



Architecture of a Quantum Multicomputer Optimized for Shor's Factoring Algorithm

A dissertation
submitted to the Department of computer science
of Keio University
in partial fulfillment of the requirements
for the degree of
doctor of philosophy

Rodney Doyle Van Meter III
July 2006

© Copyright by Rodney Doyle Van Meter III 2006
All Rights Reserved

Abstract

Quantum computers exist, and offer tantalizing possibilities of dramatic increases in computational power, but scaling them up to solve problems that are classically intractable offers enormous technical challenges. Distributed quantum computation offers a way to surpass the limitations of an individual quantum computer. I propose a *quantum multicomputer* as a form of distributed quantum computer. The quantum multicomputer consists of a large number of small nodes and a *qubus* interconnect for creating entangled state between the nodes. The primary metric chosen is the performance of such a system on Shor’s algorithm for factoring large numbers: specifically, the quantum modular exponentiation step that is the computational bottleneck.

This dissertation introduces a number of optimizations for the modular exponentiation, including quantum versions of the classical carry-select and conditional-sum adders, improvements in the modular arithmetic, and a means for reducing the amount of expensive, error-prone quantum computation by increasing the amount of cheaper, more reliable classical computation. Parallel implementations of these circuits are evaluated in detail for two abstract architectural models, one (called AC) which supports long-distance communication between quantum bits, or *qubits*, and one which allows only communication between nearest neighbors in a linear layout (called NTC). My algorithms reduce the latency, or circuit depth, to complete the modular exponentiation of an n -bit number from $O(n^3)$ to $O(n \log^2 n)$ for AC and $O(n^2 \log n)$ for NTC. Including improvements in the constant factors, calculations show that these algorithms are one million times and thirteen thousand times faster on AC and NTC, respectively, when factoring a 6,000-bit number. These circuits also reduce the demands on quantum error correction from $\sim 210n^4$ to $\sim 12n^3 \log_2 n$ for AC and $\sim 3n^4$ for NTC, potentially reducing the number of levels of error-correction encoding or allowing execution on more error-prone hardware.

Extending to the quantum multicomputer, I calculate the performance of several types of adder circuits for several different hardware configurations. Five different

qubus interconnect topologies and two different node sizes are considered, and two forms of carry-ripple adder are found to be the fastest for a wide range of performance parameters. Small nodes (up to five logical qubits) and a linear interconnection network provide adequate performance; more complex networks are unnecessary until n reaches several hundred bits. As node size grows, it is important that the I/O bandwidth of a node grow, as well, or performance can actually decline despite the overall decrease in network activity. The links in the quantum multicomputer are serial; parallel links would provide only very modest improvements in system reliability and performance. Two levels of the Steane $[[23,1,7]]$ error correction code will adequately protect our data for factoring a 1,024-bit number even when the qubit teleportation failure rate is one percent.

Acknowledgements

I had the good fortune to become acquainted very early with some characters of very high standing, and to feel the incessant wish that I could even become what they were.

Thomas Jefferson, *Autobiography*

Many, many people have demonstrated a faith in me that can never be repaid, starting with my parents, who never even suggested, so far as I recall, that there were any limits to what I could accomplish (despite sometimes overwhelming evidence to the contrary). (Though, at the same time, I have no recollection that they ever suggested I had a future in the NBA.)

Most especially, I must thank my daughters Sophia and Esther and my wife Mayumi, who put up with many hours of Daddy being physically present but mentally elsewhere. My sisters Sheila and Lera for nearly forty years have suffered the indignities and logistical difficulties of a weird, sartorially challenged older brother who lives thousands of miles away. To my grandparents, aunts, uncles, cousins and brother-in-law in a large and close family I also owe an apology for living so far away.

Every life has its cusps, its turning points that forever change you. The biggest was Caltech, but joining ISI was an unanticipated stroke of fortune. The friends and mentors I made in the Caltech and ISI days still carry me forward. Ross Berteig dragged me to the three most life-changing classes I took at Caltech (Feynman, Ayres, and Scudder), including the one that led me to ISI. At ISI, I met Wook, and my life would never be the same in ways beyond enumerating; I owe no one a greater debt. Dale Chase taught me how to be a good employee and person (and how to play team volleyball). Andi, Bobo, Brenda, Daryll, Dave, Dennis, Edie, Gabrielle, Grace, Greg, Harold, Hugo, Irene, Jessica, John, John, Kevin, Kyu, Liralen, Mimi, Michelle, Min, Myles, Pam, Rick, Ryuji, Sandy, Steve, Suz, Tiger, Yosufi and the entire CINC-PAC, WoW, volleyball, Half Moon Bay, Quantum, Nokia, NII, Keio, and Network Alchemy

crowds, just for being there (wherever “there” happens to be).

Thanks to Jim Hughes for help on classical cryptography, Reagan Moore for supercomputing advice, and the rest of the MSSTC EC for years of companionship and learning.

Without the support and encouragement of Takashi and Nobunori Shigezaki, Mark Holzbach and the folks at Asaca and ShibaSoku, and the teaching of Yuko Yamaguchi at Kichijoji Language School and Misaki-sensei at Keio, Japan would have remained a remote, foreign land rather than the second home it has become.

When I began working on quantum computing three years ago, I received important early encouragement from Prof. Kohei Itoh and Eisuke Abe of Keio University, Prof. Kunihiro of the University of Electro-Communications, Drs. Kawano and Takahashi of NTT CRL, Prof. Iwama of Kyoto University, Prof. Yamashita of NAIST, Dave Bacon of Washington, Mark Oskin of Washington, and Dr. Yamaguchi of Stanford. Professors Yoshi Yamamoto, Seth Lloyd, Isaac Chuang, Andrew Steane, Mio Murao, Hiroshi Imai, Seigo Tarucha and Akira Furusawa, and Yasunobu Nakamura and J.W. Tsai of NEC, and many researchers at NTT provided access to their labs and students, without which I would never understand how to actually build a quantum computer. Prof. Yamamoto and the others who created and staffed the summer schools in Okinawa and Kochi not only taught me but brought me into their community. I look forward to deepening collaborations with all of you over the coming years.

Although my name goes on the thesis, my coauthors on the half-dozen papers that are incorporated deserve much of the credit: Kohei Itoh, Mark Oskin, Thaddeus Ladd, Kae Nemoto, and Bill Munro. Thaddeus gets a special call out for writing advice as well as teaching me physics. Joe Touch, Ted Faber, Bill Manning and Nick Burke all read (sometimes awful) drafts of various papers and provided other important support. Kevin Binkley’s stochastic engine, especially the genetic algorithms, provided insight into optimization problems that remain open. Suzanne and Bob Diller get credit for cogent advice on the title and abstract of my dissertation, as well as providing years of friendship. Michael Cohen and Prof. Sagawa of Aizu-Wakamatsu and Prof. Jun Murai, Ryuji Wakikawa and Shoko Mikawa at the School of Internet ASIA Project provided teaching opportunities which turned into wonderful learning experiences for me. Chip Elliott and others at BBN have provided important encouragement, as well.

The music of Tatopani, Billy Higgins, John Coltrane, Louis Armstrong, King Crimson, Kodo, and a plethora of others kept me sane. Surprisingly, we have no favorite chef

in this country (our favorite anywhere is Jose Luis Ugalde of Cafe Gibraltar), but everyone who has fed me startling and wonderful meals – you keep me going.

Without the cooking and baby-sitting of the indomitable Kazuko Arai, this thesis would have taken a decade to complete, if it ever got done at all.

This work was supported in part by Ken Adelman and Dave Kashtan under the Network Alchemy basic research funding plan, and by CREST-JST. Kae Nemoto also provided funding for travel and a desk at NII. Karl and Pattie and Danner and Jenny put me up in Cambridge.

This thesis was created using 100% free software. Thanks to the creators of Linux, X, TeX and L^ATeX, GNU Emacs, xfig, dia, POVray, maxima/MACSYMA, octave, gnuplot, bison, flex, gcc, and more — and, in some cases, to the researchers on whose work these tools are founded, though the code base has changed. And thanks to the creators of the arXiv, scholar.google.com, researchindex.org, and citebase, without which I would have missed much important research, and probably been forced to recreate it poorly and tediously on my own.

I thank Y. Nakamura, T. Yamamoto, D. Wineland, and K. M. Itoh for the figures. Thanks to all of the patient physicists who have put up with my slowness, including Viv Kendon for help with Shor’s algorithm.

I have had, in effect, four advisers: Fumio Teraoka in computer networking, Kohei Itoh in experimental physics, and Kae Nemoto and Bill Munro in theoretical physics. All four have been outstanding. Kae worked harder on reviewing this dissertation than anyone else; it would not be as clear and correct without her. Bill is the one person *not* on my committee without whom this technical work could not have been done. Thanks. Thanks to Profs. Amano and Yamasaki, my other committee members. I have also had six godfathers and mentors: Wook, Darrell Long, Paul Mockapetris, Jun Murai, Rick Carlson, and Bob Hinden. Without your advice and encouragement, I wouldn’t be finishing a doctorate in such a challenging and fascinating subject.

Contents

Abstract	iii
Acknowledgements	v
Table of Contents	ix
List of Tables	xv
List of Figures	xvii
1 Introduction	3
1.1 Computing Frontiers: Why Study Quantum?	4
1.2 Defining Quantum Computer Architecture	6
1.3 The Quantum Multicomputer	7
1.4 This Dissertation	9
1.4.1 Contributions	11
1.4.2 Contents and Structure	13
1.4.3 How to Read This Dissertation	14
1.5 What We're Not Going to Talk About	14
1.6 Summary	16
2 Reversible and Quantum Computation	18
2.1 Reversible Classical Computation	18
2.1.1 History and Importance	19
2.1.2 Two-Bit Gates	20
2.1.3 Three-Bit Gates: Toffoli and Fredkin	21
2.1.4 Ancilla Management	22
2.2 Introduction to Quantum Computing	24

2.2.1	Notation and a Few Linear Algebra Notes	25
2.2.2	Schrödinger's Equation	26
2.2.3	Qubits	27
2.2.4	Manipulating Qubits	34
2.2.5	DiVincenzo's Criteria	41
2.2.6	Quantum Algorithms	43
2.2.7	Distributed Quantum Computation	45
2.3	Error Management in Quantum Computers	46
2.3.1	Error Models	47
2.3.2	Quantum Error Correction Codes	48
2.3.3	Fault Tolerance	53
2.3.4	Threshold Calculations and Concatenation	53
2.3.5	Why QEC Suppresses Over-Rotation Errors	55
2.3.6	Other Error-Suppression Techniques	57
2.4	Summary	58
3	Shor's Algorithm for Factoring Large Numbers	60
3.1	The Importance of Factoring	61
3.2	Historical Progress in Factoring	62
3.3	The Quantum Fourier Transform	64
3.4	Prior Art in Quantum Adders	66
3.4.1	Arithmetic Performance Notation	67
3.4.2	Linear-Time Adders	67
3.4.3	$O(\log n)$ Adders	71
3.4.4	Ultimate Limits on Performance of Addition	73
3.4.5	Summary	74
3.5	Quantum Modular Exponentiation	75
3.5.1	VBE, BCDP and Others	76
3.5.2	Cleve-Watrous Parallel Multiplication	77
3.5.3	Schönhage-Strassen	79
3.6	Shor's Algorithm	79
3.7	Summary	81
4	Taxonomy of Quantum Computing Technologies	83
4.1	Taxonomy Framework	83

4.1.1	Basic Features	83
4.1.2	Algorithmic Efficiency Features	85
4.1.3	Time and Gate Characteristics	87
4.1.4	Other Features	89
4.1.5	Manufacturing and Operating Environment	90
4.2	Quantum Technologies	92
4.2.1	Solution NMR	92
4.2.2	Josephson Junction	98
4.2.3	All-Silicon NMR	100
4.2.4	Scalable Ion Trap	101
4.2.5	All-Optical	102
4.2.6	Quantum Dot	102
4.2.7	Kane Solid-State NMR	104
4.2.8	Optical Lattice	105
4.3	Summary	106
5	Networking	107
5.1	Qubus Entanglement Protocols	107
5.2	Teleportation	110
5.2.1	Teleporting Data	111
5.2.2	Teleporting Gates	112
5.3	Multicomputer Networks	113
5.4	Summary	116
6	Performance of Large-Scale Systems	118
6.1	Managing Performance	119
6.1.1	Error Correction, Architecture, and Clock Speed	121
6.1.2	AC and NTC Architectural Models	122
6.1.3	Notation	123
6.2	Trading Classical for Quantum Computation	124
6.2.1	Introduction	125
6.2.2	Indirection	126
6.2.3	The <i>b</i> Array	126
6.2.4	The Algorithm	130
6.2.5	Evaluating Cost and Selecting Word Length	130

6.3	New Adder Types	132
6.3.1	Basic Carry-Select Adder	133
6.3.2	$O(\sqrt{n})$ Carry-Select Adder	135
6.3.3	$O(\log n)$ Conditional Sum Adder	136
6.3.4	Summary	138
6.4	Monolithic Shor Performance	138
6.4.1	Mapping Adders to Architectures	140
6.4.2	Acceleration	142
6.4.3	Example: Exponentiating a 128-bit Number	145
6.4.4	Asymptotic Behavior	148
6.4.5	Results	150
6.4.6	Error Correction Needs	152
6.5	Summary	154
7	The Quantum Multicomputer	156
7.1	System Overview	156
7.2	An Engineer's Definition of Scalability	157
7.2.1	Economics	158
7.2.2	Infrastructure Needs	158
7.2.3	Performance	159
7.2.4	Single-Device Physical Limitations	160
7.3	System Overview	161
7.3.1	Hardware Overview	161
7.3.2	Node Architecture	162
7.3.3	Network Topologies	165
7.3.4	Software	165
7.3.5	Summary	167
7.4	Distributed QEC and Bus Design	168
7.4.1	Distributed Logical Zeroes	169
7.4.2	Distributed Data	170
7.4.3	Implications for Link Design	175
7.4.4	Summary	177
7.5	Distributed Form of Shor's Algorithm	178
7.5.1	Algorithm	179
7.5.2	Performance	182

7.6	Summary	191
8	Conclusion	193
8.1	Complete Performance Estimates	195
8.2	Future Work	197
8.3	Prospects	199
8.4	Final Words	201
A	Glossary	202
B	List of Papers and Presentations	205
	Bibliography	208

List of Tables

2.1	CNOT truth table.	21
2.2	CCNOT (Toffoli gate) truth table.	22
2.3	Control-SWAP (Fredkin gate) truth table.	22
2.4	Erasing ancillae.	24
3.1	Transform values of the coefficients in the QFT.	65
3.2	Transform of different offsets into phase via the QFT.	66
4.1	Qubit technology basic characteristics	93
4.2	Features affecting algorithm efficiency	94
4.3	Clock speed and gate characteristics	95
4.4	Other Features	96
4.5	Manufacturing and operating environment	97
5.1	Some common interconnect topologies.	114
6.1	Qubit technologies and recommended choice of adder	141
6.2	Parameters for our algorithms, chosen for 128 bits	145
6.3	Latency to factor a 128-bit number	146
6.4	Approximate KQ for some different adder circuits	152
6.5	Approximate KQ for complete modular exponentiation circuits	154
7.1	Characteristics of our five network topologies.	166
7.2	Strawman system summary	167
7.3	Number of teleportations necessary for modular exponentiation	169
7.4	Breakpoints for the Steane $[[7,1,3]]$ code	171
7.5	An estimate of the necessary teleportation error rate	174
7.6	Estimate of adder latency using monolithic teleportation blocks	185
7.7	Estimated latency for adders using decomposed teleportation blocks	187

8.1	Number of teleportations and adder calls for modular exponentiation . .	195
8.2	Estimated time to complete distributed modular exponentiation	196

List of Figures

1.1	Quantum computer architecture	8
1.2	High-level quantum multicomputer block diagram	10
1.3	Current subsystem status	11
2.1	Reversible gates	23
2.2	The Bloch sphere.	28
2.3	Basic quantum gates	36
2.4	Our CCNOT construction	41
2.5	Error propagation in two-qubit gates.	48
2.6	Parity measurement for quantum error correction.	49
2.7	Circuit to create the $ 0_L\rangle$ state for the Steane $[[7,1,3]]$ code.	52
2.8	Fault-tolerant error syndrome measurement algorithm.	54
3.1	Length of factored RSA Challenge numbers	63
3.2	Scaling of number field sieve	64
3.3	An eight-bit VBE adder.	69
3.4	Building blocks for the CDKM adder.	71
3.5	An eight-bit CDKM adder.	72
3.6	An eight-bit carry-lookahead adder.	73
3.7	Concurrent modular multiplication	78
3.8	Cleve-Watrous parallel multiplication	78
4.1	A pair of coupled Josephson-junction charge qubits	99
4.2	Schematic of the all-silicon NMR computer	100
4.3	A six-zone ion trap	103
5.1	Physical configuration of a qubus.	108
5.2	Phase space diagram of the qubus entanglement protocol.	109
5.3	Logical equivalent of the qubus entanglement protocol.	109

5.4	Teleporting a single qubit.	111
5.5	A teleported control-NOT (CNOT) gate.	113
5.6	Five important interconnect network topologies.	115
6.1	CCNOT constructions for our architectures AC and NTC	123
6.2	Quantum-Addressable Classical Memory (QACM)	127
6.3	3-bit Quantum Select Circuit (Q-SEL)	128
6.4	Implicit indirection using a classical memory	129
6.5	Argument setting for indirection for different values of w	129
6.6	Multiplication Using Indirection, Based on Vedral's Circuit	131
6.7	Total Cost	131
6.8	Three-bit carry-select adder (CSLA) with multiplexer (MUX)	134
6.9	In-place post-select circuit	135
6.10	Block-level diagram of four-group carry-select adder	135
6.11	$O(\log n)$ MUX for conditional-sum adder	137
6.12	Scaling of number field sieve	139
6.13	Optimized, concurrent three bit VBE ADDER for NTC	141
6.14	More efficient modulo adder	144
6.15	Execution time for our algorithms for space $100n$	148
6.16	Execution time v. space for our algorithms for 128 bits	149
6.17	Scaling of number field sieve (NFS) and Shor's algorithms	151
6.18	Cleve-Watrous parallel multiplication	153
7.1	The five physical topologies analyzed in this thesis.	166
7.2	Distributed circuit to create the $ 0_L\rangle$ state for the Steane $[[7,1,3]]$ code.	171
7.3	Teleporting logical state using local QEC only	172
7.4	Teleporting logical state using intermediate, teledata distributed QEC.	175
7.5	Local QEC only, no intermediate QEC, serial interface.	176
7.6	Details of a distributed 2-qubit VBE adder	180
7.7	Visual approach to determining cost for distributed VBE adder	181
7.8	Visual approach to determining cost for distributed CDKM adder	182
7.9	(Telegate) Performance of different adders on three different networks	189
7.10	(Teledata) Performance of different adders on three different networks	190
7.11	(Teledata) CDKM+line to carry-lookahead+2fully comparison	191

For my family

Chapter 1

Introduction

We are just started on a great venture.

Dwight Eisenhower, November 1942

The designer usually finds himself floundering in a sea of possibilities, unclear about how one choice will limit his freedom to make other choices, or affect the size and performance of the entire system. There probably isn't a 'best' way to build the system, or even any major part of it; much more important is to avoid choosing a terrible way, and to have clear division of responsibilities among the parts.

I have designed and built a number of computer systems, some that worked and some that didn't.

Butler Lampson, "Hints for Computer System Design" [199]

As VLSI features continue to shrink, computers that depend on quantum mechanical effects to operate are inevitable; indeed, quantum effects are predicted to affect device behavior within a decade [236, 226, 51, 152, 110, 53]. The fundamental architectural issue in these future systems is whether they will attempt to hide this quantum substrate beneath a veneer of classical digital logic, or will expose quantum effects to the programmer, opening up the possibilities of dramatic increases in computational power [114, 94, 93, 39, 42, 296, 135, 3, 211, 248].

Small and unreliable they are, but quantum computers of up to a dozen nuclear spins [243] and eight ions [139] exist. In these machines, the spin state of an atomic nucleus or the energy level of an ion can represent a quantum bit, or *qubit*, the smallest

unit of quantum information. The three most famous quantum algorithms are Deutsch-Jozsa [94], Grover's search [135], and Shor's factoring [296]. All three of these algorithms have been experimentally implemented for small-scale problems [161, 76, 74, 174, 330, 339, 340, 138]. A further extremely broad range of experiments has demonstrated numerous building blocks [347, 33, 313, 181, 239, 70, 268, 164] based on the one- and two-qubit technology demonstrations we will see in Chapter 4. Although many theoretical and practical questions remain open, it seems reasonable to assert that implementation of quantum computation is on the verge of moving from a scientific problem to an engineering one. It is now time to ask what we *can* build, and what we *should* build. Various computer architecture researchers have begun investigating the former question, working from the bottom up [84, 155, 256, 255, 324, 154]; this dissertation and the related papers address the latter question, working from the top down [334, 337, 336, 332, 333, 335].

1.1 Computing Frontiers: Why Study Quantum?

Why should computer engineers study quantum computation, and why now? Certainly the field of classical computer architecture is not moribund, and offers far more immediate impact for much less intellectual risk. Work that increases parallelism, reduces power consumption, improves I/O performance, increases gate speed or reduces data propagation delays is much more likely to be used in the real world, and far sooner than quantum technologies. Intel began sampling a billion-transistor microprocessor chip in October 2005, a 580 square-millimeter chip built in a 90 nanometer process. Some researchers consider integration levels of a trillion transistors per silicon chip possible [228], though we are hardly done digesting the implications of a billion transistors on a chip [262, 190, 61]. Clearly there is room on-chip for many architectural advances. Ubiquitous computing, sensor networks, augmented reality, and mobile systems will no doubt be among the most transformative technologies of the coming decades, relegating today's 3G Internet-connected mobile phones to the status of Neolithic stone adzes [278]. In "back end" systems, continued research on computational grids and storage are critical. Among computing exotica, electrical circuits fabricated with nanotechnology [363, 36, 220, 322, 284], DNA computing [10], and amorphous computing are all other possible fields of pursuit [6]. So, why quantum?

Different researchers have different reasons for studying quantum computing. Physicists are learning fundamental facts about the quantum behavior of both individual particles and mesoscopic systems. Theoretical computer scientists are finding many fascinating new questions (and answering some of them). But to a computer systems person, quantum computation is about one thing: *the pursuit of performance*. If practical large-scale quantum computers can be built, we may be able to solve important problems that are classically intractable. Potential applications include cryptographically important functions such as factoring, which appears to offer a superpolynomial speedup, and scientifically important problems such as simulations of many-body quantum systems, which may offer exponential speedup, though recent questions have been raised about whether exponential speedup is achievable as the desired error bound is tightened [58]. Quantum computers therefore hold out the possibility of not just Moore's Law increases in speed, but a change in computational complexity class and consequent acceleration on these, and possibly other, problems.

I will not directly address criticisms of the possibility of quantum computation [104, 169], except to note that my response is different from that of Aaronson, who is excited by the inherent beauty and theoretical importance of quantum mechanics while searching for the ultimate limits to computation [3]. I, too, admire these factors, but more importantly I believe it is inevitable, as silicon devices continue to scale down in size, that we will have to deal with quantum effects. Many researchers are directing their efforts at mitigating these effects; in my opinion, we will do better by embracing them, even if "quantum computing" ultimately proves to have no computational advantage over classical.

Studying quantum computing indirectly benefits classical systems, as well. Quantum effects are being explored for direct exploitation as classical logic, for example, the recent work on magnetic quantum dot cellular automata [153]. *Plasmonics*, the study of electromagnetic waves propagating in the surface of a material, is developing rapidly, and might offer improvements in how we move data within classical chips [258]. More broadly, the whole area called *spintronics*, directly or indirectly manipulating the spin of small numbers of electrons, is already having an impact through the creation of technologies such as magnetic RAM (MRAM) [329, 351]. Quantum computers depend on, and have served as an impetus for developing, thermodynamically reversible computing. It has been suggested that classical computers must employ reversible logic to exceed 10^{22} floating point operations per second (10 zettaFLOPS) [91]. Quantum computation serves as an excellent training ground for engineers destined to work in

these areas, as well as providing both fundamental and practical results that influence the technological development of these areas.

My analogy is to the field of robotics. It has been more than eighty years since the original use of the term *robot* to mean an autonomous, mechanical humanoid (though the idea goes back to antiquity) [65], and several decades since the debut of robotics as a respectable field of inquiry. Yet the humanoid robots of science fiction do not roam the streets of Tokyo in the first decade of the twenty-first century. This does not mean that robotics as a field has been barren; indeed, robots dominate many forms of manufacturing, and related technologies spun off from robotics research are nearly ubiquitous. Robotics depends on, and serves as an impetus for, research as diverse as computer vision, speech recognition, fuzzy logic, virtual reality, and many mechanical advances. The road to development has been long, and the results to date look nothing like what mid-twentieth century science fiction writers such as Isaac Asimov anticipated [22], but the results have been extremely valuable nonetheless. So I expect it to be with quantum computing.

1.2 Defining Quantum Computer Architecture

Quantum computer architecture is an emerging field, spanning the gap between device physics and algorithms. If large-scale quantum computers are to be built, an overall structural plan must be established; we refer to this plan as the machine architecture of the quantum computer. Figure 1.1 shows a representation of the relationship among some subfields of quantum computing, and which subfields are part of the broader area of quantum computer architecture. I include in this field essentially everything above device physics up to the design and performance analysis of machines for specific algorithms. The component which has (rightly) been the focus of the most work to date has been quantum error correction, though effective high-level structures (including physical connection topologies), control structures, efficient algorithm implementation, and performance analysis are all receiving increased attention. Quantum computer architecture can draw heavily on classical computer architecture, but presents a number of unique challenges.

In most quantum computing technologies, a qubit is the state of a physical device, more like the state of a flip-flop than a signal propagating through a circuit. Qubits that are physically far apart cannot directly interact, so data must be shuffled from place to place as they are required to interact with other qubits. Architects and compiler writers

must cooperate to make this shuffling as efficient as possible. In the figure this topic is represented as “interconnection technologies and topologies”. Solutions to this kind of data transport problem form one of the key themes of this thesis.

Although they are not explicitly represented in the figure, quantum programming languages and compilers, designed for programming quantum computers, can be viewed as the interstitial glue that holds the whole system together [128]. Quantum programs are executed classically, and must be able to manipulate both quantum and classical data, and make branch and loop decisions based on classical data. The ability to look at quantum data during program execution is extremely limited, as we will see when we discuss measurement in Section 2.2.3; the operations on the quantum data are performed more or less blind, without examining the data itself. In this sense, programming a quantum computer is like programming a Connection Machine or systolic array, though the analogy between qubit and CM processor is weak [312].

Because quantum computer architecture is a young field, many issues have not yet been addressed in the depth required to evaluate design choices. Often clock speed and other architectural features are ignored as issues in quantum computing devices, assuming that the quantum speed-up will dominate, making quantum algorithms practical on any physically realizable quantum computer. However, this is not necessarily so. For example, Shor’s factoring algorithm runs in polynomial time and resources, but the details of the polynomial matter: what degree is the polynomial, and what are the constant factors? How much parallelism can be extracted from both the hardware and software to reduce the wall-clock time consumed? All of these issues are of concern to architects.

Some of these issues are attacked in this thesis. We will see others in Section 8.2, on future work, at the end of the dissertation.

1.3 The Quantum Multicomputer

My thesis is the design of a *quantum multicomputer*. Any single, monolithic quantum computer will have an ultimate limit to its storage capacity and performance. Borrowing from classical multicomputer design and building on the foundations of distributed quantum computation that have been laid, these limitations can be overcome. This dissertation describes the architecture of a system suitable for running highly optimized forms of Shor’s factoring algorithm, and examines the scaling of the performance from sixteen to 1,024 nodes. This broad range of sizes allows us to see clearly the important

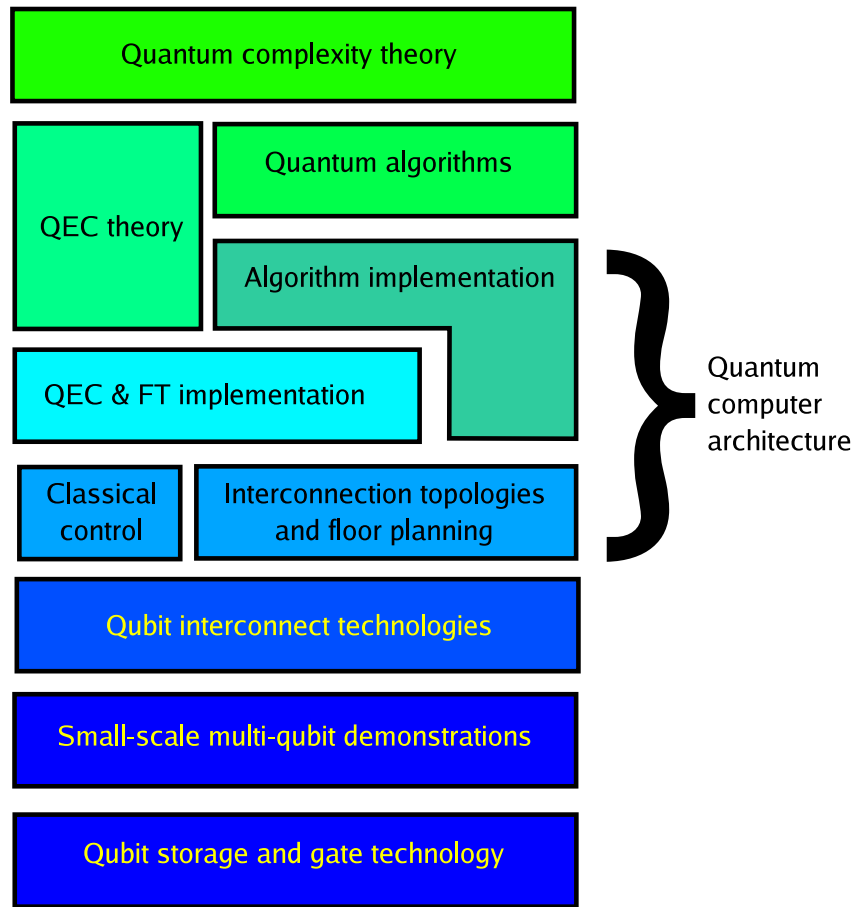


Figure 1.1: Quantum computer architecture among some subfields of quantum computation.

inflection points in behavior as the system scales up, ending at a performance point well above the capabilities of classical systems.

A high-level block diagram of the hardware is shown in Figure 1.2. Like all proposed quantum computers, it is actually a hybrid quantum-classical system, and to achieve performance balance the classical portion will be coupled to a supercomputer-class machine. The classical front end is responsible for overall coordination, download of programs and final upload of data, but has only a loose role in the execution of a program. The nodes perform the actual computation. Each node consists of two halves, the quantum part (Qnode), which holds the quantum data, and the classical part (Cnode), which contains the real-time measurement and control circuitry (including program execution) for the quantum device. There are two real-time interconnects, one classical and one quantum; the quantum interconnect is based on the *qubus* approach for its link technology [303, 237]. These interconnects may be switched, node-to-node direct, or shared; a major portion of this thesis is analysis of the traffic on the qubus-based quantum interconnect for different possible topologies. We will not address the classical portions of the system, except that classical communication and instruction execution are implicitly included in our timing estimates.

A well-designed architecture can outlive the technological environment in which it was originally created. However, some constraints are necessary as we discuss the initial implementation target, or we are left adrift on Lampson's Sea. I have chosen a solid-state qubit technology, such as Josephson-junction qubits (described in Sec. 4.2.2), as a basis on which to build. Very, very roughly, I have chosen to limit the estimated production cost to one hundred million U.S. dollars, and the size of the system to one hundred meters square of floor space.

1.4 This Dissertation

The quantum multicomputer consists of three primary subsystems: the quantum computational node hardware, the quantum interconnect hardware, and the software to run on the system. The status of some of these subsystems is represented in Figure 1.3. Node hardware is not a primary focus of this thesis; we leave it to other researchers to meet the hardware requirements outlined in Chapter 7.1. Interconnect hardware consists of basic link technologies and the manner of assembling a complete system, namely the topology and any necessary lower-level switching mechanisms; finding an appropriate topology is one of the primary contributions of this thesis. Finally, although

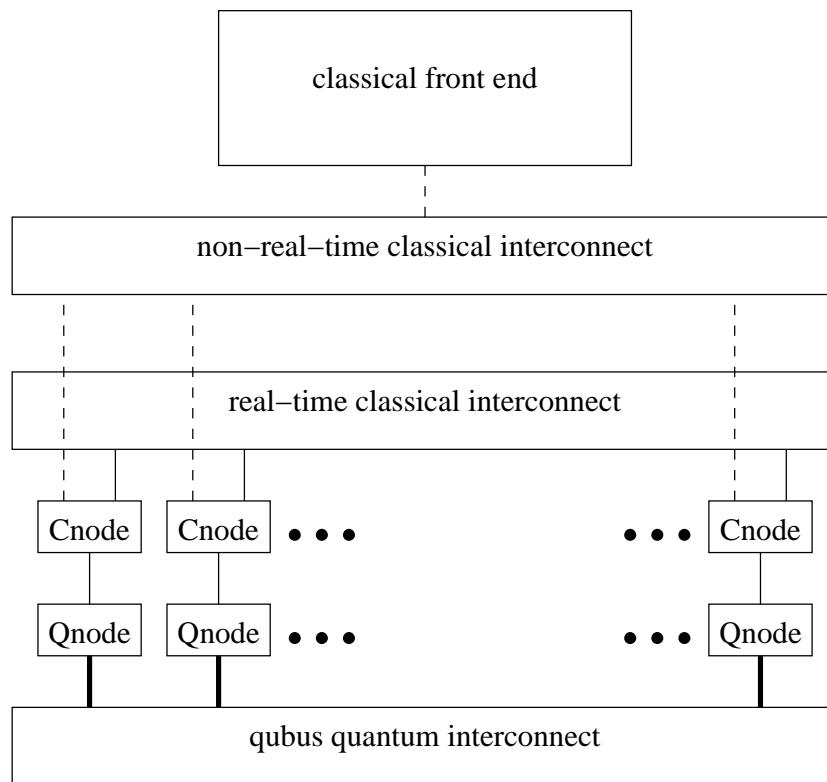


Figure 1.2: High-level quantum multicomputer block diagram. Dashed lines are non-real-time communication; solid lines are real-time communication, either classical (thin lines) or quantum (thick lines). Cnode, classical node; Qnode, quantum node.

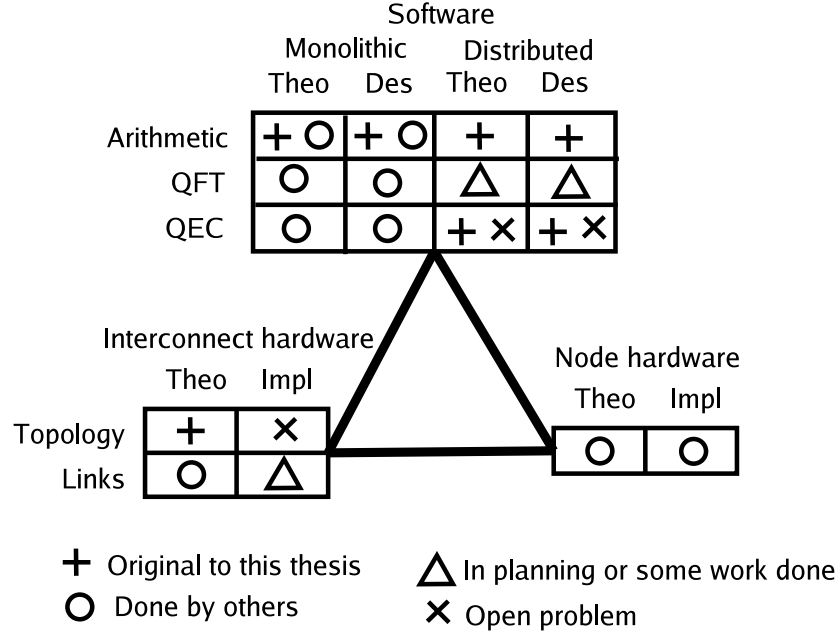


Figure 1.3: The status, or relative maturity level, of various subsystems within the quantum multicomputer. QFT, quantum Fourier transform; theo, theory; des, design; impl, implementation.

the arithmetic and quantum Fourier transform (QFT) algorithms that make up Shor’s factoring algorithm have been described at a high level, we make significant advances in the former in this thesis. Although this thesis makes some progress on distributed quantum error correction (QEC), I believe this is very much an open problem, so it is marked with both symbols in the figure.

1.4.1 Contributions

The primary contribution of this thesis is the architecture of a quantum multicomputer. To validate design choices, a target workload of Shor’s algorithm for factoring large numbers is used. This validation entails analysis and optimization of the performance of arithmetic, especially adders, on both monolithic and multicomputer quantum systems. I have designed new types of reversible adder circuits, analyzed the parallelism available in Shor’s algorithm, optimized Shor’s algorithm, and mapped it to various architectures, following through with performance analysis for two monolithic machine types and a variety of adder circuits. From there, I extend to a multicomputer. I define the capabilities necessary for a node. Detailed analysis shows that the interconnect links may be serial, rather than parallel, and that a linear network topology will be adequate

into the high hundreds of nodes, when a switched network becomes more appropriate. The performance is analyzed assuming nodes are built on high-speed solid-state qubits, and the performance is found to be good. Finally, I investigate very loosely the practical constraints on the construction of such a system, including cooling, floor space, packaging, interconnects, control equipment, and economics.

In summary, the contributions of this thesis are:

- Fast, architecturally realistic quantum modular exponentiation algorithms.
 - Based on known and new principles, improvements in both asymptotic performance and constant factors in the time required for modular exponentiation. To factor a 6,000-bit number, for example, the performance improvement ranges from 13,000 times to one million times, depending on architecture, compared to the previous best-known algorithm. The asymptotic performance (circuit depth, or latency) improves from $O(n^3)$ to $O(n^2 \log n)$ or $O(n \log^2 n)$, again depending on architecture.
 - A classical/quantum tradeoff that reduces the number of quantum gates that must be performed.
 - New square root-depth and logarithmic-depth adder circuits, used in some forms of my modular exponentiation algorithms.
 - Analysis of the demands of arithmetic circuits on the strength of quantum error correction, showing that my new algorithms are substantially less demanding, and hence have higher probability of success and/or can be executing using weaker QEC.
 - A proposed *architectural* taxonomy of qubit technologies, complementary to the DiVincenzo criteria that establish minimal necessary functionality.
 - The most detailed architectural performance analysis to date.
- Architecture of a quantum multicomputer.
 - Analysis of performance of adder circuits on various network topologies showing that a linear network is adequate up to moderately large problem sizes.
 - Design of link transfer protocols based on quantum teleportation and QEC, establishing that serial links perform adequately.

- Delineation of required traits for the computational nodes.
- A high-level analysis of the overall system requirements, including floor space and economics, assuming a solid-state qubit technology.

1.4.2 Contents and Structure

This dissertation is divided into eight chapters. The first and last are the overview and conclusions, respectively. Chapter 2 consists primarily of a review of existing classical and quantum material. Chapter 3 presents Shor’s algorithm. Chapter 4, the taxonomy of quantum technologies, reviews the work of experimentalists, but the structure of the taxonomy is original. Chapter 6 describes my contributions to understanding and improving the performance of the modular exponentiation for Shor’s algorithm, and Chapter 7 describes the architecture and performance of my quantum multicomputer.

Sections 2.1 and 2.2 introduce the fundamental concepts of reversible classical and quantum computation, including the graphical and mathematical notations used throughout this dissertation. Chapter 3 describes the quantum portions of Shor’s algorithm for factoring large numbers, including adder circuits developed by various researchers over the last decade to support Shor’s algorithm. The taxonomy in Chapter 4 describes existing experimental approaches to quantum computing developed in many research organizations; I attempt to extract common themes in these technologies and organize the information so that it is possible to determine the architectural promise of each technology. Chapter 5 is a quick sketch of the mechanisms we need for transferring data in our quantum multicomputer: the qubus approach to creating entanglement, quantum teleportation, and the classical concepts of multicomputer networks.

The first section of Chapter 6 addresses the practical implications of scalability for large quantum computing systems, including such mundane issues as economics and floor space. The rest of the chapter details the mapping of the entire quantum modular exponentiation necessary for Shor’s algorithm to abstract quantum architectures. Section 6.1 describes the management of performance, introducing the AC and NTC architectural models and our performance notation and summarizing the techniques presented in the following material. Section 6.2 accelerates the quantum portion of the algorithm in exchange for more onerous classical computation. Section 6.3 details two new reversible quantum adder algorithms, the $O(\sqrt{n})$ -depth carry-select and $O(\log n)$ -depth conditional sum circuits. Section 6.4 brings all of the techniques together and shows overall performance speedups for both architectural models.

Chapter 7 advances the state of the art in distributed quantum computation by creating specific hardware models and performance estimates for the quantum multicomputer, starting with a system overview. Section 7.4 covers the distributed form of quantum error correction and its impact on link design, and shows that serial links are acceptable. Finally, Section 7.5 brings us to the goal of analyzing the behavior of Shor’s algorithm on realistic hardware models.

A small glossary is provided as Appendix A.

1.4.3 How to Read This Dissertation

The primary target audience of this dissertation is computer systems researchers with little or no prior background in quantum computing. As such, the mathematics are limited and informal, but heavy on examples. Systems researchers will probably benefit most from reading the dissertation linearly from beginning to end.

Physicists who are already familiar with quantum computing may want to skip most of Chapters 2 and 3, though they may find enough new tidbits in Section 2.1 to repay the time invested. Such readers may be less familiar with some of the concepts in Section 3.4 and Chapter 5, and are encouraged to skim Chapter 4 for some insight into the technology issues that matter to a system architect.

For those readers interested in only the major results, besides the overview and conclusion chapters, the most important sections are 6.4, 6.3, 6.2, and especially 7.5.

1.5 What We’re Not Going to Talk About

Quantum information processing (QIP), despite its youth, is already a very broad field, and there are many important and fascinating topics that I am *not* going to present in this dissertation. This section merely identifies a few for completeness, and provides some pointers to further literature for those whose curiosity is piqued by this dissertation. Readers interested in more depth are referred first to popular [349, 245] and technical [248, 177, 126, 273] texts on the subject.

Probably the most important area not addressed is computational complexity. Computer science theorists are rapidly advancing our understanding of what quantum computers are, and are not, capable of computing efficiently [42, 354, 48, 2, 3]. This research is also advancing our knowledge of classical computational complexity, and has the potential to ultimately shed light on the fundamental $P \stackrel{?}{=} NP$ question.

Feynman originally conceived of a quantum computer as a device for quantum simulation [114, 211, 50, 7, 63, 58, 23]. Quantum simulation may very well be the first production use of quantum computing technology. However, it bears less resemblance to a general-purpose, programmable machine derived from known classical architectural principles, which is my goal in this thesis.

Other important algorithms besides Shor's factoring algorithm have been developed. The first quantum algorithm invented was Deutsch-Jozsa, which can determine whether a function is *constant* (returns the same value for all inputs) or *balanced* (returns zero for half of its inputs and one for the other half), using only a single call to the function [94]. Grover's search algorithm can search an unstructured space of N possibilities in $O(\sqrt{N})$ time. It is sometimes referred to as *amplitude amplification* and has been found to be useful for quantum counting, and as a wrapper for other algorithms [135, 137, 55]. Although they are important, we will not delve into Simon's algorithm [299], Hallgren's [143], or the fascinating topic of quantum random walks [13, 166].

Quantum networking, especially as typified by quantum key distribution, is a vital and fascinating area, and the only area of QIP in which products are already available [108, 261, 44]. Dense coding is also a clever and important idea by Bennett and Wiesner [223, 47] which essentially allows one system to "presend" half of the bits in a message to its partner *before* computing the data. Many researchers have worked on various aspects of quantum information theory, including quantum channel capacities analogous to Shannon's capacity for a classical channel. The last third of Nielsen and Chuang deals with this topic, including derivation of quantum error correction from this point of view [248].

Perhaps the most interesting advance in quantum computing theory in recent years is the development of *cluster state computing*, or *one-way computing* [277, 246]. We refer to cluster state occasionally in this dissertation, but will not have the space to deal seriously with it.

Researchers have begun designing programming languages for quantum computers [254], and several workshops have been held. Gay's survey and extensive bibliography is a good place to start studying this topic [128].

All of the quantum computers being seriously discussed today are essentially hybrid computers: some of the data is quantum, but other data and all of the program are classical. We will confine ourselves to such systems for this thesis, though some researchers have investigated the next advance in quantum computer architecture: true *quantum*

programs, leading to a quantum instruction set architecture (ISA) [247, 149, 264, 282].

Quantum games [231, 106], quantum computing through wormholes [27] and relativistically accelerated devices [275], and the amount of computation that can be performed by given amounts of matter [212] or even the Universe as a whole [213] are mind-boggling ideas. We are not discussing quantum cellular automata (QCA) or quantum Turing machines [39, 93, 126], despite their importance (quantum wires and the original Lloyd model of a quantum computer are forms of QCA [210, 256]). We are not going into any significant detail on entanglement theory. We are also not going to discuss qutrits, or continuous quantum variables (qunats).

And, of course, even in a work the length of a thesis it is impossible to go into any topic in the depth it truly deserves; the device technologies we discuss in Chapter 4 are but a few of the dozens of proposed and even instantiated types. In addition to the taxonomy and references in this dissertation, I recommend the ARDA road map for its breadth [20] and Chapter 7 of Nielsen and Chuang for its clarity of exposition [248].

1.6 Summary

The fundamental principles of small-scale quantum computing have been demonstrated experimentally, and matching theory is progressing nicely, though both have plenty of challenges ahead. What has been much less clear is whether truly scalable systems can be built; indeed, the real-world feasibility of creating entanglement across thousands of qubits remains very much open to question. Distributed quantum computation is one possible way to overcome the limitations of an individual quantum computer. The basic idea of distributed quantum computation is straightforward, but detailed analysis of its implementation has been lacking: what hardware will it run well on, under what conditions is it robust, and can it bring improvements in both qubit storage capacity and algorithmic performance? This thesis clarifies these issues. The quantum multicomputer framework, like a good classical architecture, has the potential to far outlive the technological environment in which it was originally conceived. Ladd has speculated that production quantum computers are likely to be built on technologies which have not yet been invented; the principles outlined here will apply even in that eventuality.

Before we can demonstrate that the quantum multicomputer has acceptable performance and reliability for large but finite problems, we must evaluate and optimize the proposed workload. Prior even to that, we begin by investigating the foundations of classical reversible and quantum computation. The road to a working, useful, reliable,

economically viable quantum computer is long, dangerous, and in large measure unknown, but, like Hokusai's stages of the Tokaido, the sights and stops along the way are beautiful, fascinating and important. In the next chapter, we take the first step.

Chapter 2

Reversible and Quantum Computation

“[A civilized man] can go up against gravitation in a balloon, and why should he not hope that ultimately he may be able to stop or accelerate his drift along the Time-Dimension, or even turn about and travel the other way?”

The Time Traveler, in H.G. Wells’ *The Time Machine*, 1895

In good time, as it were, we will come to our performance analysis of the arithmetic necessary to run Shor’s algorithm for factoring large numbers, and our *quantum multicomputer* architecture designed to run the algorithm. Let us begin prior to the genesis of quantum computation, with the development of *reversible computing*. Gates in quantum computation depend on concepts developed for reversible classical computing, which is sometimes also called “conservative logic”. Once we understand the basics of reversible classical computation, it will be easier to understand the circuits and algorithms for quantum computation presented in the second and third parts of this chapter, first the basic principles of quantum computing then the major topic of quantum error correction.

2.1 Reversible Classical Computation

In a reversible computation, it is possible to recover the complete initial state of the system having only the final state. A NOT gate, for example, is reversible; applying a second NOT gate recovers the initial state with no loss of information. An AND gate is not reversible; from the single output bit it is not always possible to determine the input state unambiguously. If the output is 1, we know that the input was 11, but if the

output is 0, we can't tell whether the input was 00, 01, or 10. Similarly, an OR gate is not reversible; if the output is 1, we don't know whether the input state was 10, 01, or 11. A single bit of output is insufficient to discriminate among the possible states of multiple bits of input. These examples suggest an important rule:

Reversible gates must have the same number of outputs as inputs, and the mapping of input to output states must be 1 : 1.

First, we briefly discuss the history and importance of reversible computation, then show the important two-bit reversible gate, followed by three-bit gates and the emulation of Boolean logic. We finish by presenting ancilla management techniques without which the space required for most interesting computations would grow unacceptably. We do not discuss the thermodynamics of computation in any detail here; interested readers will find this topic covered in the papers referenced here.

2.1.1 History and Importance

Reversible computation was developed in the early 1970s by Charles Bennett [40], acting on inspiration from Landauer's discovery that the *erasure* of information requires an increase in entropy [200, 41]. In traditional logic, erasing information may involve, for example, discharging a capacitor, which dissipates energy. At first glance this appears to be an implementation-dependent fact, but Landauer proved that it is in fact fundamental. Bennett initially proposed reversible Turing machines, and discussed reversibility in the context of the contents of several tapes. We shall discuss reversibility in the form of circuits and gates, rather than Turing machines, in this thesis. In order to be computationally complete, single-bit and even two-bit gates are not enough; at least one three-bit operation is necessary. Fredkin and Toffoli invented the two most commonly used three-bit reversible gates, discussed below [123].

Studying reversible computation is interesting in its own right [112]: Kerntopf has identified more than sixty research papers on the topic, including a variety of basic logic gates that we will not detail here [168]. Perhaps the most famous classical example of reversible computing is the billiard ball computer developed by Fredkin, Feynman, and others, in which colliding billiard balls compute functions ¹. Such a system is easier to design when conserving billiard balls, making reversible logic the obvious choice. For more practical circuits, Bruce et al. recently designed reversible carry-ripple and

¹Ross Berteig, Takako Matoba and I implemented a small-scale circuit based on these principles in 1985, when taking Feynman's class on "Potentialities and Limitations of Computing Machines".

carry-skip adders using Fredkin gates, intended to be implemented in silicon [60]. Hall designed a reversible instruction set equivalent to a PDP-10 [38] more than a decade ago, before quantum computation became a hot research topic [142]. More recently, Vieri, Frank and others, working in the Tom Knight group at MIT, designed and fabricated a reversible microprocessor known as Pendulum [344, 343]. They developed not only the microprocessor, but also a small compiler. Frank's thesis discusses in detail topics such as options for subroutine call and branch structure, and operating systems for reversible computers; as reversible and quantum computer architectures advance, this thesis will be a valuable resource [122].

Reversible computation benefits the thermodynamics of a system. The minimum amount of energy that a circuit must dissipate is proportional to the number of bits of information that are *erased*. Although the minimum amount of energy to erase a bit is very small, this factor eventually must be addressed in classical systems. Athas, Koller and their collaborators have investigated its importance for lowering power consumption in adiabatic CMOS and found that power distribution and clocking issues are manageable, but that the increase in chip area required is significant [25, 188]. They suggest occasionally relaxing the constraints on reversibility, discarding a few intermediate results to reduce the area consumed. Their chips operate far above the theoretical minimum for irreversible logic, but take advantage of adiabatic charging and discharging of capacitors to reduce power consumption. DeBenedictis has argued that building a high-performance computer system capable of exceeding $\sim 10^{26}$ logic gates per second or 10 zettaFLOPS (10^{22} floating point operations per second), roughly 6-7 decimal orders of magnitude more than the current most powerful systems, within a realistic power budget (750 kilowatts to the active logic components) will require the use of reversible logic [91].

2.1.2 Two-Bit Gates

Classically, the only important one-bit gate is the NOT gate, and, as noted, it is reversible. For two-bit gates, we have the CNOT and SWAP, and construct FANOUT.

First, let us look at the controlled-NOT gate, or CNOT. One variable (or input) is designated as the control line, and the other as the target. If the control bit is one, a NOT gate is performed on the target bit; if the control bit is zero, the target bit is left unchanged. The output is the exclusive OR (XOR) of the two bits, and one of the input bits: $(a, b) \rightarrow (a, a \oplus b)$. Table 2.1 shows the truth table for a CNOT with A as the

input		output	
A	B	A	B
0	0	0	0
0	1	0	1
1	0	1	1
1	1	1	0

Table 2.1: CNOT truth table.

control bit and B as the target bit. Applying a CNOT gate twice to the same bits returns to the system to its original state, $(a, b) \rightarrow (a, a \oplus b) \rightarrow (a, a \oplus b \oplus b) = (a, b)$.

Swapping two bits is an important capability. Physically, if data signals are propagating through a circuit, routing of wires may accomplish the swap. However, if two register bits are to be swapped, and no temporary storage location is available, we need a different approach. In standard logic, three consecutive XORs will swap two bits or two entire registers without the use of intermediate, temporary variables [37]. A similar trick, using three CNOTs, can be done in reversible computation, as shown in Figure 2.1 on page 23.

In reversible notation, we must explicitly specify the fanout of a signal, an operation generally done implicitly with a wire in irreversible logic. A CNOT performed with the variable to be copied as the control and a zero in the target bit accomplishes this task for us.

2.1.3 Three-Bit Gates: Toffoli and Fredkin

The two seminal reversible three-bit gates are the Toffoli and Fredkin gates. Table 2.2 shows the truth table for the control-control-NOT (CCNOT), or Toffoli gate. If both control lines, A and B, are one, then a NOT gate is performed on the target bit, C, otherwise, no action is performed. Table 2.3 shows the control-SWAP, or Fredkin, gate. This gate has one control line (A) and two target lines (B and C). If the control is one, the two targets have their values swapped; if the control is zero, the targets are unaffected. Either of these gates is adequate to perform universal computation; any computable circuit or equation can be reduced to a set of Toffoli gates or a set of Fredkin gates. Smaller gates, such as the CNOT and NOT, can of course be simulated by setting one or two of the inputs to the gate to zero or one, as appropriate.

Graphic symbols for these gates are shown in Figure 2.1. In all circuit diagrams in this thesis, time flows left to right, a horizontal line represents a single bit through time,

input			output		
A	B	C	A	B	C
0	0	0	0	0	0
0	0	1	0	0	1
0	1	0	0	1	0
0	1	1	0	1	1
1	0	0	1	0	0
1	0	1	1	0	1
1	1	0	1	1	1
1	1	1	1	1	0

Table 2.2: CCNOT (Toffoli gate) truth table.

input			output		
A	B	C	A	B	C
0	0	0	0	0	0
0	0	1	0	0	1
0	1	0	0	1	0
0	1	1	0	1	1
1	0	0	1	0	0
1	0	1	1	1	0
1	1	0	1	0	1
1	1	1	1	1	1

Table 2.3: Control-SWAP (Fredkin gate) truth table.

and vertical line segments represent gates. A filled dot indicates a control variable, while an open circle represent a NOT gate on that variable – the target of the gate, for a CNOT or CCNOT.

2.1.4 Ancilla Management

Every temporary variable created — every term in a logical expression — consumes a bit. For example, in the simple expression $(A \wedge B) \vee (C \wedge D)$, the terms $(A \wedge B)$ and $(C \wedge D)$ each require a temporary bit during the calculation of the final result. These temporary variables, in reversible logic terminology, are *ancillae*. Without a method for recovering these ancillae, the space required for a computation would grow in direct proportion to the length of the computation. Of course, since we are using only reversible gates in this computation, we could clean our ancillae (collect our garbage) by applying the exact same set of gates in the reverse order. Unfortunately, that would return the state of the entire system to the initial state, including resetting our desired output to zero. We need a way to keep the output but clean up the garbage, and maybe

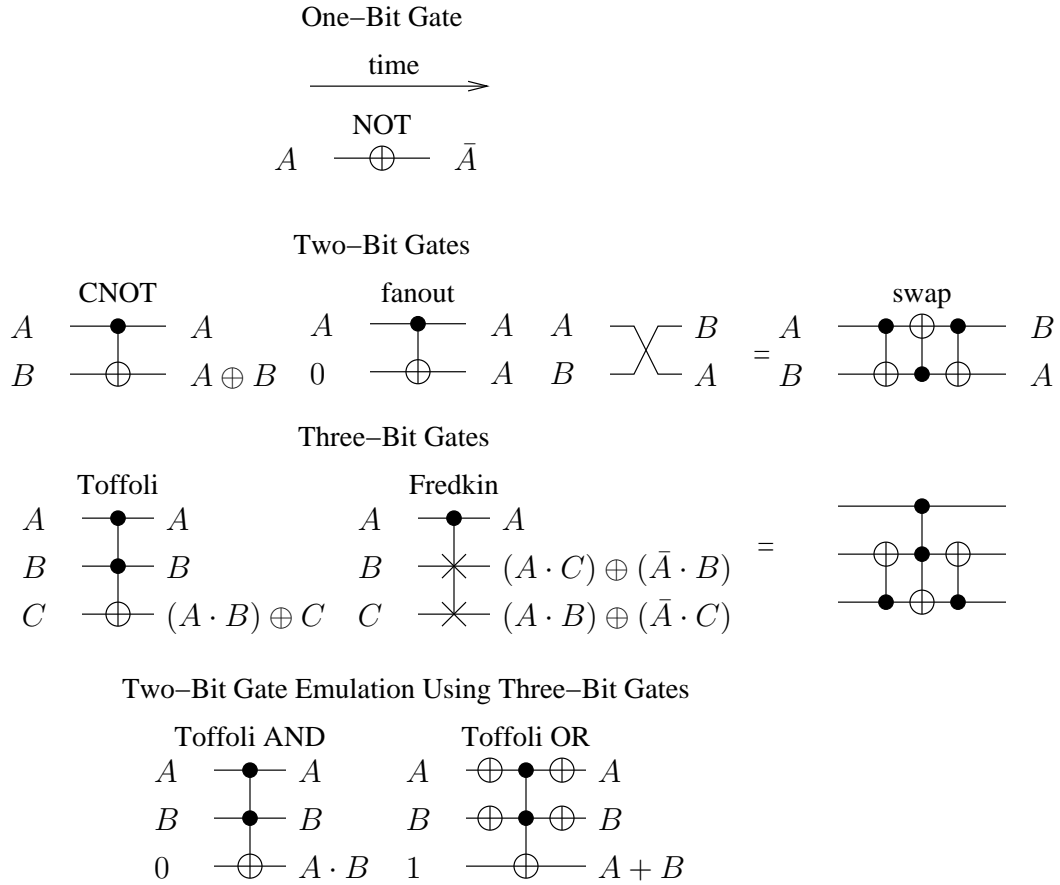


Figure 2.1: Reversible gates: CNOT, CCNOT (Toffoli), control-SWAP (Fredkin), NOT, fanout and swap, and emulation of Boolean AND and OR using the Toffoli gate.

Step	action	INPUT	TEMPVARS	TEMPOUT	OUTPUT
0.	initial state	input	0	0	0
1.	forward computation	input	garbage	result	0
2.	“copy” using CNOT fanout	input	garbage	result	result
3.	reverse computation	input	0	0	result

Table 2.4: Erasing ancillae.

even “delete” the input if what we really want to keep is just the output.

Bennett discovered a method for cleaning ancillae while retaining the important results bits. He originally constructed this method for Turing machines; we will describe it in terms of circuits and registers. We will illustrate the computation in terms of three registers used in the computation itself (the INPUT, TEMPVARS for intermediate variables, and TEMPOUT, which holds the result immediately after completing the computation), though in practice the roles assigned to bits may not be that clearly delineated. A fourth register, OUTPUT, gets the final result. The computation is run forward (step 1), then the results are “copied” out to the OUTPUT register (step 2)², then the ancillae are returned to their initial (generally, zero) state by reversing the computation (step 3). This is illustrated in Table 2.4. Bennett also defined a seven-step method for doing in-place computation (erasing the input state, leaving only the output), and Feynman stated that he had a method for doing a $2n$ -step irreversible computation reversibly in only $3n$ steps, though as far as I can tell he did not publish this result and it has never been replicated [113].

2.2 Introduction to Quantum Computing

Alice laughed. “There’s no use trying,” she said: “one can’t believe impossible things.”

“I daresay you haven’t had much practice,” said the Queen. “When I was your age, I always did it for half-an-hour a day. Why, sometimes I’ve believed as many as six impossible things before breakfast.”

Lewis Carroll, *Through the Looking Glass*, 1871

²In this thesis, we use the term “copy” to mean the fanout operation described above.

A *quantum computer* is a device that takes advantage of quantum mechanical effects to perform certain computations faster than a purely classical machine can. It relies on *quantum parallelism*, using physical phenomena that can be held, like Schrödinger's cat, in more than one state at once, allowing us to compute on all of those states at the same time, using a single operation. Quantum parallelism is best understood in the context of the concepts of *superposition*, *entanglement* and *measurement*; of course, we must also learn how quantum data is represented and manipulated. A quantum computer performs, in principle, exponentially many computations simultaneously; however, exponentially many *results* of those computations cannot be read out, leaving us with the fascinating problem of how to use such a machine to accelerate computations that interest us. The most famous result in quantum computing to date, Shor's algorithm for factoring large numbers (which we will discuss in more detail in the next chapter), appears to offer superpolynomial speedup, but no general method for finding quantum analogs to classical algorithms is known.

This section reviews the basics of quantum computing. We begin with quantum mechanics, presenting Dirac's *ket* notation, with a few notes on linear algebra, then Schrödinger's equation and Hamiltonian dynamics. We then informally define a qubit, discuss its state-vector and Bloch sphere representations and corresponding manipulations. Two-qubit gates and their relationship to the reversible gates presented above are explained, along with constructions for the Toffoli gate. Once we have begun to understand these fundamentals, we can discuss DiVincenzo's criteria for physical realization of quantum computation. We end the chapter with a discussion of distributed quantum computation, which is the purpose of our proposed quantum multicomputer. Readers are also referred to both popular [245, 349] and technical [177, 248] texts on the topic for more breadth and depth.

2.2.1 Notation and a Few Linear Algebra Notes

First, let us introduce the notation commonly used in quantum computing. We will not give rigorous definitions, instead limiting ourselves to a few of the practical matters that a working engineer needs to understand.

$|\psi\rangle$ is Dirac's *ket* notation for vectors, and this can be referred to as the state-vector representation of a qubit. $\langle\psi|$ is the *bra* corresponding to the ket. The bra is a complex-conjugate row vector and the ket is a column vector. $\langle\psi_1|\psi_2\rangle$ is the dot product of the two vectors ψ_1 and ψ_2 , and $|\psi_1\rangle\langle\psi_2|$ is their outer product.

For a single qubit, $|0\rangle$ is the zero state, and $|1\rangle$ is the one state. For a multiple-qubit register, we will often write the binary expansion of the state as e.g. $|0111\rangle$ (a four-qubit state with the value seven). This state can also be written $|0\rangle|1\rangle|1\rangle|1\rangle$ or $|0\rangle \otimes |1\rangle \otimes |1\rangle \otimes |1\rangle$, emphasizing that it is the tensor product of four separate two-level systems. Sometimes, we will write $|7\rangle$ as the state of the set of qubits. Although the number may be written base ten for convenience, it is represented in binary in the quantum register (many physical phenomena, such as the energy levels of an atom, may have more than two levels and therefore may use e.g. $|2\rangle$ to represent the third level, but we will confine ourselves to two-level qubits in this thesis). The size of the register will usually be understood from context, and if the integer is small the high-order bits are of course understood to be zero. Occasionally, it may be necessary to write $|0\rangle^{\otimes k}$ to indicate a set of k qubits all in the zero state.

We describe an arbitrary n -qubit quantum gate via the $2^n \times 2^n$ matrix U , which must be a *unitary* transform. A unitary matrix obeys the equation $U^\dagger U = U U^\dagger = I$, where U^\dagger is the adjoint of U . In keeping with normal matrix multiplication rules, a series of gates or transforms applied to a register can be written

$$U_k \cdots U_3 U_2 U_1 |\psi\rangle \quad (2.1)$$

where U_1 is the first gate applied, U_2 is the second, etc. This can be confusing, as we draw circuit diagrams with time flowing left to right. We introduced the graphical notation for reversible gates in Chapter 2; we extend that to quantum gates in Section 2.2.4, and larger circuits will appear in later chapters.

2.2.2 Schrödinger's Equation

Schrödinger's equation

$$i\hbar \frac{\partial |\psi\rangle}{\partial t} = H |\psi\rangle \quad (2.2)$$

describes the dynamics of a quantum system. Solutions describing the time evolution of the system are of the form

$$|\psi\rangle \rightarrow e^{-iHt/\hbar} |\psi\rangle = U |\psi\rangle. \quad (2.3)$$

H , in this equation, is an operator (represented as a matrix) known as the *Hamiltonian* of the system, and U is the corresponding unitary transform. Solutions to the

Schrödinger equation can be weighted, linear combinations of any of the possible solutions, such that the weights all add up to 1. Experimentalists usually describe the behavior of the system in terms of its Hamiltonian to emphasize the temporal nature of the evolution, but we are interested in specific types of behavior achieved by using fixed time intervals, so it will be easiest for us to use the unitary operators. Unitary operators can, in turn, be expressed as gates, which we will use throughout this thesis.

2.2.3 Qubits

What's a Qubit?

A *qubit* is either a true two-level system, such as the direction of polarization of a photon or the direction of spin of an electron, or a pseudo-two-level system, such as two energy levels of an atom that can be treated as a two-level system. We will see more examples in Chapter 4. Of course, an electron spins in either the “up” or “down” direction, not zero and one, so we chose to label the two states as our zero and one states, much as we choose e.g. +5 volts to be a logical one and ground to be a logical zero in classical circuits. The difference between a classical bit and a qubit is that a qubit can be in a *superposition* of the two states; it can be partially zero and partially one. The state of a qubit can be written as

$$|\psi\rangle = \alpha|0\rangle + \beta|1\rangle \quad (2.4)$$

where α and β are complex numbers, $|\alpha|^2$ is the probability of finding the qubit in the state 0, and $|\alpha|^2 + |\beta|^2 = 1$: the qubit must be found to be in one state or the other.

The above expression can also be written

$$|\psi\rangle = \begin{bmatrix} \alpha \\ \beta \end{bmatrix} \quad (2.5)$$

showing the same probabilities for finding the states 0 and 1, implicit in the position within the vector. The top element of the vector corresponds to the zero state, and the bottom element to the one state. Technically, the 0 and 1 inside the ket are labels for the states; we could choose to represent any two basis vectors by $|0\rangle$ and $|1\rangle$, but in this

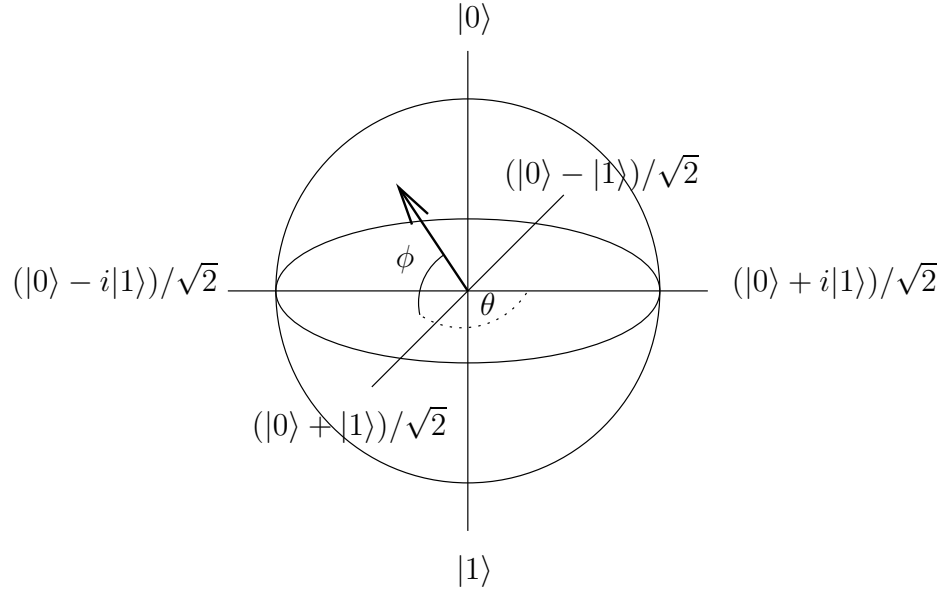


Figure 2.2: The Bloch sphere.

dissertation we will always use the convention that

$$|0\rangle \equiv \begin{bmatrix} 1 \\ 0 \end{bmatrix}, |1\rangle \equiv \begin{bmatrix} 0 \\ 1 \end{bmatrix}. \quad (2.6)$$

The state of a single qubit is often thought of in terms of the *Bloch sphere* representation, in which the state of a qubit is a unit vector, as shown in Figure 2.2 (this sphere is often called the Poincaré sphere by researchers working in optics). If the vector points at the north pole, our qubit is in the $|0\rangle$ state, and if it points at the south pole, the qubit is in the $|1\rangle$ state. The north-south axis is the Z axis, the positive X axis is toward the reader (out of the page or screen, for a 2-D representation), and the Y axis is right-left. When the unit vector points toward you, that is the $(|0\rangle + |1\rangle)/\sqrt{2}$ state, when it points away from you that is the $(|0\rangle - |1\rangle)/\sqrt{2}$ state. The positive Y axis is $(|0\rangle + i|1\rangle)/\sqrt{2}$, and the negative Y axis is $(|0\rangle - i|1\rangle)/\sqrt{2}$. The *phase* is the position of our vector about the Z axis (the angle θ in the figure).

Physicists, especially theorists, occasionally refer to a large unitary transform as a *quantum gate*, but in this dissertation we will restrict the use of the term to smaller units, which for most proposed implementations will be more physically realistic. Our gates will be one-, two-, and three-qubit transforms only.

Quantum Registers and Weighted Probabilities

We will refer to a related set of two or more qubits as a *quantum register*. Two classical bits can be in any of the four states 00, 01, 10, and 11. Two qubits can be in a weighted combination of all four states at the same time. For two qubits, we can write

$$|\psi\rangle = \alpha|00\rangle + \beta|01\rangle + \gamma|10\rangle + \delta|11\rangle \quad (2.7)$$

where $|\alpha|^2 + |\beta|^2 + |\gamma|^2 + |\delta|^2 = 1$. For example, if $\alpha = \delta = 1/\sqrt{2}$ and $\beta = \gamma = 0$, we have a fifty percent probability of finding $|00\rangle$ and a fifty percent probability of finding $|11\rangle$, but no chance of finding the other states.

Similarly, three qubits can be in eight states, and n qubits can be in all 2^n possible states at once,

$$|\psi\rangle = \sum_{i=0}^{2^n-1} \alpha_i |i\rangle, \quad (2.8)$$

subject to the constraint that their total weights α_i must sum to 1,

$$\sum |\alpha_i|^2 = 1. \quad (2.9)$$

Of course, some of the α_i may be zero.

Entanglement

Two quanta can be in a shared state in which operations on one affect the other. The quanta are said to be *entangled*. One consequence is that the probabilities of two entangled qubits are not independent (but see Section 2.2.3 below for an important caveat). If the state of the system is e.g. $(|00\rangle + |11\rangle)/\sqrt{2}$ ($\alpha = \delta = 1/\sqrt{2}$, in the above notation), when we measure the system, we will find either that both qubits are zero, or that both qubits are one. Although each qubit has a 50% probability of being zero and a 50% probability of being one, their state is not independent. Starting from this state, we will never find one qubit to be zero and the other qubit to be one.

Entanglement is a continuous phenomenon, not discrete. There are numerous measures of the amount of entanglement present in a system, but they all use a scale running from zero to one, where zero is completely unentangled and one is fully entangled (see Munro et al. and references therein [238].) For the purposes of this thesis, our primary interest will be in fully-entangled and fully-unentangled pairs of qubits, though the process of purifying a set of partially entangled pairs of qubits into fully-entangled pairs

will figure into the qubus network protocol (Chapter 5 and Section 7.4) [77, 43, 303].

Decoherence

Quantum states are very fragile: excited atoms decay and spins of electrons and atomic nuclei spontaneously flip. Any quantum system can be affected by interacting with its environment, leaking information about its state out into the environment where we cannot recover or use the information. We call this gradual decay of the state of a system *decoherence*. When decoherence sets in, measurement of the system probably will not produce the desired results, causing the failure of our quantum algorithm. The two key measures of decoherence are the T_1 and T_2 times. T_1 is the energy relaxation time, and T_2 is the phase relaxation time. Both processes are memoryless, with probabilistic behavior. The amount of time we can count on the state of a qubit remaining in a usable state is the minimum of T_1 and T_2 . Researchers determine these values experimentally, and an important area of device research is extending these times by careful engineering of the environment and control system.

Pure and Mixed States and the Density Matrix

Quantum states can be either *pure* or *mixed*. So far, we have discussed only pure states. “Pure” does not mean that the superposition, when written out in state-vector form, contains only one term; pure means that it is *possible* to write the state in state-vector form. For example, $|\psi\rangle = |0\rangle$ and $|\psi\rangle = (|0\rangle + |1\rangle)/\sqrt{2}$ are both pure states. However, not all quantum states can be written out completely in the state-vector form. Experimentalists often prefer to write the state using the $2^n \times 2^n$ *density matrix* form, which can represent a more complex state of the system. In particular, the density matrix representation allows us to write down a representation of the state of the system when the complete state cannot be known, such as when part of the information in the quantum state has leaked out into the environment. Using the example of our basic entangled state, $|\psi\rangle = (|00\rangle + |11\rangle)/\sqrt{2}$, our density matrix is

$$\rho = |\psi\rangle\langle\psi| = \frac{1}{2}|00\rangle\langle 00| + \frac{1}{2}|00\rangle\langle 11| + \frac{1}{2}|11\rangle\langle 00| + \frac{1}{2}|11\rangle\langle 11| = \begin{bmatrix} \frac{1}{2} & 0 & 0 & \frac{1}{2} \\ 0 & 0 & 0 & 0 \\ 0 & 0 & 0 & 0 \\ \frac{1}{2} & 0 & 0 & \frac{1}{2} \end{bmatrix}. \quad (2.10)$$

The entries along the diagonal of the density matrix correspond to the probability of finding the system in a particular state. To be a valid density matrix, the trace (the sum of the diagonal) must be one, written $\text{Tr}(\rho) = 1$. The trace must be one because, when measured, the system will be found to be in *some* state. For pure states, the square of the density matrix also has trace one, $\text{Tr}(\rho^2) = 1$. If the density matrix is diagonalized (achieved via an appropriate change of basis), a pure state will have only a single non-zero element. The eigenvector corresponding to this eigenstate is the state of the system. The Bloch sphere can be used to visualize mixed states of a single qubit as points inside the sphere; the closer the state is to pure, the closer the length of the vector is to unity.

In Section 2.2.3 above, we referred to a caveat on our definition of entanglement; with this understanding of the difference between pure and mixed states we are now ready to discuss it. The state of two qubits can, in fact, be dependent, without being entangled, if the state is mixed. In contrast to the state in Equation 2.10, we can also have the state

$$\frac{1}{2}(|00\rangle\langle 00| + |11\rangle\langle 11|) = \frac{1}{2} \begin{bmatrix} 1 & 0 & 0 & 0 \\ 0 & 0 & 0 & 0 \\ 0 & 0 & 0 & 0 \\ 0 & 0 & 0 & 1 \end{bmatrix}. \quad (2.11)$$

In this mixed state, the state of the two qubits is not independent, but they are not entangled; actions on one qubit cannot affect the state of the other. In this particular case, the density matrix now represents classical dependent probabilities.

Measurement

Measurement of a qubit causes the collapse of the wave function, forcing the state of the system into just one term of the superposition. In the famous thought experiment of Schrödinger, measurement is opening the box containing his cat and finding out if the cat is dead or alive. Until measurement takes place, the state of the system can be in the superposition state, with various histories and outcomes only determined probabilistically. When we measure the system, the state and history pick one consistent “storyline” that the system must have followed, in effect choosing among possible pasts based on their relative probabilities. If we measure such that more than one history is possible, the system remains in a state that is consistent with all of them, as in the double-slit quantum interference experiment (see, for example, V. I Ch. 37 of the

Feynman Lectures [115]).

In our basic example of $|\psi\rangle = |0\rangle$, we know the system is 100% in the zero state. Measurement of the qubit's state will definitely produce a zero³. For $|\psi\rangle = (|0\rangle + |1\rangle)/\sqrt{2}$, zero and one each have a fifty percent probability of being found. Once our measurement determines the state (e.g., 0), the entire system will be forced to a state consistent with the idea that our qubit has been zero all along.

For two or more qubits, we can measure either the entire system, or only part. Measuring a single qubit can alter the state of the system. For example, consider our two-qubit state $|\psi\rangle = (|00\rangle + |11\rangle)/\sqrt{2}$. If we measure the low-order bit (the right-hand one of our pair), we have a fifty percent probability of each outcome, and our result will force the system to a matching state. We can write the measurement outcome and the resulting state as

$$0 : |\psi\rangle \rightarrow |0\rangle \quad (2.12)$$

$$1 : |\psi\rangle \rightarrow |1\rangle. \quad (2.13)$$

In this case, measuring one qubit has determined the state of the other. For the state $|\psi\rangle = (|00\rangle + |10\rangle)/\sqrt{2}$, we can factor the state as $|\psi\rangle = (|0\rangle + |1\rangle)|0\rangle/\sqrt{2}$. Measuring the low-order qubit will clearly always yield the result 0. The state of the system then moves to $(|0\rangle + |1\rangle)/\sqrt{2}$; the high-order qubit (now our only qubit) has not changed. We can say that two qubits were *separable*; there was no entanglement between them.

Measurement is a complex and sometimes counter-intuitive topic. It is important and deep enough that books and conferences are devoted to it [17]. One good place to start studying this topic is Preskill's lecture notes [273]. We will see an example of how to use measurement in the discussion of quantum error correction in Section 2.3.

The Partial Trace

We are now ready to discuss the *partial trace* of a system. We use the partial trace for various purposes, including expressing the loss of a photon in optical quantum computing or the “leaking” of information about the state out into the environment.

We can discuss the state of a system in terms of the *system* and the *reservoir*, where system in this case refers to the qubits we are interested in and have control over, and reservoir refers to the rest of the world. Initially, the system and the reservoir are not

³Assuming the measurement is performed along the Z (0/1) axis; we will not deal with measurements in other bases in this dissertation.

entangled; that is, they are separable, and the state can be written

$$\rho = \rho_S \otimes \rho_R \quad (2.14)$$

where ρ is our overall state, ρ_S is the state of the quantum system, and ρ_R is the state of the reservoir (which we can never know fully). Over time, information leaks out of the quantum system into the larger world, or the reservoir. If $\rho(t)$ is the state at time t ,

$$\rho = \rho_S \otimes \rho_R, \rho_S(t) = \text{Tr}_R(\rho(t)) \quad (2.15)$$

where Tr_R is the partial trace with respect to the reservoir.

For a two-qubit system, numbering our qubits 0 and 1, in keeping with normal computer architecture convention, we will let ρ^0 be the density matrix for the system traced out over qubit 1, and ρ^1 be traced out over qubit 0. Defining the partial trace as

$$\rho^0 = \text{Tr}_1(\rho) = \langle 10|\rho|01\rangle + \langle 11|\rho|11\rangle, \quad (2.16)$$

where $|0_1\rangle$ is the basis vector for the zero state for qubit one. Noting that $\langle 0|0\rangle = \langle 1|1\rangle = 1$ and $\langle 0|1\rangle = \langle 1|0\rangle = 0$, and that the trace is linear, the partial trace for the example in equation 2.10 is

$$\begin{aligned} \rho^0 &= \text{Tr}_1(\rho) = \frac{1}{2} \text{Tr}_1(|00\rangle\langle 00|) + \frac{1}{2} \text{Tr}_1(|11\rangle\langle 00|) + \frac{1}{2} \text{Tr}_1(|00\rangle\langle 11|) + \frac{1}{2} \text{Tr}_1(|11\rangle\langle 11|) \\ &= \frac{1}{2} \langle 10|00\rangle\langle 00|0_1\rangle + \frac{1}{2} \langle 10|11\rangle\langle 00|0_1\rangle + \frac{1}{2} \langle 10|00\rangle\langle 11|0_1\rangle + \frac{1}{2} \langle 10|11\rangle\langle 11|0_1\rangle \\ &\quad + \frac{1}{2} \langle 11|00\rangle\langle 00|1_1\rangle + \frac{1}{2} \langle 11|11\rangle\langle 00|1_1\rangle + \frac{1}{2} \langle 11|00\rangle\langle 11|1_1\rangle + \frac{1}{2} \langle 11|11\rangle\langle 11|1_1\rangle \\ &= \frac{1}{2} |0\rangle\langle 0| + \frac{1}{2} |1\rangle\langle 1| \\ &= \begin{bmatrix} \frac{1}{2} & 0 \\ 0 & \frac{1}{2} \end{bmatrix}. \end{aligned} \quad (2.17)$$

$\text{Tr}((\rho^0)^2) = 1/2$, indicating that our state is now a mixed state. Our pure state has become mixed with the environment, and we can no longer write down a definitive description of the quantum register alone.

Interference

The state of a quantum system is a wave function that matches Schrödinger's equation. As with classical wave mechanics, two waves can *interfere*, depending on the relative phases of the waves. That interference can be positive, enhancing the amplitude (hence, probability) of a particular state, or negative, decreasing the probability. Since the phase of a state is actually complex, the addition of phases is also complex.

As a simple example, consider the state created by application of a Hadamard gate (which we will define below) to the $|0\rangle$ state,

$$|\psi\rangle = \frac{|0\rangle + |1\rangle}{\sqrt{2}} = \frac{1}{\sqrt{2}} \begin{bmatrix} 1 \\ 1 \end{bmatrix}. \quad (2.18)$$

The state now consists of two terms, a superposition of two states. Applying a second Hadamard gate will return the system to its original state by interfering the two terms,

$$H|\psi\rangle = \frac{1}{2} \begin{bmatrix} 1 & 1 \\ 1 & -1 \end{bmatrix} \begin{bmatrix} 1 \\ 1 \end{bmatrix} = \frac{1}{2} \begin{bmatrix} 1+1 \\ 1-1 \end{bmatrix} = \begin{bmatrix} 1 \\ 0 \end{bmatrix} = |0\rangle. \quad (2.19)$$

The top element in the array exhibits positive interference ($1 + 1$), and the bottom element shows negative interference ($1 - 1$).

2.2.4 Manipulating Qubits

Quantum computation proceeds by taking a set of qubits, modifying their state such that a “computation” of some interest is performed, and reading out the result so that we learn what happened. Feynman originally conceived of quantum computers as systems designed to simulate the physical behavior of many-body systems, which are hard to examine experimentally or in classical simulation, solving quantum mechanical problems directly in an analog fashion rather than via numerical calculation of properties of the wave function [114, 211, 7, 63]. This approach is similar to e.g. simulating a set of mechanical resonators using a set of electrical resonators, as is done in analog computing [189, 129, 224]. However, this is not the only way to use quantum phenomena to solve problems. A quantum computation can be defined as a circuit, in which the system is built and programmed and behaves roughly analogously to a classical digital computer. Recent advances include adiabatic quantum computing [111, 313, 12] and cluster-state computing [277, 246, 347]. All of these are equivalent in computational

power, but are believed to be very different in how useful algorithms are found. In this dissertation, we will deal almost exclusively in terms of the circuit model, which is the basis for Shor's factoring algorithm and most of the other important quantum algorithms discovered to date.

What's a Quantum Gate?

In the circuit model, quantum computations are decomposed into separate gates, and can be organized more or less along the lines of classical circuits. These gates are based on the concepts of reversible computing discussed in the last section, extended to accommodate the Bloch sphere. In order for our computational capabilities to be “universal”, we must be able to reach any point on the Bloch sphere for a single qubit, and we must be able to entangle two qubits. First we discuss the individual gates that compose a quantum computation, and in the next subsection we discuss larger circuits in more detail.

Single-Qubit Gates and the Bloch Sphere

Only one interesting single-bit operation, the NOT gate, exists in the classical world (ignoring setting and resetting the bit). In the quantum world, a single-qubit operation can be any rotation on the Bloch sphere. Rotations about the axes of the Bloch sphere can be described in terms of the *Pauli matrices*. The transforms for 180° rotations are

$$X = \sigma_x = \begin{bmatrix} 0 & 1 \\ 1 & 0 \end{bmatrix} \quad (2.20)$$

$$Y = \sigma_y = \begin{bmatrix} 0 & -i \\ i & 0 \end{bmatrix} \quad (2.21)$$

$$Z = \sigma_z = \begin{bmatrix} 1 & 0 \\ 0 & -1 \end{bmatrix}. \quad (2.22)$$

For rotation of an angle θ about each axis, the transforms (modulo a global phase factor we will ignore) are (from Nielsen & Chuang [248]):

$$R_x(\theta) = e^{-i\theta X/2} = \begin{bmatrix} \cos \frac{\theta}{2} & -i \sin \frac{\theta}{2} \\ -i \sin \frac{\theta}{2} & \cos \frac{\theta}{2} \end{bmatrix} \quad (2.23)$$

$$\begin{array}{lcl}
\text{---} \oplus \text{---} = \text{---} \boxed{\text{X}} \text{---} & \begin{bmatrix} 0 & 1 \\ 1 & 0 \end{bmatrix} & \text{---} \boxed{\text{H}} \text{---} \frac{1}{\sqrt{2}} \begin{bmatrix} 1 & 1 \\ 1 & -1 \end{bmatrix} \\
\text{---} \boxed{\text{T}} \text{---} & \begin{bmatrix} 1 & 0 \\ 0 & e^{i\pi/4} \end{bmatrix} & \text{---} \boxed{\text{S}} \text{---} \begin{bmatrix} 1 & 0 \\ 0 & i \end{bmatrix} \\
\begin{array}{c} \text{---} \bullet \text{---} \\ | \\ \text{---} \oplus \text{---} \end{array} & \begin{bmatrix} 1 & 0 & 0 & 0 \\ 0 & 1 & 0 & 0 \\ 0 & 0 & 0 & 1 \\ 0 & 0 & 1 & 0 \end{bmatrix} & \begin{array}{c} \text{---} \oplus \text{---} \\ | \\ \text{---} \bullet \text{---} \end{array} \begin{bmatrix} 1 & 0 & 0 & 0 \\ 0 & 0 & 0 & 1 \\ 0 & 0 & 1 & 0 \\ 0 & 1 & 0 & 0 \end{bmatrix} \\
\begin{array}{c} \text{---} \bullet \text{---} \\ | \\ \text{---} \boxed{\text{Z}} \text{---} \end{array} = \begin{array}{c} \text{---} \boxed{\text{Z}} \text{---} \\ | \\ \text{---} \bullet \text{---} \end{array} & \begin{bmatrix} 1 & 0 & 0 & 0 \\ 0 & 1 & 0 & 0 \\ 0 & 0 & 1 & 0 \\ 0 & 0 & 0 & -1 \end{bmatrix} & \begin{array}{c} \text{---} \text{X} \text{---} \\ \text{---} \text{X} \text{---} \end{array} \begin{bmatrix} 1 & 0 & 0 & 0 \\ 0 & 0 & 1 & 0 \\ 0 & 1 & 0 & 0 \\ 0 & 0 & 0 & 1 \end{bmatrix}
\end{array}$$

Figure 2.3: Basic one-qubit NOT (X), Hadamard (H), $\pi/8$ (T), and phase (S) gates (top two rows), and two-qubit CNOTs, control-phase, and swap gates (bottom two rows).

$$R_y(\theta) = e^{-i\theta Y/2} = \begin{bmatrix} \cos \frac{\theta}{2} & -\sin \frac{\theta}{2} \\ \sin \frac{\theta}{2} & \cos \frac{\theta}{2} \end{bmatrix} \quad (2.24)$$

$$R_z(\theta) = e^{-i\theta Z/2} = \begin{bmatrix} e^{-i\theta/2} & 0 \\ 0 & e^{i\theta/2} \end{bmatrix} \quad (2.25)$$

which we will need only for the quantum Fourier transform and for our decomposition of the Toffoli gate.

Universal quantum computation requires that we be able to reach any location on the Bloch sphere starting from any other. Naturally, we do not need arbitrary rotations about all three axes in order to achieve this; two will do. Moreover, arbitrary rotations can be approximated using a small set of fixed rotations. Figure 2.3 shows one such set of gates, with their graphic representations and unitary transform matrices. The particular set shown is technically redundant; the control-Z and swap gates can be constructed from the others.

As a simple example, consider the state created by application of a Hadamard gate to the $|0\rangle$ state,

$$|\psi\rangle = H|0\rangle \rightarrow \frac{1}{\sqrt{2}} \begin{bmatrix} 1 & 1 \\ 1 & -1 \end{bmatrix} \begin{bmatrix} 1 \\ 0 \end{bmatrix} = \frac{1}{\sqrt{2}} \begin{bmatrix} 1 \\ 1 \end{bmatrix} \rightarrow \frac{|0\rangle + |1\rangle}{\sqrt{2}}. \quad (2.26)$$

The state now consists of two terms, a superposition of two states. Likewise, applying the Hadamard to the $|1\rangle$ state, we have

$$|\psi\rangle = H|1\rangle \rightarrow \frac{1}{\sqrt{2}} \begin{bmatrix} 1 & 1 \\ 1 & -1 \end{bmatrix} \begin{bmatrix} 0 \\ 1 \end{bmatrix} = \frac{1}{\sqrt{2}} \begin{bmatrix} 1 \\ -1 \end{bmatrix} \rightarrow \frac{|0\rangle - |1\rangle}{\sqrt{2}}. \quad (2.27)$$

Geometrically, we visualize the Hadamard gate as a 180° (π) rotation about the Z axis, followed by a 90° ($\pi/2$) rotation about the Y axis. The rotation about the Z axis does not directly affect the probability of finding either a 0 or a 1 if the state is measured right away, but this two-step manipulation shows clearly the importance of the phase (angle about the Z axis).

Unfortunately, visualizing the state of more than one qubit is more complicated than a set of spheres, one per qubit. If it were that easy, there would be no exponential growth in the complexity of our states, and quantum computation would be uninteresting. It is possible to visualize the state of more than one qubit as a *set* of points on the Bloch sphere, in what is called the *Majorana representation*. Its utility is limited to pure states; there are not enough degrees of freedom to represent mixed states [219].

Two-Qubit Gates

In Chapter 2, we discussed classical reversible computation using control-NOT (CNOT) gates as our primary two-qubit gate. The CNOT is an extremely useful gate in quantum computation, as well, and will figure prominently in our quantum arithmetic. However, the CNOT is not the only type of two-qubit quantum gate. As with the one-qubit gates, we must consider the phase of the system, resulting in analog gates equivalent to the rotations about the axes we saw for single-qubit gates. We can create a “control- U ” two-qubit gate, where U is any single-qubit unitary gate.

First, let us look at the unitary transforms for single-qubit gates applied to two-qubit systems, so we can see the form the matrices take. For operations on multi-qubit registers, we will let U_i be the single-qubit unitary operation U on the i th qubit in the register. We will number qubits from zero, with qubit zero being the “low order” qubit in the system. Qubit i then corresponds to the value 2^i in the binary expansion (note that this is in keeping with common computer architecture practice, but physicists usual number from qubit 1, starting at the left, or high-order, bit). In circuit diagrams, the low-order qubit will be the bottom qubit. The transform for a Hadamard gate on the

low-order qubit is

$$H_0 \equiv I \otimes H = \frac{1}{\sqrt{2}} \begin{bmatrix} 1 & 1 & 0 & 0 \\ 1 & -1 & 0 & 0 \\ 0 & 0 & 1 & 1 \\ 0 & 0 & 1 & -1 \end{bmatrix} \quad (2.28)$$

and for one on the high-order qubit is

$$H_1 \equiv H \otimes I = \frac{1}{\sqrt{2}} \begin{bmatrix} 1 & 0 & 1 & 0 \\ 0 & 1 & 0 & 1 \\ 1 & 0 & -1 & 0 \\ 0 & 1 & 0 & -1 \end{bmatrix} \quad (2.29)$$

where I_i is the identity operation on qubit i and H_i is the Hadamard on qubit i . Because the two gates operate on independent qubits, the order in which we compose the larger unitary in does not matter,

$$H_0 H_1 = H_1 H_0 = \frac{1}{2} \begin{bmatrix} 1 & 1 & 1 & 1 \\ 1 & -1 & 1 & -1 \\ 1 & 1 & -1 & -1 \\ 1 & -1 & -1 & 1 \end{bmatrix}. \quad (2.30)$$

The two-qubit swap gate has a very simple transform,

$$SWAP = \begin{bmatrix} 1 & 0 & 0 & 0 \\ 0 & 0 & 1 & 0 \\ 0 & 1 & 0 & 0 \\ 0 & 0 & 0 & 1 \end{bmatrix}. \quad (2.31)$$

When we write a CNOT gate, occasionally it will be necessary to distinguish which qubit is which. In that case, the first subscript will be the control qubit and the second subscript the target qubit, e.g.,

$$CNOT_{1,0} = \begin{bmatrix} 1 & 0 & 0 & 0 \\ 0 & 1 & 0 & 0 \\ 0 & 0 & 0 & 1 \\ 0 & 0 & 1 & 0 \end{bmatrix} \quad (2.32)$$

and

$$CNOT_{0,1} = \begin{bmatrix} 1 & 0 & 0 & 0 \\ 0 & 0 & 0 & 1 \\ 0 & 0 & 1 & 0 \\ 0 & 1 & 0 & 0 \end{bmatrix}. \quad (2.33)$$

In some physical implementations, a control-phase gate is the natural Hamiltonian. The control-phase or control-Z unitary is

$$CZ_{1,0} = \begin{bmatrix} 1 & 0 & 0 & 0 \\ 0 & 1 & 0 & 0 \\ 0 & 0 & 1 & 0 \\ 0 & 0 & 0 & -1 \end{bmatrix}, \quad (2.34)$$

or, more generally, for an arbitrary rotation by an angle θ about the Z axis,

$$CZ_{1,0}(\theta) = \begin{bmatrix} 1 & 0 & 0 & 0 \\ 0 & 1 & 0 & 0 \\ 0 & 0 & 1 & 0 \\ 0 & 0 & 0 & e^{i\theta} \end{bmatrix}, \quad (2.35)$$

which is not quite what we need for most logic. However, we can construct a CNOT gate from CZ easily, by wrapping the CZ in a pair of Hadamards on the target qubit:

$$H_0 CZ_{1,0} H_0 = CNOT_{1,0}. \quad (2.36)$$

DiVincenzo described other related constructions in an early paper [99]. The control-phase gate is actually symmetric; it does not matter which of the two qubits we treat as the control and which we treat as the target. The change in the system state is the same. This fact is illustrated in Figure 2.3 on page 36 with the control-Z gate both “right side up” and “upside down”. This feature can result in unwanted error propagation, as discussed in Section 2.3.

Three-Qubit Gates

We have already discussed the importance of the Toffoli and Fredkin gates in classical reversible computation. They form the two most important three-qubit gates in the quantum domain, as well. Most quantum algorithms are defined using Toffoli gates.

The transform for the Toffoli CCNOT gate with the low-order qubit being the target is

$$CCNOT = \begin{bmatrix} 1 & 0 & 0 & 0 & 0 & 0 & 0 & 0 \\ 0 & 1 & 0 & 0 & 0 & 0 & 0 & 0 \\ 0 & 0 & 1 & 0 & 0 & 0 & 0 & 0 \\ 0 & 0 & 0 & 1 & 0 & 0 & 0 & 0 \\ 0 & 0 & 0 & 0 & 1 & 0 & 0 & 0 \\ 0 & 0 & 0 & 0 & 0 & 1 & 0 & 0 \\ 0 & 0 & 0 & 0 & 0 & 0 & 0 & 1 \\ 0 & 0 & 0 & 0 & 0 & 0 & 1 & 0 \end{bmatrix}, \quad (2.37)$$

and the transform for the Fredkin control-SWAP gate with the high-order bit being the control is

$$CSWAP = \begin{bmatrix} 1 & 0 & 0 & 0 & 0 & 0 & 0 & 0 \\ 0 & 1 & 0 & 0 & 0 & 0 & 0 & 0 \\ 0 & 0 & 1 & 0 & 0 & 0 & 0 & 0 \\ 0 & 0 & 0 & 1 & 0 & 0 & 0 & 0 \\ 0 & 0 & 0 & 0 & 1 & 0 & 0 & 0 \\ 0 & 0 & 0 & 0 & 0 & 1 & 0 & 0 \\ 0 & 0 & 0 & 0 & 0 & 0 & 1 & 0 \\ 0 & 0 & 0 & 0 & 0 & 0 & 0 & 1 \end{bmatrix}. \quad (2.38)$$

The CCNOT cannot be implemented directly on most quantum technologies, so we need a breakdown into two-qubit gates. The breakdown we choose uses a two-qubit gate which we will call the “square root of X ”,

$$\sqrt{X} = \frac{1}{2} \begin{bmatrix} 1+i & 1-i \\ 1-i & 1+i \end{bmatrix} \quad (2.39)$$

and its adjoint

$$\sqrt{X}^\dagger = \frac{1}{2} \begin{bmatrix} 1-i & 1+i \\ 1+i & 1-i \end{bmatrix}. \quad (2.40)$$

Our graphic representation is shown in Figure 2.4. We will use this construction and an additional variant in Section 6.1, when we discuss the interaction of architecture and gates in more detail.

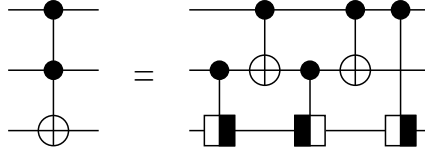


Figure 2.4: Our CCNOT construction. The box with the bar on the right represents the square root of X , and the box with the bar on the left its adjoint.

Quantum Circuits

A quantum computation, in the abstract, is a unitary transformation on the initial state of the system, creating a desired output. The complete unitary transform on n qubits, of course, is a $2^n \times 2^n$ matrix, so direct construction of the unitary to implement a complex function of more than a few qubits is difficult. The physical phenomena used for quantum computation do not, in general, lend themselves well to direct implementation of complex transforms. Moreover, human beings are not good at imagining such large systems, but are very good at composing large systems from smaller components. Thus, the abstraction of a *quantum circuit* is important. A quantum circuit effects the overall transform via a series of smaller gates (generally, one- to three-qubit gates) applied in a prescribed order on the appropriate qubits.

Researchers have found several methods for decomposing a specific unitary transform into a series of small gates or operations that we know how to implement. Some methods find optimal evolution paths (not necessarily composed of discrete gates) but are highly theoretical, and it is not immediately clear how to compile a large program by employing these methods [251, 66]. Using the most general method, the number of gates grows exponentially as the size of the problem increases, negating any advantage in computational complexity that quantum computing appears to offer [290]. Most of the work on quantum programming languages and tools for them essentially defers the decomposition problem to the programmer [128, 254, 14, 316]. Fortunately, many quantum algorithms depend on a few basic building blocks that have known efficient decompositions (such as the quantum Fourier transform), or on ideas translated directly from classical analogues (such as arithmetic).

2.2.5 DiVincenzo's Criteria

DiVincenzo [97] enumerated five abilities which are necessary for real-world quantum computing devices. A quantum computer must:

1. Be a scalable physical system with well-defined qubits;
2. Be initializable to a known state prior to computation;
3. Have adequately long decoherence times;
4. Have a universal set of quantum gates; and
5. Permit high efficiency quantum measurements.

Two additional criteria focus on moving quantum information between two different quantum computers. A viable quantum communications technology must:

6. Be able to convert between physical realizations of qubits that are stationary and moving; and
7. Be able to faithfully transmit a physical realization of a qubit between specified locations.

The first criterion means there must be some physical entity, such as energy levels of an ion, polarization of a photon, or spin of an electron, that is the actual carrier of the qubit. It must meet basic criteria of quantum behavior and support two distinct states which can be treated as zero and one. Item 1 also refers to “scalability”, which means different things in different contexts; we will explore its system aspects beginning in Chapter 7.2.

The second item may seem obvious, but some qubits, especially nuclear spins, are difficult to “reset” to zero. Schulman and Vazirani developed a method for taking a poorly-initialized machine and improving the state, “cooling” the system algorithmically [291].

The third item, decoherence, has important implications for quantum computer architecture. In order to fault tolerantly compute on a quantum computer, the native error rate must be below a certain threshold. Aharonov and Ben-Or initially calculated the threshold (“errors per quantum gate”) to be 10^{-6} [11]. However, this factor is architecture dependent, with real architectures requiring substantially lower thresholds. Furthermore, in order to not have undue overhead from error correction processes as the size of the computation scales, quantum technologies really need to achieve error rates well below this critical threshold [308].

The fourth criterion requires that a quantum computer be able to compute any quantum function. It must be able to rotate a single qubit by any angle, and must be able to entangle a pair of qubits. The single-qubit rotations may be difficult to achieve, so a

small number of “universal” gates that can be used to synthesize larger, more complex gates serves as an alternative, at polynomial cost [30, 176, 145, 118]. This is equivalent to saying that a classical computing technology should be able to perform at least a NOR or NAND operation. For quantum computers, one such set of universal gates is X, H, T, and CNOT, the gates we have already introduced in Figure 2.3 on page 36. X, H and CNOT are relatively simple to make fault tolerant, while T requires a more complex circuit; nearly one hundred gates in one construction [118].

Item 5 is the measurement we discussed above; there must be a reliable way to read out the state of a qubit. However, as noted, measurement is far more important than retrieving results at the end of a computation; it occurs almost continuously as part of quantum error correction and the fault-tolerant execution of gates on encoded bits [297, 64, 308, 132, 307].

Items 6 and 7 deal specifically with moving quantum information across long distances for purposes of computation. Criterion 6 only applies to systems that compute complex quantum algorithms via shared state. It does not apply to other uses of quantum effects, such as quantum cryptography [44, 108] and basic demonstrations of quantum teleportation [45, 125] (though teleportation may be used in quantum computer architectures [133, 136]).

These criteria have been used as a basis for evaluation of quantum computing *technologies* [248, 302, 20]. They are a necessary set of capabilities, but not sufficient to understand the difficulty of building a quantum computer or its speed and utility once built. Ladd has suggested that DiVincenzo’s five criteria can be restated as three [195]. A complementary set of criteria for quantum computer *systems* is discussed in Chapter 4.

2.2.6 Quantum Algorithms

We observed in Section 2.2.3 that an n -qubit quantum register can be in a superposition of all possible 2^n states $|0\rangle$ to $|2^n - 1\rangle$ at the same time. Usually, quantum algorithms begin by placing one input register in this superposition. This effect allows a quantum computer to calculate a function on all possible inputs at the same time, in a single pass. The hard part is getting a useful answer out. At the end of the calculation, the result register is a superposition of all of the results, one for each of the 2^n possible inputs. However, we can’t directly read out all of those results. If we measure the result register to get our answer, the superposition collapses into a single state with

a probability according to the weights discussed above. Then we have only a single value; our end result is no better than if we had used a classical computer to compute the function for one possible input chosen at random. How do we structure a quantum algorithm so that useful results come out, taking advantage of these quantum effects to accelerate computation? We must find a way to drive the system toward the state where the weights α_i from Equation 2.8 of undesirable states are zero and desirable states (the solutions to our problem) have large weights.

Deutsch discovered the key to a quantum algorithm [94]: use quantum interference to increase the probability that a useful state is found when the quantum register is measured. Deutsch's algorithm, later refined in collaboration with Jozsa, classifies an unknown function as one of two types. One type of function will create interference so that the register cannot read 0; the other type of function creates interference so that all of the non-zero values cancel, leaving only the state 0. This is perhaps the most profound observation in all of quantum computing: we can take advantage of the wave nature of particles to achieve computation.

What we colloquially call quantum algorithms are, in reality, hybrid algorithms with both classical and quantum components. Moreover, the quantum portion of many algorithms is probabilistic, often necessitating multiple runs to get the desired result (even ignoring the physical issues of decoherence). The complete cycle of a "quantum" computation is as follows:

1. Pre-calculate certain classical factors.
2. Repeat:
 - (a) Initialize quantum computer.
 - (b) Prepare input state.
 - (c) Execute quantum portion of the algorithm.
 - (d) Measure output register.
 - (e) Post-process output to determine if desired result achieved.
 - (f) Exit if desired result.
3. Finish post-processing.

We will see in Section 2.3 that this process is applied recursively in the implementation of quantum error correction. The quantum computer can be initialized starting

from a partially-initialized state using quantum algorithms, as well, using this procedure for step 2.a [291].

2.2.7 Distributed Quantum Computation

Distributed quantum computation (DQC) is the cooperative use of multiple, independent quantum computers working to solve a single problem. The theoretical foundations of DQC have been laid, but very little work on designing a machine to run DQC has been done. Early suggestions of distributed quantum computation include Grover [136], Cirac et al. [77], and Steane and Lucas [311]. A recent paper has proposed combining the cluster state model [277, 246] with distributed computation [207]. D'Hondt has done work on formal models of distributed quantum computation, drawing on formal classical techniques [96]; D'Hondt and Tani et al. have worked on the leader election problem, one of the few true distributed quantum algorithms [321]. A distributed system generally requires the capability of transferring qubit state from one physical representation to another, such as nuclear spin \leftrightarrow electron spin \leftrightarrow photon, as in DiVincenzo's seventh criterion [227, 159, 71].

Yenez distinguished between distributed computation using entanglement between nodes, which he called type I, and without inter-node entanglement (i.e., classical communication only), which he called type II [355]. Our quantum multicomputer is a type I quantum computer. Jozsa and Linden showed that Shor's algorithm requires entanglement across the full set of qubits, concluding that a type II quantum computer cannot achieve exponential speedup [162, 215]. Much of the work on our multicomputer involves creation and management of that shared entanglement.

Yimsiriwattana and Lomonaco have discussed a distributed version of Shor's algorithm [356], based on one form of the Beckman-Chari-Devabhaktuni-Preskill modular exponentiation algorithm [35]. The form they use depends on complex individual gates, with many control variables, inducing a large performance penalty compared to using only two- and three-qubit gates. Their approach is similar to our telegate (Sec. 5.2.2), which we show to be slower than teledata (Sec. 5.2.1). They do not consider differences in network topology, and analyze only circuit complexity, not depth (time performance).

2.3 Error Management in Quantum Computers

By failing to prepare, you are preparing to fail.

Benjamin Franklin

There are no mistakes, save one: the failure to learn from a mistake.

Robert Fripp

O throw away the worser part of it,
And live the purer with the other half.

Shakespeare's *Hamlet*, quoted by Lampson

A bewildering array of error processes bedevil quantum computing technologies. There are normal, independent errors of decay (T_1 and T_2 memoryless processes) that affect a single qubit only, correlated error processes caused by environmental defects that affect more than one qubit, unwanted interactions between qubits, stochastic gate errors, propagation of errors by gates, “hot” and “cold” gates, accidental measurement of qubits, leakage of information into the environment creating mixed states, and finally, loss of the qubits themselves (photons or, occasionally, ions).

Error management in quantum computers is accordingly a rich and complex field. In this section, we provide a general introduction to quantum error correction (QEC), including a look at how QEC helps reinforce the digital nature of quantum computing, and briefly present the notion of a *threshold*. We then skim over other error control techniques such as decoherence-free subspaces and composite gate sequences, very different from error-correcting codes and more tightly bound to the quantum nature of the data we are protecting. Our goal in this section is not to cover the mathematics of quantum errors or to provide complete coverage of the topic, but to give computer architects a feel for the nature of the problems and the solutions. For a more thorough understanding, see Chapter 10 of Nielsen & Chuang [248] (which runs seventy-five pages) and the many papers referenced both there and in this chapter. Keyes' paper is a good introduction to some of the physical concerns associated with solid-state systems [169]. In my opinion, the single most important paper for engineers to read and understand, for the practicality of its results, is one by Steane [308]. This topic alone would easily warrant development of a full book.

2.3.1 Error Models

As suggested above, there are many ways in which quantum data can be damaged. Error processes also operate at many time scales: errors may occur at fabrication time, over the course of many gates, or over the course of a single gate. Atoms are identical, but fabricated structures are not, and the resulting differences may alter e.g. oscillation frequencies, affecting gate time and coupling of qubits. Temperatures drift over time, influencing behavior. Atoms may vary their position relative to a laser beam or optical cavity, altering the ideal gate time on a moment-by-moment basis. Stray magnetic fields may influence large groups of qubits.

This plethora of problems suggests that we should look for similarities and simplifying abstractions. The first models of errors in quantum computation assumed that independent errors occurred before or after the execution of logical gates. If we assume independent, random errors (an assumption we will gradually relax), it can be shown that all errors can be reduced to X or Z gate errors on individual qubits.

Error Propagation

In classical circuits, whether analog or digital, we are accustomed to errors propagating from source to target; an error in an AND gate creates an incorrect result, but does not affect its inputs. In the quantum world, we have the same kind of errors, but additionally have errors that propagate in counter-intuitive fashion.

In Figure 2.5, we show how errors propagate through quantum gates. An X error (a NOT error, drawn as \oplus in the figures) on the target qubit of a CNOT gate behaves the same before or after the qubit. An X error on the control bit before the gate execution, in contrast, propagates the error to both the control and target qubits at the output; our single error has become two errors. Worse, a Z error (drawn as a box with a Z in it in the figure) on the target qubit of a CNOT prior to the gate propagates a Z back to the control, as well; our intuition about the flow of errors in the system fails us in this case. This effect affects our ability to correctly execute quantum error correction itself, which we will see below.

Steane's Error Models

The basic model introduced above correctly models the *logic* of errors as single-qubit gates that occur before or after the execution of logic gates. For accurately assessing the *probability* of errors, it is somewhat simplistic; we will see in Section 3.4 that,

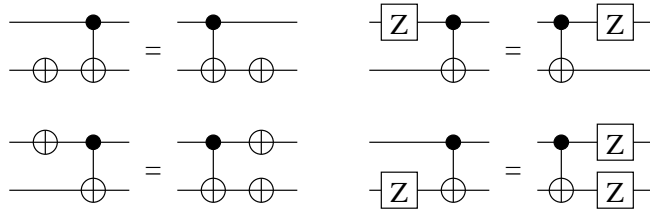


Figure 2.5: Error propagation in two-qubit gates.

for many calculations, many of the qubits sit idle for long periods of time. A better model will therefore take into account memory errors and gate-induced errors. Steane introduced just such a model, which we will call the KQ model or the *space-time* model [308]. Letting K be the number of logical qubits in the computation and Q be the number of time steps to complete the computation, then the accuracy of our logical operations must be related to the inverse of the space-time product, $\sim 1/KQ$. In this remarkable paper, Steane went further and discussed the difference between the gate error probability, which he labeled γ , and memory error probability, which he labeled ϵ , and produced numerical values for the size of computations (KQ) achievable for various system characteristics.

2.3.2 Quantum Error Correction Codes

Until the advent of quantum error correction, many researchers believed that these problems were insurmountable [169, 104, 328] or at least limited the range of problems to which quantum computing can be applied [75, 31]. However, in 1995, almost simultaneously, several researchers discovered and developed mechanisms for applying classical error correction codes, such as Reed-Solomon codes, to quantum data [297, 64, 304]. The most important class of quantum error correction (QEC) codes is now called the Calderbank-Shor-Steane codes, after its inventors, and includes quantum analogs of Hamming, Golay, and other types of classical error correcting codes.

In classical systems, we often use multiple levels of error correction. The same principle can be applied in quantum systems, in a manner called *concatenation*. In a concatenated system, physical qubits are grouped to encode a logical qubit, and a group of logical qubits is further encoded (using the same or a different code) to provide greater protection against errors. We discuss concatenation in Section 2.3.4.

First, let us examine how to correct bit-flip errors in a quantum state. The CSS codes, like classical codes, redundantly encode information so that an error in one component qubit can be detected by comparing to the other qubits, and the error corrected.

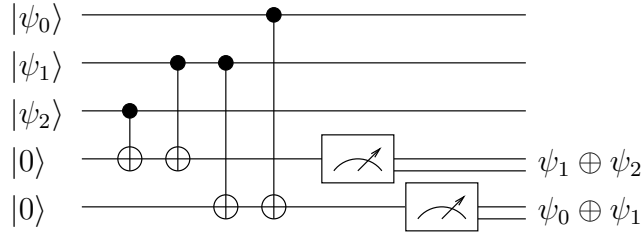


Figure 2.6: Parity measurement for quantum error correction.

In the simplest example, one qubit is encoded by making two fanout “copies”⁴ of the qubit. Three ones will be our logical one, and three zeroes will be our logical zero, i.e.

$$|0\rangle \rightarrow |0_L\rangle \equiv |000\rangle \quad (2.41)$$

$$|1\rangle \rightarrow |1_L\rangle \equiv |111\rangle. \quad (2.42)$$

Our canonical unknown single-bit state then becomes

$$|\psi\rangle = \alpha|0\rangle + \beta|1\rangle \rightarrow |\psi_L\rangle = \alpha|0_L\rangle + \beta|1_L\rangle = \alpha|000\rangle + \beta|111\rangle. \quad (2.43)$$

Now that we have our proposed logical states, how do we execute gates, and how do we perform our actual error correction? Taking the second question first, error correction is done by a series of parity calculations and measurements. Letting $|\psi_j\rangle$, $j = 2, 1, 0$ be the three qubits in our logical state $|\psi_L\rangle$, we want to calculate the parity of the 0-1 pair and the 1-2 pair. If the state is still unmarred, both calculations will return zero (even parity). However, if we find, for example, that the 1-2 pair is even but the 0-1 pair is odd, we can infer that bit 0 is in error, and needs to be corrected. If both pairs are odd, we can infer that bit 1 is in error. The basic circuit for these parity measurements is shown in Figure 2.6.

Although it is not immediately obvious, this parity measurement will *not* disrupt our qubit state, causing the collapse of the wave function and ruining our computation. We saw in Section 2.2.3 that measurement of a single qubit in a superposition takes out one qubit, shrinking the entangled state of the system. Intuitively, this is reasoned by considering what we *learn* from the measurement. By doing a parity measurement, we learn only whether the two qubits are the same, not whether they are one or zero. When the states are correct, both bits will be one, or both bits will be zero, in accordance with

⁴Again, be careful that when we use the term “copy”, we are referring to a fanout, rather than an independent, cloned copy of the state, which we know is impossible [352].

the usual behavior of entangled qubits.

The error case works the same. Our error model assumes a bit *flip*, not a qubit being *set* to either one or zero. Thus, an error on bit 1, for example, would lead to the state $\alpha|010\rangle + \beta|101\rangle$. Parity measurement of the 0-1 pair produces a 1 (odd parity). Writing out both the correct case and the case of an error on bit 1, adding a parity qubit whose state is created using the circuit in Figure 2.6, we have

$$\alpha|000\rangle + \beta|111\rangle \rightarrow \alpha|0000\rangle + \beta|1110\rangle = (\alpha|000\rangle + \beta|111\rangle)|0\rangle \quad (2.44)$$

$$\alpha|010\rangle + \beta|101\rangle \rightarrow \alpha|0101\rangle + \beta|1011\rangle = (\alpha|010\rangle + \beta|101\rangle)|1\rangle \quad (2.45)$$

where the right-hand factoring makes it explicit that measuring the last qubit will not affect the prior state, neither collapsing the superposition nor altering the values of α and β .

Once the parity has been calculated and measured, we know whether or not an error occurred, and if so, on which qubit. Assuming we found an error on qubit 1, we correct by applying an X gate,

$$X_1|\psi_L\rangle = X_1(\alpha|010\rangle + \beta|101\rangle) = \alpha|000\rangle + \beta|111\rangle \quad (2.46)$$

and our desired state is restored.

The second type of error we must correct is phase errors. When a phase error occurs on our three-bit encoded state,

$$\alpha|0_L\rangle + \beta|1_L\rangle \rightarrow \alpha|0_L\rangle - \beta|1_L\rangle \quad (2.47)$$

regardless of which qubit the phase error affected. Obviously, our three-bit code does not detect such errors. However, if we apply a Hadamard to the three-qubit state before an error occurs, then we shift into a space where a phase error will show up as a bit error when the parities are calculated. Combining a three-bit code for protecting against bit flips and a three-bit code for protecting against phase flips, we have a nine-bit encoding for a single logical qubit known as the *Shor nine-bit code* [297].

QEC traditionally depends on interleaving measurement and logic gates, and there has been recent experimental progress on this front [281]. However, it is possible to perform QEC without measurement, at a cost of a number of ancillae that grows with the number of applications of error correction [248]; this approach is not supportable in a large computation, but may be applied in short sequences.

QEC builds on concepts from classical error correcting codes. *Stabilizer codes* represent an important advance in the mathematical representation of QEC, providing a more compact representation of the code word states and simplifying construction of fault-tolerant operations [131].

QEC demands to be taken into account when designing a quantum computer. Indeed, Steane has referred to a quantum computer as a machine whose purpose is to execute error correction; computation is a side effect [307]. Currently, some researchers are analyzing the behavior of QEC on proposed architectures and attempting to design machines that are well-adapted to performing QEC [317, 87, 120, 307, 83, 255, 62, 95, 230, 229], or exploring the interaction of QEC with *cluster state computing* [250]. Others are demonstrating QEC and decoherence-free subspaces (DFS, described below) experimentally, either partially or completely, on NMR [181], optical [268], Josephson junction [164], or ion trap systems [140, 281, 70]. Knill et al. have even suggested that the ability to run QEC be used as a reliability benchmark for quantum computing technologies [181].

CSS Codes and Larger Blocks

Now that we understand the basics of the error correction processes, surely we will want more efficient codes than the Shor nine-bit code. To discuss the efficiency of the encoding of various schemes, we need a notation. We will describe a quantum error correcting code using the notation $[[n,k,d]]$, where n is the number of physical bits, k is the number of logical bits encoded, and d is the Hamming distance ($(d-1)/2$ errors can be corrected by the code). In this notation, the nine-bit Shor code is $[[9,1,3]]$. Nine physical qubits encode a single logical qubit, and can correct any single-qubit error, whether bit flip or phase flip (or both).

More efficient encodings for a single qubit are known. The most commonly used example is the $[[7,1,3]]$ Steane code [304]. Thus, for the Steane 7-bit code, we encode each logical qubit in seven physical qubits, and this state can correct a single error. In this code, logical zero and logical one are [64]

$$\begin{aligned}
 |0_L\rangle &= \frac{1}{\sqrt{8}}(|0000000\rangle + |1101001\rangle + |1011010\rangle + |0110011\rangle \\
 &\quad + |0111100\rangle + |1010101\rangle + |1100110\rangle + |0001111\rangle) \\
 |1_L\rangle &= \overline{X}|0_L\rangle.
 \end{aligned} \tag{2.48}$$

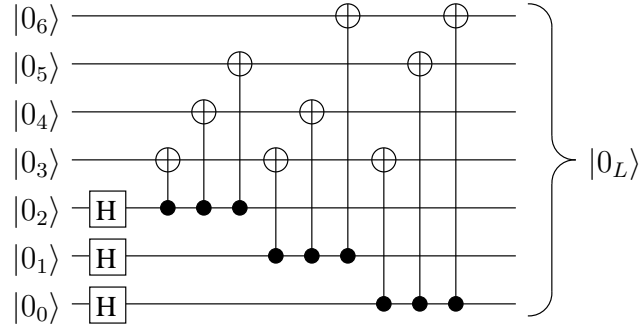


Figure 2.7: Circuit to create the $|0_L\rangle$ state for the Steane $[[7,1,3]]$ code.

In the equation, we have underlined the last three bits and ordered the terms in the superposition to emphasize that all of the binary values 0 to 7 appear there. Figure 2.7 shows a circuit that can create the logical zero state; the Hadamards on the bottom three qubits give us our superposition of 0 to 7 from which the rest of the state is built. The subscripts in the figure are the bit number in the QEC block, with qubit 6 being the leftmost bit in the state as written in Equation 2.48. The quality of the state must be verified after creation and before use.

This seven-bit code is still not the limit for a single qubit; within months of the elucidation of the basic concepts of quantum error correction, two groups had discovered a $[[5,1,3]]$ code, which was demonstrated experimentally on an NMR system in 2001 [198, 46, 181]. However, this code is difficult to work with; executing many kinds of logical gates on the logical states for this code requires long sequences of physical gates.

As with classical error correction, we can encode more than a single qubit into a block that is collectively protected. In classical systems, even with strong codes, in practice the overhead is rarely more than 30%. Unfortunately, in the quantum world, even with modest-sized blocks, the overhead runs to a factor of three or so. Steane described codes as efficient as $[[63,39,5]]$, with an overhead of only 1.6, but this one can correct only two errors in the entire block, and the other efficient codes likewise trade protection for space. Steane recommends a $[[23,1,7]]$ code based on a classical Golay code as giving higher error tolerance (a larger possible application-level KQ) for a given overhead in storage, when multiple layers of QEC are concatenated. For a concatenated code, he recommends $k = 1$ for the lowest level(s) of the system, it being much easier to construct higher-level codes in this case [308].

2.3.3 Fault Tolerance

Fault tolerance, as the term is usually applied in quantum computing, means that dynamic errors in our state do not propagate uncontrollably throughout the system. The system can tolerate individual errors and still successfully compute. Thus, fault tolerance is primarily a set of techniques for controlling error propagation. Fault tolerance does not mean, as the term is often used in classical systems, that the quantum computer is prepared to deal with near-permanent failure of large hardware subsystems.

As we saw above, errors can propagate from one qubit to another as gates are executed. For this reason, errors are especially dangerous to QEC blocks that contain more than one logical qubit. A code that can correct only a single error across multiple qubits can never be robust against a logical gate error when the gate is applied between two qubits in the same QEC code block. Therefore, to execute a gate between qubits in the same block, one logical qubit must first be swapped out. Next, we apply the gate laterally between blocks and perform error correction separately in each block, after which the qubit can be swapped back in to its original location, if desired.

Figure 2.6 on page 49 shows a simple, ideal circuit for calculating the error syndromes. To prevent the kind of error propagation described in Section 2.3.1, we cannot use this circuit directly; we must have a scheme which prevents phase error propagation. Steane described an algorithm for this, based on earlier work by himself, Shor, Zalka, and others [308]. Figure 2.8 shows Steane's algorithm, slightly reformulated. In actual implementation, the creation of the logical $|0_L\rangle$ state will be decoupled from the syndrome measurement part of the subroutine. The syndrome measurement will draw from a pool of logical zeroes that is refilled continuously, tuned to guarantee that logical zeroes are available when necessary, and as fresh as possible, while minimizing the number of qubits required.

Many researchers have studied fault tolerance, including the composition of fault-tolerant logical gates [310, 62, 118]. We will not delve further into this topic here.

2.3.4 Threshold Calculations and Concatenation

Error correction only improves the quality of the state of our system if, on average, it repairs more errors than it introduces. If the resulting error rate is still inadequate, we can concatenate multiple levels of QEC, pushing down the net error rate to the necessary level.

In an h -level concatenated encoding, the effective error probability is $(cp)^{2^h}/c$,

```

subroutine get_one_syndrome:
  repeat
    prepare n qubits in state  $|0\rangle$ 
    apply circuit to create logical  $|0\rangle$ 
    verify logical  $|0\rangle$  state
  until logical  $|0\rangle$  state is good
  couple  $|0\rangle$  to data block
  Hadamard transform  $|0\rangle$ 
  measure
  return result
endsubroutine

routine syndrome:
  get_one_syndrome
  if syndrome = 0 then
    return 0
  else
    repeat r-1 times
      get_one_syndrome
    if more than chosen limit of r syndromes agree then
      return syndrome
    else
      fail
endroutine

```

Figure 2.8: Fault-tolerant error syndrome measurement algorithm.

where c is the *threshold* value and p is the error probability (which is assumed to be the same at each level, for the moment). The threshold, in this equation, is the number of operations required to execute a single level of error correction. If $cp < 1$, then each level of encoding we add to the system decreases our net probability of failure. If an encoding level uses n qubits from the level below to encode a single qubit, our total cost per logical qubit is n^h physical qubits. In two-level concatenated QEC, with different inner and outer codes, $[[n_i, 1, d_i]]$ and $[[n_o, k, d_o]]$, respectively, we use $n_i n_o$ physical qubits to represent k logical qubits.

Aharonov and Ben-Or were among the first to calculate a numerical value for a threshold [11]. They found a value of $\sim 10^{-6}$ for a particular set of assumptions. That is, if more than one gate out of a million fails (a level *well* beyond experimental capabilities for all quantum technologies at the moment), using fault tolerant techniques actually makes the state of the system worse rather than better. If less than one in a million gates fails, fault tolerance makes the state of the system better, and via repeated application of fault tolerance we can reach an arbitrary level of reliability. Aharonov and Ben-Or also proved (without providing a numerical figure) that a threshold exists even when the qubits are arranged in a linear nearest neighbor-only topology, which we will see in Section 6.1. Thresholds have been calculated many times for different sets of physical assumptions and error correcting codes, with answers varying by several orders of magnitude in both directions [185, 90, 120, 132, 183, 318, 131, 274]; Knill has suggested that, under some conditions, error rates as high as 1% might be acceptable [180]. In this dissertation, we will work with the Steane algorithm and memory/gate error assumptions described above, working toward a finite computation of a particular size and ignoring the issues around thresholds.

2.3.5 Why QEC Suppresses Over-Rotation Errors

One counter-intuitive aspect of operating on encoded states is the suppression of over-rotating gates (gates running “hot”) or under-rotating gates (gates running “cold”) [233]⁵. It is easy to see that QEC corrects a single gate error, but if all of the physical gates comprising a logical gate over-rotate by similar amounts, can that be corrected?

Examining the three-bit encoding once again,

$$|\psi_L\rangle = \alpha|000\rangle + \beta|111\rangle \quad (2.49)$$

⁵This is a key factor in the “quantum computation is not analog computation” argument.

an X gate that runs hot on a single qubit will actually perform the gate

$$X_\epsilon = R_X((1 + \epsilon)\pi) = \begin{bmatrix} \sin \frac{\epsilon}{2} & \cos \frac{\epsilon}{2} \\ \cos \frac{\epsilon}{2} & \sin \frac{\epsilon}{2} \end{bmatrix}. \quad (2.50)$$

The logical X gate for this encoding is $\overline{X} = XXX$ (X gates on all three component qubits), where the over-line indicates a logical operation. A mis-rotation at the *logical* level is

$$\overline{X}_\epsilon |\psi\rangle = (\alpha \sin \frac{\epsilon}{2} + \beta \cos \frac{\epsilon}{2})|000\rangle + (\alpha \cos \frac{\epsilon}{2} + \beta \sin \frac{\epsilon}{2})|111\rangle \quad (2.51)$$

but $\overline{X}_\epsilon \neq X_\epsilon X_\epsilon X_\epsilon$! It is easy to be confused about how the system distinguishes between a deliberate attempt to rotate by π and 1.1π . The answer is that this construction $X_\epsilon X_\epsilon X_\epsilon$ suppresses the (apparent) over-rotation and *forces* $X_\epsilon X_\epsilon X_\epsilon \sim \overline{X}$. This fact can be seen by doing the vectors explicitly.

$$X_\epsilon X_\epsilon X_\epsilon |\psi\rangle = \begin{bmatrix} \alpha \sin^3 \frac{\epsilon}{2} + \beta \cos^3 \frac{\epsilon}{2} \\ \alpha \sin^2 \frac{\epsilon}{2} \cos \frac{\epsilon}{2} + \beta \cos^2 \frac{\epsilon}{2} \sin \frac{\epsilon}{2} \\ \alpha \sin^2 \frac{\epsilon}{2} \cos \frac{\epsilon}{2} + \beta \cos^2 \frac{\epsilon}{2} \sin \frac{\epsilon}{2} \\ \alpha \sin \frac{\epsilon}{2} \cos^2 \frac{\epsilon}{2} + \beta \cos \frac{\epsilon}{2} \sin^2 \frac{\epsilon}{2} \\ \alpha \sin^2 \frac{\epsilon}{2} \cos \frac{\epsilon}{2} + \beta \cos^2 \frac{\epsilon}{2} \sin \frac{\epsilon}{2} \\ \alpha \sin \frac{\epsilon}{2} \cos^2 \frac{\epsilon}{2} + \beta \cos \frac{\epsilon}{2} \sin^2 \frac{\epsilon}{2} \\ \alpha \sin \frac{\epsilon}{2} \cos^2 \frac{\epsilon}{2} + \beta \cos \frac{\epsilon}{2} \sin^2 \frac{\epsilon}{2} \\ \alpha \cos^3 \frac{\epsilon}{2} + \beta \sin^3 \frac{\epsilon}{2} \end{bmatrix} \quad (2.52)$$

before applying the error correction. This encoding suppresses the angular error to $O(\sin^2 \frac{\epsilon}{2}) = O(\epsilon^2)$, even without going through the QEC correction step, but it's easier to see once we've applied the QEC. Assuming perfect QEC, the final result is

$$\begin{aligned} |\psi'_L\rangle &= (\alpha \sin^3 \frac{\epsilon}{2} + \beta \cos^3 \frac{\epsilon}{2} \\ &\quad + 3\alpha \sin^2 \frac{\epsilon}{2} \cos \frac{\epsilon}{2} + 3\beta \cos^2 \frac{\epsilon}{2} \sin \frac{\epsilon}{2})|000\rangle \\ &\quad + (\alpha \cos^3 \frac{\epsilon}{2} + \beta \sin^3 \frac{\epsilon}{2} \\ &\quad + 3\alpha \cos^2 \frac{\epsilon}{2} \sin \frac{\epsilon}{2} + 3\beta \sin^2 \frac{\epsilon}{2} \cos \frac{\epsilon}{2})|111\rangle \end{aligned} \quad (2.53)$$

and we see that the angular rotation error is in the \sin^2 terms.

Mathematicians would say, of the deliberate attempt to rotate by 1.1π , that “it’s not

in the Clifford group,” or “it’s not in the normalizer.” The importance of this mathematical distinction is that there are only a few gates, such as the X gate, that are easily constructed by applying the same gate in a transverse fashion to all elements of our logical qubit. It is not possible to (easily) construct a deliberate rotation by 1.1π on the logical state. We will not delve further into these mathematical issues or terminology, though they affect compilation of efficient programs and cluster-state computing as well as quantum error correction, and are influenced by the natural gate for a specific technology [145, 118].

2.3.6 Other Error-Suppression Techniques

Other forms of error management techniques exist, some based on deep theoretical insights. One particularly intriguing one, from a theoretical point of view, is *topological quantum memory*, in which a 2-D array or torus of qubits is entangled in various patterns to make a logical qubit [92]. The state is stable because it is the patterns of the connections, rather than the value or phase of any single qubit, that determines the logical state. The resources required are large, and it is not immediately clear how to implement this scheme on a physical system.

QEC works best on systems with uncorrelated errors on separate qubits. When error processes are more likely to affect groups of nearby qubits, a technique known as *decoherence free subspaces* (DFS) helps to mitigate these problems [206, 140, 205]. In a DFS, the logical value is encoded in the relative, rather than absolute, state of a group of qubits. A stray magnetic field that caused them all to flip, for example, would not affect the logical state.

In optical systems, the principal source of error is loss of photons. In this case, *erasure codes* (in contrast to *error correcting codes*) work well [183]. Erasure codes can be as simple as a parity check. Reconstruction of the state is straightforward when the position of the missing qubit is known. Erasure codes are used in RAID arrays, where the position of the disk spindle that has failed plus a simple parity check provide enough information to reconstruct the original data [263].

As we noted above, individual gates can run hot or cold, over- or under-rotating compared to the intended angle. Besides using (digital) quantum error correction, analog techniques for improving the accuracy of gates have been developed. Composite pulses break down a rotation into a series of steps designed so that similar errors in each step cancel [338, 81]. As a simple example, a rotation from the north pole to the south

pole can be broken down into a 90° rotation about the X axis, then a 180° rotation about the Y axis, then another 90° rotation about X . If the X rotations both under-rotate, the Y rotation will compensate by mirroring the position about the equator between X rotations. Realistic sequences for arbitrary (and unknown) starting positions and gates are substantially more complex but valuable. Some sequences can reduce an error of ϵ in each step of the process to an error $O(\epsilon^6)$ in the final outcome.

2.4 Summary

Reversible computation allows us to reverse the arrow of time and return to the starting point of a computation, recovering all inputs to the system. This is possible because information is conserved, rather than destroyed, as in common Boolean logic; each gate has an inverse that undoes its operation. In reversible classical logic, the inverse of a gate is the same gate, but in quantum that is not necessarily so, as we saw in Section 2.2.4. In reversible classical logic, we need a three-bit gate in order to have universal computation; we have also seen that in quantum computation we can construct the three-bit gates from many types of two-bit gates.

When Bennett, Feynman, Fredkin, Toffoli and others originally developed the concepts behind reversible computing in the 1970s, they were searching for the ultimate limits to the energy consumption of a computation, as well as playing with remarkable intellectual facets of information. They probably had no notion that beginning just a few years later they would help to found the fields of quantum computation, quantum information theory and quantum communication, and that their names would be indelibly linked with those fields. Feynman, Benioff and Deutsch conceived of quantum computing in the 1980s as utilizing quantum effects to, potentially, dramatically accelerate computation of certain functions [39, 114, 94].

Quantum computing must be contrasted with classical computation performed using quantum phenomena. Of course, the behavior of semiconductors can be viewed as an analog quantum phenomenon, but transistors currently use large numbers of charge carriers, allowing us to treat transistors as classical digital devices. As device size continues to decrease according to Moore's Law, we will soon move into the range where individual electrons are used [236, 110]. Other approaches involve using quantum cellular automata as logic gates, or more directly manipulating the spin of small numbers of electrons for e.g. magnetic RAM and logic devices, in a field broadly called *spintronics* [153, 329, 351]. Although the physics of the devices and the technology for

manipulating such states have much in common with the experimental techniques for quantum computation, there is a key difference. In what we refer to as quantum computation, we are attempting to take direct advantage of the key aspects of superposition and entanglement, whereas in quantum-executed classical computation, the goal is to suppress these effects as unwanted, and maintain a clear binary state.

A quantum bit, or qubit, can be in a superposition of states, rather than the definite zero or one state of a classical bit. In this chapter, we have presented the basic concepts of qubit state, starting with the relationship between the wave function and the probability of getting certain results. We discussed representing the state of a single qubit as a point on the Bloch sphere; visualization of the state of multiple qubits is much harder, and if the qubits are entangled they cannot be represented independently. We discussed the basic principles of quantum superposition, entanglement, measurement, and decoherence. We can entangle multiple qubits and interfere the terms in the superposition, driving the system toward our desired states. Measuring the system will produce values that would be difficult to calculate using only classical computers, in some cases, exponentially more difficult. Designing algorithms that generate superpositions with useful speedups has proved to be a difficult problem.

We have outlined some of the coherence and computational accuracy problems inherent in quantum computing devices, and shown a variety of ways of mitigating these problems. In particular, we focused on quantum error correction (QEC). Besides simple bit errors, QEC must be able to correct phase errors as well. This fact results in substantially less efficient codes than in the classical case. The counter-intuitive propagation of phase errors also forces complex fault-tolerance mechanisms. The state of a qubit is something of an analog phenomenon, with a continuum of states for the phase and probabilities of different states; fortunately, as we have seen, QEC helps to suppress analog errors, at the expense of requiring more complex processes to effect many logical qubit rotations.

This chapter has described the building blocks of quantum computation. The material presented so far gives only the vaguest notion how these concepts cooperate to give us the power of quantum computation. We will gradually elaborate on these topics, beginning in the next chapter with Shor's algorithm for factoring large numbers.

Chapter 3

Shor's Algorithm for Factoring Large Numbers

"I am fairly familiar with all forms of secret writings, and am myself the author of a trifling monograph upon the subject, in which I analyze one hundred and sixty separate ciphers, but I confess that this is entirely new to me. The object of those who invented the system has apparently been to conceal that these characters convey a message, and to give the idea that they are the mere random sketches of children."

Sherlock Holmes in "The Adventure of the Dancing Men," Sir Arthur Conan Doyle, 1903.

Before we can design a computer, we have to understand how it will be used. Characterizing the workload of a proposed system is the first important task in the design process. For our quantum multicomputer design, we have chosen Shor's algorithm as our primary target application [296, 107]. Shor's algorithm requires arithmetic and the quantum Fourier transform (QFT), both of which are considered fundamental building blocks of other algorithms. Moreover, Shor's algorithm is a famous and important result in its own right. This chapter presents an informal overview of the algorithm. Our discussion does not detail the theoretical mathematics of the algorithm, instead covering the importance and structure of the algorithm, and its relationship to the quantum mathematical building blocks which are the primary focus of this thesis. The chapter begins by discussing the factoring problem, then presents the QFT, followed by arithmetic algorithms for reversible and quantum addition and modular exponentiation, then

combines the parts into Shor's overall algorithm.

3.1 The Importance of Factoring

Authentication of identity is one of the key factors in computer security. To authenticate yourself, you prove in some fashion that you are who you claim to be (or, at least, have rights that you claim to have). Authentication is often said to depend on something you have, something you are, or something you know (but that is not known to other people). A door key, for example, is one way to authenticate that you are allowed to pass through the corresponding door; it is something you have. Biometric sensors, such as fingerprint or iris readers, are canonical examples of "something you are" authentication. A computer password is something you know.

The RSA algorithm (Rivest-Shamir-Adelman, named for its developers) is the most important authentication mechanism on the Internet today [280, 289]. RSA is a classic example of a *public key*, or *asymmetric*, encryption algorithm. RSA is used primarily for authentication, rather than encryption of bulk data, because it is expensive to calculate relative to other encryption algorithms. In RSA, a cryptographic key has two parts, the public key and the private key. The public key can be disclosed to anyone, and should be made available via some trustworthy means. This trustworthy publication of the public key is beyond the scope of our discussion, but can be recursive use of the same authentication mechanism leading back to a trusted source such as a friend or the RSA Corporation, or an out-of-band trust mechanism such as publication in the New York Times. The private key is used to calculate a function whose result can be disclosed publicly. Using the result and the previously-announced public key, any party can then verify that the function result was calculated by the holder of the private key, thereby authenticating the identity of the creator.

Factoring a large integer into its components would seem to be a rather esoteric problem, but in fact, it is directly relevant to this issue of authentication. The difficulty of cracking RSA is known to be related to the difficulty of factoring a large, composite number into its prime factors. Letting C be the ciphertext and M be the original message, the function calculated in RSA is

$$C = M^e \bmod n \quad (3.1)$$

$$M = C^d \bmod n. \quad (3.2)$$

The *encryption key*, or public key, is (e, n) , and the *decryption key*, or private key, is (d, n) . n is chosen to be a simple composite number, the product of two primes, $n = pq$. d is a large, random number which is relatively prime to $(p-1)(q-1)$. e must then be the multiplicative inverse of d , modulo $(p-1)(q-1)$, such that

$$ed = 1 \bmod (p-1)(q-1). \quad (3.3)$$

From this, we can easily see that the ability to factor n into p and q would allow the encryption scheme to be broken. Thus, the security of RSA is said to depend on the computational difficulty of the factoring problem.

3.2 Historical Progress in Factoring

The factoring problem has never been *proved* to be impossible to solve classically in polynomial time, though many researchers strongly believe it to be impossible. The best known classical algorithm, the general Number Field Sieve (NFS), consumes total resources that are superpolynomial in the length of the number [187]. Its asymptotic computational complexity on large numbers is

$$O(e^{(nk \log^2 n)^{1/3}}) \quad (3.4)$$

where n is the length of the number, in bits, and $k = \frac{64}{9} \log 2$.

RSA, the company founded by the inventors of the RSA algorithm, which owns the (now expired) patents on the RSA algorithm and much related software, issues an ongoing series of public challenges to the factoring community, in the form of numbers to be factored. These challenges carry with them cash prizes that are currently modest but grow into the hundreds of thousands dollars for longer numbers [283]. Figure 3.1 shows the progress of the RSA Challenge factoring records since 1991.

RSA places no restrictions on the amount or type of computing power to be used in the challenge. At a constant dollar value of computing power used, in the current range of ~ 600 bits, Moore's Law applied to CPU power alone (ignoring memory and I/O, and software improvements) suggests that the longest number factorable using NFS should be growing at about 18 bits per year. In the data through 2003, we see roughly this trend. The line on the plot is a least-squares fit to the records through 2003. The current world record for factoring is 663 bits; a German team (Bahr, Boehm,

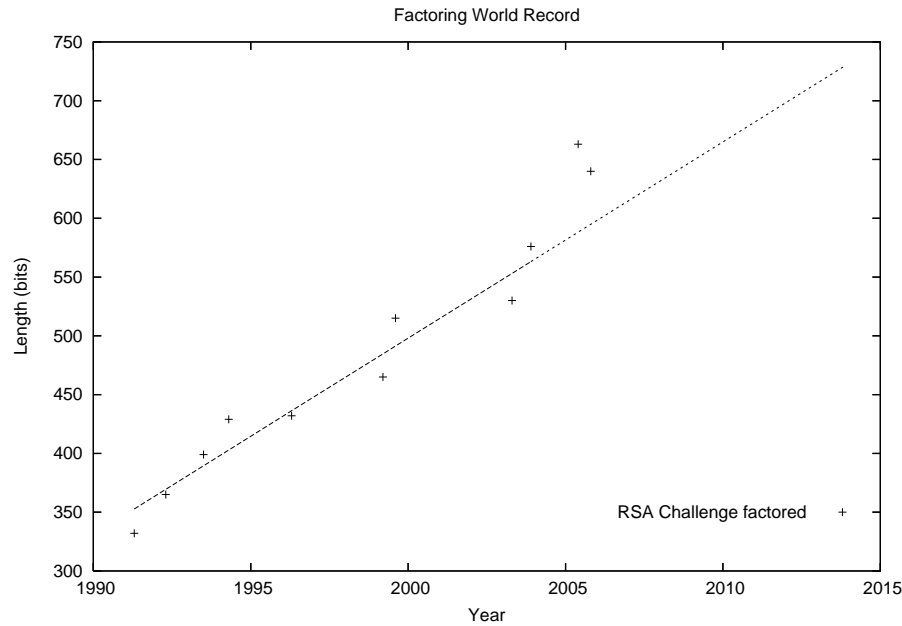


Figure 3.1: Length of RSA Challenge numbers successfully factored, in bits, plotted versus date accomplished.

Franke, and Keinjung) announced the factoring of the RSA-200 challenge number in May, 2005. This data point appears to be an anomalously large leap; whether it represents a shift in the long-term trend remains to be seen. Cavallar et al. estimated in 2000 that a 768-bit RSA key will be factored by 2010, and a 1024-bit one by 2018 [67]; progress appears to be on track to meet those predictions. Lenstra et al. have also noted that NFS scales well to large numbers of parallel processors and is amenable to custom hardware acceleration; they suggest that a machine that could factor a 1,024-bit number in one year could be built for US\$10M using 2003 technology [203]. It may be possible to use an Internet-scale distributed system, such as the Berkeley Open Infrastructure for Network Computing (BOINC), to attack this problem [150, 19]. BOINC, upon which SETI@home is based, has the potential to manage 100,000 or more nodes simultaneously attacking the same problem, a 1,000-fold increase over the size of systems deployed to date on factoring problems. We can infer that, at this point, moderately large jumps in factoring records are primarily a matter of commitment of resources.

The execution time to factor a number using NFS on a set of on classical computers is shown in Figure 3.2. The left curve is extrapolated performance based on the previous world record, factoring a 530-bit number in one month, established using 104 PCs and workstations made in 2003 [283]. The right curve is speculative performance using 1,000 times as much computing power. This could be 100,000 PCs in 2003, or, based

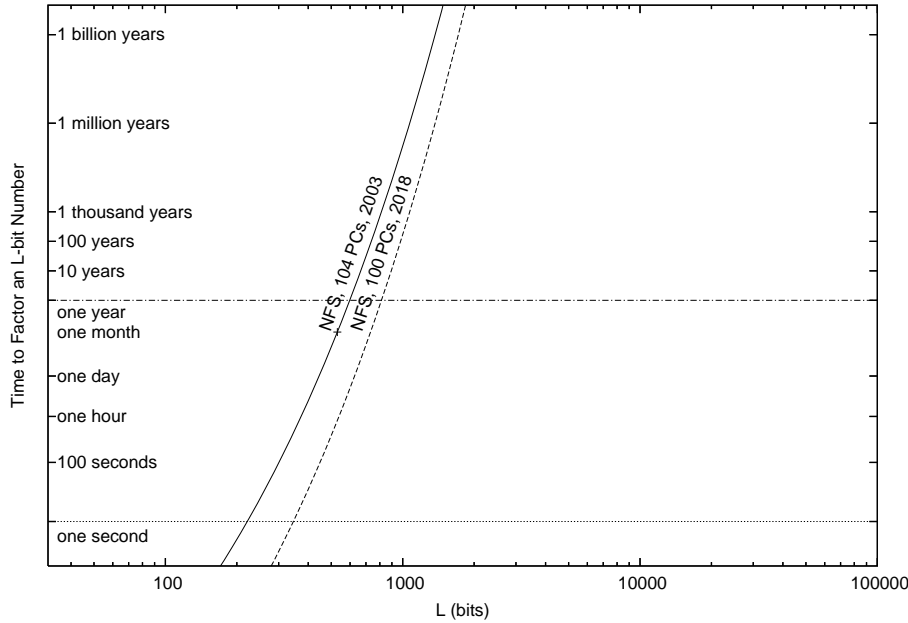


Figure 3.2: Scaling of number field sieve (NFS) on classical computers. Both horizontal and vertical axes are log scale. The horizontal axis is the size of the number being factored, in bits.

on Moore's law, 100 PCs in 2018. From these curves it is easy to see that Moore's law has only a modest effect on our ability to factor large numbers. Factoring a 1,000-bit number is only a matter of time, but a 2,000-bit number awaits either some theoretical advance or the advent of large-scale quantum computers.

3.3 The Quantum Fourier Transform

We have noted several times that quantum parallelism effectively calculates exponentially many functions at the same time, but that the difficulty lies in extracting useful information from the superposition of results. Shor's remarkable insight showed the path to creating a desirable superposition by interfering periodic elements. Some problems exhibit periodicity in their results, but with a changing offset from zero. Classically, one method for finding a period in such an environment is to Fourier transform the data, which eliminates phase (the offset) and leaves the frequency (or period) information.

The quantum Fourier transform (QFT) transforms each individual basis state in the

r	input α_j								output β_k								L/r
	$j = 0$	1	2	3	4	5	6	7	$k = 0$	1	2	3	4	5	6	7	
8	1	0	0	0	0	0	0	0	1	1	1	1	1	1	1	1	1
4	1	0	0	0	1	0	0	0	1	0	1	0	1	0	1	0	2
2	1	0	1	0	1	0	1	0	1	0	0	0	1	0	0	0	4
1	1	1	1	1	1	1	1	1	1	0	0	0	0	0	0	0	8

Table 3.1: Transform values of the coefficients in the QFT.

following way:

$$|j\rangle \xrightarrow{\text{QFT}} \frac{1}{\sqrt{L}} \sum_{k=0}^{L-1} e^{2\pi i j k / L} |k\rangle \quad (3.5)$$

where L is 2^l , and l is the length of our state in bits. Writing out the entire transform for $l = 3$ and letting $\omega = e^{2\pi i / 8} = \sqrt{i}$, we have

$$\frac{1}{\sqrt{8}} \begin{bmatrix} 1 & 1 & 1 & 1 & 1 & 1 & 1 & 1 \\ 1 & \omega & \omega^2 & \omega^3 & \omega^4 & \omega^5 & \omega^6 & \omega^7 \\ 1 & \omega^2 & \omega^4 & \omega^6 & 1 & \omega^2 & \omega^4 & \omega^6 \\ 1 & \omega^3 & \omega^6 & \omega & \omega^4 & \omega^7 & \omega^2 & \omega^5 \\ 1 & \omega^4 & 1 & \omega^4 & 1 & \omega^4 & 1 & \omega^4 \\ 1 & \omega^5 & \omega^2 & \omega^7 & \omega^4 & \omega & \omega^6 & \omega^3 \\ 1 & \omega^6 & \omega^4 & \omega^2 & 1 & \omega^6 & \omega^4 & \omega^2 \\ 1 & \omega^7 & \omega^6 & \omega^5 & \omega^4 & \omega^3 & \omega^2 & \omega \end{bmatrix}. \quad (3.6)$$

Let us look at the input and output of the QFT in more detail ¹. In Table 3.1, α_j are the coefficients of the values j in the input superposition $\sum \alpha_j |j\rangle$. β_k are the coefficients in the output superposition. The top left entry, for example, has a one in the leftmost α_j column, corresponding to the state $|0\rangle$. The next line includes $|0\rangle$ and $|4\rangle$, corresponding to the two ones. r is the period of repetition, that is, how often ones appear in the fully-written-out superposition. The table can be used, for example, to see the following transformation:

$$\frac{1}{\sqrt{2}}(|0\rangle + |4\rangle) \xrightarrow{\text{QFT}} \frac{1}{2}(|0\rangle + |2\rangle + |4\rangle + |6\rangle) \quad (3.7)$$

What happens if the values in the superposition are period four, but not $|0\rangle$ and $|4\rangle$, perhaps being $|1\rangle$ and $|5\rangle$ instead? Such an offset difference shows up in a difference in

¹These examples are borrowed from Lieven Vandersypen's thesis [339].

input α_j								output β_k							
$j = 0$	1	2	3	4	5	6	7	$k = 0$	1	2	3	4	5	6	7
1	0	0	0	1	0	0	0	1	0	1	0	1	0	1	0
0	1	0	0	0	1	0	0	1	0	i	0	-1	0	$-i$	0
0	0	1	0	0	0	1	0	1	0	-1	0	1	0	-1	0
0	0	0	1	0	0	0	1	1	0	$-i$	0	-1	0	i	0

Table 3.2: Transform of different offsets into phase via the QFT.

the *phase* of the output, as shown in Table 3.2, giving e.g.

$$\frac{1}{\sqrt{2}}(|1\rangle + |5\rangle) \xrightarrow{\text{QFT}} \frac{1}{2}(|0\rangle + i|2\rangle - |4\rangle - i|6\rangle). \quad (3.8)$$

After the transform, *all* of the period four superpositions will have an equal chance of returning 0, 2, 4, or 6 when the register is measured, regardless of their original input values (this discarding of offset or phase is a characteristic of the classical Fourier transform, as well).

Thus, when we have an unknown superposition that we suspect consists of some terms $|j\rangle$ where the j s have a periodic relationship, the quantum Fourier transform will allow us to extract that period. Shor has used quantum interference to cause undesirable terms to cancel when transformed. This remarkable result concentrates portions of our total probability into superposition terms that tell us something useful about the entire superposition when measured, holding out the tantalizing possibility of an exponential increase in computational power.

Shor built on work by Simon to develop his algorithm [299]. Many researchers have examined the QFT in more detail, including describing how to implement it, and discussing the necessity of exponentially small rotations in the low-order bits [31, 69, 80, 82, 141, 332, 121]. We will leave off discussing the QFT, and move on to arithmetic, which we also need for Shor's algorithm.

3.4 Prior Art in Quantum Adders

Shor's factoring algorithm depends on the creation of a superposition consisting of the modular integer exponentiation of a randomly-chosen number x raised to all powers 0 to $2^{2n} - 1$, for an n -bit number. Exponentiation, of course, depends on integer multiplication, which in turn depends on addition. In this section we will review several types of quantum adders developed by other researchers, which will be used to construct the

complete modular exponentiation in the following section.

Classically, engineers have found many ways of building adders and multipliers; choosing the correct one is a technology-dependent exercise [109]. The performance of an adder depends primarily on how quickly the information about the carry can propagate from bit to bit. The most obvious methods result in latency that is linear in the number of bits to be added, but more complex techniques can reduce that to $O(\sqrt{n})$ or even $O(\log n)$. Classical multipliers are usually built by deferring the carry calculation, allowing the n additions necessary for a multiplication to be completed in much less than n times the latency of an individual adder; we will see below that this is less attractive for quantum arithmetic. Only a few of these classical techniques have been explored for quantum computation. We review these circuits in this chapter. For our purposes, we need only unsigned integer arithmetic, so the standard unsigned integer representation is used.

We begin by explaining our notation for performance, then analyze progressively faster types of adders developed by other researchers, saving the presentation of my new adder types for Section 6.3. Rather than the details of why these circuits work, we are more interested in how to implement them and evaluate their performance.

3.4.1 Arithmetic Performance Notation

We express the circuit cost using the notation (CCNOTs; CNOTs; NOTs) or (CNOTs; NOTs). The values may be total gates or circuit depth (latency), depending on context. The notation is sometimes enhanced to show required concurrency and space, (CCNOTs; CNOTs; NOTs) $\#(\text{concurrency; space})$.

t is time, or latency to execute an algorithm, and S is space, subscripted with the name of the algorithm or circuit subroutine. When t or S is superscripted with AC or NTC, the values are for the latency of the construct on that architecture, as described in Section 6.1.2. Equations without superscripts are for an abstract machine assuming no concurrency. R is the number of calls to a subroutine, subscripted with the name of the routine.

3.4.2 Linear-Time Adders

The two most commonly cited modular exponentiation algorithms are those of Vedral, Barenco, and Ekert [342], which we will refer to as VBE, and Beckman, Chari, Devabhaktuni, and Preskill [35], which we will refer to as BCDP. Both the BCDP and VBE

algorithms build multipliers from variants of carry-ripple adders, the simplest but slowest method. Draper designed an adder that acts in the Fourier transform space whose principal advantage is its smaller size [102]. Cuccaro, Draper, Kutin and Moulton have more recently shown the design of a smaller, faster carry-ripple adder, which we call (CDKM) [88], which appears to make the Fourier adder obsolete.

VBE Carry-Ripple

We use the VBE adder in several of our algorithmic variants described in Chapter 6. In this algorithm, the values to be added in (the convolution partial products of x^a , in the overall modular exponentiation) are programmed into a temporary register (combined with a superposition of $|0\rangle$ as necessary) based on a control line and a data bit via appropriate CCNOT gates. Here we examine just the adder itself.

The latency of ADDER², assuming *no* concurrent gate execution, is

$$t_{ADD} = (4n - 4; 4n - 3; 0) \# (1; 3n) \quad (3.9)$$

that is, $4n - 4$ CCNOT times plus $4n - 3$ CNOT times and zero NOT times, executing only one gate at a time and using $3n$ qubits. Since we are assuming no concurrent gate operations, this value is the same as the total number of gates in the circuit. In Figure 3.3, we have drawn the circuit with multiple gates being executed in some time slots; the actual expression for the performance of the circuit as drawn is

$$t_{ADD}^{AC} = (3n - 3; 2n - 3; 0) \# (3; 3n) \quad (3.10)$$

It requires that at least 3 gates can be executed concurrently in order to meet the performance specified, and uses $3n$ qubits during the calculation. These numbers are calculated assuming that gates on independent qubits can be executed concurrently, and that CCNOTs take longer to execute than CNOTs.

Figure 3.3 shows the circuit for an eight-bit VBE adder, adding the A and B registers, with the C register used as temporary variables that begin in the zero state and must be returned to that state at the end. The graphical notation used for quantum circuits is a superset of the classical reversible notation introduced in Figure 2.1 on page 23; we will introduce new gates as necessary. The structure of the circuit is straightforward.

²When we write ADDER in all capital letters, we mean the complete VBE n -bit construction, with the necessary undo; when we write adder in small letters, we are usually referring to a smaller or generic circuit block.

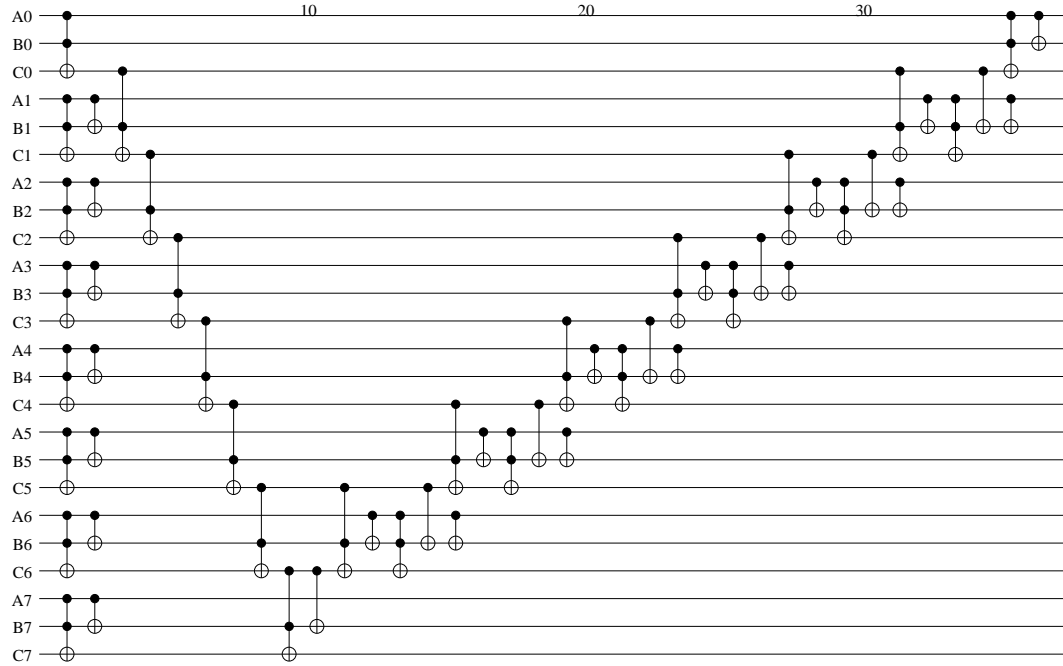


Figure 3.3: An eight-bit VBE adder.

Along the left-hand edge, all of the partial sums are computed concurrently (as drawn, the concurrency used is n , but it is easy to see that doing the partial sums in a “just in time” fashion would result in a concurrency of 3). Next, descending from the top edge, we see a chain of CCNOT gates; these propagate the carry from one bit to the next. The entire latter two-thirds of the circuit cleans up the ancillae we have used, leaving the A register in its original state and the B register containing the eight-bit value $A + B$, with $C7$ the output carry. The numbers across the top of the diagram are clock cycles. These numbers are counted assuming that all gates require the same amount of time, which is not the case in most systems, so the numbers should be treated as a guideline rather than an actual performance figure.

Murali et al. experimentally demonstrated a half-adder subunit of the VBE carry-ripple on an NMR system [239]. This experiment and the NMR implementation of Shor’s algorithm to factor the number fifteen [340] are, to the best of my knowledge, the only experimental demonstrations of quantum arithmetic circuits.

BCDP Carry-Ripple

The BCDP algorithm is also based on a carry-ripple adder. It differs from VBE in that it more aggressively takes advantage of classical computation, adding a classical number into the register conditional on a quantum enable bit. However, for our purposes, this

makes it harder to use some of the optimization techniques presented in later chapters. Beckman et al. present several optimizations and tradeoffs of space and time, slightly complicating the analysis. The latency of their adder is

$$t_{OADDN} = (6n - 2; 2n; 2) \quad (3.11)$$

which, assuming CCNOT gates are slower than CNOTs, is slower than the VBE adder.

Gossett Carry-Ripple

Shortly after the publication of the VBE and BCDP algorithms, Gossett realized that it is possible to do much better than carry-ripple arithmetic, drawing on the important classical Boolean techniques of *carry-save arithmetic* [130]. Gossett does not provide a full modular exponentiation circuit, only adders, multipliers, and a modular adder. Carry-save arithmetic is particularly well suited to incorporation into a larger multiplier structure, but in this case a large penalty in the number of qubits required must be paid. Unfortunately, the paper's secondary contribution, Gossett's carry-ripple adder, as drawn in his figure 7, seems to be incorrect. Once fixed, his circuit optimizes to be similar to VBE.

Draper QFT-based Adder

Draper developed a clever method for doing addition on Fourier-transformed representations of numbers [102]. It uses only $2n$ qubits, but it requires n concurrent gates. Moreover, the comparison operations necessary for modular arithmetic are difficult in the Fourier space, necessitating frequent transformation of the representation between integer and Fourier forms. The accuracy required in the gate rotations is very high, which may be difficult to achieve. Finally, although the latency is $O(n)$, I believe the constant factors to actually implementing this circuit on encoded logical states will be large, making it ultimately an unattractive option for most purposes.

CDKM Carry-Ripple

Cuccaro et al. have recently introduced a carry-ripple circuit, which we will call CDKM, which uses only a single ancilla qubit [88]. The authors do not present a complete modular exponentiation circuit; we will use their adder in our algorithms **F**

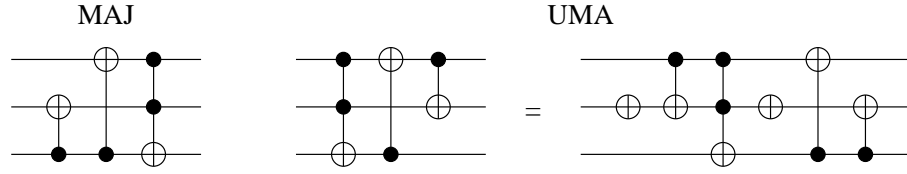


Figure 3.4: Building blocks for the CDKM adder.

and **G** (Section 6.4). This adder, we will see in section 6.4.3, is the most efficient known for some architectures.

Figure 3.4 shows the building blocks of the CDKM adder. MAJ is the majority function; the bottom qubit winds up holding zero if two or three of the bits are zero, and one if two or three of the bits are one. It is the basis of the carry calculation chain. UMA is unmajority and add, undoing the MAJ calculation while turning the middle bit into the correct, carry-adjusted final sum. Two ways to construct the UMA function are shown. A full adder circuit is illustrated in Figure 3.5, using the right-hand construct for UMA, which is more gates than the left-hand construct but can be pipelined more effectively, overlapping the execution of multiple gates and reducing the total latency.

The latency of their adder is

$$t_{CDKM} = (2n - 1; 5; 0) \# (6; 2n + 2). \quad (3.12)$$

This circuit uses only $2n + 2$ qubits and runs perhaps one and a half times as fast as the VBE adder (again, depending on implementation details), but requires higher concurrency in gate operations. This factor affects the performance of the distributed forms of our algorithms, presented in Section 7.5.

3.4.3 $O(\log n)$ Adders

Carry-save, carry-lookahead and conditional-sum (see Sec. 6.3.3) are all adder types that reach $O(\log n)$ performance by deferring carry computation or by communicating the carry to distant parts of the circuit more rapidly.

Gossett Carry-Save

Gossett’s arithmetic is pure quantum, as opposed to the mixed classical-quantum of BCDP. Gossett’s carry-save adder [130], the primary contribution of the paper, can run in $O(\log n)$ time. More importantly, carry-save adders are designed to combine well

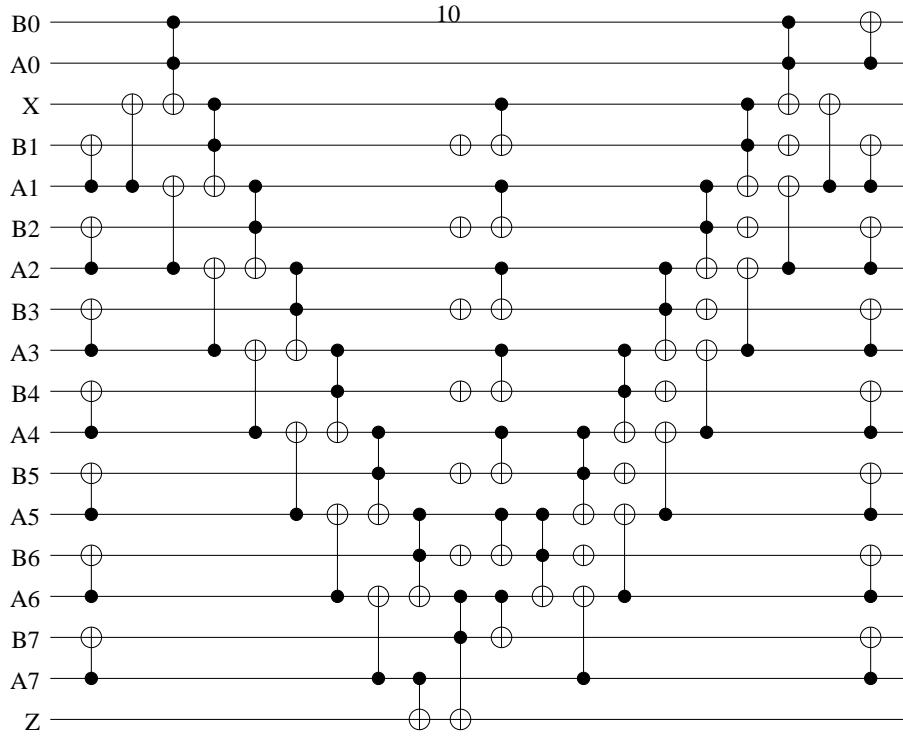


Figure 3.5: An eight-bit CDKM adder. X is a temporary variable, and Z is the carry out.

into fast multiplier circuits. However, such a circuit will remain impractical for the foreseeable future due to the large number of qubits required; Gossett estimates $8n^2$ qubits for a full multiplier, which would run in $O(\log^2 n)$ time. It bears further analysis because of its high speed and resemblance to standard fast classical multipliers.

Carry-Lookahead

Draper, Kutin, Rains, and Svore have recently designed a carry-lookahead adder, which we call QCLA [103]. This method allows the latency of an adder to drop to $O(\log n)$. The latency and storage of their adder is

$$t_{LA} = (4 \log_2 n + 3; 4; 2) \# (n; 4n - \log n - 1). \quad (3.13)$$

This circuit is illustrated in Figure 3.6. Although an eight-bit carry-lookahead adder is not faster than a CDKM carry-ripple adder, the logarithmic advantage quickly becomes apparent as n grows. When looking at this figure, it is immediately obvious that the circuit is denser than the carry-ripple adders. All quantum carry-ripple adders exhibit

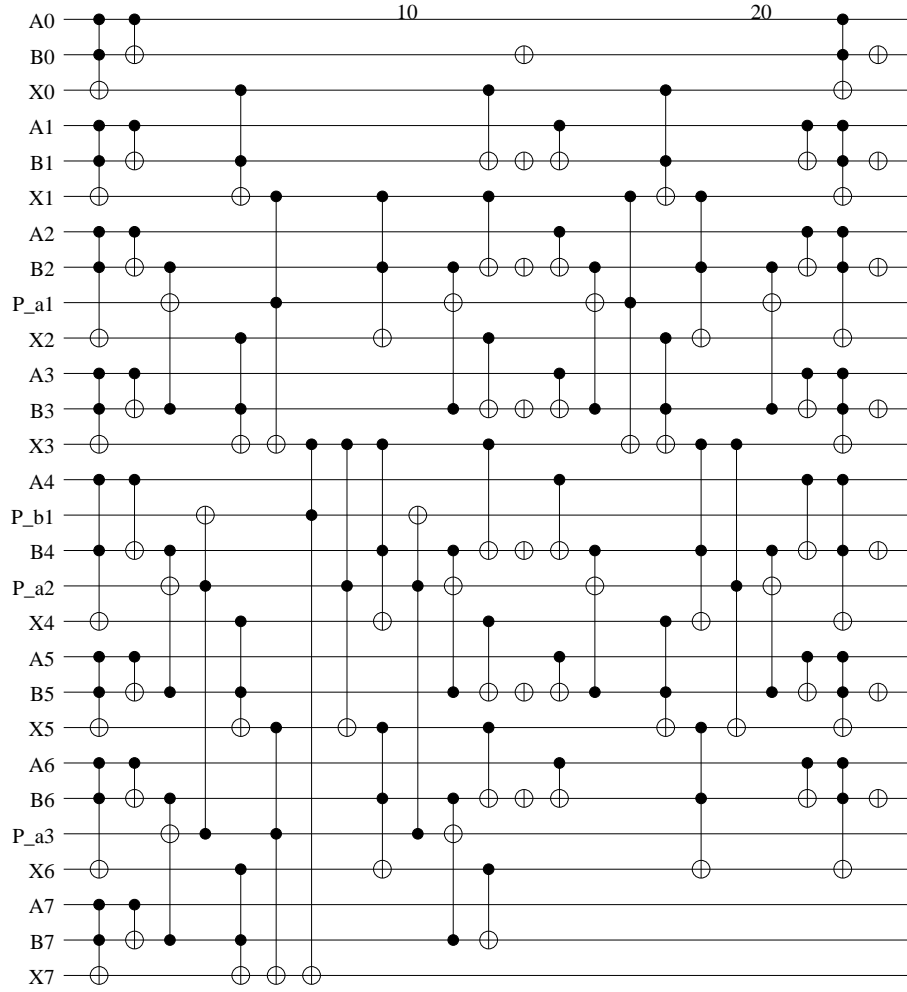


Figure 3.6: An eight-bit carry-lookahead adder.

a “V” shape in which many of the qubits sit idle for long periods while the carry propagates down and back the length of the register. In the carry-lookahead adder, various carry signals leapfrog up and down the register, with the overall state gradually converging on the correct value. In the figure, this leapfrogging is illustrated by gates that stretch is much as half the height of the total circuit. We will see shortly that such gates are not always practical, and that this issue will place limits on our achievable performance.

3.4.4 Ultimate Limits on Performance of Addition

The performance of any circuit must be specified with respect to a particular architecture. Architectural assumptions are implied in the numbers provided throughout this chapter; we will detail these more carefully in Section 6.4.

Engineers tend to use the $O(\cdot)$ notation more loosely than theorists. The behavior of an algorithm is generally understood to hold only for a particular range of problem size, or as long as a certain set of assumptions holds. In particular, signal propagation times are often approximated to be zero, an assumption which clearly does not hold indefinitely. *All* algorithms which require any signal to propagate to all parts of a computation are ultimately limited to $O(\sqrt[3]{n})$ for any system in which bits occupy a finite volume, as the signal propagation is constrained to the finite speed of light and bits can only be packed in three dimensions. This constraint holds for addition; our assertion above that certain adders can reach $O(\log n)$ performance holds only until signal propagation effects come into play. We will present the system behavior for more realistic conditions when we discuss both monolithic and distributed computation.

3.4.5 Summary

Recent focus on quantum arithmetic has provided a bounty of new reversible addition algorithms. With the exception of Draper's quantum Fourier transform-based adder, all of the adder circuits we have just presented will benefit classical reversible logic, as well. In Boolean logic, the carry-ripple adder is so straightforward that there are not many distinctions to be made. In the reversible and quantum arenas, we now have the VBE, BCDP, and CDKM carry-ripple circuits, using different numbers of ancillae qubits and having different performance characteristics. We also have various more complex adder circuits that reach square-root or logarithmic depth instead of the linear depth of carry-ripple. These faster circuits include the carry-save adder, the carry-lookahead adder, and my two circuits, the conditional-sum and carry-select adders, which we will see in Section 6.3. All of these adders except the carry-ripple ones require qubits that are some distance apart to interact. Classically, the choice of adder circuit in modern systems is made not based on actual gate count, but on the time and space required for the wiring to connect the bits; this approach will inevitably be necessary in quantum computing, as well.

Integer arithmetic, of course, is the foundation of all computer arithmetic, but has been extended in many ways to make more complex functions, including integer multiplication and floating-point arithmetic. Research into these areas for reversible logic remains very basic. The next section introduces two methods for composing the complete quantum modular exponentiation, and several optimizations, but multiplication is still created by serial execution of addition.

3.5 Quantum Modular Exponentiation

We now come to the part of the algorithm most relevant to this thesis. The modular exponentiation of a random integer is the most computationally intensive portion of Shor's algorithm, and is our benchmark for the behavior of our quantum multicomputer. These algorithms are introduced here and improved throughout Chapter 6.

To factor the number N using Shor's algorithm [296], a quantum computing device must evolve to hold the state

$$\frac{1}{2^n} \sum_{a=0}^{2^{2n}-1} |a\rangle |x^a \bmod N\rangle. \quad (3.14)$$

for a randomly chosen, fixed x , where n is the bit length of N . $|a\rangle$ is the register that holds the superposition of all values $0..2^{2n} - 1$, created by applying a Hadamard gate to each qubit in $|a\rangle$. Depending on the algorithm chosen for modular exponentiation, x may appear explicitly in a register in the quantum computer, or may appear only implicitly in the choice of instructions to be executed.

In general, quantum modular exponentiation algorithms are created from building blocks that do modular multiplication,

$$|\alpha\rangle|0\rangle \rightarrow |\alpha\rangle|\alpha\beta \bmod N\rangle \quad (3.15)$$

where β and N may or may not appear explicitly in quantum registers. This modular multiplication is built from blocks that perform modular addition,

$$|\alpha\rangle|0\rangle \rightarrow |\alpha\rangle|\alpha + \beta \bmod N\rangle \quad (3.16)$$

which, in turn, are usually built from blocks that perform addition and comparison.

In most modular exponentiation algorithms, the multiplication step is performed $2n$ times, once for each bit in the register $|a\rangle$ [342, 35]. The running product is multiplied by a value held in a quantum register. That value is either 1, if the corresponding bit of $|a\rangle$ is zero, or x^{2^i} , if the corresponding bit is one. Let $d_i = x^{2^i}$, and $a_{n-1}a_{n-2}..a_0$ be the binary expansion of a . The d_i can be calculated classically, but $|a\rangle$ is a quantum register. The value $x^a \bmod N$ can be rewritten [191, 342] as

$$\prod_{j=0}^{2n} d_j^{a_j} \bmod N. \quad (3.17)$$

Fundamentally, quantum modular exponentiation is $O(n^3)$; that is, the number of quantum gates or operations scales with the cube of the length in bits of the number to be factored [296, 342, 35]. It consists of $2n$ modular multiplications, each of which consists of $O(n)$ additions, each of which requires $O(n)$ operations. However, $O(n^3)$ operations do not necessarily require $O(n^3)$ time steps. On an abstract machine, it is relatively straightforward to see how to reduce each of those three layers to $O(\log n)$ time steps, in exchange for more space and more *total* gates, giving a total running time of $O(\log^3 n)$ if $O(n^3)$ qubits are available and an arbitrary number of gates can be executed concurrently on separate qubits. Such large numbers of qubits are not expected to be practical for the foreseeable future, so much interesting engineering lies in optimizing for a given set of constraints.

3.5.1 VBE, BCDP and Others

Both the VBE and BCDP algorithms construct modular multiplication from a straightforward series of modular additions. Each modular addition is performed by adding in the chosen number, comparing to N to see if the result has overflowed, and subtracting N if so. This method results in a large number of additions and subtractions, which can easily be reduced, as will be demonstrated in Chapter 6.

The VBE algorithm [342] builds full modular exponentiation from smaller building blocks. The bulk of the time is spent in $20n^2 - 5n$ calls to ADDER. The full circuit requires $7n + 1$ qubits of storage: $2n + 1$ for a , n for the other multiplicand, n for a running sum, n for the convolution products, n for a copy of N , and n for carries.

In this algorithm, the values to be added in, the convolution partial products of x^a , are programmed into a temporary register (combined with a superposition of $|0\rangle$ as necessary) based on a control line and a data bit via appropriate CCNOT gates. The latency t_V of the complete VBE algorithm is

$$\begin{aligned} t_V &= (20n^2 - 5n)t_{ADD} \\ &= (80n^3 - 100n^2 + 20n; 96n^3 - 84n^2 + 15n; \\ &\quad 8n^2 - 2n + 1). \end{aligned} \tag{3.18}$$

The BCDP algorithm is similar in structure to VBE, but uses more complicated gates and presents numerous engineering tradeoffs. Borrowing from their equation

6.23, the latency t_B of the complete BCDP algorithm is

$$\begin{aligned} t_B = & (54n^3 - 127n^2 + 108n - 29; \\ & 10n^3 + 15n^2 - 38n + 14; \\ & 20n^3 - 38n^2 + 22n - 4). \end{aligned} \quad (3.19)$$

The exact sequence of gates to be applied is also dependent on the input values of N and x , saving space but making it less suitable for hardware implementation with fixed gates (e.g., in an optical system). In the form we analyze, it requires $5n + 3$ qubits, including $2n + 1$ for $|a\rangle$.

Beauregard has designed a circuit for doing modular exponentiation in only $2n + 3$ qubits of space [34], based on Draper's clever method for doing addition on Fourier-transformed representations of numbers [102]. The depth of Beauregard's circuit is $O(n^3)$, the same as VBE and BCDP. However, we believe the constant factors on this circuit are very large; every modulo addition consists of four Fourier transforms and five Fourier additions. Moreover, its primary advantage, reduction of the scratch space used in addition, has been partially nullified by the development of a carry-ripple adder that likewise uses only $2n + 1$ qubits [88].

Fowler, Devitt, and Hollenberg have simulated Shor's algorithm using Beauregard's algorithm, for a class of machine they call *linear nearest neighbor* (LNN) [119, 95]. LNN corresponds approximately to our NTC. In their implementation of the algorithm, they found no significant change in the computational complexity of the algorithm on LNN or an AC-like abstract architecture, suggesting that the performance of Draper's adder, like a carry-ripple adder, is essentially architecture-independent.

3.5.2 Cleve-Watrous Parallel Multiplication

Modular exponentiation is often drawn as a string of modular multiplications, but Cleve and Watrous pointed out that these can easily be parallelized, at linear cost in space [80]. We always have to execute $2n$ multiplications; the goal is to do them in as few time-delays as possible.

To go (almost) twice as fast, use two multipliers. For four times, use four. Naturally, this can be built up to n multipliers to multiply the necessary $2n + 1$ numbers, in which case a tree recombining the partial results requires $\log_2 n$ quantum-quantum (Q-Q) multiplier latency times, as shown in Figure 3.8. We will analyze this method in

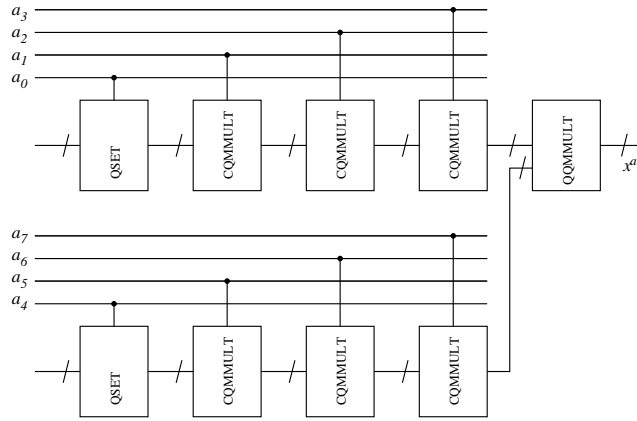


Figure 3.7: Concurrent modular multiplication in modular exponentiation using two multipliers. QSET simply sets the sum register to the appropriate value.

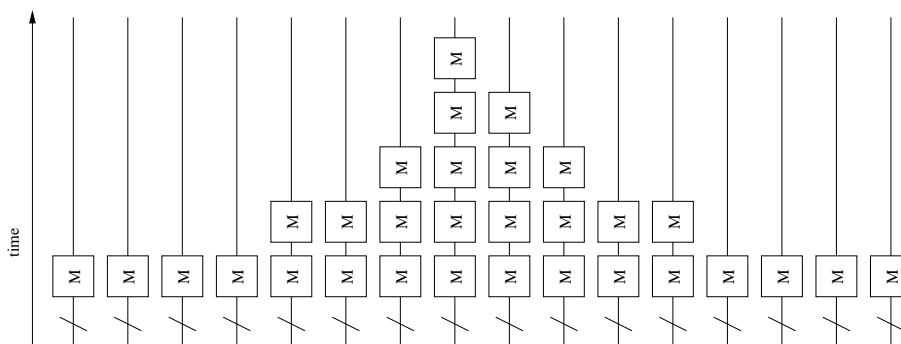


Figure 3.8: Cleve-Watrous parallel multiplication (rotated ninety degrees relative to other graphs, with time flowing bottom to top).

more detail in Section 6.4.2.

3.5.3 Schönhage-Strassen

The Schönhage-Strassen multiplication algorithm is often quoted in quantum computing research as being $O(n \log n \log \log n)$ in complexity for a single multiplication [362, 187]. However, simply citing Schönhage-Strassen without further qualification is misleading for several reasons. Most importantly, the constant factors matter. Shor noted this in his original paper, without explicitly specifying a bound. Quantum modular exponentiation based on Schönhage-Strassen is only faster than basic $O(n^3)$ algorithms for more than approximately 32 *kilobits*³. In this thesis, we will concentrate on smaller problem sizes, and exact, rather than $O(\cdot)$, performance. Note also that this bound is for a Turing machine; a random-access machine can reach $O(n \log n)$ using Schönhage-Strassen.

3.6 Shor's Algorithm

Finally, we come to Shor's factoring algorithm itself. The algorithm consists of both classical and quantum portions, with the quantum portion being a period-finding method based on the QFT and arithmetic to calculate the modular exponentiation of two integers. The period-finding method operates on two quantum registers, the control register and the function result register; in the end, we will actually measure the *control* register to find the period of the function (this is perhaps the most counter-intuitive feature of the algorithm).

To factor a number N whose length is n bits, we begin by checking that the number is not even and determining that it not an integer power, a^b , for $a \geq 1$ and $b > 2$. Efficient classical methods are known for this calculation and for finding the greatest common divisor (gcd), which we will not present. Next, choose an integer $2 < x < N$, and check that $\gcd(x, N) = 1$; if not, return $\gcd(x, N)$. The value of x need not be strictly random, but is not important except that repeating the algorithm after a failure sometimes requires that x be changed.

Next, use the quantum period-finding method to determine the order r of x modulo N . If r is even and $x^{r/2} \not\equiv -1 \pmod{N}$, calculate $\gcd(x^{r/2} - 1, N)$ and $\gcd(x^{r/2} + 1, N)$.

³Zalka found that his approach would be faster for 8kilobits, using a slightly different set of assumptions.

One of these should be a factor of N . If not, or if r is odd, repeat the algorithm, choosing a different x .

The order of x modulo N is found by noting that we can calculate the modular exponentiation $x^a \bmod N$ for all a . We use two quantum registers, which will hold, respectively, a and $x^a \bmod N$. The register for a must be $2n$ qubits long. Starting from the state

$$\frac{1}{2^L} \sum_{a=0}^{2^{2L}-1} |a\rangle|1\rangle \quad (3.20)$$

in which all of the qubits are disentangled, the modular exponentiation then produces the state

$$\frac{1}{2^L} \sum_{a=0}^{2^{2L}-1} |a\rangle|x^a \bmod N\rangle. \quad (3.21)$$

Once we have that entangled state [167], we apply the QFT *to the first register*, measure both registers, and use the value in the first register (discarding the second) to find the order of x modulo N , and from there the factors of N .

How the QFT creates a state that can tell us the order of the function is mysterious, almost spooky, and certainly difficult to grasp. To make this more concrete, let's look at an example. 15 is the smallest number upon which Shor's algorithm works properly, and we will choose $x = 7$ as a good example. For reasons we won't go into here, we really need at least one bit more in our a register than the length of N itself, but we will restrict ourselves to four bits for a to keep the size of the example manageable. This gives us

$$\begin{aligned} \frac{1}{4} \sum_{a=0}^{15} |a\rangle|x^a \bmod N\rangle &= \frac{1}{4}(|0\rangle|1\rangle + |1\rangle|7\rangle + |2\rangle|4\rangle + |3\rangle|13\rangle \\ &\quad + |4\rangle|1\rangle + |5\rangle|7\rangle + |6\rangle|4\rangle + |7\rangle|13\rangle \\ &\quad + |8\rangle|1\rangle + |9\rangle|7\rangle + |10\rangle|4\rangle + |11\rangle|13\rangle \\ &\quad + |12\rangle|1\rangle + |13\rangle|7\rangle + |14\rangle|4\rangle + |15\rangle|13\rangle) \\ &= \frac{1}{4}((|0\rangle + |4\rangle + |8\rangle + |12\rangle)|1\rangle \\ &\quad + (|1\rangle + |5\rangle + |9\rangle + |13\rangle)|7\rangle \\ &\quad + (|2\rangle + |6\rangle + |10\rangle + |14\rangle)|4\rangle \\ &\quad + (|3\rangle + |7\rangle + |11\rangle + |15\rangle)|13\rangle). \end{aligned} \quad (3.22)$$

The second form makes it clear that what we have accomplished so far is to *group the*

values of a based on $x^a \bmod N$. Each of these groups – 0-4-8-12, 1-5-9-13, etc. – has elements that skip four values, but with an offset that differs from group to group. This information – the length of that stride between elements of the superposition in each group – is what will allow us to find the order. But how can we extract that piece of information?

If we were to apply the QFT to our original raw a register $\frac{1}{4} \sum_{a=0}^{15} |a\rangle$, the result would simply be $|0\rangle$. The grouping created by the modular exponentiation now creates sets of elements that can effectively be Fourier transformed independently. The Fourier transform, as noted, eliminates the offset, “hiding” it in the phase of the elements of the superposition and leaving the frequency components in the numeric values. The QFT of Equation 3.22 is

$$\begin{aligned}
 & \text{QFT}\left(\frac{1}{4}(|0\rangle + |4\rangle + |8\rangle + |12\rangle)|1\rangle\right. \\
 & \quad + (|1\rangle + |5\rangle + |9\rangle + |13\rangle)|7\rangle \\
 & \quad + (|2\rangle + |6\rangle + |10\rangle + |14\rangle)|4\rangle \\
 & \quad \left. + (|3\rangle + |7\rangle + |11\rangle + |15\rangle)|13\rangle\right) \\
 & = \left(\frac{1}{4}(|0\rangle + |4\rangle + |8\rangle + |12\rangle)|1\rangle\right. \\
 & \quad + (|0\rangle + i|4\rangle - |8\rangle - i|12\rangle)|7\rangle \\
 & \quad + (|0\rangle - |4\rangle + |8\rangle - |12\rangle)|4\rangle \\
 & \quad \left. + (|0\rangle - i|4\rangle - |8\rangle + i|12\rangle)|13\rangle\right). \tag{3.23}
 \end{aligned}$$

Now, when we measure the two registers, we will always find one of 0, 4, 8, or 12 in the first register, with equal probability. If we find 0, the algorithm has failed and we must repeat. Otherwise, we use the number found as r , and apply Euclid’s algorithm for finding greatest common denominators to find the GCD of N and $x^{r/2} - 1$, and of N and $x^{r/2} + 1$, as described above.

3.7 Summary

In this chapter, we have introduced Shor’s algorithm for factoring large numbers, and discussed its significance. The creation of a machine that executes Shor’s algorithm would have implications for security on the Internet, breaking the widely-used RSA public-key crypto system. Most of the tasks assigned to RSA can be accomplished

via other mechanisms, including symmetric, private-key encryption, but such solutions may be less efficient in using resources both locally and globally [289].

Shor's algorithm rests on the breakthrough insight that certain functions produce the same results for inputs that are separated by a specific period, and that the quantum Fourier transform can extract that period efficiently. For factoring large composite integers, the function of interest is the exponentiation of a random number modulo N , the number to be factored. The modular exponentiation is constructed in a straightforward fashion from integer addition and comparison, and we saw various circuits for addition. We will see in later chapters how to implement these operations efficiently; we turn next to a taxonomy of quantum computing technologies which might be used to build systems on which Shor's algorithm can be run.

Chapter 4

A Taxonomy of Quantum Computing Technologies

In this chapter we present a classification scheme for quantum computing technologies, based on the characteristics most relevant to computer systems architecture, and apply it to analyze several candidate technologies. This taxonomy is complementary to the DiVincenzo criteria introduced in Section 2.2. Whereas the DiVincenzo criteria help define whether or not it is *possible* to build a quantum computer based on the specified technology, in our taxonomy we are concerned with whether or not it is *practical*. This taxonomy will be used in our definition of a scalable system (Section 7.2), and the performance-relevant portions will affect our analysis of systems throughout the remainder of this thesis. We will describe each criterion as well as some of its high-level architectural implications. In the last section, we will use this taxonomy to evaluate several proposed computing technologies.

4.1 Taxonomy Framework

4.1.1 Basic Features

Stationary, flying and mobile: Quantum computing technologies can be divided into two categories: those in which the qubits are represented by constantly moving phenomena (photons) and those in which qubits are represented by static phenomena (nuclear or electron spins). For phenomena that move, gates are physical devices which affect qubits as they flow through the gate. These are called “flying qubits”. Optical implementations generally fall into this category, where photons are qubits and e.g.

beam splitters serve as gates. For “stationary” phenomena, qubits occupy a physical place and gate operations from an application are applied to them. The “stationary” notion applies *only* during gate operation. Some stationary technologies, such as the proposed scalable ion trap [170], permit the physical qubit carrier to be moved prior to application of a gate; we will call these “mobile” qubits.

The key reason to make the distinction between stationary and flying implementations is dynamic control. In a flying qubit device, the order and type of gates must typically be fixed in advance, often at device construction time; different program execution is achieved by classical control of switches that route qubits through different portions of the circuit. A stationary qubit device has more flexibility to reconfigure gates. In this sense, using stationary devices is like classical programming, while flying qubit designs are more like classical circuit design [354].

Single system versus ensemble: A significant distinction in quantum computing technologies is the choice of *ensemble* computing or *singleton* computing. In ensemble computing, generally implemented on stationary qubit systems, there are many identical quantum computers, all receiving the same operators and executing the same program on the same data (except for noise). Singleton systems have the ability to directly control a single physical entity that is used to represent the qubit.

From a technology perspective, ensemble systems are easier to experiment with, as techniques for manipulating and measuring large numbers of atoms or molecules are well understood. Hence, the largest quantum computing system demonstrations to date have all been on bulk-spin NMR [340, 52], which uses an ensemble of molecules to compute.

Quantum I/O: There are a variety of reasons why we may want to move quantum data from one place to another: we may simply be aggregating multiple devices into a larger machine, or the far node may provide different computational capabilities (e.g. long-term storage) or have access to different data. In some cases, we may wish to move quantum data between devices of different technologies [222]. In our quantum multicomputer, we will be aggregating homogeneous nodes into a larger system using the qubus protocol described in Chapter 5.

Quantum I/O (QIO) is a very error-prone process. Therefore, it is done by first using QIO on “empty” qubits, which we will call QIO sites or transceiver qubits, creating an entangled state between a pair of devices. Once the existence of the entangled state is

confirmed through a process called purification [43, 77, 259], it can be used to transfer any desired quantum state by using quantum teleportation (Chapter 5).

Question marks appear in the QIO entries in table 4.1 because experimental demonstration in structures similar to those expected to be used in quantum computers has not yet been done, or because adequate fidelity has not been shown. In some cases, basic experimental confirmation or proposals backed by relatively solid analysis exist; in others, only a few sentences in a longer paper.

Measurement: In Section 2.2.3 we discussed measurement in the abstract, and in Chapter 2.3 we saw its importance for quantum error correction. Four architectural features characterize different measurement schemes: (1) Can measurements of multiple quantum bits be performed in parallel or must they be serialized? (2) Does measurement of a quantum bit require interaction with another “clean” qubit in order to produce a result? (3) Is the speed of measurement about as fast (in the same order of magnitude) as performing an operation? (4) Can measurement be performed almost anywhere, or must the physical entities that are used to represent the qubits be moved to specialized measurement sites?

Reliably computing on a quantum system will mean that many of the total quantum operations will be measurements, as we discussed in the last chapter. From an architectural perspective, if measurements must be performed serially, or are inordinately slow, then Amdahl’s Law [18] will apply and measurement will be the bottleneck in computation. Furthermore, if additional ancillae qubits are required for measurement to take place, then we must plan for the initialization of those qubits to occur frequently. Similarly, if technologies restrict where measurement can occur, then those restrictions will need to be designed into the architecture and algorithms.

4.1.2 Algorithmic Efficiency Features

Many features of the various quantum computing proposals will have profound implications for the execution of quantum algorithms on realistic architectures.

Concurrency (control parallelism): The most fundamental feature required to accelerate quantum computation is concurrent execution of gates. This is useful at the algorithmic (logical) level, but critical at the physical level, where concurrent operation is required in order to execute quantum error correction frequently enough to prevent

decoherence of large numbers of qubits.

Despite the advantages in computational complexity class that some quantum algorithms promise, it is still important to extract parallelism from quantum algorithms. If all operations had to be sequentialized, then on some proposals, such as silicon NMR [300], it would still require significant time to factor large values. For example, Kunihiro [193] has estimated the sequential running time of Shor's algorithm factoring a 530-bit number at 1.18 years for a 1kHz device (approximately NMR speeds), 10 hours for a 1MHz device, or 37 seconds for a 1GHz device.

Fortunately, there is significant parallelism available [235] in quantum software (error correction [308] and factoring [80, 334]). The ability to exploit this parallelism, however, requires technologies with parallel control. This parallel control will require significant classical support circuitry. If this circuitry cannot be located "on chip" near the qubits then a high-bandwidth interface between a classical device generating control pulses and a quantum device containing the actual qubits will be required. This may be a control line per qubit, or may be multiplexed across the wire, reducing the need for I/O pads at the cost of reduced concurrent operation (and longer times between QEC cycles). Thaker et al. have designed a large-scale ion trap with separate storage and gate action sites (see below), and investigated the use of the carry-lookahead adder on this system, finding that performance grows only linearly due to limited application-level concurrency [324].

Total available qubits: The feature with the single largest impact on the scalability, usefulness, and reliability of the computer is the actual number of physical qubits available. Clearly, too few qubits and the ability to execute on large data sizes will be inhibited. Additional qubits can be utilized for increased reliability via error correction, as well as algorithmic parallelism.

All entries in table 4.2 are followed by question marks because of very high uncertainty; in some cases, even which factors will prove to be the practical limits are not yet clear. As most researchers are still focusing on very small numbers of qubits, they have not yet attempted to circumscribe this upper limit.

Wiring topologies: Optimization of the architecture to support the data movement of a useful class of algorithms is one of the key areas where computer architects can contribute. In many proposed technologies, only neighboring qubits are allowed to perform two-qubit gates. Either the physical entities representing the qubits (using a

control process [170]) or just the state (using quantum wires [256]) must be moved around the machine to support computation. In some cases, technological constraints limit the interconnection topology to a one-dimensional line; in others, a loose two-dimensional lattice, full 2-D mesh, or even 3-D structure have been proposed [210]. A few proposals support long-distance gates with various tradeoffs, such as limited concurrency [359].

Addressability: In some systems, addressing specific qubits is difficult, because localization of the classical control required (e.g., microwave-frequency electromagnetic field) to just the small region the qubit occupies is difficult. One solution, the original Lloyd model, proposes forming small groups of qubits into cellular automata [210]. One suggested implementation is long molecular chains with a repeating pattern in which each unit is a C.A. Each qubit position in the automaton can be addressed via a specific electromagnetic frequency. Each automaton follows the same program, effected by electromagnetic radiation blanketing the whole device, which is, in effect, a fully concurrent SIMD machine. One technique for turning a cellular automata into a more-easily-controlled serial machine is to include in the cellular automata a token that is passed from automaton to automaton; only the automaton holding the token performs the indicated action. We expect that designing architectures and software systems for technologies without the ability to address and operate on specific qubits will be difficult.

Operations on all qubits: In most physical implementations, all qubits are identical; any qubit can have any operation performed on it during any clock cycle. A few technologies, however, notably the scalable ion trap, separate storage and action locations, so that qubits (e.g., individual atoms) must be physically moved from a storage location to an action location before a gate can be executed on the qubit.

4.1.3 Time and Gate Characteristics

Decoherence time: We discussed decoherence in Section 2.2.3. The upside to good isolation from environmental effects is long *coherence time*, or the time which a qubit can be “kept”. As a broad generalization, those technologies relying upon electrons to maintain quantum state have short coherence times because electrons are fairly mobile and tend to interact with their surrounding environment. Technologies that utilize

nuclear effects are more stable. However, the downside to good isolation from environment effects is relatively slow operation times for two-qubit gates. Across the technologies we examine, the gate speed and decoherence time vary over eight orders of magnitude or more [197]. Coherence time is an especially important research area and will be subject to potentially large advances as QC technology progresses. Gate operation time, however, is often tied directly to physical processes with limited flexibility in engineering parameters.

Measurement time: How long does it take to accurately measure the state of a qubit? For many technologies the measurement time is longer than a gate time, dominating the time for a quantum error correction cycle and hence the logical clock speed.

Single-qubit and two-qubit gate clock speeds: In some cases, the time it takes to perform a one-qubit gate can be vastly different from the time for a two-qubit gate, so we must specify both.

Natural two-qubit gate: Various sets of gates have been shown to form elementary basis sets [30, 98]. The standard set of universal gates presented in Section 2.2.5 (X, H, T, CNOT) is just one example, and all serious proposals for quantum computing technologies include enough operations to provide this or an equivalent universal set. Beyond universality, however, are three important characteristics. (1) Does the technology provide an arbitrary single qubit rotation, or must it be synthesized from X, H and T; (2) How complex are the syntheses for a CNOT and three qubit controlled-controlled-not (a TOFFOLI gate), which is commonly used in quantum algorithms [30]; (3) Do specific gates have unwanted effects on qubits that are *not* the intended operands (that is, are other qubits being implicitly manipulated)? We will discuss these in more detail below.

Several of most common physical interactions result in a controllable exchange (SWAP), the J coupling [339], and a controlled phase shift, which, when applied for the appropriate amounts of time, give us possible two-qubit natural gates with these

unitary transforms:

$$\sqrt{\text{SWAP}} = \begin{bmatrix} 1 & 0 & 0 & 0 \\ 0 & \frac{1}{\sqrt{2}} & \frac{1}{\sqrt{2}} & 0 \\ 0 & \frac{1}{\sqrt{2}} & -\frac{1}{\sqrt{2}} & 0 \\ 0 & 0 & 0 & 1 \end{bmatrix} \quad (4.1)$$

$$J = \begin{bmatrix} -i & 0 & 0 & 0 \\ 0 & i & 0 & 0 \\ 0 & 0 & i & 0 \\ 0 & 0 & 0 & -i \end{bmatrix} \quad (4.2)$$

$$\text{CZ} = \begin{bmatrix} 1 & 0 & 0 & 0 \\ 0 & 1 & 0 & 0 \\ 0 & 0 & 1 & 0 \\ 0 & 0 & 0 & -1 \end{bmatrix}. \quad (4.3)$$

From these three possible entangling two-qubit gates, we can construct a CNOT with only a few single-qubit rotations on the two qubits.

In stationary qubit devices such as ion traps or NMR systems, several electromagnetic pulses are generally required to implement each gate. A typical number is five or six, though the exact number and timing are dependent on the gate to be executed. One side effect in NMR systems is that nearby qubits are affected by these pulses and are implicitly operated on by them. To overcome this, additional control sequences called *decoupling pulses* are required [35, 204].

4.1.4 Other Features

Logical Encoding: Quantum algorithms are written to manipulate abstract, logical qubits. Logical qubits, however, are not always represented by a single physical phenomenon such as a single ion or photon. We call the entities that software manipulates “logical qubits” (or “encoded qubits” when quantum error correction is involved) and the entities that technologies use to implement them “elementary qubits” or “physical qubits”. This is not the same as the ensemble / singleton distinction outlined above.

In some technologies, such as electron count (charge) in quantum dots, a “dual rail” encoding is used. Similarly, a single photon may take either the left or right path through a circuit, corresponding to logical different quantum states (i.e. 0 or 1). In both of these technologies, it is possible to talk about a single quantum dot (or path) as a single qubit, but we arrange computation and measurement to take place on the encoded pair.

Gate-Level Timing Control: Because the state of an individual qubit is something of an analog phenomenon, precise timing of gates is critical. What will limit our ability to achieve the necessary precision? And, in the case of photons or other flying qubits, how do we dynamically adjust their arrival times so that multiple qubits can be in the right place at the same time? Most qubits oscillate; how do we keep the relative phases of multiple qubits right?

Scalability Limits: Scaling to large numbers of qubits is, for most architectures, a function of all of the above factors and more. Other factors not yet described are technology specific. For example, in lithography-based systems, they include I/O pads on the chip, the supporting infrastructure such as rack-mount microwave generators, and the practical challenge of simply providing enough control wires to such a small device. Few of the proposals suggest that an actual numerical upper bound exists because of any of these factors, yet they are critical to the success of building systems. In the next section we will highlight what the primary scalability limit is perceived to be for each technology.

4.1.5 Manufacturing and Operating Environment

At the moment, all scalable quantum computing technologies are proposals and significant advances in manufacturing will be required to bring them to reality. Nevertheless, some proposals have less onerous technological hurdles in front of them than others. Furthermore, certain proposed technologies integrate better with existing classical silicon-based computing.

Fabrication challenges: To what extent do the proposed technologies rely on difficult-to-achieve advances in manufacturing? For example, the Kane silicon-based NMR technology relies upon the ability to dope silicon with precisely placed individual phosphorus atoms, and to align those with overlaid structures created using standard VLSI

lithography [163]. All of the solid-state circuit techniques require classical control lines (e.g., [124, 242]), which may benefit from expected improvement in VLSI feature sizes following Moore's Law [236, 110]. In our taxonomy we will highlight the major technological challenges facing each quantum computing proposal and discuss the latest advances in overcoming them.

Operating temperature: In order to control noise, most proposals call for extremely low temperatures achievable only with liquid helium. Others, such as superconducting qubits and quantum dot qubits, require still colder *millikelvin* temperatures achieved through a dilution refrigerator. A dilution refrigerator, or dil fridge, uses the different condensation characteristics of helium-3 and helium-4 to cool things down to millikelvin temperatures [86].

Although there are numerous models, the dil fridges made by Oxford Instruments seem to be popular. The most commonly used ones are almost two meters tall and a little under a meter in diameter. The researcher loads the test sample in from the top on a long insert, so another two meters' clearance above (plus a small winch) are required. The lowest temperature a dil fridge can reach is limited in theory to approximately 7 millikelvin, and in practice to higher values depending on model. A dil fridge can typically extract only a few hundred microwatts of heat from the device under test, which is limited to a few cubic centimeters. This thermal limit will limit the number of devices per chip and the operating speed of the devices, imposing an important constraint on scalability. These low temperatures are not only operationally challenging, but also affect the ability of classical circuits to operate, complicating the design of the control process [256].

The atom chip [117] and ion trap [78] operate by cooling individual atoms to extremely low temperatures using lasers and electrical and magnetic control fields, but the devices themselves are kept at room temperature and no elaborate cooling mechanisms are required.

Supporting equipment: Some technologies require complex supporting equipment, notably high-frequency microwave and voltage signal generators and high-precision lasers. One or more of these per qubit may be needed; as systems scale, switching or sharing of this equipment or direct integration into on-chip systems are likely to be required.

4.2 Quantum Technologies

In this section we survey a variety of proposed quantum computing technologies using the taxonomy framework described in the last section. We have chosen to focus on eight technologies: Si-NMR, P-NMR, solution NMR, quantum dot charge, scalable ion traps, Josephson junction charge, linear optics, and optical lattice. This selection should by no means be interpreted as exhaustive; several dozen viable proposals exist [117, 294, 265, 71]. These systems were chosen for their near and long term implementability, and/or scalability and/or pedagogical interest. It is also worth noting that the fundamental technology, in some case, can lead to several possible qubit representations, such as spin, energy level, or particle count. The information is summarized in Tables 4.1-4.5. Below we will briefly discuss each technology and its architectural implications.

4.2.1 Solution NMR

Probably the most complete demonstrations of quantum computation to date are the solution NMR experiments [340, 52, 182]. In an NMR system, the qubit is represented by the spin of the nucleus of an atom. When placed in a magnetic field, that spin precesses, and the spin can be manipulated via microwave radiation. In solution NMR, a carefully-designed molecule is used. Some of the atoms in the molecule have nuclear spins, and the frequency of radiation to which they are susceptible varies depending on their position in the molecule, so that different qubits are addressed by frequency. In some cases, isotopic composition must be carefully controlled. Many copies of the molecule are held in a liquid solution; each molecule is a separate quantum computer, run independently, with the large numbers providing adequate signal strength for read-out. This is the canonical ensemble system. Solution NMR has been used to factor the number 15 using Shor's algorithm, which required 720 milliseconds [340]. The largest demonstration to date is 12 qubits [243].

No special cooling apparatus is required for this ensemble system. However, its scalability is believed to be quite limited due to falling signal/noise ratio as the number of qubits increases.

- **strengths:** good decoherence time, room temperature operation, advanced experimental verification
- **weaknesses:** slow gates, poor scalability, difficult concurrent operations

technology	stationary/ flying/mobile	single/ ensemble	QIO?	measurement	references
Si NMR	stationary	ensemble	N	mechanical vibration, concurrent, frequency analysis	[196]
solution NMR	stationary	ensemble	N	concurrent, frequency analysis	[340]
quantum dot charge	stationary	single	Y?	concurrent, on-chip auxiliary structures, similar to quantum dots in size and structure	[214]
scalable ion trap	mobile	single	Y?	limited concurrent, optically induced fluorescence	[78, 170]
JJ charge	stationary	single	Y?	concurrent, on-chip charge probe	[260, 360]
Kane model	stationary	single	N?	concurrent, single-electron spin measurement	[163]
LOQC	flying	single	Y	single qubit polarization via single photon number resolving optical detectors	[184]
optical lattice	stationary	single	N?	fluorescence, but resolution of individual atoms difficult	[56, 157, 326]

Table 4.1: Qubit technology basic characteristics. Question marks under QIO indicate that experimental verification has not yet been shown. JJ: Josephson junction, LOQC: linear optics quantum computing

technology	concurrency	max qubits	wiring topologies	addressability	ops on all qubits?
Si NMR	limited by ability to suppress activity of uninvolved qubits	hundreds?	linear nearest neighbor	by frequency, all independent	Y
solution NMR	limited by ability to suppress activity of uninvolved qubits	low tens?	linear nearest neighbor, limited non-neighbor	by frequency, all independent	Y
quantum dot charge	limited by control mechanism	large?	linear nearest neighbor	localized, independent control via on-chip systems	Y
scalable ion trap	limited by # of action sites with lasers	large?	open, irregular, up to 2-D?	individual ions and chains moved from addressable storage to action sites	N
JJ charge	limited by coupling mechanism	large?	1-D, 2-D?, long-distance possible?	localized, independent control via on-chip systems	Y
Kane model	limited by control mechanism	large?	1-D or 2-D?	localized, independent control via on-chip systems	Y
LOQC	unlimited?	large?	physical routing, essentially unlimited	physical position	Y
optical lattice	mandatory	thousands?	1-, 2-, or 3-D neighbors	none	Y

Table 4.2: Features affecting algorithm efficiency on specific qubit technologies. The maximum number of qubits in all technologies remains undetermined with any reliability. Question marks in topologies indicate that the natural area for layout is 2-D, but practical engineering constraints may limit full 2-D layout.

technology	decoherence time	measurement time	single-qubit gate clock speed	two-qubit gate clock speed	natural two-qubit gate
Si NMR	25s	long	40kHz	400Hz	J coupling
solution NMR	seconds	long	50kHz	50Hz	J coupling
quantum dot charge	a few ns	10-100ns [124, 214]	10GHz	10GHz	exchange [214]
scalable ion trap	1ms-20s	100 μ s [230] to 10msec [288]	can trade off speed for gate fidelity in the range of 14kHz to 100kHz; also limited by ion movement times to \sim 20kHz		conditional phase shift
JJ charge	a few ns	10ns	10GHz	10GHz	conditional phase shift
Kane model	long?	long	75kHz	75kHz	J coupling
LOQC	limited by scattering and absorption	5-10ns	< 1 ns	limited by detector time	several possibilities, including conditional phase shift
optical lattice	seconds?	N/A	160kHz	5kHz	conditional phase shift

Table 4.3: Clock speed and gate characteristics

technology	logical: elementary encoding	gate-level timing control	scalability limit
Si NMR	1:1	slow gates make precise timing feasible	quality of initialization (no more than $1/n$ copies may be mis-polarized for large n , to achieve adequate SNR), precision of placement in static magnetic field, area of high-quality magnetic field
solution NMR	1:1	slow gates make precise timing feasible	SNR falls exponentially in n
quantum dot charge	1:3	gates must be precise, but jitter is not a problem	external wiring/control
scalable ion trap	1:1	recommends use of decoherence-free subspace to reduce jitter	probably ability to accurately track large numbers of individual ions, and their movement times
JJ charge	1:1	active control of phases	cross-qubit interference; inductance of Josephson junctions; large numbers of rack-mount microwave generators and getting wires into the dilution refrigerator
Kane model	1:1		manufacturing complexity
LOQC	1:1 but many auxiliary photons used	“stopped” light [116]	skew and jitter in both input generation and gates; single-photon photodetector efficiencies of ~ 0.9 will scale poorly when used for large numbers of independent qubits; deep circuits subject to loss
optical lattice	1:1	slow gates make precise timing feasible	region of high-quality lattice tens of sites per side?

Table 4.4: Other Features

technology	fabrication	operating environment	supporting equipment
Si NMR	Si micromachining	4 K, 7 T magnetic field	r.f. signal generator
solution NMR	chemical	room temperature, 11 T magnetic field	r.f. signal generator
1-D quantum dot charge	GaAs lithography	20 mK	GHz voltage pulse generator (per qubit?)
scalable ion trap	macroscopic electromechanical assembly	supercooled ions in room temperature vacuum	multiple lasers (gates and measurement), electronic signal generators (ion movement control), CCD cameras (state detection)
JJ charge	Si lithography	30 mK	GHz voltage pulse generator (per qubit?)
Kane model	P implanted in Si lithography	1.5 K, 2 T magnetic field	
LOQC	macroscopic electromechanical assembly	dependent on optical detectors; liquid helium to room temperature	high speed optical switches, atomic clocks
optical lattice	vacuum chamber, lasers, macroscopic electromechanical assembly	ultracold atoms in room temp. vacuum	multiple lasers

Table 4.5: Manufacturing and operating environment. K, degrees Kelvin; mK, millikelvin.

4.2.2 Josephson Junction

Josephson junction-based (JJ) quantum computing devices are superconducting systems [295]. They come in four flavors: those that represent qubits using charge (such as the device shown in figure 4.1) [242, 260], those that use flux [234, 72, 271], those that use phase [361, 221], and a recently-designed high-temperature form [32]; most of the information in the tables applies to all but the latter. Fabrication is done using conventional electron-beam lithography and shadow evaporation of Al onto an SiN_x insulating substrate. In the JJ charge qubit, a sub-micron size superconducting box (essentially, a small capacitor) is coupled to a larger superconducting reservoir. In a superconductor, electrons move in pairs known as Cooper pairs. The qubit representation is the number of Cooper pairs in the box, controlled to be either zero or one, or a superposition of both. Similarly, for the flux qubit, Cooper pairs are introduced into a superconducting ring, where they circulate and induce a quantized magnetic flux. Because the flux qubit has slower gate times but a relatively even longer coherence time, experimental efforts appear to be shifting toward the flux qubit approach.

Josephson junction technologies can couple qubits in a variety of ways [49, 216, 85, 252, 208, 209, 272]. In one proposed scalable form of the charge qubit, neighboring qubits are linked in a one-dimensional structure that supports only nearest-neighbor gates, but concurrent gates on independent qubits may be allowed [201]. In another proposal, it is possible to address any two qubits and couple them through a shared inductance [359]. In this case, the restriction of operations involving only neighboring qubits in a linear array is removed, but execution is limited to one gate at a time. Rigetti et al. have proposed a scheme that borrows ideas from NMR to couple neighboring qubits of either flux or charge type [279]; their proposal has the benefit that slight differences in fabrication between qubits are a help rather than a hindrance.

The high-temperature JJ device requires complex fabrication and careful alignment to crystal lattice axes. “High temperature”, in this case, refers to the materials potentially being superconductors at liquid nitrogen temperatures, but the experiments described are conducted at 15mK to minimize other sources of decoherence.

- **strengths:** very fast gates, advanced experimental demonstration, straightforward fabrication (for all but the high-temperature device)
- **weaknesses:** low coherence time relative to measurement time, sensitivity to background charge fluctuations and local magnetic fields

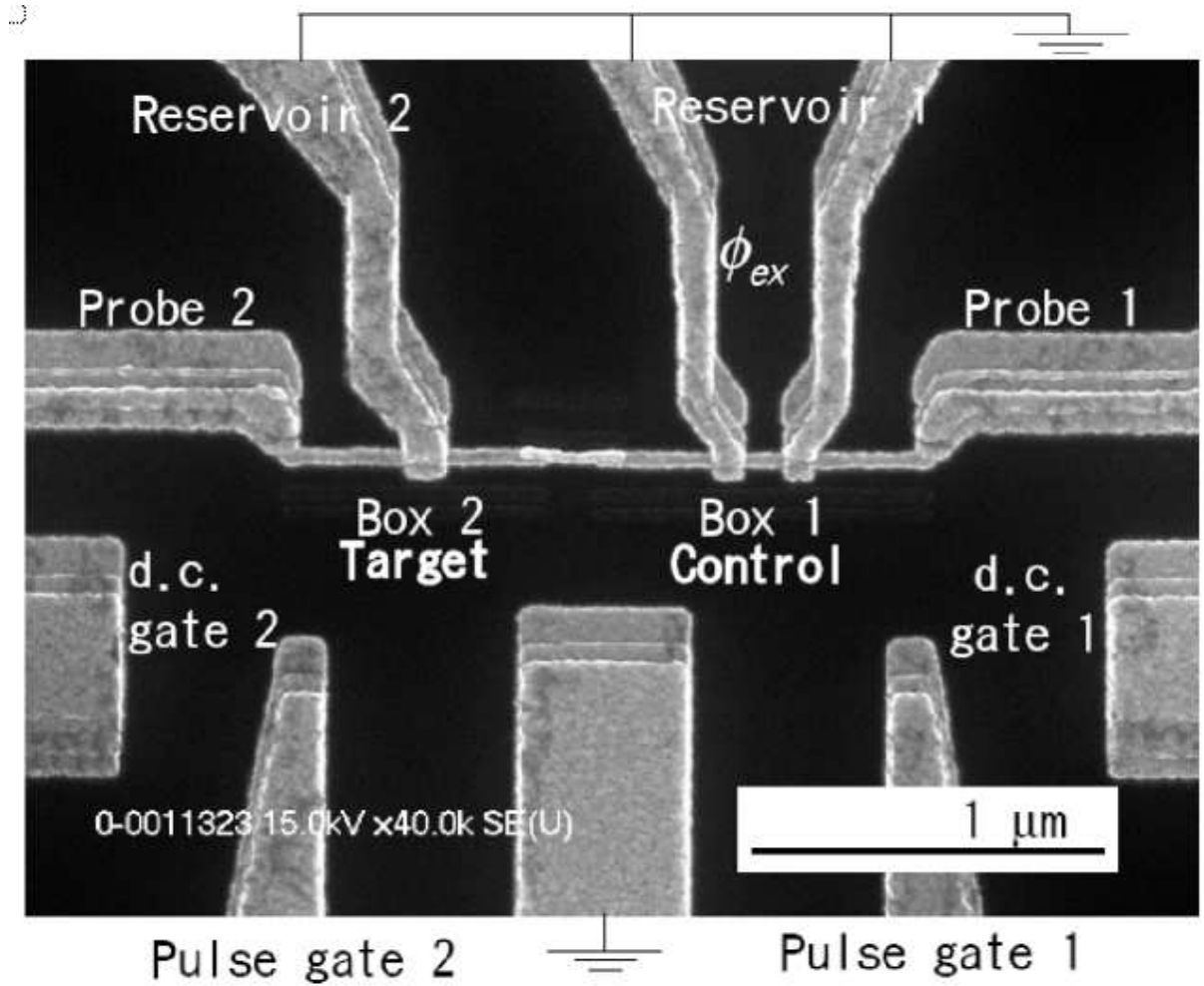


Figure 4.1: A pair of coupled Josephson-junction charge qubits (labeled Box 1 and Box 2). This device is designed to execute a two-qubit gate between the qubit labeled “Control” and the one labeled “Target”. The coupling between the two qubits is fixed in hardware in this device. Image courtesy of Y. Nakamura and T. Yamamoto, NEC.

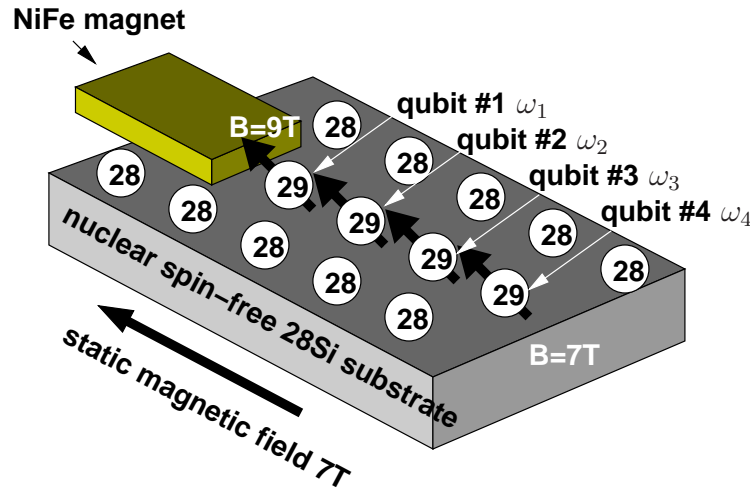


Figure 4.2: Schematic of the all-silicon NMR computer. Qubits are the spin of ^{29}Si nuclei on a spin-free base of ^{28}Si . Distance from the micromagnet determines oscillation frequency ω_i and provides individual qubit addressability. Image courtesy of K. M. Itoh, Keio University.

4.2.3 All-Silicon NMR

Ladd et al. have proposed an all-silicon NMR-based quantum computer which stores qubits in the nuclear spin of a chain of ^{29}Si (spin 1/2 nucleus) in a substrate of spin 0 nuclei (^{28}Si and ^{30}Si). In one form, the ^{29}Si atoms are laid down in a line across a micromechanical bridge [196]. Readout is done via magnetic resonance force microscopy (MRFM), reading oscillations of the bridge. Other measurement schemes for the same basic architecture are being pursued, as well [156]. This is an ensemble system; 10^5 copies are required to get an adequate signal for measurement. One form of the system is illustrated in Figure 4.2. Only one chain of ^{29}Si is shown. Initialization is done via electrons whose spin is set with polarized light (optical pumping). Operations are done via microwave radiation directed at the device. A micromagnet provides a high field gradient, allowing individual atoms to be addressed by frequency. The device is fabricated via near-atomically precise machining, then refined by passing electrical current through it in a carefully controlled fashion [292, 358, 348].

- **strengths:** longest known decoherence time
- **weaknesses:** slow gates, no QIO, measurement still being designed, difficult fabrication

4.2.4 Scalable Ion Trap

One of the few systems which explicitly separates storage areas from interaction areas is the scalable ion trap [170, 350, 173, 230, 309, 29, 324, 9, 147]. Initially designed and built at NIST, this is a proposal to scale up an ion trap quantum computer [78, 305, 301, 288]. In ion trap systems, qubits are usually stored in the energy levels of individual ions. In early ion trap experiments, small numbers of ions were held in a single trap known as an RF Paul trap. In the scalable trap system, which is a large system of interconnected, individually controllable traps, the ions are kept suspended in a vacuum in a channel in the device and are literally moved around using magnetic fields until they reach locations in the system designated for operations, as shown in Figure 4.3. Small numbers of ions are brought together and formed into chains to execute multi-qubit gates. Gates are effected by laser pulses; readout is also accomplished by laser pulses creating fluorescence (interpreted as a 1) or not (0). Gate times are moderate, but overall system performance will likely be driven by ion movement times (which naturally depend on distance and topology), times for creating and splitting chains of atoms, time to cool atoms heated by the movement process, and multiplexing of gate operations. For both gates and measurement in scalable ion trap systems, many laser beams must excite many ions. Complex optics and photon detectors may be required to read out the state of many qubits at once; CCD cameras involve a direct tradeoff of speed versus noise, while avalanche photodiodes are difficult to integrate and photon counters require cryogenic operation [173].

The Monroe group has recently shown the ability to move ions around corners, a fundamental engineering advance in control of individual atoms [147]. As noted above, the efficiency of algorithms implemented on ion traps will depend on realizable concurrency, and on the time to move and cool ions.

In Table 4.3, we list the decoherence time of ions as a range of 1 millisecond to 20 seconds. The lifetime of individual ions has been shown to be in the millisecond range, but Häffner et al., in the Blatt group in Austria, recently encoded a state on a pair of ions using a decoherence free subspace and experimentally measured a lifetime of 20 seconds [140]. Other experiments from both the Blatt group and the Wineland group at NIST have recently confirmed the existence of entangled groups of 6, 7, and 8 ions, prompting the coining of the term “qubyte” [139, 202]. While these accomplishments do not yet surpass the size of the Cory group’s 12 qubit NMR system, researchers are excited because ion trap technology is viewed as a strong candidate for a scalable

system. It will be interesting to see when it becomes possible to draw a “Moore’s Law” parallel for the size of an entangled system, graphing the doubling time of the largest entanglement demonstrated in ion traps.

- **strengths:** scalability of storage
- **weaknesses:** slow gates [306]; limitations on concurrent operations and measurements

4.2.5 All-Optical

All-optical systems come in two flavors: those that depend on non-linear effects to execute gates, and those in which the only necessary non-linearity is measurement, known as *LOQC* (linear optics quantum computation) [184]. Research on all-optical systems has focused on photon sources capable of generating precise numbers of photons with the necessary timing precision [286], gates based on measurement [184, 287, 179, 59, 357], and high-quality single-photon detectors [232, 345, 158].

Measurement-based gates are inherently probabilistic in nature, though it has been shown that these gates can be built into a scalable feed-forward network [184, 276]. Much of the current experimental work is focusing on this approach, and individual gates have been shown to work [270, 253, 269, 127, 285].

Jitter and skew are likely to be managed by “stopped light”, created by electromagnetically induced transparency [116, 144], which has also recently been shown to be useful for creating and managing single photons both directly [105] and in combination with other techniques [68].

- **strengths:** well-understood physics and easy fabrication
- **weaknesses:** photon losses; for non-linear systems, weak non-linear effects give poor gate quality; high resource requirements for probabilistic gates; large physical size of systems

4.2.6 Quantum Dot

A “quantum dot”, as used in quantum information processing, is a lithographically-defined structure that confines electrons at the boundary layer between two materials, creating a two-dimensional electron gas (2DEG). By varying the surrounding electrical

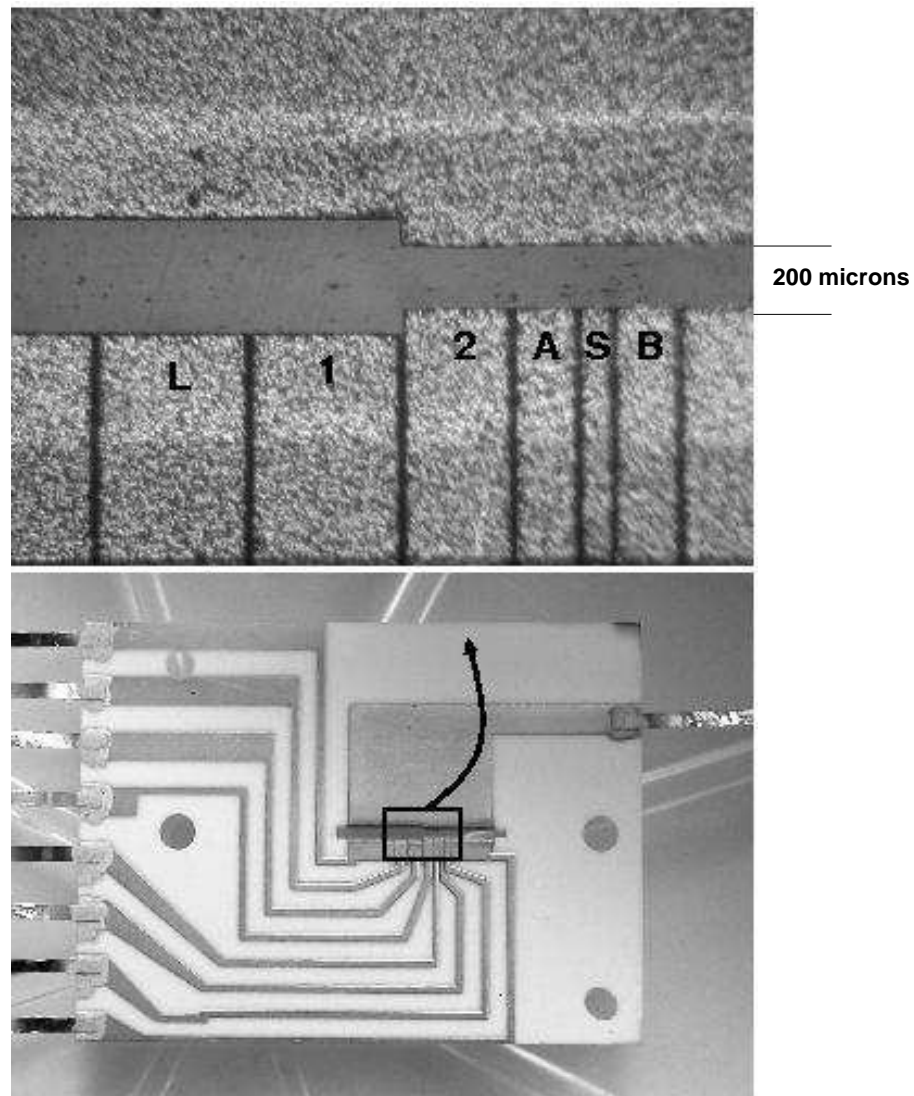


Figure 4.3: A six-zone ion trap capable of moving individual ions. Ions are inserted in the landing zone L, and manipulated in the zones A, S, and B. Image courtesy of D. Wineland, NIST.

potential, individual electrons can be confined to a small area, called the quantum dot. A qubit can be defined based on the number of electrons in a quantum dot or the spin or energy levels of a single electron held in a quantum dot.

Several quantum dot devices are under development; one experimentally advanced approach uses a pair of quantum dots as a dual-rail encoded logical qubit, with a single electron in the left dot representing a logical 0, and the electron in the right dot representing a logical 1 [124, 323]. Another approach uses a linear array of single-electron quantum dots, and encodes the qubit in the spin of the excess electron [214].

In a third approach, DiVincenzo et al. proposed that the only operation needed is an exchange between two neighboring qubits, accomplished by lowering the electrical potential and allowing the electrons to tunnel [100, 214, 240]. This is easier to accomplish than precise control of a magnetic field, which would be required in order to effect gates on specifically addressable bits. Perhaps the biggest drawback of this approach is that exchange-only computation requires encoding a single logical qubit onto multiple physical qubits. A CNOT, for example, requires each logical qubit to be encoded in three physical qubits, and the exchange times must be controlled fairly precisely. The CNOT on neighboring logical qubits requires 19 exchange operations [100], though Myrgren and Whaley have found interesting optimizations that allow non-neighbor operations to be effected in 28% fewer total operations than the obvious formulation of repeated use of the 19-exchange CNOT [240]. Continued compiler work may reduce the encoded execution time penalty further, though the important storage penalty remains.

- **strengths:** advanced fabrication
- **weaknesses:** low coherence time

4.2.7 Kane Solid-State NMR

Kane has proposed a solid-state NMR system with excellent scalability, built on VLSI techniques for control [163], and Clark et al. have made progress in fabrication [79]. In this system, individual phosphorus atoms are embedded in a silicon substrate, and standard photolithography techniques are used to build control structures on the surface. The qubit is held in the spin of the phosphorus nucleus, and interactions between neighboring qubits are mediated by electrons coupled to the nuclei via hyperfine interactions. The shape of the electron wave function is controlled via the control structures built on the Si surface; the distance between neighboring P atoms and the accuracy of

aligning the control gates to the P impurities will determine the quality of qubit interactions. Some Si isotopes have a nuclear spin; the presence of atoms of these isotopes could potentially disrupt the operation of the Kane structure. Abe et al. have studied the behavior of such a system as the isotopic composition of the Si substrate is varied [5, 4]. Oskin, Copsey et al. have performed engineering studies, suggesting that teleportation may be required to move qubits long distances even for error correction, and that matching the pitch of the necessary lithographically-created control structures to the desirable atomic spacing is difficult [256, 84].

- **strengths:** long coherence time
- **weaknesses:** difficult fabrication, creating adequate overlap in electron wave functions

4.2.8 Optical Lattice

In an optical lattice, qubits are the internal states of individual atoms [157, 56, 326]. The optical lattice itself is a set of standing waves of light, creating magnetic fields that hold individual atoms in place in an array, suspended in a vacuum. Two-qubit gates are executed by adjusting the positions of the peaks and troughs of the light waves so that neighboring atoms collide. This basic approach is similar to trapping of ions, but since the atoms are neutral rather than charged, they do not interact with the environment as strongly, and hence have the potential to have much longer lifetimes. The lifetime of a Bose-Einstein condensate (a coherent quantum state rather different from qubits) has been measured in seconds in a lattice [134]. The lattice may work well in multiple dimensions. The principal drawbacks to this approach are that individual addressing and readout of atoms have not been shown. Each pair of atoms in the lattice acts exactly the same, and the spacing between the atoms is too small for optical resolution for fluorescent readout. The “atom chip” approach uses similar physics for the qubits and gates, but is a dramatically different engineering approach, using lithographically created structures to move individual atoms at will, something like the scalable ion trap [117, 326, 175].

- **strengths:** long coherence time, easy fabrication
- **weaknesses:** no individual addressability for gates or readout

4.3 Summary

DiVincenzo laid down the defining characteristics of a viable quantum computing technology [97]. Many engineering factors extend beyond the DiVincenzo criteria to determine how practical it is to build a machine based on a given technology [337]. These factors include such basic issues as possible measurement schemes, the difficulty of building and operating large-capacity devices, and several issues affecting performance, notably clock speed, the qubit-to-qubit layout topology and possible concurrent operation. For our purposes, some quantum I/O mechanism is necessary; without one, we cannot build a quantum multicomputer, and the system's scalability with respect to number of qubits (and possibly concurrent operation) will be quite limited. In the next chapter, we will develop the *qubus* mechanism and accompanying *teleportation* techniques that we will use to connect quantum computers together.

This chapter organizes information about quantum computers in a way that specifically focuses on scalability, implementability, and architectural implications. The evaluation criteria we have laid out should make it possible to compare technologies and determine which will be useful in different roles of a system, and how application algorithms can be mapped to and compiled for various architectures.

Each of the technologies discussed here has its own particular set of technological hurdles to overcome before it can be considered practical. NMR-based systems have slow gate times, but have good coherence times; if a QIO mechanism can be designed [346], they will make excellent storage devices, but pure NMR systems are unlikely to make adequate factoring machines. Josephson-junction devices and quantum dots have extremely fast gate times, but have poor coherence times. Both of these systems have yet to demonstrate scalability in implementation and addressing of qubits, though both have been designed. Pure optical systems need more efficient single-photon detectors. Ion traps have many desirable features that make them scalable architecturally.

The complex tradeoffs in controlling a quantum computer include trading speed for coherence time. The quantum wiring and classical control are under investigation in both technology-dependent and -independent fashions, but many scaling questions remain. Work on both programming language design to support quantum computation and back-end optimization for specific architectural characteristics has just begun [254, 14, 241, 165]. The mapping of algorithms to these architectures will determine the performance and practicality of particular architectures.

Chapter 5

Networking

True and serious traveling is no pastime, but is as serious as the grave.

Henry David Thoreau

Our quantum multicomputer will require a quantum network, as illustrated in Figure 1.2 on page 10. The physical layer of the network must be quantum, of course, but the techniques for describing and understanding classical networks can be applied easily to quantum networks. In this chapter, we take a quick look at the qubus physical layer for creating entangled pairs, and the classical ways of describing network topologies and their performance.

5.1 Weak Nonlinearity and Qubus Entanglement Protocols

EPR pairs, or Einstein-Podolsky-Rosen pairs, are pairs of particles or qubits which are entangled so that actions on one affect the state of the other, such as the state $(|00\rangle + |11\rangle)/\sqrt{2}$ (which can also be called a Bell pair). EPR pairs can be created in a variety of ways, including reactions that simultaneously emit pairs of photons whose characteristics are related and many quantum gates on two qubits. For an ion trap system, for example, two ions can be moved together, an entangling operation performed, and the ions separated. As long as the quantum state remains coherent, the ions can be separated by any physical distance and their state will remain related. In the next section, we will see how to use EPR pairs both to move data and to execute gates remotely,

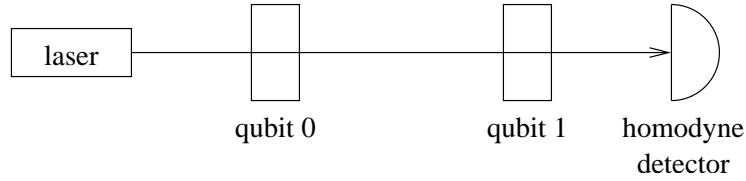


Figure 5.1: Physical configuration of a qubus.

via a process known as quantum teleportation. In this section, we present our mechanism for making the EPR pairs. Technically, an EPR pair is a maximally entangled pair; that is, operations on one qubit have the strongest possible influence on the other. In this thesis, we use the term somewhat more loosely, including pairs whose entanglement has decayed somewhat from the maximum, or whose entangling operations failed to produce a perfect pair.

Our approach to creating EPR pairs contains no direct qubit-qubit interactions and does not require the use of single photons, as e.g. Kimble’s team has recently demonstrated [73]. We use the invention of Munro, Nemoto and Spiller, which uses laser or microwave pulses as a *probe beam* [244, 237]. Two qubits are entangled indirectly through the interaction of qubits with a common quantum field mode created by the probe beam – a continuous quantum variable – which can be thought of as a communication bus, or “qubus” [303]. We call this process the qubus entanglement protocol (QEP).

Physically, the qubus consists of a laser or microwave source, a pair of qubits and some means of interacting them with the probe beam, and a *homodyne detector* [21], as shown in Figure 5.1. The distance between the qubits can be arbitrarily large, limited only by losses in the probe beam. The probe beam consists of a large number of photons, each of which interacts minutely with the qubits. If the qubits are single photons, this is accomplished using a type of crystal with a property known as a *cross-Kerr nonlinearity*.

For some solid state qubit systems, we can put the qubits in a microwave resonant cavity and use a microwave pulse to create the qubus effect. The interaction with a bus mode takes the effective form of a cross-Kerr nonlinearity, analogous to that for optical systems, described by an interaction Hamiltonian of the form

$$H_{int} = \hbar \chi \sigma_z a^\dagger a. \quad (5.1)$$

In this equation, a^\dagger and a are, respectively, the creation and annihilation operators,

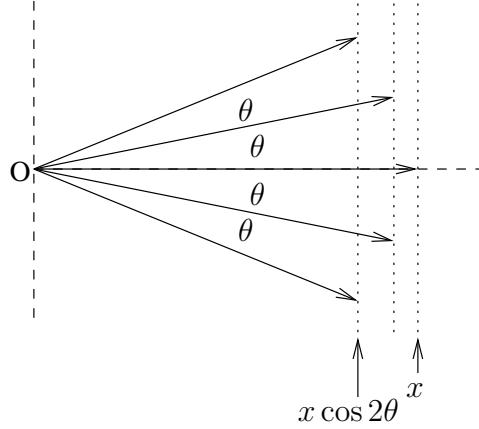


Figure 5.2: Phase space diagram of the qubus entanglement protocol.

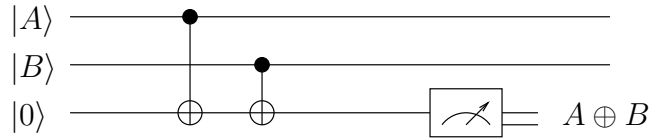


Figure 5.3: Logical equivalent of the qubus entanglement protocol.

representing the raising or lowering of the number of photons present in the probe beam. When acting for a time t on a qubit-bus system where the nonlinear interaction is of strength χ , this interaction causes a rotation in phase space by an angle $\pm\theta$ on a bus coherent state, where $\theta = \chi t$ and the sign depends on the qubit computational basis amplitude. In a phase space diagram, the horizontal and vertical axes correspond to the quadrature amplitudes of two variables. They are commonly referred to as position (x) and momentum (p), respectively, due to mathematical similarities in their behavior, but they do not physically represent these quantities. The diagram for this interaction is shown in Figure 5.2. By interacting the probe beam with the qubit, the probe beam picks up a θ phase shift if it is in one basis state (e.g., $|0\rangle$) and a $-\theta$ phase shift if it is in the other (e.g., $|1\rangle$). If the same probe beam interacts with two qubits, it is straightforward to see that the probe beam acting on the two-qubit states $|0\rangle|1\rangle$ and $|1\rangle|0\rangle$ picks up no net phase shift because the opposite-sign shifts cancel, while the probe beam acting on the states $|0\rangle|0\rangle$ and $|1\rangle|1\rangle$ picks up phase shift $\pm 2\theta$.

The homodyne measurement projects the point in phase space onto the x axis (position). This projection determines whether the probe beam has been phase shifted (in effect taking the absolute value of the angular shift), projecting the qubits into either an even parity state or an odd parity state. The measurement shows only the parity

of the qubits, not the actual values, leaving them in an entangled state. If the homodyne measurement returns $x \cos 2\theta$, we know that the state is either $|00\rangle$ or $|11\rangle$. If the measurement returns x , we know that the state is either $|01\rangle$ or $|10\rangle$. In the latter case, we can apply a NOT gate to either qubit, moving the state into $|00\rangle$ or $|11\rangle$. Figure 5.3 shows a circuit that is logically similar to QEP, differing only in its possible error propagation characteristics, which we will not detail.

Although the qubus is physically asymmetric, with a probe beam source and homodyne detector at opposite ends of the physical layout and a definite ordering of qubits along the bus, this layout does not influence the logic of the qubus. The qubus is used to create EPR pairs, which are symmetric. Each teleportation operation, as we will see in the next section, consumes one EPR pair to send a qubit from node to node. We can schedule use of the bus as if it is a *half-duplex* bus.

This procedure is general, and can be applied to any pair of qubits to determine their parity. If all of the terms of the superposition have the same parity, the state of the superposition is not affected by the parity measurement, beyond a small phase change which can be corrected with single-qubit gates. If we start with both qubits in the state $(|0\rangle + |1\rangle)/\sqrt{2}$, we are left with the state $(|00\rangle + |11\rangle)/\sqrt{2}$, which is a good state for beginning the teleportation protocols described in the next section.

5.2 Teleportation

Teleportation, discovered by Bennett and his collaborators, transfers the state of one quantum to another by using EPR pairs. Teleportation of quantum states has been known for more than a decade [45]. It has been demonstrated experimentally [125, 54], and has been suggested as being necessary for moving data long distances within a single quantum computer [256, 229]. Teleportation can also form part of the process of transferring quantum state from one physical representation to another.

For our quantum multicomputer, we propose using the qubus entanglement protocol (QEP), described in the last section. Entanglement is a continuous, not discrete, phenomenon, and several weakly entangled pairs can be used to make one strongly entangled pair using a process known as *purification* [43, 77]. Purification starts with EPR pairs in a known (but possibly degraded) state, then essentially performs an error correction protocol that is specific to that state. This is more efficient than full-fledged quantum error correction.

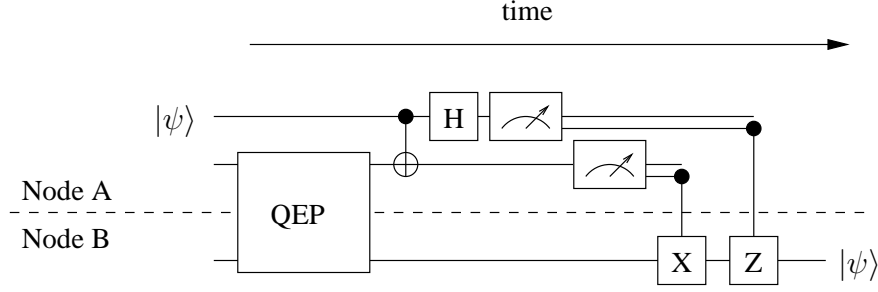


Figure 5.4: Teleporting a single qubit.

5.2.1 Teleporting Data

Figure 5.4 shows the basic teleportation circuit to move a single qubit from one location to another. The box labeled QEP is the qubus entanglement protocol; the output of the box is the EPR pair. The near and far ends of the teleportation each hold one member of the entangled pair. To teleport the qubit $|\psi\rangle = \alpha|0\rangle + \beta|1\rangle$, the first step is to perform a CNOT at the source between the qubit and the source-side EPR member, causing the change

$$|\psi\rangle \frac{|00\rangle + |11\rangle}{\sqrt{2}} \rightarrow \frac{\alpha}{\sqrt{2}}|000\rangle + \frac{\alpha}{\sqrt{2}}|011\rangle + \frac{\beta}{\sqrt{2}}|110\rangle + \frac{\beta}{\sqrt{2}}|101\rangle \quad (5.2)$$

where the qubits in our written representation correspond top to bottom to the qubits in the figure. That is, the left-most qubit in our notation is the original qubit, the middle one is the source-side EPR pair member, and the right-most qubit is the member of the EPR pair at the destination. We then apply a Hadamard gate to the original qubit, moving to the state

$$\begin{aligned} & \frac{\alpha}{2}|000\rangle + \frac{\alpha}{2}|100\rangle + \frac{\alpha}{2}|011\rangle + \frac{\alpha}{2}|111\rangle - \frac{\beta}{2}|101\rangle - \frac{\beta}{2}|110\rangle + \frac{\beta}{2}|001\rangle + \frac{\beta}{2}|010\rangle \\ &= \frac{1}{2}(|00\rangle(\alpha|0\rangle + \beta|1\rangle) + |01\rangle(\beta|0\rangle + \alpha|1\rangle) + |10\rangle(\alpha|0\rangle - \beta|1\rangle) + |11\rangle(-\beta|0\rangle + \alpha|1\rangle)). \end{aligned} \quad (5.3)$$

The last representation makes it clear that the destination qubit now has some relationship to the state of the original qubit. In the first term, if the first two qubits are zero, then the last qubit holds the state of our original qubit, $\alpha|0\rangle + \beta|1\rangle$. In the other three terms, the state of the last qubit is a simple permutation of the original qubit, which can be recovered via an X gate, a Z gate, or both. The four terms correspond to the states 00, 01, 10, and 11 in the first two qubits. Thus, if we force the state of the system into

one of those four states, we can determine which gates to apply to “fix” the destination qubit, so that it ends in the starting state of the qubit we wanted to send, $|\psi\rangle$.

In the figure, this is shown by the measurements, followed by “control” X and Z gates. Of course, the outcomes of the measurements are classical bits, so our control, in this case, is a classical choice to apply an X gate or not, depending on the measured bit. After the measurements but before the control gates, the original qubit and the source-side EPR pair member have both been “destroyed” (the physical carriers of the qubits likely still exist, but we no longer have a useful quantum state, as the superposition has collapsed).

As an example, assume that the node A bits are measured, and produce the value 11. This value is then transmitted via classical means to node B. At node B, we now know that the state of the destination qubit is $-\beta|0\rangle + \alpha|1\rangle$. We apply both X and Z gates, and the state shifts to $\alpha|0\rangle + \beta|1\rangle$, recovering the original qubit $|\psi\rangle$ at the destination.

The “spooky action at a distance” of entangled pairs of particles was one of Einstein’s concerns about quantum mechanics, especially because it appears to violate relativity. Part of the answer to his concern is that *information* cannot travel faster than the speed of light. Thus, although the state of the qubit at the destination may change “instantaneously” as we perform the measurements at the source, the state of the qubit remains in the indeterminate state until we receive the classical, relativity-limited information telling us which gates to apply to recover the pure state we are teleporting.

5.2.2 Teleporting Gates

So far, we have discussed the teleportation of data. It is also possible to teleport gates. Gottesman and Chuang showed that teleportation can be used to construct a control-NOT (CNOT) gate [133]. Their original teleported gate requires two EPR pairs. We use an approach based on parity gates that consumes only one EPR pair, as shown in figure 5.5 [237]. Locally, the parity gates can be implemented with two CNOT gates and a measurement (outlined with dotted lines in the figure). Double lines are classical values that are the output of the measurements; when used as a control line, we decide classically whether or not to execute the quantum gate, based on the measurement value. The last gate involves classical communication of the measurement result between nodes. As shown, this construction is not fault tolerant; it must be built over fault-tolerant gates. Alternatively, the qubus approach can be used as the node-internal interconnect. Its natural gate is the parity gate, and is fault tolerant; this is the approach

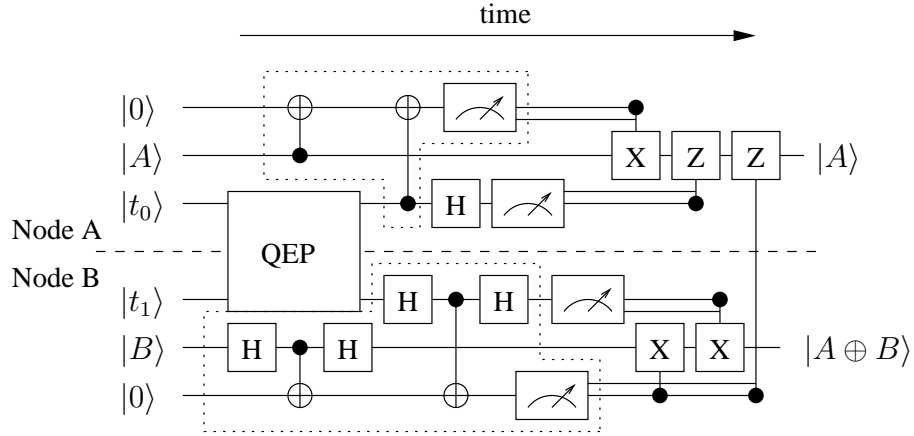


Figure 5.5: A teleported control-NOT (CNOT) gate.

we will use when we come to distributed computing in Chapter 7.

5.3 Multicomputer Networks

The theme of this dissertation is the design of a quantum multicomputer, a collection of smaller quantum computers connected via a message-passing network so as to collaborate to solve a single problem [24]. A multicomputer is a distributed-memory multiprocessor, in which processing units run programs independently, and cannot directly access the memory of other processing units. All shared computation is accomplished by exchanging messages through an interconnection network. In this section, we take a very brief, technology-independent look at the interconnection networks that turn a group of individual computers into a multicomputer. In Chapter 7, we will apply these principles to our quantum system, designing an interconnect network to create EPR pairs.

Networks consist of *nodes* and *links*. A node is a computational element, where data is stored and manipulated. A link transfers messages from one node to another. A link may be serial, with one data line, or parallel, with several. A serial link requires only a single *transceiver*, whereas a parallel link requires one per wire, or the *bus width*. The current trend in local-area networks and peripheral buses (such as Fibre Channel, USB, and serial ATA) is serial links, which allow tighter packaging, lower power requirements, simpler cabling, etc. The savings in those areas offset the cost of a single higher-speed transceiver, generally meaning that serial networks wind up being roughly as fast as the parallel ones they replace.

For multicomputer networks [146, 151, 89], as with all networks, we have most of

Topology	degree	diameter	avg. dist.	bisection	tot. BW (links)
Bus	1	1	1	1	1
Line	2	$N - 1$	$N/2$	1	$N - 1$
2D Mesh	4	$2(\sqrt{N} - 1)$	$2\sqrt{N}/3$	\sqrt{N}	$2N - 2\sqrt{N}$
Hypercube(2-cube)	$\log_2 N$	$\log_2 N$	$(\log_2 N)/2$	$N/2$	$(N \log_2 N)/2$
Fully Connected	$N - 1$	1	1	$N^2/4$	$N(N - 1)/2$

Table 5.1: Some common interconnect topologies. N , number of total nodes.

what we need to know about the topology when we know four characteristics:

- **degree** The number of links from each node.
- **diameter** The maximum distance across the network, measured in hops.
- **average distance** The average distance between any two nodes.
- **bisection** The minimum number of links you must cut to chop the machine in half.

This assumes, generally, a regular network, though the same principles apply for arbitrary topologies. For a link, we also need to know the link latency, bandwidth, and protocol and processing overhead; we will mostly ignore those issues and express our results in units of a single transfer, or EPR pair creation. We also include aggregate system bandwidth in our analysis.

These characteristics give us some guidelines and hint at the generality (or lack thereof) of a particular network. What ultimately matters, of course, is how long it takes to execute the application algorithm(s) that comprise our workload. In most cases, this is a function of both the network topology and the message-passing pattern of the algorithm. “Incast” problems (two nodes trying to send to the same destination at the same time) inevitably cause contention (competition for access to resources); we will see some of the effects of contention in Section 7.5.

Table 5.1 and Figure 5.6 show five topologies. The *bus* is a single, shared medium on which any node can send a message directly to any other node, but only one pair can be communicating at a time; this configuration roughly corresponds to the original Ethernet scheme and most computer buses. In a *line* configuration, each node has a neighbor to the left and a neighbor to the right, and can exchange messages with both of them simultaneously. In a *2D mesh*, each node has four neighbors, north, east, south and west, and the nodes are laid out in a two-dimensional grid; the Intel Touchstone

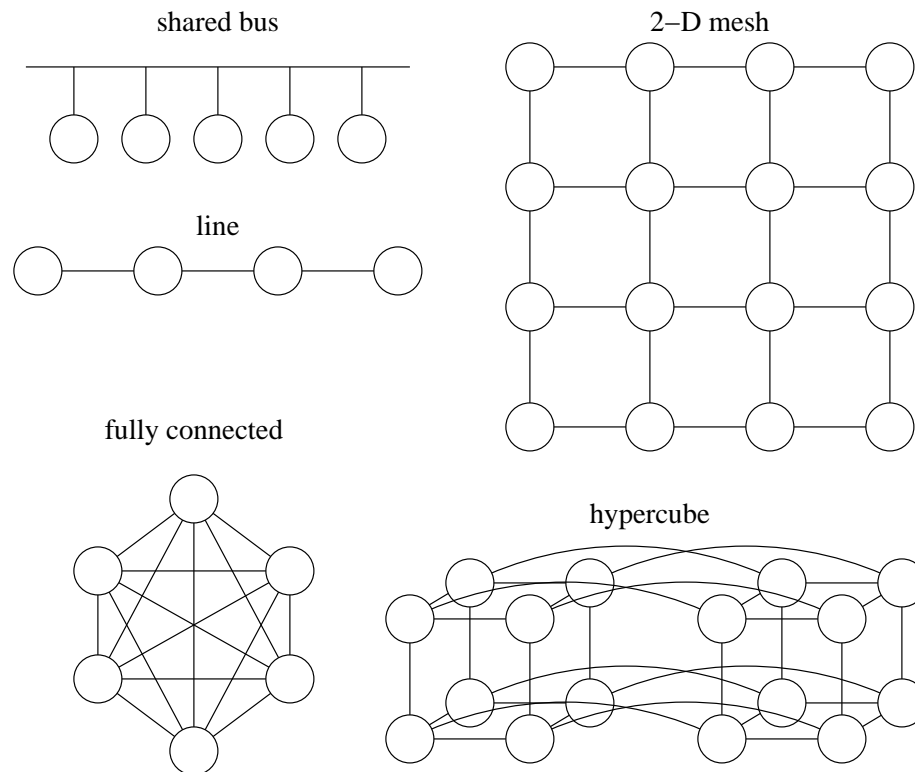


Figure 5.6: Five important interconnect network topologies.

Delta and other large-scale systems found this topology to be a good choice. The original Caltech Cosmic Cube was a hypercube, with each of the 64 nodes connected to $\log_2 64 = 6$ neighbors. Scaling this system up is difficult, as each doubling of the number of nodes requires adding a link to each one of the existing nodes; packaging constraints quickly become a problem. In a fully-connected network, each node can communicate directly with each other node. Given that this requires $O(N^2)$ links, it is clearly impractical, but serves as a theoretical upper bound.

All of these topologies are *direct network*, also sometimes called *distributed switch*, topologies, where the hardware to route messages from location to location resides with the compute nodes. It is also possible to use *indirect network*, also called *centralized switch* topologies, such as crossbars and fat trees. In indirect networks, packets must pass through switching nodes in the middle of the network whose sole purpose is routing packets. For reasons that will become clear in later chapters, we ignore indirect network systems.

The performance of a system depends on several factors besides the topology. Although a hypercube offers excellent theoretical properties, with no node more than

$\log_2 N$ hops away, if each hop is slow, the overall system suffers. The most straightforward implementation, *store and forward*, requires waiting for an entire message to arrive at a node before beginning the retransmission along the next hop. Based on this experience, 2D meshes such as the Intel Touchstone Delta were implemented with *wormhole routing*, allowing the start of a message to begin transmitting while the tail is still arriving, giving excellent overall performance with more scalable hardware. These issues matter less in our environment.

For most of the 1980s and 1990s, with fine-grained parallelism and many processors attempting to send messages at the same time, careful matching of applications to network topologies and management of resources (principally, access to the network) were required. In recent years, the availability of fast, cheap, general-purpose networking hardware and improving software tools for larger-grained parallel systems, such as Beowulf, MPI, and BOINC, have largely decoupled parallel applications from the need for such hardware-specific tuning [314, 101, 19].

The field of interconnection networks for distributed, parallel computation is a vast one; here we have hardly begun to even hint at the scope [89, 146]. Our current needs for a quantum multicomputer are modest, so this level of analysis will suffice.

5.4 Summary

In this chapter, we have introduced the disparate concepts needed to build a quantum multicomputer: the fundamental qubus technology we intend to use to create entangled pairs of qubits (EPR pairs), the teleportation of both quantum data and quantum gates that will use EPR pairs to effect distributed quantum computation, and the principles of store-and-forward multicomputer networks that will determine how efficient the system can be.

We now come to the end of not only the chapter on the qubus, but of the entire first part of this thesis, covering the fundamentals of quantum computation. We have studied the basic ideas of quantum computation, seen Shor's algorithm for factoring large numbers, which we will use as our target application, explained how to control errors, and discussed many different quantum computing technologies. And finally, we presented quantum teleportation and the qubus protocol upon which we will build our quantum multicomputer.

We now set aside the distributed nature of our system for a while, and move into

the detailed analysis of the performance and limitations of a monolithic quantum computer. Once that analysis is complete, we will return to the quantum multicomputer in Chapter 7.

Chapter 6

Performance of Large-Scale Systems

[T]he period matters little until the acceleration itself is admitted. The subject is even more amusing in the seventeenth than in the eighteenth century, because Galileo and Kepler, Descartes, Huygens, and Isaac Newton took vast pains to fix the laws of acceleration for moving bodies, while Lord Bacon and William Harvey were content with showing experimentally the fact of acceleration in knowledge...

Henry Adams, “A Law of Acceleration,” 1905

We are now prepared to design the architecture of a quantum computer and evaluate its performance. Up to this point, we have examined what it means to do quantum computation, discussed what a quantum computer could be used for, and analyzed the technologies available to build such a system. In Section 2.2.5, we saw DiVincenzo’s five criteria which must be met by any useful quantum computing technology [97]. In addition to these criteria, a useful quantum computing technology must also support a quantum computer *system architecture* which can run one or more quantum algorithms in a usefully short time. This observation subsumes into one requirement several issues which, while not strictly necessary to build a quantum computer, will have a strong impact on the possibility of engineering a practical, useful system; we presented our analysis of those requirements in Chapter 4.

The process of adapting abstract algorithms to quantum computers naturally depends on the architecture, but the application of classical computer architecture principles to quantum computers has only just begun, making it difficult to definitively

pronounce that a certain quantum computer will be “useful” in solving real-world problems. In this chapter, my aim is to advance our understanding of this design process, including designing some specific algorithmic subroutines that are appropriate for certain architectures. I analyze and optimize the performance of the modular exponentiation that forms the largest part of Shor’s factoring algorithm, based on the Vedral-Barenco-Ekert algorithm as discussed in Section 3.5. We have found ways to improve the scaling of performance with respect to the length of the number being factored; the acceleration is thousands of times for important problem sizes, reaching one million times when factoring a 6,000-bit number. We show that this acceleration depends on the architecture of the system, and how to optimize for certain constraints. We also show that the faster modular exponentiation algorithms reduce the demands on the error management subsystems and increase the fidelity of our calculation.

The first section of this chapter provides a brief overview of the techniques we use to accelerate arithmetic, then discusses the impact of architecture on quantum error correction, and presents our architectural models and notation. The next two sections explain the tradeoff between classical and quantum computation and present our new adder designs, the carry-select and conditional-sum adders. Section 6.4 closes this chapter with our major analytical and numerical results for the complete modular exponentiation algorithm. The material presented here should help other researchers analyze the performance of systems they design, both large and small; in the next part of this dissertation, I use these techniques to analyze the behavior of a quantum multicomputer based on an overall structure I propose.

6.1 Managing Performance

The realized performance of a system is a product of both the underlying technology and the architecture imposed above it. In Sections 4.1.2, 4.1.3 and 4.1.5, we introduced the technological factors that affect performance of the system: physical and logical clock speed, concurrency or parallelism, the number of available qubits, the ability of qubits to communicate with each other (the “wiring topology”), addressability of individual qubits, and the decomposition of logical gates into physical ones. From this point forward in the dissertation, we will ignore addressability and assume individual control over qubits. For our purposes (primarily arithmetic circuits), the issue of direct or polynomial approximation of arbitrary rotations only concerns us as described below, in the breakdown of CCNOT. The ability of a system to retire application instructions as

quickly as possible derives from more than the clock speed; extracting parallelism and moving data as efficiently as possible strongly impact behavior, and these issues drive much of the rest of this dissertation.

Concurrent quantum computation is the execution of more than one quantum gate on independent qubits at the same time. We generally use the term *concurrency* rather than parallelism, to avoid confusion with the concept of quantum parallelism. Utilizing concurrency, the latency, or circuit depth, to execute a number of gates can be smaller than the number of gates. We discussed parallel multipliers in Section 3.5.2. Circuit depth is also explicitly considered in Cleve and Watrous’ parallel implementation of the quantum Fourier transform [80], various types of arithmetic [88, 103, 334, 130], and Zalka’s Schönhage-Strassen-based implementation of modular exponentiation [362]. Moore and Nilsson define the computational complexity class **QNC** to describe certain parallelizable circuits, and show which gates can be performed concurrently, proving that any circuit composed exclusively of Control-NOTs (CNOTs) can be parallelized to be of depth $O(\log n)$ using $O(n^2)$ ancillae on an abstract machine [235]. In Chapter 4, we discussed the capability of different technologies to perform concurrent gates; in this part of the thesis, we combine the theoretical and practical concerns to analyze the demands of the algorithms.

Here we summarize the techniques which are detailed in following sections. Our fast modular exponentiation circuit is built using the following optimizations:

- Trade classical for quantum computation, to reduce the length of the expensive and difficult quantum portions (Section 6.2).
- Move to better adders; our algorithms concentrate on the use of the conditional-sum adder (Section 6.3.3), carry-lookahead adder (Section 3.4.3), and CDKM carry-ripple adder (Section 3.4.2).
- Look for concurrency within addition; our concurrent version of VBE forms our baseline case, and the other adder circuits are defined with concurrency in mind.
- Do multiplications concurrently, using Cleve-Watrous (Sections 3.5 and 6.4.2).
- Reduce modulo comparisons, only subtract N on overflow; this incurs a small space penalty and requires some cleanup at the end, in exchange for a nearly $5\times$ reduction in the number of calls to the adder routine (Section 6.4.2).

- Select correct qubit layout and subsequences to implement gates, then hand optimize [339, 14, 165, 192, 320, 354, 15].

6.1.1 Error Correction, Architecture, and Clock Speed

A basic understanding of the pressures that quantum error correction and fault tolerance place on architecture is critical. As we saw in Chapter 2.3, QEC and FT demand the continuous preparation and measurement of a set of ancillae (temporary work qubits), and raise the overall cost of quantum computation by as much as four orders of magnitude for *each* level of QEC built into the system – and it appears that two or more levels may be necessary. The logical clock speed of the system will correspond roughly to the QEC cycle time, and is correspondingly slower than the physical clock speed, though the exact ratio will depend on both technology- and machine-dependent details.

QEC codes encode one or more qubits into a code word. The error syndromes on this code word are continuously calculated and measured, and corrective actions applied to the code word. The measurement of the syndrome actually effects a key portion of the error control process; it forces (“projects”) the state either back into a good state (with high probability) and returns a zero (no error) syndrome, or an error state (with low probability) and returns a non-zero syndrome. When the syndrome is non-zero, one or two corrective gates are indicated and applied. Unfortunately, this syndrome calculation and measurement process may also introduce errors. Technologies that support nearest-neighbor-only interactions require swapping of qubits in order to calculate the error syndrome, with the swap gates possibly introducing errors themselves, making the threshold requirements for effective error correction more stringent; in some studies, as much as 175 times worse [317, 308, 11, 120, 318]. The parity calculations necessary to retrieve the error syndrome cannot be carried out directly, but must operate indirectly using a logical zero ($|0_L\rangle$) state to defend against propagation of errors. That state preparation requires as many qubits as the code word itself, and may be the driver of the cycle time for QEC. Measurement of qubit state on some technologies is slow compared to the gate time, so this also figures prominently into the cycle time.

As qubits are subject to error processes when idle, as well as while being used, the total amount of error correction in the system is dependent on the size of the machine, as well as the number of logical gates being executed. If each qubit must be “refreshed” at one-tenth the QEC cycle rate, for example, then we must build a system in which one-tenth of the qubits can all be undergoing QEC at the same time. Longer

waits for correction increase the probability of error; this must be balanced against the number of levels of QEC and the engineering difficulties of initialization and measurement. Quantum dots and superconducting qubits require additional on-chip structures to perform measurement [266], limiting layout flexibility and consuming die space. If possible, it will be desirable to perform entire QEC sequences on-chip; however, in the short run, it may be necessary to use off-chip signal generators and control circuitry, requiring a wide, high-bandwidth I/O interface from the chip itself.

To manage errors effectively, then, we can say that a technology must support large numbers of concurrent qubit state preparations, gates, and measurements. As the required operations are much more complex than a DRAM refresh cycle, and are close to the universal gate set, a large-scale difference in structure akin to the CPU/RAM dichotomy is unlikely. However, at the small scale, systems which store qubits in nuclear spins while idle and shift to electron spins for active gates have been proposed [311, 163, 227, 159, 71].

6.1.2 AC and NTC Architectural Models

This dissertation analyzes two separate architectures, still abstract but with some important features that help us understand performance. For both architectures, we assume any qubit can be the control or target for only one gate at a time. The first, the AC, or *Abstract Concurrent*, architecture, is our more abstract model. It supports CCNOT (the three-qubit Toffoli gate, or Control-Control-NOT), arbitrary concurrency, and gate operands any distance apart without penalty. It does not support arbitrary control strings on control operations, only CCNOT with two ones as control. AC corresponds to the machine we have implicitly assumed to this point. The second, the NTC, or *Neighbor-only, Two-qubit-gate, Concurrent* architecture, is similar but does not support CCNOT, only two-qubit gates, and assumes the qubits are laid out in a one-dimensional line, and only neighboring qubits can interact. The 1D layout will have the highest communications costs among possible physical topologies.

The NTC model is a reasonable description of several important experimental approaches, including a one-dimensional chain of quantum dots [214], the original Kane proposal [163], and the all-silicon NMR device [196]. Superconducting qubits [260, 359] may map to NTC, depending on the details of the qubit interconnection.

For NTC, which does not support CCNOT directly, we compose CCNOT from a set of five two-qubit gates [30], as shown in figure 6.1. The box with the bar on the right

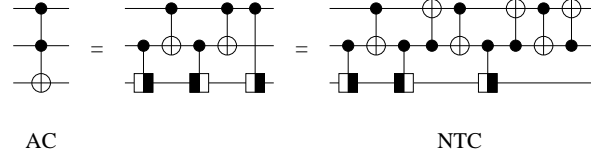


Figure 6.1: CCNOT constructions for our architectures AC and NTC. The box with the bar on the right represents the square root of X , and the box with the bar on the left its adjoint.

represents the square root of X , $\sqrt{X} = \frac{1}{2} \begin{bmatrix} 1+i & 1-i \\ 1-i & 1+i \end{bmatrix}$ and the box with the bar on the left its adjoint. We assume that this gate requires the same execution time as a CNOT.

The difference between AC and NTC is critical; beyond the important constant factors as nearby qubits shuffle, we will see in Section 6.4 that AC can achieve $O(\log n)$ performance on addition where NTC is limited to $O(n)$. Most real, scalable architectures will have constraints with this flavor, if different details, so AC and NTC can be viewed as bounds within which many real architectures will fall. The layout of variables on this structure has a large impact on performance; what is presented here is the best we have discovered to date, but we do not claim it is optimal.

6.1.3 Notation

In the rest of this dissertation, as in Chapter 3, where we introduced Shor's factoring algorithm, we will use N as the number to be factored, and n to represent its length in bits. For convenience, we will assume that n is a power of two, and that the high bit of N is one. x is the random value, smaller than N , to be exponentiated, and $|a\rangle$ is our superposition of exponents, with $a < 2N^2$ so that the length of a is $2n + 1$ bits.

As described in Section 3.4.1, when discussing circuit cost, the notation we use is $(\text{CCNOT}s; \text{CNOT}s; \text{NOT}s)$ or $(\text{CNOT}s; \text{NOT}s)$. The values will usually be circuit depth (latency), but may be total gate count, depending on context. The notation is sometimes enhanced to show required concurrency and space, $(\text{CCNOT}s; \text{CNOT}s; \text{NOT}s) \# (\text{concurrency}; \text{space})$.

t is time, or latency to execute an algorithm, and S is space, subscripted with the name of the algorithm or circuit subroutine. When t is superscripted with AC or NTC, the values are for the latency of the construct on that architecture. Equations without superscripts are for an abstract machine assuming no concurrency, equivalent to a total

gate count for the AC architecture. R is the number of calls to a subroutine, subscripted with the name of the routine.

m , g , f , p , b , and s are parameters that determine the behavior of portions of our modular exponentiation algorithm. m , g , and f are part of our carry-select/conditional-sum adder (Section 6.3). p and b are used in our indirection scheme (Section 6.2). s is the number of multiplier blocks we can fit into a chosen amount of space (Section 6.4.2).

6.2 Trading Classical for Quantum Computation

Any software problem can be solved by adding another layer of indirection.

David Wheeler

This section discusses balancing the overall *system* performance. With a classical computer as much as 10^{15} times as fast as quantum computer ¹, we can afford to trade many classical operations for a single quantum one [333]. The same principle applies if the metric of interest is economic cost, rather than time performance; quantum gates will remain many orders of magnitude more expensive than classical ones for the foreseeable future.

As we saw in earlier chapters, modular exponentiation is the most expensive portion of Shor's algorithm, consisting of $2n$ multiplication operations to exponentiate an n -bit number. Here, I show that it is possible to reduce the number of quantum modular multiplications necessary by a factor of w , at a cost of performing 2^w times as many classical modular multiplications and adding temporary storage space and associated machinery for a table of 2^w entries. The storage space may be quantum-addressable classical memory, pure quantum memory, or pure classical memory. Values of w from 2 to 30 seem attractive; physically feasible values depend on the implementation of the memory.

¹Very, very roughly, a modern microprocessor has 10^9 transistors, of which perhaps 10% are involved in a "gate" in a clock cycle, of which there are 10^9 per second, yielding some 10^{17} gates/second. In contrast, the slowest quantum devices (liquid NMR) may run at only a few tens of gates per second, *before* applying quantum error correction. Note that this ignores both parallel classical computation and faster quantum devices, but the point is still valid.

6.2.1 Introduction

To factor the number N using Shor's algorithm [296], a quantum computing device must evolve to hold the state

$$\frac{1}{2^n} \sum_{a=0}^{2^{2n}-1} |a\rangle |x^a \bmod N\rangle. \quad (6.1)$$

This is the *modular exponentiation* step discussed in Section 3.5, the first major quantum step in the order-finding process. We also saw that the value $x^a \bmod N$ can be rewritten [191, 342] as

$$\prod_{j=0}^{n-1} d_j^{a_j} \bmod N \quad (6.2)$$

where $d_i = x^{2^i}$, and $a_{n-1}a_{n-2}..a_0$ is the binary expansion of a . The d_i can be calculated classically, but $|a\rangle$ must be a quantum register.

This approach treats $|a\rangle$ as a sequence of *bits*; my approach to reducing the number of multiplications is to treat $|a\rangle$ as a series of short *words*. Dividing $|a\rangle$ up into l words of length w , let $|t_k(a)\rangle$, the k th word in $|a\rangle$, be $|t_k(a)\rangle = |a_{w(k+1)-1}a_{w(k+1)-2}..a_{wk+1}a_{wk}\rangle$ for $0 \leq k < l$, $l = \lceil n/w \rceil$. $|t_k(a)\rangle$, as part of $|a\rangle$, will hold a superposition of all values 0 to $2^w - 1$.

We can reduce the $2n$ quantum multiplications to l by iterating over the words in $|a\rangle$, using the superposition $|t_k(a)\rangle$ as a quantum index into a memory array holding the 2^w n -bit entries with values $b_{m,k} = x^{m2^{wk}} \bmod N$, where m is the index into the array and k is the iteration number, 0 to $l - 1$. The superposition of values retrieved from the memory is multiplied with the current value, giving

$$\frac{1}{2^n} \sum_{a=0}^{2^{2n}-1} |x^a \bmod N\rangle = \frac{1}{2^n} \sum_{a=0}^{2^{2n}-1} \left| \prod_{j=0}^{l-1} b_{t_j(a),j} \bmod N \right\rangle. \quad (6.3)$$

A total of $lw2^w = n2^{w+1}$ classical and l quantum modular multiplications must be performed, compared with $2n$ classical and $2n$ quantum modular multiplications using Vedral's formulation [342].

6.2.2 Indirection

In a computer, arguments to an instruction (or function) can be passed *by value* or *by reference*. By value arguments appear directly in the bits of the instruction. When accessing arguments by reference, the address of the argument is held in the instruction; the actual value must be retrieved from memory before the function can be evaluated. The address is called a *pointer* or an *index*. *Indirection* is a generalization of by reference, in which the value retrieved from memory may itself be a pointer which must in turn be dereferenced.

In the straightforward, bit-based implementation of quantum modular exponentiation, the d_i values are classical values programmed into a register with a superposition of 0, based on the matching bit in the superposition $|a\rangle$. In the word-oriented approach, the $b_{m,k}$ values are held in a table. Logically, a portion of the $|a\rangle$ superposition is used as an index into that table, fetching one of the values to use as the multiplicand (more correctly, fetching a superposition of the $b_{m,k}$ values to use as the multiplicand). That is, we are accessing the arguments for our multiplication through a single level of indirection.

6.2.3 The b Array

The b array is our bridge from classical computation to quantum. Each entry is n bits. We must compute 2^w values for the table, requiring w classical modular multiplications each, before each of the l quantum multiplications. Then, we must figure out how to get $b_{m,k}$ values into the multiplicand register, in superposition. We can use quantum memory, classical memory, or a type of mixed device to hold the data.

Quantum-Addressable Classical Memory

The array can be held using a quantum addressable classical memory (QACM) [249]. In such a device, memory cells (the modular exponentiation values) are classical, but a quantum superposition is used as an address, and the read out value is a superposition of each classical value in proportion to the “amount” of its address present in the address superposition. One such possible device is an optical plate, with photons steered through the various cells according to the value of specific address bits. Figure 6.2 shows a 3-bit example. At the top, the input (generally $|0\rangle$) is steered left or right according to the high-order bit of the address superposition (carried on a control line not

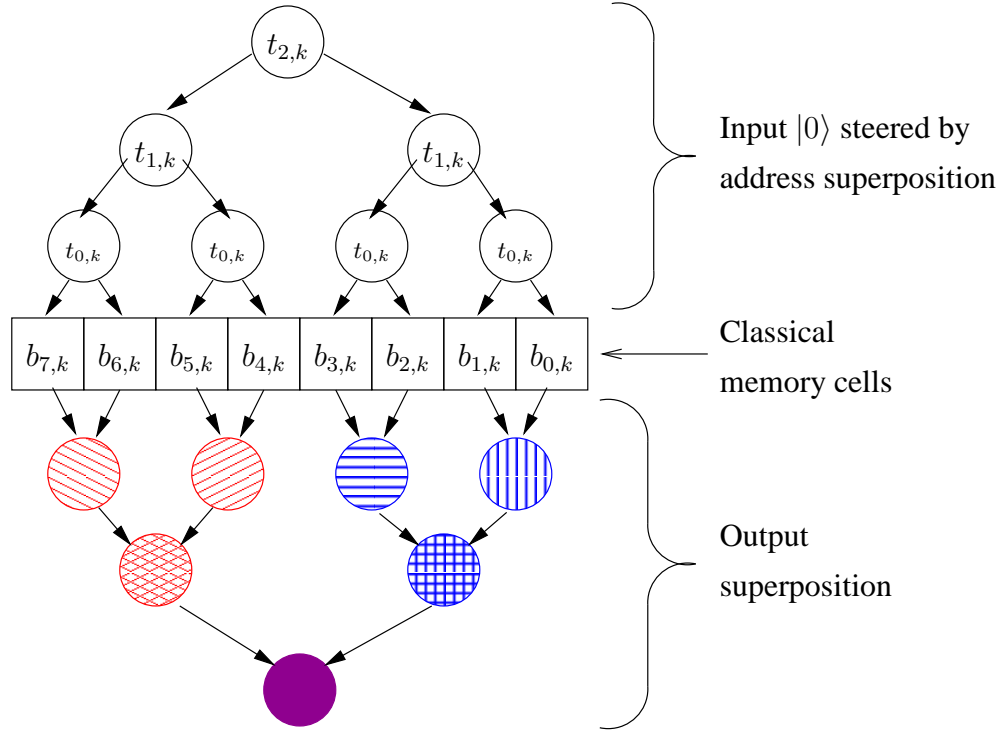


Figure 6.2: Quantum-Addressable Classical Memory (QACM)

shown in the figure). Subsequent circles steer left or right according to their address bits, to reach the appropriate classical data memory cells. The values retrieved from the memory are combined to give the full output superposition, in weights according to the address superposition.

Pure Quantum Memory

An equivalent array of qubits can be used in place of the QACM. However, in that case, the cost of filling the table must be accounted for, and our limitation will be the number of available qubits. Figure 6.3 shows a 3-bit select circuit composed of Fredkin gates which will choose from among the 8 possible arguments for the modular multiplier. The desired value $c_k = b_{t_k,k}$ occupies the location as shown on the right of the figure; it is then used as the argument to the modular multiplier. This select circuit can be reversed following the multiplication to restore the original locations of the $b_{j,k}$ values.

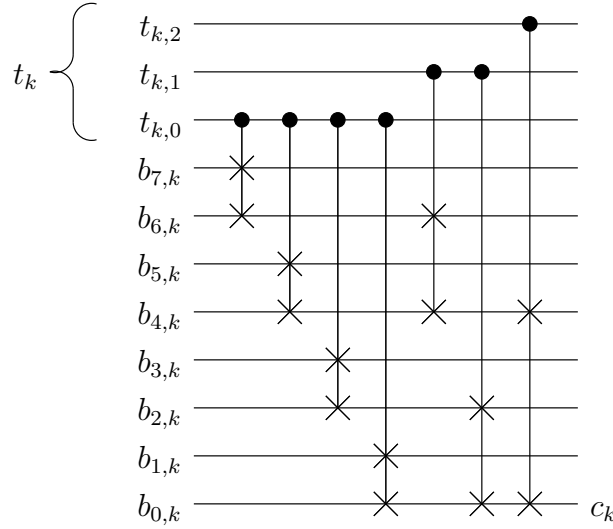


Figure 6.3: 3-bit Quantum Select Circuit (Q-SEL)

Classically-Driven Setting of Multiplicand Register

In the VBE algorithm, the multiplicand register is filled using CNOTs, with the appropriate bit of $|a\rangle$ as the control. For our word-oriented approach, we can implicitly perform the lookup by choosing which gates to apply while setting the argument. In Figure 6.4, we show the setting and resetting of the argument for $w = 2$, where the arrows indicate CCNOTs to set the appropriate bits of the 0 register to 1. The x^i values are classically calculated and stored; we are setting the $|0\rangle$ register to a superposition of the b values. The actual implementation can use a calculated enable bit to reduce the CCNOTs to CNOTs. Only one of the values x^0 , x^1 , x^2 , or x^3 will be enabled, based on the value of $|a_1 a_0\rangle$.

The setting of this input register may require propagating $|a\rangle$ or the enable bit across the entire register. Use of a few extra qubits (2^{w-1}) will allow the several setting operations to propagate in a tree. The cost of setting the argument is

$$t_{ARG} = \begin{cases} 2^w(1; 0; 1) = (4; 0; 4)w = 2 \\ 2^w(3; 0; 1)w = 3, 4 \end{cases} . \quad (6.4)$$

For $w = 2$ and $w = 3$, we calculate that setting the argument adds $(4; 0; 4)\#(4, 5)$ and $(24; 0; 8)\#(8, 9)$, respectively, to the latency, concurrency and storage of each adder. We create separate enable signals for each of the 2^w possible arguments and pipeline flowing them across the register to set the addend bits. We consider this cost only when using indirection. Figure 6.5 shows circuits for $w = 2, 3, 4$.

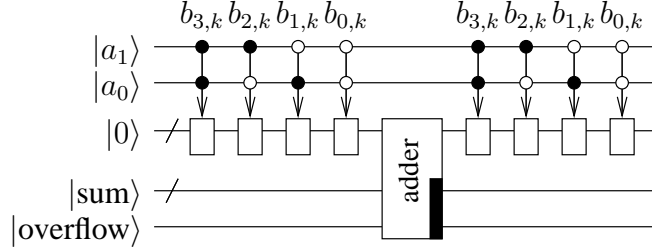


Figure 6.4: Implicit indirection using a classical memory. The arrows pointing to blocks indicate the setting of the multiplicand register to the value above, based on the control lines.

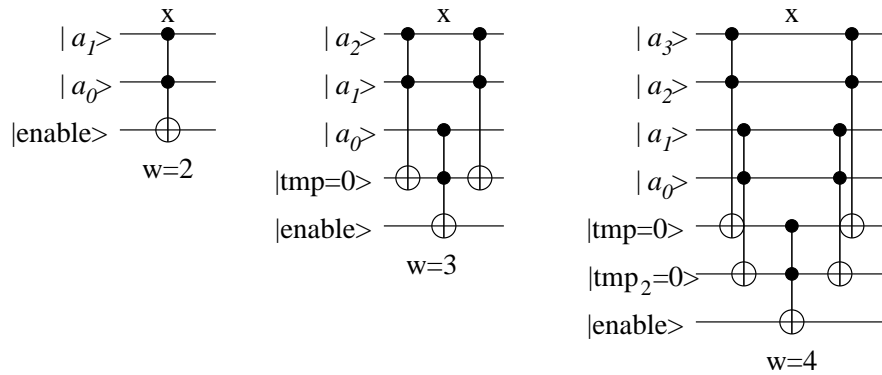


Figure 6.5: Argument setting for indirection for different values of w . For the $w = 4$ case, the two CCNOTs on the left can be executed concurrently, as can the two on the right, for a total latency of 3.

6.2.4 The Algorithm

In essence, the algorithm involves moving from a bit-oriented breakdown of the multiplications to a word-oriented breakdown. The algorithm consists of two main parts: classically calculating the b array values, and calculating their products in the quantum domain. We pay the classical cost in step 1b in the algorithm below, and the quantum cost in step 3c.

The cost of setting up to use the k th iteration of the b array is technology dependent; only one of steps 1c and 3a is necessary. $O(n2^w)$ gates may be required to set a quantum memory, or only the change of a single pointer or position if a QACM is large enough to hold the entire b array at once.

1. Calculate the b array elements:
 - (a) Classically calculate $b_{j,0} = x^j$ for all $j, 0 \leq j < 2^w$
 - (b) For k from 1 to $l - 1$, classically square (modulo N) all 2^w elements $b_{j,k-1}$ w times to create $b_{j,k}$
 - (c) (Store all $b_{j,k}$ into QACM)
2. Initialize $|p\rangle$ to 1
3. For k from 0 to $l - 1$, do
 - (a) (Set up to use $b_{j,k}$ values: store into QACM or quantum memory)
 - (b) In quantum domain, use $|t_k(a)\rangle$ as index into b , $|c_k\rangle = |b_{t_k(a),k}\rangle$
 - (c) $|p\rangle = |c_k p \bmod N\rangle$

Figure 6.6 shows a portion of a modified form of Vedral's circuit using indirection. The dashed box indicates where update of the b array takes place, if necessary; only one-qubit gates are required. Note also that Q-SEL and its reverse are used, but, unlike Vedral's circuit, we do not need the reverse of multiplication to free up our argument. The degenerate case of $w = 1$ is therefore faster than Vedral's circuit.

6.2.5 Evaluating Cost and Selecting Word Length

The goal of this work is to minimize the cost of executing Shor's algorithm, for some metric of cost important to the user. In Figure 6.7 we show the total cost of calculating the modular exponentiation, as a function of word length w . "Cost" in this graph is an

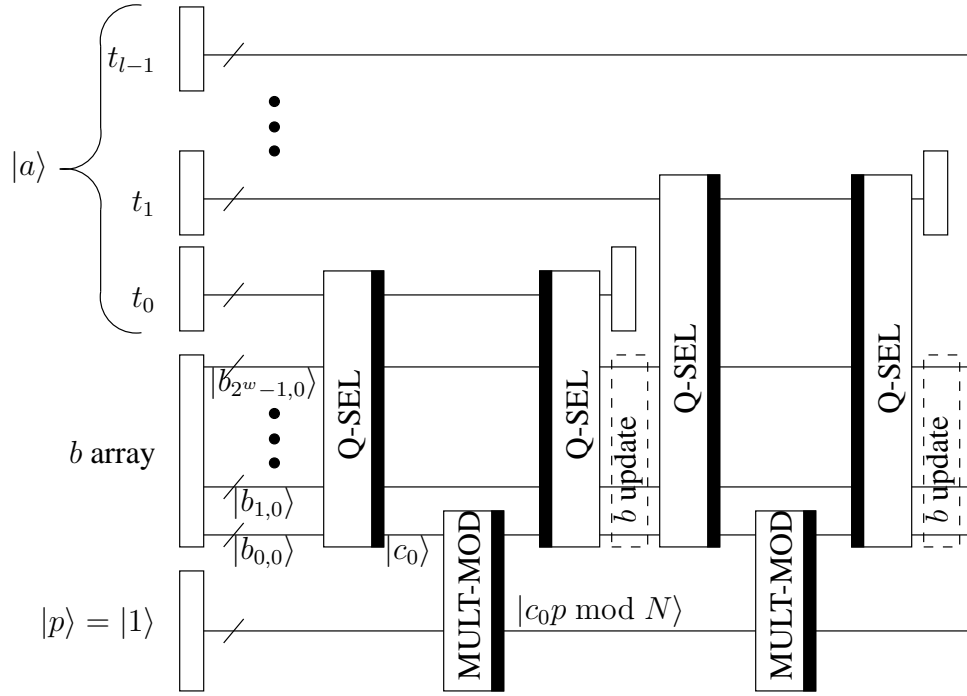


Figure 6.6: Multiplication Using Indirection, Based on Vedral's Circuit

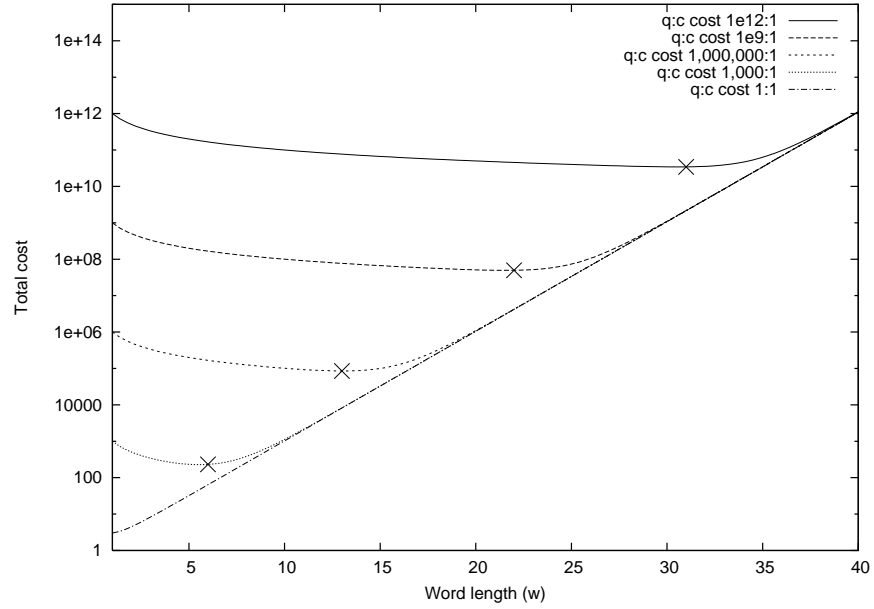


Figure 6.7: Total Cost

arbitrary metric; it may be wall clock time, total time on parallel machines, price tag, or some other economic cost of quantum and classical machines. Perhaps the easiest cost to consider is simply time to perform a modular multiplication. The five curves represent total cost at different ratios of quantum: classical cost, ranging from 1:1 to 10^{12} :1. The 'x' marks on each curve are the nearest integer value of w to the minimum. This recommended word length increases by approximately eight bits for each factor of one thousand the relative quantum cost increases.

This graph is somewhat simplified, in that the cost ratio is treated as fixed. In reality, the QACM cost will almost certainly depend on the word length.

Commodity microprocessors may be as much as 10^{15} times as fast as quantum computing devices, even before accounting for quantum error correction. Faster technologies, ranging up to gigahertz clock rates, still leave several orders of magnitude difference between classical and quantum aggregate gate rates. Combined with the success probability, it is clear that the limitation on w will be the practical size of the b array rather than computational cost.

This section has shown that the standard computer science technique of indirection can be used in the quantum domain to accelerate the modular exponentiation that is the primary cost of Shor's algorithm. This technique reduces the number of multiplications necessary, and is independent of the multiplication algorithm chosen. The price we pay for this is a large classical/quantum tradeoff; we perform 2^w more multiplications in the classical domain in exchange for reducing the quantum multiplications by a factor of w . This basic technique will likely apply to other algorithms, as well.

6.3 New Adder Types

"I only took the regular course...Reeling and Writhing, of course, to begin with, and then the different branches of Arithmetic – Ambition, Distraction, Uglification and Derision."

the Mock Turtle, in **Lewis Carroll's *Alice's Adventures in Wonderland*, 1865**

Quantum versions of the classical carry-select and conditional-sum adders deepen the toolbox of arithmetic routines available for matching software to hardware [109, 334]. The basic carry-select adder concurrently calculates two possible results without knowing the value of the carry in, one assuming that the carry in will be zero, one

assuming that the carry in will be one. Once the carry in becomes available, the correct output value is selected using a multiplexer (MUX). The type of MUX determines whether the latency of the circuit is $O(\sqrt{n})$ (called a carry-select adder) or $O(\log n)$ (called a conditional-sum adder).

Zalka has proposed a carry-select adder, without calling it by name [362]. He did not present a full circuit, making it difficult to reproduce his results, and my circuit produces slightly different numbers than his.

6.3.1 Basic Carry-Select Adder

First, we present the basic carry-select adder, then show the MUX structure that completes the circuit. To add two n -bit numbers, we will divide the numbers into groups and run an adder for each group. The bits are divided into g groups of m bits each, $n = gm$. The first group may have a different size, f , than m , since it will be faster, but for the moment we assume they are the same. The carry-select adder for a single group we will call CSLA.

VBE-Based Adder

Figure 6.8 shows a three-bit carry-select adder, CSLA, plus an example MUX. This generates two possible results, assuming that the carry in will be zero or one. All of the outputs without labels are ancillae to be garbage collected. The circuit shown here is based on the Vedral-Barenco-Ekert (VBE) carry-ripple adder described in Section 3.4.2. As drawn, a full carry-select circuit requires $5m - 1$ qubits to speculatively add two m -bit numbers. The MUX can be implementing using the optimization of the Fredkin gate shown in Figure 2.3 on page 36.

A larger m -bit carry-select adder can be constructed so that its internal delay, as in a normal carry-ripple adder, is one additional CCNOT for each bit, although the total number of gates increases (because we are essentially running two additions at the same time) and the distance between gate operands increases. The latency for the CSLA block is

$$t_{CS} = (m; 2; 0). \quad (6.5)$$

Note that this is not a “clean” adder; we still have ancillae to return to the initial state.

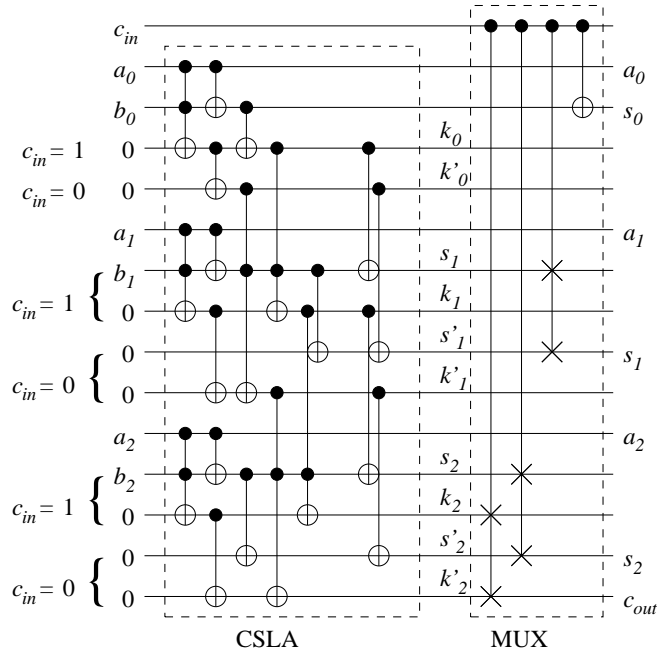


Figure 6.8: Three-bit carry-select adder (CSLA) with multiplexer (MUX). a_i and b_i are addends. The control-SWAP gates in the MUX select either the qubits marked $c_{in} = 1$ or $c_{in} = 0$ depending on the state of the carry in qubit c_{in} . s_i qubits are the output sum and k_i are internal carries.

CDKM-Based Adder

It is possible that a design optimized for space could reduce the number of qubits required, perhaps by utilizing the Cuccaro-Draper-Kutin-Moulton (CDKM) carry-ripple adder (Section 3.4.2), which is more space-efficient. The CDKM adder uses only $2n+2$ bits to add two n -bit numbers (including the carry out). By simply fanning out a “copy” of both the A and B input registers and running separate adders in parallel, it is easy to reduce the $5m - 1$ qubits required above to $4m$, a noticeable savings in space. Figure 6.9 outlines one approach to performing the demultiplexing in place; this approach results in *very* fast availability of the result, but the ancillae garbage collection is slow. The circuit in the figure is general; applying it to carry-select addition, A and B are almost identical, but disentangling the carry in signals slows down the total circuit. I am still in the process of designing this adder, and expect to report on its performance at a later date.

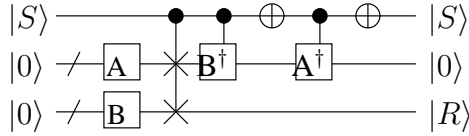


Figure 6.9: In-place circuit and MUX to post-select either $R = A|0\rangle$ or $R = B|0\rangle$, based on the select signal S .

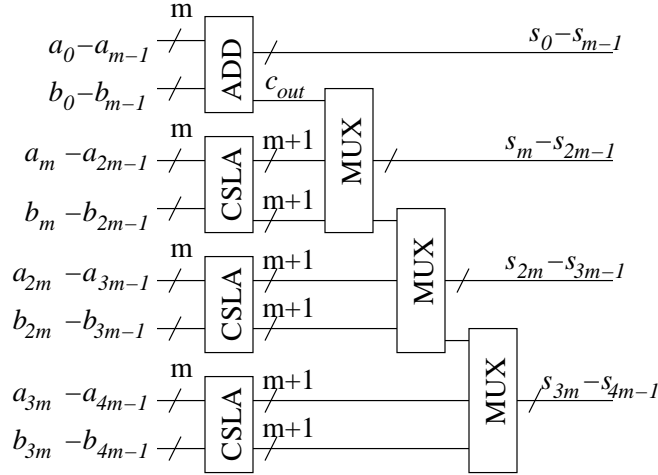


Figure 6.10: Block-level diagram of four-group carry-select adder. a_i and b_i are addends and s_i is the sum. Additional ancillae not shown.

6.3.2 $O(\sqrt{n})$ Carry-Select Adder

The right-hand portion of Figure 6.8 is the MUX which selects the output to use; it is constructed from Fredkin gates using the carry in as the control bit. Notice that the carry in is not used until after all of the adder blocks have completed. This feature allows the parallelism that makes the carry-select adder structure fast. One CSLA for each of the g groups is used; all of the CSLAs are executed concurrently, then the output MUXes are cascaded, as shown in Figure 6.10.

The most difficult implementation problem will be creating an efficient MUX. Figure 6.10 makes it clear that the total carry-select adder is only faster than the carry-ripple adder if the latency of MUX is substantially less than the latency of the full carry-ripple adder. The delay of the initial part of the VBE adder for a group of m qubits would be $(m; 0; 0)$. If the carry out from the MUX requires less than m CCNOT times, it may be faster. The carry out can be generated in a constant number of time steps by prioritizing the last bit in the addition as the first to be MUXed out. The latency of the carry ripple from MUX to MUX (not qubit to qubit) can be arranged to give a total MUX cost of $(4g + 2m - 6; 0; 2g - 2)$.

Within the block, it is certainly easy to see how the MUX can use a fanout tree consisting of more ancillae and CNOT gates to distribute the carry in signal, as suggested by Moore [235], allowing all MUX Fredkin gates to be executed concurrently. A full fanout requires an extra m qubits in each adder. For intermediate values of m , we will use a fanout of 4, reducing the MUX latency to $(4g + m/2 - 6; 2; 2g - 2)$ in exchange for 3 extra qubits in each group. The space used for the full, clean, VBE-based adder is $(6m - 1)(g - 1) + 3f + 4g$ when using a fanout of 4.

The total latency of the CSLA, MUX, and the CSLA undo is

$$\begin{aligned} t_{SEM} &= 2t_{CS} + t_{MUX} \\ &= (4g + 5m/2 - 6; 6; 2g - 2). \end{aligned} \quad (6.6)$$

Optimizing, based on equation 6.6, the delay will be the minimum when $m \sim \sqrt{8n/5}$, giving asymptotic performance $O(\sqrt{n})$.

6.3.3 $O(\log n)$ Conditional Sum Adder

To reach $O(\log n)$ performance, we must add a multi-level MUX to our carry-select adder. This structure is called a conditional sum adder, which we will label CSUM. Rather than repeatedly choosing bits at each level of the MUX, we will create a multi-level distribution of MUX select signals, then apply them once at the end. Figure 6.11 shows only the carry signals for eight CSLA groups. The e signals in the figure are our effective swap control signals. They are combined with a carry in signal to control the actual swap of variables. In a full circuit, a ninth group, the first group, will be a carry-ripple adder and will create the carry in to the rest of our tree; that carry in will be distributed concurrently in a separate tree.

The total adder latency will be

$$\begin{aligned} t_{CSUM} &= 2t_{CS} + \\ &\quad (2\lceil \log_2(g - 1) \rceil - 1) \times (2; 0; 2) \\ &\quad + (4; 0; 4) \\ &= (2m + 4\lceil \log_2(g - 1) \rceil + 2; 4; \\ &\quad 4\lceil \log_2(g - 1) \rceil + 2) \end{aligned} \quad (6.7)$$

where $\lceil x \rceil$ indicates the smallest integer not smaller than x .

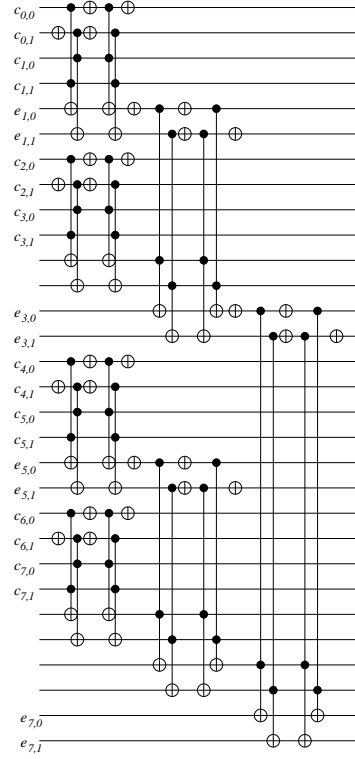


Figure 6.11: $O(\log n)$ MUX for conditional-sum adder, for $g = 9$ (the first group is not shown). Only the $c_{i,j}$ carry out lines from each m -qubit block are shown, where i is the block number and j is the carry in value. At each stage, the span of correct effective swap control lines $e_{i,j}$ doubles. After using the swap control lines, all but the last must be cleaned by reversing the circuit. Unlabeled lines are ancillae to be cleaned.

For large n , this generally reaches a minimum for small m , which gives asymptotic behavior $\sim 4 \log_2 n$, the same as the carry-lookahead adder from Section 3.4.3. CSUM is noticeably faster for small n , but requires more space. The MUX uses $\lceil 3(g-1)/2 \rceil - 2$ qubits in addition to the internal carries and the tree for dispersing the carry in. Our space used for the full, clean adder is $(6m-1)(g-1) + 3f + \lceil 3(g-1)/2 \rceil - 2 + (n-f)/2 \approx 6n$. Section 6.4 details the tradeoffs in overall system design caused by the extra space required.

Maslov et al. have recently improved on the performance of this MUX by reducing the pair of CCNOTs to one CCNOT and two CNOTs, using the breakdown of the Fredkin gate from Figure 2.1.

6.3.4 Summary

Carry-select addition speculatively executes two additions in parallel, one assuming a carry in of zero, and one assuming a carry in of one. After completion of the addition, when the input carry becomes available, one result is chosen and the other discarded, in direct analog to the speculative execution of instructions in modern microprocessors. The basic concept of a carry-select addition process is a flexible framework allowing different choices of group size, inner adder type, and multiplexer structure. This structure can even, in theory, be applied to other operations besides addition, by using the general circuit in Figure 6.9. The adders I have designed have latency of $O(\log n)$ or $O(\sqrt{n})$ to add two n -bit numbers, when evaluated for the abstract ACarchitecture. We turn next to the mapping of these and other algorithms to specific sets of hardware constraints, primarily restrictions on the distance of gate operands on the NTC architecture.

6.4 Performance of Shor's Algorithm on a Monolithic Quantum Computer

In Chapter 3, particularly Figure 3.2 and Section 3.5.1, we introduced the performance of factoring on classical machines and quantum computers, but left that analysis incomplete. We know that Shor's algorithm is polynomial in the length of the number being factored, which will be a straight line on a log-log plot, but where should it fall on the graph? We were missing a key piece of information, namely, the logical clock speed of the quantum system, as discussed in Section 6.1. A comparison of the execution time to factor a number on classical and quantum computers is shown in

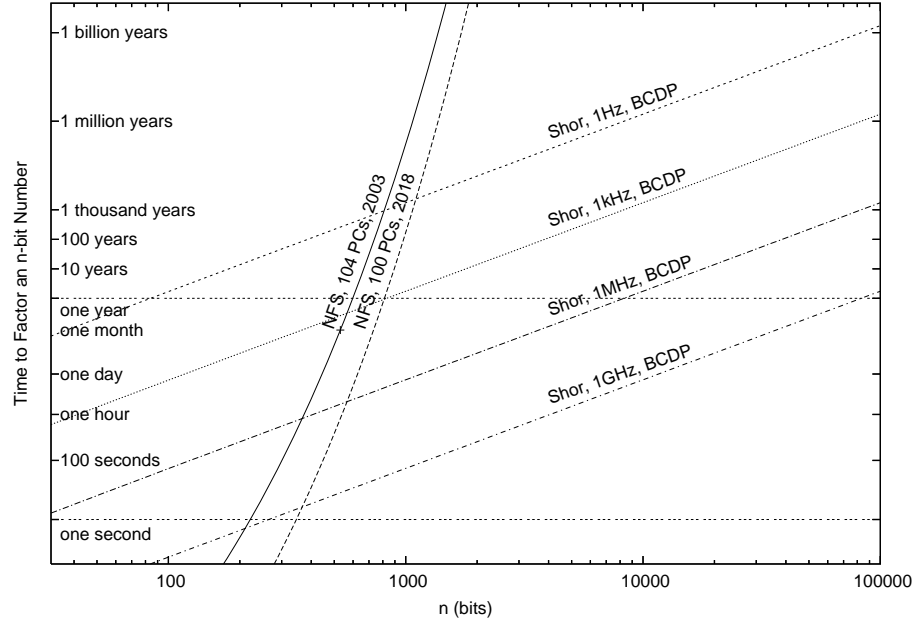


Figure 6.12: Scaling of number field sieve (NFS) on classical computers and Shor's algorithm for factoring on a quantum computer, using BCDP modular exponentiation with various clock rates. Both horizontal and vertical axes are log scale. The horizontal axis is the size of the number being factored, in bits.

Figure 6.12. It compares the performance of Shor's algorithm on a quantum computer using the Beckman-Chari-Devabhaktuni-Preskill (BCDP) modular exponentiation algorithm [35] to classical computers running the general Number Field Sieve. The steep curves are for NFS on a set of classical computers. The shallower curves on the figure are predictions of the performance of a quantum computer running Shor's algorithm, using the BCDP modular exponentiation routine, which uses $5n$ qubits to factor an n -bit number, requiring $\sim 54n^3$ gate times to run the algorithm on large numbers. The four curves are for different logical clock rates from 1 Hz to 1 GHz. The performance scales linearly with clock speed. Factoring a 576-bit number in one month of calendar time requires a clock rate of 4 kHz. A 1 MHz clock will solve the problem in about three hours. If the clock rate is only 1 Hz, the same factoring problem will take more than three hundred years.

The execution time shown in Figure 6.12 can be improved by understanding that relationship of architecture and algorithm. The performance of the VBE and BCDP carry-ripple adders, and by extension their entire modular exponentiation algorithms, is almost independent of architecture. Carry-ripple adders, which use only nearby qubits

during their execution, do not take advantage of long-distance gates even when the architecture supports them, so any architectural analysis based solely on these algorithms is likely to conclude that long-distance gates are not useful. However, the performance of most polynomial-time algorithms, including other types of adder, varies noticeably depending on the system architecture.

6.4.1 Mapping Adders to Architectures

Figures 3.3 and 3.6 on pages 69 and 73 showed two types of quantum adder circuits, the Vedral-Barenco-Ekert (VBE) carry-ripple adder [342] and the Draper-Kutin-Rains-Svore carry-lookahead adder [103]. The first, most obvious difference between the two is how “busy” the diagrams appear. The carry-ripple adder shows that most of the qubits sit idle during most of the computation, waiting for the carry to ripple across the circuit (and back, as a cleanup operation). The carry-lookahead adder is much denser, accomplishing its work in fewer time steps by executing more gates in parallel.

The second most prominent visual difference is the span of the gates (vertical line segments). Carry-ripple adders operate only on qubits that are nearby, while the carry-lookahead adder leapfrogs long distances. This gives the carry-ripple adder $O(n)$ latency, compared to $O(\log n)$ for the carry-lookahead — if long-distance gates are supported.

Figure 6.13 shows a fully optimized, concurrent, but otherwise unmodified version of the VBE ADDER for three bits on a neighbor-only machine (NTC architecture). The latency is

$$t_{ADD}^{NTC} = (20n - 15; 0) \# (2; 3n + 1) \quad (6.8)$$

or 45 gate times for the three-bit adder. A 128-bit adder will have a latency of (2545; 0). The diagram shows a concurrency level of three, but simple adjustment of execution time slots can limit that to two for any n , with no latency penalty.

Table 6.1 lists recommendations for adders that match various technologies. For example, the Fourier adder [102] uses only $2n$ space, compared to the $3n$ of standard carry-ripple adders [342, 35]. Unfortunately, it requires n concurrent gates to achieve the $O(n)$ time bound when performing the quantum Fourier transform (QFT) required to move numbers into and out of the Fourier representation, compared to concurrency of 2 for carry-ripple. The Fourier adder also requires precise rotations similar to those in the QFT, which may be hard to implement accurately. The newly designed CDKM carry-ripple adder (Section 3.4.2) uses only $2n$ space and small concurrency, making it

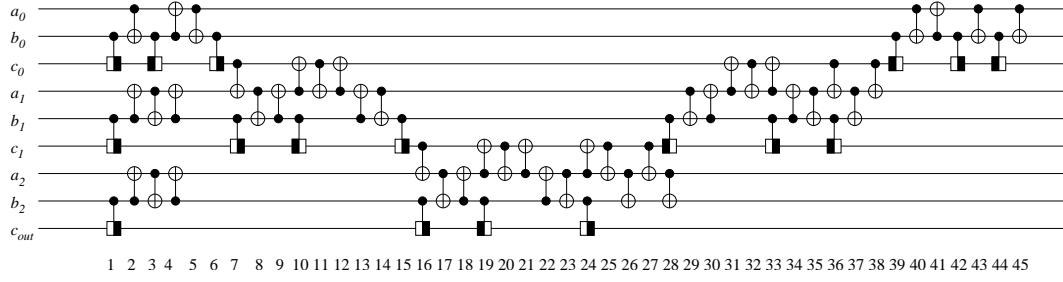


Figure 6.13: Optimized, concurrent three bit VBE ADDER for the NTC architecture. Numbers across the bottom are time steps.

technology	adder	conc.	latency
Si NMR	carry-ripple	2	$O(n)$
solution NMR	carry-ripple	2	$O(n)$
1-D quantum dot	carry-ripple, Fourier	2 or n	$O(n)$
1-D JJ charge	carry-ripple, Fourier	2 or n	$O(n)$
1-D Kane model	carry-ripple, Fourier	2 or n	$O(n)$
scalable ion trap	carry-lookahead, conditional-sum	n or $2n$	$O(\log n)$
Oskin lattice	carry-lookahead, conditional-sum	n or $2n$	$O(\sqrt{n})$
all-optical	carry-lookahead, conditional-sum	n or $2n$	$O(\log n)$

Table 6.1: Qubit technologies and recommended choice of adder. conc., required application-level concurrency

now the preferred choice in many cases [88].

Likewise, some entries recommend both the conditional-sum and carry-lookahead adders, which have almost identical $O(\log n)$ latencies. A conditional-sum adder requires more space and concurrency than carry-lookahead. However, it has different locality characteristics which might make it map better to an irregular architecture.

Irregular architectures, or those with regular but more complex layouts, complicate the analysis. In particular, the scalable ion trap has limited concurrency, but the distance an ion must move may have a factor of two or more performance impact, making locality desirable. Although the design of such a system is not yet advanced enough to definitively choose between the two proposed types of adders, Thaker et al. have begun analyzing the performance of the carry-lookahead adder on one proposed system [324]. In their analysis, the carry-lookahead adder is limited in performance by available application-level concurrency, leading us to suggest that the CDKM carry-ripple adder may provide similar performance while using fewer qubits. For the two-dimensional layout of the Kane lattice, an ideal $O(\log n)$ adder can reach latency of only $O(\sqrt{n})$ due to the communications cost of moving qubits.

For the Josephson-junction qubits, we recommend using long-distance inductive or capacitive transfer structures only if concurrent operations can be preserved for at least some qubits. Alternating cycles of a single long-distance interaction and many nearest-neighbor interactions would be adequate. Designs in which only some of the qubits can transfer long distances while others execute concurrent nearest-neighbor operations seem physically plausible, and would result in intermediate performance, possibly using a carry-select or conditional-sum adder. Concrete performance analysis will depend on the details of such a heterogeneous architecture. Vartiainen has done some analysis on such a structure [341].

The common format of circuit diagram abstracts away the physical layout of qubits, and for any layout other than linear nearest neighbor, gives the wrong impression of “nearby”. Therefore, we have begun animating the action of some circuits for more complex topologies [331].

6.4.2 Acceleration

This section presents an engineering tradeoff analysis of parallelizing the multiplication steps, an improved modulo arithmetic method, and a brief analysis of the indirection method of Section 6.2, in the context of Shor’s algorithm.

Concurrent Exponentiation

In Section 3.5, we discussed Cleve and Watrous' method for parallelizing multiplication, as shown in Figure 3.7 on page 78. For s multipliers, $s \leq n$, each multiplier must combine $r = \lfloor (2n + 1)/s \rfloor$ or $r + 1$ numbers, using $r - 1$ or r multiplications (the first number being simply set into the running product register), where $\lfloor x \rfloor$ indicates the largest integer not larger than x . The intermediate results from the multipliers are combined using $\lceil \log_2 s \rceil$ quantum-quantum multiplication steps.

For a parallel version of VBE, the exact latency, including cases where $rs \neq 2n + 1$, is

$$R_V = 2r + 1 + \lceil \log_2(\lceil (s - 2n - 1 + rs)/4 \rceil + 2n + 1 - rs) \rceil \quad (6.9)$$

times the latency of our multiplier. For small s , this is $O(n)$; for larger s ,

$$\lim_{s \rightarrow n} O(n/s + \log s) = O(\log n) \quad (6.10)$$

Reducing the Cost of Modulo Operations

The VBE algorithm does a trial subtraction of N in each modulo addition block; if that underflows, N is added back in to the total. This accounts for two of the five ADDER blocks and much of the extra logic to compose a modulo adder. The last two of the five blocks are required to undo the overflow bit.

Figure 6.14 shows a more efficient modulo adder than VBE, based partly on ideas from BCDP and Gossett. It requires only three adder blocks, compared to five for VBE, to do one modulo addition. The first adder adds x^j to our running sum. The second conditionally adds $2^n - x^j - N$ or $2^n - x^j$, depending on the value of the overflow bit, *without* affecting the overflow bit, arranging it so that the third addition of x^j will overflow and clear the overflow bit if necessary. The blocks pointed to by arrows are the addend register, whose value is set depending on the control lines. Figure 6.14 uses n fewer bits than VBE's modulo arithmetic, as it does not require a register to hold N .

In a slightly different fashion, we can improve the performance of VBE by adding a number of qubits, p , to our result register, and postponing the modulo operation until later. This works as long as we don't allow the result register to overflow; we have a redundant representation of modulo N values, but that is not a problem at this stage of

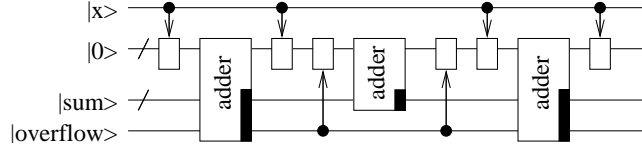


Figure 6.14: More efficient modulo adder. The blocks with arrows set the register contents based on the value of the control line. The position of the black block indicates the running sum in our output.

the computation.

The largest number that doesn't overflow for p extra qubits is $2^{n+p} - 1$; the largest number that doesn't result in subtraction is $2^{n+p-1} - 1$. We want to guarantee that we always clear that high-order bit, so if we subtract bN , the most iterations we can go before the next subtraction is b . The largest multiple of N we can subtract is $\lfloor 2^{n+p-1}/N \rfloor$. Since $2^{n-1} < N < 2^n$, the largest b we can allow is, in general, 2^{p-1} . To perform b modular additions requires $2b + 1$ ADDER calls. For example, adding three qubits, $p = 3$, allows $b = 4$, reducing the 20 ADDER calls VBE uses for four additions to 9 ADDER calls, a 55% performance improvement.

We must use $3p$ adder calls at the end of the calculation to perform our final modulo operation. As p grows larger, the cost of the adjustment at the end of the calculation also grows and the additional gains are small. Calculations suggest that p of up to 10 or 11 continues to improve in speed.

This approach almost eliminates the penalty for doing modulo arithmetic instead of ordinary integer arithmetic. The number of calls to our adder block necessary to make an n -bit modulo multiplier is reduced from the $5n$ in VBE to $3n$ using Figure 6.14 to

$$R_M = n(2b + 1)/b \quad (6.11)$$

for the overflow approach described in these last few paragraphs; this last expression is only slightly above two adder calls per modulo addition for reasonable values of b .

Indirection

Adapting equation 6.9 to both indirection and concurrent multiplication, we have a total latency for our circuit, in multiplier calls, of

$$R_I = 2r + 1 + \lceil \log_2(\lceil (s - 2n - 1 + rs)/4 \rceil + 2n + 1 - rs) \rceil \quad (6.12)$$

algo.	adder	modulo	indirect	s	space	concurrency
cVBE	VBE	VBE	N/A	1	897	2
D	CSUM($m = 4$)	$p = 11, b = 1024$	$w = 2$	12	11969	$126 \times 12 = 1512$
E	QCLA	$p = 10, b = 512$	$w = 2$	16	12657	$128 \times 16 = 2048$
F	CDKM	$p = 10, b = 512$	$w = 4$	20	11077	$20 \times 2 = 40$
G	CDKM	fig. 6.14	$w = 4$	1	660	2

Table 6.2: Parameters for our algorithms, chosen for 128 bits. s , number of independent multiplier units.

where $r = \lfloor \lceil (2n + 1)/w \rceil / s \rfloor$.

6.4.3 Example: Exponentiating a 128-bit Number

In this section, we combine these techniques into complete algorithms and examine the performance of modular exponentiation of a 128-bit number. We assume the primary engineering constraint is the available number of qubits. In Section 6.4.2 we showed that using twice as much space can almost double our speed, essentially linearly until the log term begins to kick in. Thus, in managing space tradeoffs, this will be our standard: any technique that raises performance by more than a factor of c in exchange for c times as much space will be used preferentially to parallel multiplication. Carry-select adders (Sec. 6.3.1) easily meet this criterion, being perhaps six times faster for less than twice the space.

Because we are interested in systems with some realistic limitations, in this section we have chosen to limit the space available to $100n$ qubits. This is a large enough number to see the effects of parallelism, but small enough to constrain the behavior of the algorithm somewhat. In later sections, we will relax this space restriction to $2n^2$ qubits, the maximum number we have found to be useful.

Algorithm **D** uses $100n$ space and our conditional-sum adder *CSUM*. Algorithm **E** uses $100n$ space and the carry-lookahead adder *QCLA*. Algorithms **F** and **G** use the Cuccaro adder and $100n$ and minimal space, respectively. Parameters for these algorithms are shown in Table 6.2. We have included detailed equations for concurrent VBE and **D** below, and numeric results for all of the algorithms in Table 6.3; the detailed equations for the other algorithms are easily derived in a similar fashion. The performance ratios are based only on the CCNOT gate count for AC, and only on the CNOT gate count for NTC.

algo.	AC		NTC	
	gates	perf.	gates	perf.
cVBE	$(1.25 \times 10^8; 8.27 \times 10^7; 0.00 \times 10^0)$	1.0	$(8.32 \times 10^8; 0.00 \times 10^0)$	1.0
D	$(2.19 \times 10^5; 2.57 \times 10^4; 1.67 \times 10^5)$	570	N/A	N/A
E	$(1.71 \times 10^5; 1.96 \times 10^4; 2.93 \times 10^4)$	727	N/A	N/A
F	$(7.84 \times 10^5; 1.30 \times 10^4; 4.10 \times 10^4)$	159	$(4.11 \times 10^6; 4.10 \times 10^4)$	203
G	$(1.50 \times 10^7; 2.48 \times 10^5; 7.93 \times 10^5)$	8.3	$(7.87 \times 10^7; 7.93 \times 10^5)$	10.6

Table 6.3: Latency to factor a 128-bit number for various architectures and choices of algorithm. AC, abstract concurrent architecture. NTC neighbor-only, two-qubit gate, concurrent architecture. perf, performance relative to VBE algorithm for that architecture, based on CCNOTs for AC and CNOTs for NTC.

Concurrent VBE

On AC, the concurrent VBE ADDER is $(3n - 3; 2n - 3; 0) = (381; 253; 0)$ for 128 bits. This is the value we use in the concurrent VBE line in Table 6.3. This will serve as our best baseline time for comparing the effectiveness of more drastic algorithmic surgery.

The unmodified full VBE modular exponentiation algorithm, consists of $20n^2 - 5n = 327040$ ADDER calls plus minor additional logic. A 128-bit VBE adder, from Equation 6.8, will have a latency of $(2545; 0)$. This gives a total latency of

$$\begin{aligned}
 t_V^{NTC} &= (20n^2 - 5n)t_{ADD}^{NTC} \\
 &= (400n^3 - 400n^2 + 75n; 0)
 \end{aligned} \tag{6.13}$$

for VBE.

Algorithm D

The overall structure of algorithm **D** is similar to VBE, with our conditional-sum adders instead of the VBE carry-ripple, and our improvements in indirection and modulo. As we do not consider CSUM to be a good candidate for an algorithm for NTC, we evaluate only for AC. Algorithm **D** is the fastest algorithm for $n = 8$ and $n = 16$. The total latency is

$$\begin{aligned}
 t_D &= R_I R_M \\
 &\quad \times (t_{CSUM} + t_{ARG}) \\
 &\quad + 3pt_{CSUM}.
 \end{aligned} \tag{6.14}$$

Expanding the terms in this equation and letting $r = \lfloor \lceil (2n + 1)/w \rceil / s \rfloor$, the latency and space requirements for algorithm **D** are

$$\begin{aligned}
 t_D^{AC} = & 2r + 1 + \lceil \log_2(\lceil (s - 2n - 1 + rs)/4 \rceil \\
 & + 2n + 1 - rs) \rceil n(2b + 1)/b \\
 & \times ((2m + 4\lceil \log_2(g - 1) \rceil + 2; 4; \\
 & 4\lceil \log_2(g - 1) \rceil + 2) + (4; 0; 4)) \\
 & + 3p(2m + 4\lceil \log_2(g - 1) \rceil + 2; 4; \\
 & 4\lceil \log_2(g - 1) \rceil + 2)
 \end{aligned} \tag{6.15}$$

and

$$\begin{aligned}
 S_D = & s(S_{CSUM} \\
 & + 2^w + 1 + p + n) + 2n + 1 \\
 = & s(7n - 3m - g + 2^w + p \\
 & + \lceil 3(g - 1)/2 - 2 + (n - m)/2 \rceil) \\
 & + 2n + 1.
 \end{aligned} \tag{6.16}$$

Algorithm E

Algorithm **E** uses the carry-lookahead adder QCLA in place of the conditional-sum adder CSUM. Although CSUM is slightly faster than QCLA, its significantly larger space consumption means that in our $100n$ fixed-space analysis, we can fit in 16 multipliers using QCLA, compared to only 12 using CSUM, as listed in Table 6.2. This allows the overall algorithm **E** to be 28% faster than **D** for 128 bits.

Algorithms F and G

The CDKM carry-ripple adder has a latency of $(10n + 5; 0)$ for NTC. This is twice as fast as the VBE adder. We use this in our algorithms **F** and **G**. Algorithm **F** uses $100n$ space, while **G** is our attempt to produce the fastest algorithm possible in the minimum amount of space.

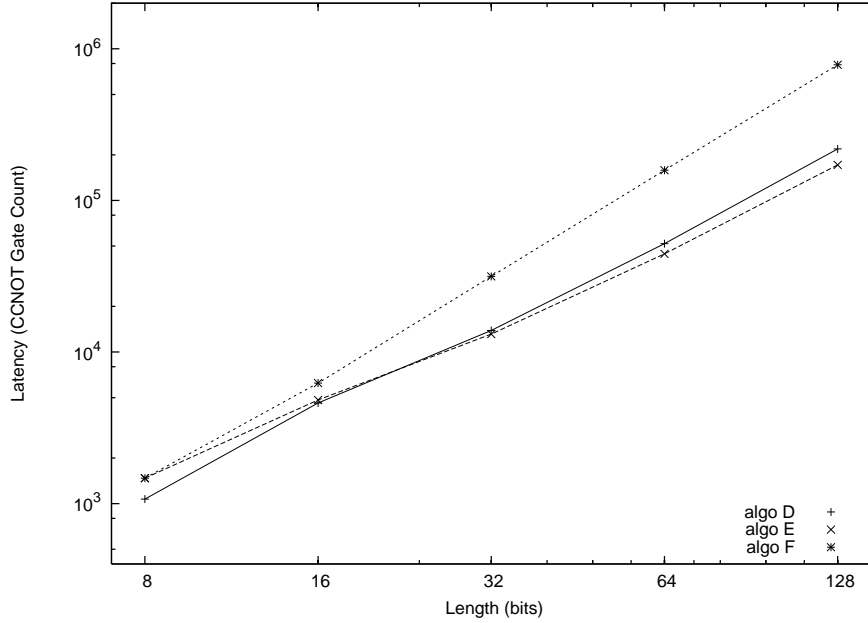


Figure 6.15: Execution time for our algorithms for space $100n$ on the AC architecture, for varying value of n .

Smaller n and Different Space

Figure 6.15 shows the execution times of our three fastest algorithms for n from eight to 128 bits. Algorithm **D**, using CSUM, is the fastest for eight and 16 bits, while **E**, using QCLA, is fastest for larger values. The latency of 1072 for $n = 8$ bits is 32 times faster than concurrent VBE, achieved with $60n = 480$ qubits of space.

Figure 6.16 shows the execution times for $n = 128$ bits for various amounts of available space. All of our algorithms have reached a minimum by $240n$ space (roughly $1.9n^2$).

6.4.4 Asymptotic Behavior

The focus of this dissertation is the constant factors in modular exponentiation for important problem sizes (up to a thousand bits or so) and architectural characteristics. However, let us look briefly at the asymptotic behavior of our circuit depth, which will tell us about the behavior of systems on very large problems. As we have mentioned before, the arbitrary-distance AC model is not physically realistic for very large systems; likewise, no one would propose carrying NTC to its extreme and building a one-dimensional line of a million or more qubits. Therefore, these expressions should be treated as “not to exceed” upper and lower bounds.

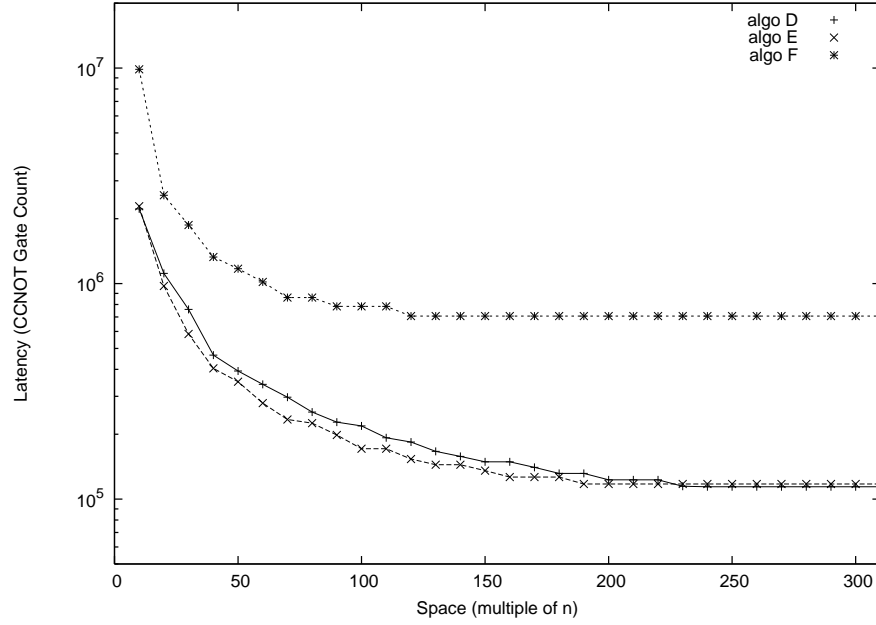


Figure 6.16: Execution time for our algorithms for 128 bits on the AC architecture, for varying multiples of n space available.

In Section 6.4.2, we showed that the latency of our complete algorithm is

$$O(n/s + \log s) \times (\text{latency of multiplication}) \quad (6.17)$$

as we parallelize the multiplication using s multiplier blocks. Our multiplication algorithm is still

$$O(n) \times (\text{latency of addition}). \quad (6.18)$$

Algorithms **D** and **E** both use an $O(\log n)$ -depth adder. Combining equations 6.17 and 6.18 with the adder cost, we have asymptotic circuit depth of

$$t_D^{AC} = t_E^{AC} = O((n \log n)(n/s + \log s)) \quad (6.19)$$

for algorithms **D** and **E**. As $s \rightarrow n$, these approach $O(n \log^2 n)$ and space consumed approaches $O(n^2)$.

Algorithm **F** uses an $O(n)$ adder, whose asymptotic behavior is the same on both AC and NTC, giving

$$t_F^{AC} = t_F^{NTC} = O((n^2)(n/s + \log s)) \quad (6.20)$$

approaching $O(n^2 \log n)$ as space consumed approaches $O(n^2)$.

These results compare favorably to the asymptotic behavior of $O(n^3)$ for VBE, BCDP, and algorithm **G**, each of which uses $O(n)$ space. The asymptotic behavior of these three algorithms is independent of whether the architecture is AC or NTC.

The ultimate limit of performance for AC will be achieved using a Gossett carry-save multiplier and large s . The carry-save multiplier consumes $O(n^2)$ space. Gossett has shown that the latency of a carry-save multiplier will be $O(\log n)$, using a tree structure to combine partial results, and the latency of the entire modular exponentiation algorithm will be $O(n \log n)$. Parallelizing the multiplication raises the space consumed to $O(n^3)$ and reduces the latency to $O(\log^3 n)$. The requirement for n^3 qubits quickly moves into the billions as n nears one thousand, and into the trillions as n nears ten thousand; none of the proposed technologies we know of are likely to reach such levels of scalability, though it is possible that nanotechnology will eventually reach levels in which large numbers of individual atoms in bulk materials are controllable.

For physically realizable systems, as we noted in Section 3.4.4, an adder will ultimately be limited to $O(\sqrt[3]{n})$ when $O(n)$ qubits are packed in three-dimensional space, because all signal propagation methods are limited to be linear in distance, and are subject to the final limit of the speed of light. The complete modular exponentiation algorithm, using $O(n^2)$ adders calls, is therefore limited to $O(n^2 \sqrt[3]{n}) = O(n^{7/3})$ latency when using $O(n)$ qubits and a nominally $O(\log n)$ adder. When using $O(n^2)$ qubits, the performance limit is $O(n^{5/3})$. When using $O(n^3)$ qubits, the distance across the entire ensemble is $O(n)$, and this turns out to be the limit of our performance, too.

Thus, we can say that modular exponentiation is ultimately limited to $O(n)$ performance, where n is limited only by the size (and age) of the Universe and the availability of matter (or energy) to implement the qubits.

6.4.5 Results

In this section, we extend our results by expanding the qubit space available, and, at last, bringing clock speed into the picture. On the AC architecture, our algorithms have shown a speed-up factor ranging from 4,000 times for factoring a 576-bit number to nearly one million for a 100,000-bit number, when using $100n$ space. This is about fifteen times the space consumption of the original VBE algorithm, at $7n$, and twenty times the space of BCDP, at $5n$. Using BCDP as our baseline, we compare the **D** and **F** algorithms, with **D** being the fastest algorithm on AC and **F** being the fastest on NTC.

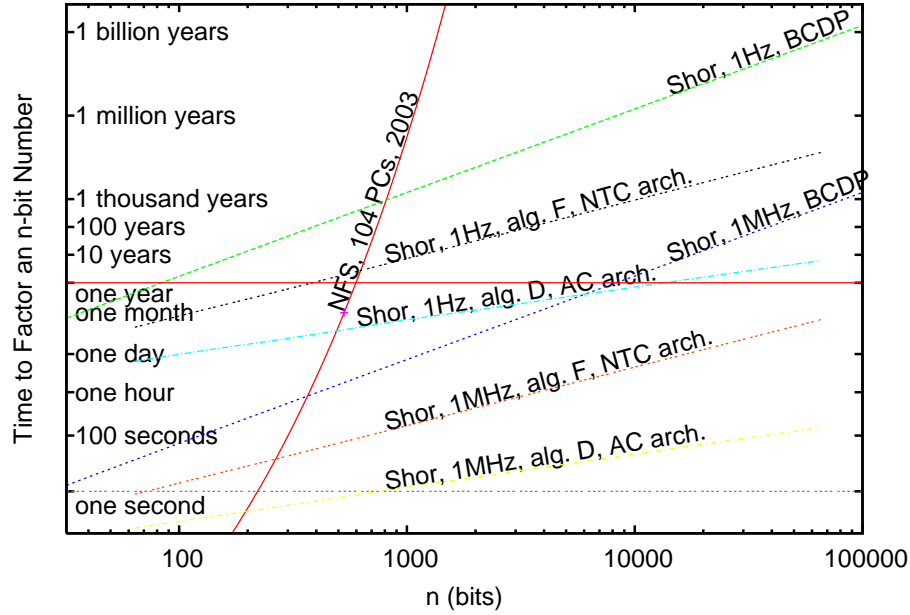


Figure 6.17: Scaling of number field sieve (NFS) and Shor's algorithms for factoring, using faster modular exponentiation algorithms and $2n^2$ space.

The values reported here for both algorithms are calculated using $2n^2$ qubits of storage to exponentiate an n -bit number, the largest number of qubits our algorithms can effectively use. Algorithm **D** with $2n^2$ qubits on AC is 13,000 times faster than BCDP at factoring a 576-bit number, and one million times faster for a 6,000 bit number. Algorithm **F** on NTC, by contrast, is only about 1,000 times faster than BCDP at factoring a 6,000-bit number. For very large n , the latency of **D** is $\sim 9n \log_2^2(n)$. The latency of **F** is $\sim 20n^2 \log_2(n)$.

Figure 6.17 updates the performance shown in Figure 6.12 on page 139, adding our fastest algorithms. We have kept the 1 Hz and 1 MHz lines for BCDP, and added matching lines for our fastest algorithms on the AC and NTC architectures at the same clock speeds. These speeds are, of course, logical clock speeds, after accounting for the overhead of fault tolerance and QEC. The clock speed is for Toffoli gates for BCDP and **D**, and for two-qubit gates for **F**. For AC, our algorithm **D** requires a clock rate of only about 0.3 Hz to factor a 576-bit number in one month. For NTC, using our algorithm **F**, a clock rate of around 27 Hz is necessary.

adder	K	Q	KQ
VBE carry-ripple	$3n$	$3n$	$9n^2$
CDKM carry-ripple	$2n$	$2n$	$4n^2$
conditional-sum	$6n$	$4 \log_2 n$	$24n \log_2 n$
carry-lookahead	$4n$	$4 \log_2 n$	$16n \log_2 n$

Table 6.4: Approximate KQ to add two n -qubit numbers using some different adder circuits, in units of qubit-Toffoli times.

6.4.6 Error Correction Needs

We saw in Section 2.3.1 that we can estimate the required strength of error correction, roughly, by calculating KQ , where K is the number of qubits and Q is the number of time steps. KQ represents the number of QEC cycles that must be performed throughout the entire system during the course of the complete computation. This approach is predicated on the observation that QEC consumes such a large percentage of the total operations in the system that the effects of the logical gates are unimportant for this analysis. Steane's analysis treats KQ somewhat abstractly; here we show that K varies over the course of the execution of an algorithm [308].

A carry-ripple adder to add two n -qubit numbers, whether VBE or CDKM, uses $O(n)$ qubits and takes $O(n)$ time steps, giving a $KQ = O(n^2)$. The carry-lookahead and conditional-sum adders likewise use $O(n)$ qubits, but run in $O(\log n)$ time steps, for $KQ = O(n \log n)$. Table 6.4 shows approximate values of KQ for the different adders. For $n = 1,024$, KQ is about four million for the CDKM adder, but only 160,000 for the conditional-sum adder, a factor of twenty five better. Of course, this analysis assumes the AC architecture's support for long-distance gates. Thus, we see that not only does AC have a better error threshold, but the demands of the application are lower. This factor will result in higher-fidelity calculations, or possibly even a reduction in the necessary strength of QEC, saving space and time.

In all of our proposed algorithms, modular multiplication consists of $O(n)$ calls to the adder routine, giving $KQ = O(n^3)$ for a multiplication when using carry-ripple adders and $KQ = O(n^2 \log n)$ when using log-depth adders. We have also proposed parallelizing multiplication using the Cleve-Watrous method. In its broadest form, as in Figure 6.18, it uses n multiplier units and requires $\log_2 n$ steps. This may appear to result in KQ being $n \log_2 n$ times the KQ of a multiplication, which would be an increase of a factor $\log_2 n$ over a simple linear string of multiplications. However, the

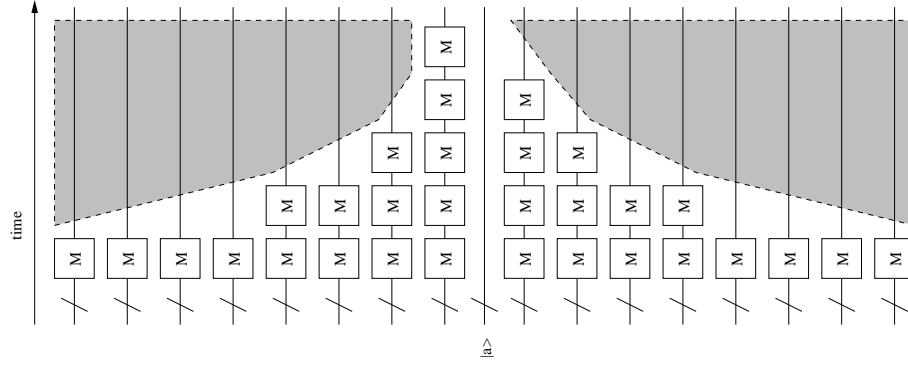


Figure 6.18: Cleve-Watrous parallel multiplication (rotated ninety degrees relative to other graphs, with time flowing bottom to top). Gray areas represent disentangled, unused qubits.

gray areas in the figure are *disentangled* from the running computation. They do not affect the results, and should not be counted in the KQ for the overall computation. (The unused resources ideally shouldn't go to waste, but that's a different problem.) Thus, regardless of the arrangement of the multipliers, the total KQ for modular exponentiation is $2n$ times the cost of a multiplier, or, when using the indirection of Sections 6.4.2 and 6.2, $2l = 2\lceil n/w \rceil$ times the cost of a multiplier. The one minor complication is that our parallel multiplications keep only a single copy of $|a\rangle$, rather than one for each multiplier unit. For algorithms **D**, **E**, **F**, and **G**, we ignore the cost of the $|a\rangle$ register in the table, it being small compared to the overall size of the system; for small values of s this approximation is not good, but the result is still within 40% or so at worst. Recognizing from Equation 6.11 that even for modest values of b , the number of adder calls R_M to make a modulo multiplier is $\sim 2n$, we can simplify our expressions for KQ and arrive at the values in Table 6.5. The terms in the expressions in the table are, in order, number of modulo multiplier calls; number of modulo adder calls per modulo multiplier; adder calls per modulo adder; adder depth; and first-order term in number of qubits. Our algorithm **G** is an order of magnitude better than VBE, and **F** is almost two orders of magnitude better, on the NTC architecture. For AC, we can use **D** and **E** for further gains. The asymptotic growth is substantially slower; numerically, for $n = 1,024$, for VBE $KQ \approx 2 \times 10^{14}$, and **E** is $\approx 2.4 \times 10^{11}$, almost three orders of magnitude better. All of these values are for indirection (Section 6.2) using $w = 2$ to $w = 4$, as shown in Table 6.2; an additional factor of 4 or more seems quite plausible, as shown in Figure 6.7 on page 131, when error correction becomes an overriding concern.

Steane calculated that, for a physical gate error rate of $\sim 10^{-5}$ and a memory error

algorithm	KQ
cVBE	$2n \times n \times 5 \times 3n \times 7n = 210n^4$
algo. D	$2l \times n \times 2 \times 4 \log_2 n \times 5n \approx 40n^3 \log_2 n$
algo. E	$2l \times n \times 2 \times 4 \log_2 n \times 3n \approx 24n^3 \log_2 n$
algo. F	$2l \times n \times 2 \times 2n \times 3n \approx 6n^4$
algo. G	$2l \times n \times 3 \times 2n \times 6n \approx 18n^4$

Table 6.5: Approximate KQ for our complete modular exponentiation circuits, in units of qubit-Toffoli times.

rate of $\sim 10^{-6}$ on an AC-like architecture, KQ of 10^{15} can be achieved using only about a factor of twelve increase in storage, via the BCH $[[127,43,13]]$ code [308]².

6.5 Summary

This chapter opened with a discussion of the performance of Shor’s algorithm on a quantum computer, showing in Figure 6.12 that logical clock speed has an important impact on the utility of a quantum computer, despite the apparent gains in computational class compared to classical computers. This fact is often under-appreciated by physicists, who tend to assume that the gain in class will prove decisive.

It is possible to significantly accelerate quantum modular exponentiation using a stable of techniques, culminating in the much-improved performance shown in Figure 6.17. I have provided exact gate counts, rather than asymptotic behavior, for the $n = 128$ case, showing algorithms that are faster by a factor of 200 to 700, depending on architectural features, when $100n$ qubits of storage are available. For $n = 1024$, this advantage grows to more than a factor of 5,000 for non-neighbor machines (AC). Neighbor-only (NTC) machines can run algorithms such as addition in $O(n)$ time at best, when non-neighbor machines (AC) can achieve $O(\log n)$ performance.

Our contribution has focused on parallelizing execution of the arithmetic through improved adders, concurrent gate execution, and overall algorithmic structure. We have also made improvements that resulted in the reduction of modulo operations, and traded some classical for quantum computation to reduce the number of quantum operations. It seems likely that further improvements can be found in the overall structure and by more closely examining the construction of multipliers from adders [109]. We also intend to pursue multipliers built from hybrid carry-save adders.

²Steane uses extra ancillae for measurement and fault tolerance, resulting in a total consumption of $\sim 4n$ physical qubits to store k logical qubits in an $[[n,k,d]]$ code.

The three factors which most heavily influence performance of modular exponentiation are, in order, concurrency, the availability of large numbers of application-level qubits, and the topology of the interconnection between qubits. Without concurrency, it is of course impossible to parallelize the execution of any algorithm. Our algorithms can use up to $\sim 2n^2$ application-level qubits to execute the multiplications in parallel, executing $O(n)$ multiplications in $O(\log n)$ time steps. Finally, if any two qubits can be operands to a quantum gate, regardless of location, the propagation of information about the carry allows an addition to be completed in $O(\log n)$ time steps instead of $O(n)$. We expect that these three factors will influence the performance of other algorithms in similar fashion.

As we alluded to in Section 6.4.1, not all physically realizable architectures map cleanly to one of our models. A full two-dimensional mesh, such as neutral atoms in an optical lattice [56], and a loose trellis topology [256] probably fall between AC and NTC. The behavior of the scalable ion trap [170] is not immediately clear, but will be controlled by ion movement times and realizable concurrency.

In this chapter, we have analyzed the performance of the modular exponentiation step of Shor's factoring algorithm for some abstract architectural models, and shown how to dramatically improve that performance. Depending on the post-quantum error correction, application-level effective clock rate for a specific technology, choice of exponentiation algorithm may be the difference between hours of computation time and weeks, or between seconds and hours. This difference, in turn, feeds back into the system requirements for the necessary strength of error correction and coherence time. The next chapter will develop a design for a machine we call a *quantum multicomputer*, designed to run Shor's algorithm in a distributed fashion, and show optimized forms of arithmetic to run on it.

Chapter 7

The Quantum Multicomputer

7.1 System Overview

The scientist describes what is; the engineer creates what never was.

Theodore Von Kármán

Music is your own experience, your own thoughts, your wisdom. If you don't live it, it won't come out of your horn. They teach you there's a boundary line to music. But, man, there's no boundary line to art.

Charlie Parker

Plan to throw one away. You will do that, anyway. Your only choice is whether to try to sell the throwaway to customers.

Frederick P. Brooks

At long last, we reach the objective of our pilgrimage: the design and analysis of a distributed quantum computer, or *quantum multicomputer*. A multicomputer is a constrained form of distributed system [24]. It is composed of nodes, each of which is an independent quantum computer, and an interconnect network of links connecting the nodes. As we noted in Section 2.2.7, distributed quantum computation requires shared entanglement; in Yepez's terminology, our quantum multicomputer is a type I system [355]. The network is used to create EPR pairs shared between pairs of nodes,

and those EPR pairs are then used to teleport qubits (teledata) or quantum gates (tele-gate). Our goal with such a system is to increase both the *storage* and *performance* of the total system well beyond what a single, monolithic quantum computer is capable of; we want our multicomputer to be *scalable*. This chapter provides an overview of the entire system, including the node and network hardware and software. The first section will justify our decision to explore distributed quantum computer architectures. Succeeding sections will go into more detail on the impact of quantum error correction and finally a performance analysis of adder circuits run on our system.

7.2 An Engineer's Definition of Scalability

What will constrain our ability to build a quantum computing system as large as we care to attempt? In this section, we discuss the practical aspects of scaling up the size (in qubits) of a quantum computer. We also reason that technological limitations on most proposed technologies make it necessary to plan to use multiple machines to solve large problems, laying the foundation for our quantum multicomputer work.

Chuang has defined scalability to mean that the combination of fault tolerant methods and a particular technology, including its base error rate, meet the threshold criterion. Combinations that meet this criterion are scalable; those that do not, are not. However, the term “scalable” has different meanings in different contexts. I am interested in building a complete, practical quantum computing system. In this context, Chuang's definition is a necessary, but not sufficient, condition. Instead, I offer the following, broader but less formal, definition.

Above all, it must be possible, physically and economically, to grow the *system* through the region of interest. Addition of physical resources must raise the performance of the system by a useful amount (for all important metrics of performance, such as calculation speed or storage capacity), without excessive increases in negative features (e.g., failure probability).

This definition refers to several important criteria, summarizing our taxonomy from Chapter 4. It also points out that scalability is never indefinite in the real world; there are always limits, and we must begin by deciding what those limits are. No one would say that a system that costs a hundred thousand dollars per qubit or that covers an optical lab bench for each gate is scalable in any practical sense. Thus, good engineers say, “This scales to...” and name a level, metric, and what part of the system constrains

the scalability. (Better engineers tell you why, and great engineers find a way around the limitations.) In this section, we provide a qualitative look at some of these issues.

7.2.1 Economics

My estimate of the price at which the first production quantum computer will be sold is four hundred U.S. dollars per qubit. The definition of “production” in this case is a machine that is bought and installed for the purpose of solving real problems. That is, it has to solve a problem for which there is not a comparable classical solution.

To arrive at this estimate, I assume that the machine will be built to run Shor’s factoring algorithm on a 1,024-bit number. That takes about five kilobits of application-level qubit space; we will multiply by fifty to support two levels of QEC. This gives a total requirement of a quarter of a million physical qubits.

One hundred million U.S. dollars is a reasonable price for a machine with unique capabilities. The U.S. government clearly spends that much on cluster supercomputers today. BlueGene, for example, built by IBM, has 131,072 processors (65,536 dual-core chips). Counting packaging, power, cooling, memory, storage, and networking, the price of such a system undoubtedly exceeds a thousand dollars per processor (all of these prices are ignoring physical plant, including the building).

Our price point, then, is $\$100\text{M}/250\text{K qubits} = \$400/\text{qubit}$. This estimate might easily be one or two orders of magnitude high or low; other applications, such as physical simulations, may require fewer qubits for a production machine (indeed, one estimate is that as few as 30 qubits might be enough to be useful [23]), or a high error rate may demand more error correction and more physical qubits.

The dollar cost is a real-world constraint that must be satisfied; a large system will not get built until it justifies itself economically.

7.2.2 Infrastructure Needs

Each technology has its own physical infrastructure requirements. Packaging, cooling, and housing a semiconductor-based quantum computer may be non-trivial. Even though a quantum computer manipulates individual quanta, the space, power, thermal, and helium budgets for such a system are large. In Section 4.1.5, we discussed the size and cooling capacity of dilution refrigerators; this will be one limit on the number of qubits we can support in each such dil fridge. For our quantum multicomputer, we plan to connect many dil fridges together into a complete system. We will call a setup of

a dil fridge and the electronics to support the qubits inside a “pod”. We will examine what constitutes a “node” in our multicomputer in Section 7.1.

Thermal engineering and packaging are serious problems. In Section 7.3.2, we will discuss this issue; here we assert that this issue will limit us to only a few logical qubits per pod, which in turn requires us to have a large number of pods. For the moment, we assume one node per pod, and again set our target at a machine for factoring a 1,024-bit number. We must have clearance around the dil fridge for operators and rack-mount equipment to move equipment down the aisles. Quite a bit of space, power, and money are required for each such setup. If each pod requires an area three meters square, we need an area approximately 100 meters by 100 meters for our total machine, a large but certainly achievable amount of floor space. However, growing an order of magnitude beyond this size seems impractical.

With dilution refrigerator prices of about \$100,000 per pod, one thousand dil fridges would consume our entire budget, leaving no money for support electronics or the qubits themselves. This clearly shows that thermal engineering and packaging will be key issues in building large-scale production systems based on quantum dot or Josephson-junction devices; we need to fit more than one node into each pod, or more qubits into each node.

This linear extrapolation from the current state of research is unlikely to be the way production systems will really be built ¹. However, this brief discussion should illustrate the problems that must be solved. Without solutions, we do not have a system that scales to reach our desired performance target.

7.2.3 Performance

We introduced performance as an issue in quantum computing back in Chapter 3. A system running an $O(n^3)$ algorithm that requires a year to solve a problem of size n is unlikely to be considered a viable choice to solve a problem of size $10n$, even if the hardware can be scaled to an appropriate level, as there are few solutions for which funders and researchers are willing to wait 1,000 years.

¹It's also worth noting that NMR, ion trap, optical lattice, and atom chip systems would require a completely different analysis.

7.2.4 Single-Device Physical Limitations

Before accepting the need to build a quantum multicomputer, we should look at the scalability of a single, large, monolithic machine. Thaker et al. estimated the size of an ion trap system to factor a 1,024-bit number to be about a tenth of a square meter of ion traps [324]; a single device of this scale is difficult to construct and operate, suggesting that smaller devices interconnected via teleportation channels will be required.

We are most interested in VLSI-based qubits. In particular, let us look at the superconducting Josephson-junction flux qubit from Dr. Semba's group at NTT [194]. Their qubit is a loop about $10\mu\text{m}$ square. This area is determined by the desired physics of the device, not limited by achievable VLSI feature size; the size of the loop determines the size of the flux quantum, which in turn determines control frequencies and gate speed. Dr. Semba's group is working on connecting qubits via an LC oscillator which includes an on-chip capacitor [160].

Once they have demonstrated interconnection among multiple qubits connected to the bus, will that meet DiVincenzo's criterion for a scalable set of qubits? In this case, we are looking for up to a quarter of a million physical qubits. At first glance, it would seem easy to fit that many qubits on a chip. Even a small 10mm square chip would fit a million 10-micron square structures. However, that estimate ignores the need for I/O pads. Equally important, the capacitor in the LC circuit is huge compared to a qubit (though only one of those is required per bus that connects a modest-sized group of qubits, and it may be possible to build the capacitor in some more space-efficient manner, or maybe even put it off-chip). Still more important, these qubits are magnetic, not charge; place them too close together, and they'll interfere. The strength of the interaction could be a problem if the qubits are only a micron apart, but at $10\mu\text{m}$ spacing, the interaction drops to order of kHz, low enough not to worry about much [293]. Control is achieved with a microwave line run past the qubit; obviously, this line cannot run that too close to other qubits. Thus, there is a lot of physics to be done even before the mundane engineering of floor-planning. Above, we discussed the need for control lines to move into/out of the dil fridge, crossing the thermal boundary. The I/O requirement applies directly to the chip, as well; now we need roughly a pin per qubit. Without major advances in integration or some form of multiplexing of control, we are probably limited to about a thousand qubits per chip, simply because of the required pin count, and each pin will conduct heat into the chip, affecting our overall thermal budget.

With an estimated limit to the number of qubits of two orders of magnitude or more below our total system requirements, we see the need to connect multiple nodes together into a quantum multicomputer. We need to create an entangled state that crosses node boundaries. The quantum I/O mechanisms discussed in Chapter 4 therefore become critical. Having a quantum I/O mechanism allows us to circumvent one entire set of scalability constraints. The governing constraints are likely to be overall ability to suppress errors, performance, or cost.

7.3 System Overview

7.3.1 Hardware Overview

We constrain all parts of the system to be geographically collocated. Short travel distances (up to a few tens of meters) between nodes reduce latency, simplify coordinated control of the system, and increase signal fidelity and reduce losses, freeing us from the need to consider placing quantum repeaters [57] in the network. We may wish, however, to use hardware proposed for quantum repeaters as our local node and interconnect technologies [71].

Figure 1.2 on page 10 showed the quantum multicomputer architecture at a high level. Here we deal only with the quantum network and the nodes' interaction with it. We choose a regular network topology, assume a dedicated network environment, and set a goal of scalability to thousands of nodes. The dedicated network assumption allows us to ignore security and contention for resources beyond the instructions we schedule, and to assume in-order delivery of data. The links may be directly connected between a pair of nodes, connected to a shared network medium, or switched at some lower physical level. Although the QEP protocol in theory supports EPR pair creation over many kilometers, our design goal is a scalable quantum computer in one location (such as a single lab). We consider a 10 nanosecond classical communication latency, corresponding roughly to 2 meters' distance between nodes. The performance figures found are insensitive to this number. The links in the multicomputer are serial; Section 7.4 shows that parallel links would have only a modest impact on performance and reliability, so we choose to avoid the additional complexity.

We concentrate on a homogeneous node technology based on solid-state qubits, with a qubus interconnect, though our results apply to essentially any choice of node and interconnect technologies, such as ion-trap nodes and single photon-based qubit

transfer interconnects [311, 346, 222]. Each node has many qubits which are private to the node, and a few transceiver qubits that can communicate with the outside world. Node size is limited by the number of elements that can practically be built into a single device, considering control structures, external signaling, packaging, cooling, and shielding constraints.

One or more nodes will be placed inside a dilution refrigerator, or dil fridge. Various rack-mount signal generators and measurement devices, classical computing and control equipment, etc. must accompany each node. We will call such a setup a “pod”. For the moment, we assume one node per pod. The exact number of nodes and qubits that can be placed in a pod will depend on volume, heat extraction, and the cabling that must cross temperature boundaries. This is perhaps *the* primary driver of system economics. A dil fridge includes multiple temperature stages, and different parts of the system will be held at different levels. The innermost, millikelvin fridge can dissipate only a few hundred microwatts. Unless the extraction rate of the dil fridge is raised substantially, each transmission line crossing the inner temperature boundary is limited to about a microwatt of thermal load, even if the device itself dissipates no energy.

Finally, economics must be considered. To be able to scale the system to 1,024 nodes, we cannot exceed about US\$100,000 per node, almost all of which will be consumed by the dil fridge if we have only one node per pod. Both cost and floor space can be reduced if more than one node can be fit into a pod, but doubling or quadrupling the number of coaxes and the heat budget is a daunting proposition on an already extremely aggressive engineering challenge. However, some researchers have begun working on these problems and expect to make dramatic improvements. We will see in this and succeeding sections that such progress is necessary to make the system viable.

These assumptions of a regular network topology and homogeneous nodes will certainly hold for the first, small-scale systems that will be built. However, as the size of systems and our experience with them grow, it is quite likely that a multi-stage network composed of heterogeneous nodes will come to be the commonly-accepted architecture.

7.3.2 Node Architecture

The basic architectural principles described in this dissertation are largely independent of the technology on which the nodes are built. A node built on a semiconducting or superconducting base technology serves as a useful model for evaluating performance.

Technology-Independent Characteristics

First, let us examine the roles each node must fulfill, regardless of the implementation:

- Each node must include enough physical qubits to represent several logical qubits, once error correction is taken into account (we will vary our expectation of the exact number in later section). The qubits must meet DiVincenzo's criteria, including adequately fast and accurate gates and measurements.
- Each node must support one or more *transceiver qubits* that can connect to the qubus. Because links are serial, only one transceiver qubit per link is required.
- Qubus operations must be fast enough, relative to memory and gate times, and high enough fidelity that state transfer of logical qubits is possible, and basic performance constraints are met.
- The technology and node implementation, including supporting equipment, must meet the physical, economic and operational constraints identified in Section 7.2.

Expanding on the first criterion, if we assume, for the moment, that each node contains three application-level qubits per node, and we use one level of Steane $[[7,1,3]]$ code and one level of $[[23,1,7]]$ code, then each node must contain about 500 physical qubits².

Hardware Constraints

Solid-state qubits, including both semiconducting quantum dot and superconducting Josephson junction-based devices, are operationally challenging due to the millikelvin temperatures required and the large number of sources of decoherence. However, they are very attractive for two reasons: among experimentally advanced technologies, they are the fastest, with gate times in the low nanoseconds, and several decades' collective experience with semiconductor design and fabrication makes it possible that physical scalability will come more easily to these technologies than some others, once the fundamental hurdles of coherence and manipulation are cleared. Josephson junction-based devices may also support node-internal interconnects, using various forms of

²This estimate ignores Steane's multiplier for multiple, concurrent QEC syndrome extraction, which would raise the number by a factor of four or so. This factor depends on the cycle time of a measurement device, which will be different for solid-state systems than ion traps.

resonators, that will transfer qubits long distances and make them algorithmically more efficient.

In general, a node will be a single chip, with off-chip quantum communication performed using the qubus protocol and teleportation. More precisely, a node consists of the set of qubits that are under unified control and clocking, and that can interact directly either as neighbors or using resonator-based interconnects. If the communication between two qubits must be mediated by an EPR pair created using the qubus protocol, those two qubits will be said to be in different nodes. Some hardware implementations may make the boundary of a node fuzzier, using teleportation internally [324, 256] or other methods externally, but we will use these simplifying assumptions.

Each qubit requires certain control structures and lines; generally, two to five signals each, including bias voltage, gate signals, measurement devices, and qubit-qubit or qubit-resonator coupling control. Some of these signals can be shared among a small group of qubits, potentially allowing an average of one to two signals per qubit. If the control structures remain off-chip, as is common today, each signal requires an I/O pad and a line to the outside. For the chip package, ball grid array packages of more than 2,000 pins exist, and the maximum number of package pins is predicted to reach 7,000 by the year 2016 [110]. At 250 qubits per chip, then, we may not be pin-limited, though the I/O pads will still demand substantial die space. For a thousand qubits or more, once system demands such as ground plane pins are met, it seems likely that packaging constraints will come into play. The engineering challenges of a bus consisting of several thousand microcoaxial cables suitable to reach external equipment are also large. These pedestrian engineering issues suggest that low-level qubit control must reside inside the dil fridge. A node may consist of several dice in a multi-chip module, or the control structures may be integrated directly into the chip. On-chip demultiplexers may reduce the width of the bus to the outside world, at the price of leaving qubits to fend for themselves for long periods of time as control is multiplexed among a group of qubits.

This linear extrapolation from the current state of research prototypes should be viewed as a strawman proposal demonstrating the range of prosaic implementation problems that must be solved to build production systems, rather than an actual proposal to implement. It is clear that, in addition to electrical and VLSI engineers for the chip itself, packaging, thermal, and cabling engineers are needed to create a production system.

7.3.3 Network Topologies

For our proposed multicomputer, we have analyzed five network topologies, as shown in Figure 7.1 and described in Table 7.1, where the “label” column corresponds to the label in the figure. The bus, line, and fully connected topologies were shown in Section 5.3. To these we have added the 2bus and 2fully topologies. In the 2bus and 2fully topologies, each node is connected to two separate networks. This set of topologies explores whether the bottleneck in performance is the network itself, or the ability to move data into and out of the nodes. The network switching elements are integrated directly into the computational nodes, except for the possibility of physical-layer switching in the fully-connected networks. There are no store-and-forward routers or other intelligent elements in the network.

For the shared bus, all nodes are connected to a single bus. Any two nodes may use the bus to communicate, but it supports only a single transaction at a time. In the line topology, each node uses two transceiver qubits, one to connect to its left-hand neighbor and one to connect to its right-hand neighbor. Each link operates independently, and all links can be utilized at the same time, depending on the algorithm. For the fully-connected network, a full set of links creating a true fully-connected network would require $n - 1$ transceiver qubits at each node; obviously this number is impractical. We assume that each node has only a single transceiver qubit, and that it can connect to any other node without penalty via some form of classical, switched network such as a micromirror device [16]. Each transceiver qubit can be involved in only one transaction at a time. 2bus and 2fully utilize two transceiver qubits per node for concurrent transfers.

The effective topology may be different from the physical topology, depending on the details of a bus transaction. For example, even if the physical topology is a bus, the system may behave as if it is fully connected if the actions *internal* to a node to complete a bus transaction are much longer than the activities on the bus itself, allowing the bus to be reallocated quickly to another transaction. Some technologies may support frequency division multiplexing on the bus, allowing multiple concurrent transactions.

7.3.4 Software

Previous chapters have discussed the entire quantum modular exponentiation that forms the most computationally intensive portion of Shor’s factoring algorithm, but here we will concentrate on the adder algorithms that are the core arithmetic routines. Section 7.5 evaluates the VBE (Sec. 3.4.2) [342] and CDKM carry-ripple adders (Sec. 3.4.2)

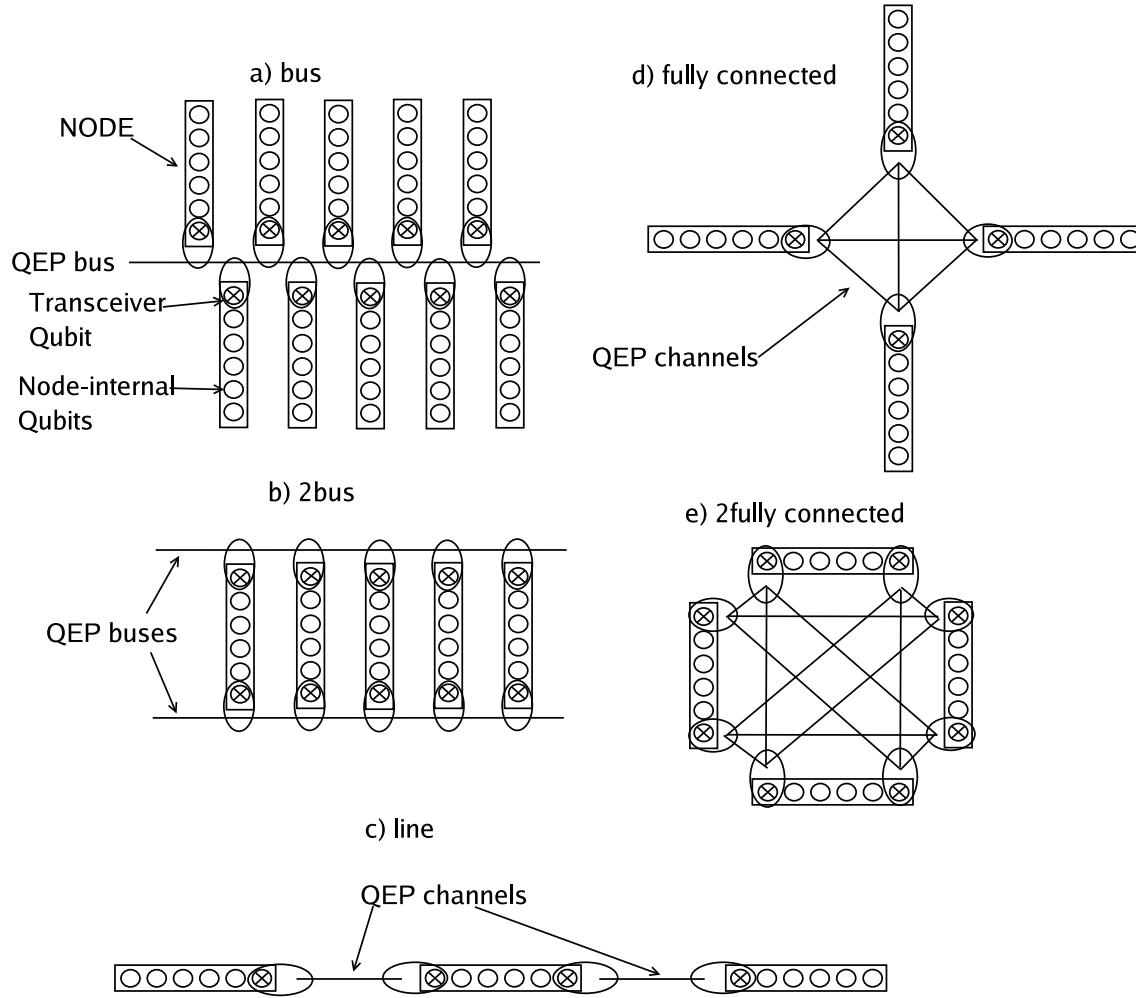


Figure 7.1: The five physical topologies analyzed in this thesis.

label	name	degree	diameter	avg. dist.	bisection	total
a	bus	1	1	1	1	1
b	2bus	2	1	1	2	2
c	line	2	$n - 1$	$(n + 1)/3$	1	$n - 1$
d	fully	1	1	1	$n - 1$	$n(n - 1)/2$
e	2fully	2	1	1	$2(n - 1)$	$n(n - 1)$

Table 7.1: Characteristics of our five network topologies.

Node hardware:	~ 500 physical qubits 2 transceiver qubits
QEC:	$[[23,1,7]]^i + [[7,1,3]]^o$
logical capacity:	3 qubits
Network:	Linear serial links
adder algorithm:	CDKM carry-ripple

Table 7.2: Summary of the strawman system proposal.

[88], and the carry-lookahead adder (Sec. 3.4.3) [103].

As in general-purpose classical multicomputers, distribution of software functionality and synchronization primitives are important for both correctness and performance. In the quantum multicomputer, the distribution of functionality is at the level of a few gates, simplifying the synchronization problem; we need not concern ourselves with interrupt handlers and packet headers and the like. Although each node executes instructions (gates) independently on its qubits, overall coordination requires that the nodes are in sync to within a fraction of a gate, or on the order of a few nanoseconds. This level of synchronization can only be achieved through the real-time classical network. Small amounts of asynchrony must be tolerated as propagation delays between nodes are significant compared to the clock cycle time for individual gates.

Finally, although only application algorithms are presented here, it is interesting to note that Magniez et al. have already discussed a boot-time quantum self-test [217].

7.3.5 Summary

We have already tipped our hand on one critical architecture issue: the choice of serial links. This decision will be justified in the next section, along with analysis showing that the $[[23,1,7]]$ Steane code is the preferred bottom-level quantum error correction code. The following chapter will show that CDKM is the preferred adder circuit, and that two-transceiver nodes with about 500 physical qubits and a linear network will be adequate to scale systems up to hundreds of nodes. Table 7.2 summarizes our strawman system proposal. Details of clock speed and the node-internal interconnect are not specified because they are subject to technological development.

The theme of the next two sections is the optimization of algorithms that require qubits stored in separate nodes to interact. The engineering choice of performing gates via teleportation, as discussed in Sec. 5.2.2, or teleporting data first, then executing the

desired gates locally (Sec. 5.2.1), is examined. We will see that teledata generally outperforms telegate for both QEC (in Section 7.4) and adder algorithms (in Section 7.5).

7.4 Distributed QEC and Bus Design

We now take up the question of how to perform quantum error correction (QEC) in our quantum multicomputer. We show that it is possible to execute QEC on a logical state where the physical qubits that make up a QEC code block are distributed across multiple nodes. We must also determine how to utilize QEC to best protect logical states as they are teleported from one node to another, and we show that the simplest approach is best.

The performance of error correction influences an important hardware design decision: should our network links be serial or parallel? We argue that the difference in both reliability and performance is likely to be small, assuming that the reliability of teleportation is less than that of quantum memory and that teleportation times are reasonable compared to the cycle time of locally-executed QEC.

Teleportation, as we saw in Chapter 5, is composed of EPR pair creation, local gates, measurements, and classical communication, and of course requires high-fidelity memory. Until we take up the issue of link design in Section 7.4.3, we will assume that local gates, memory, and measurements are perfect, or at least much better than EPR pair creation. Therefore, when we talk about limits on the failure rate of teleportation, we are really referring to the quality of the EPR pair. The quality can be improved via purification, which has a cost logarithmic in the starting fidelity; in this dissertation, we will not pursue further the best way to achieve EPR pairs of the necessary quality. We denote the failure probability of a single teleportation as p_t .

First, let us briefly consider the failure probability assuming no error correction on our qubits. The probability of success of the entire computation, then, rests on the success of *all* of the individual teleportation operations. If t is the total number of teleportations we must execute for the complete computation, our success probability is

$$p_s = (1 - p_t)^t = 1 - \binom{t}{1}p_t + \binom{t}{2}(-p_t)^2 \cdots \approx 1 - tp_t \quad (7.1)$$

for small p_t . Our failure probability grows linearly with the number of teleportations we must execute, requiring $p_t \ll 1/t$. Obviously, we need to do better than that, so we quickly conclude that error correction on the logical states being transferred is

length	teleportations (t)
16	14000–125000
128	8×10^6 – 10^8
1024	4×10^9 – 6×10^{10}

Table 7.3: Number of teleportations necessary to execute the full modular exponentiation for different problem sizes.

necessary.

The argument here falls much along the lines of the threshold argument for quantum computation in general, as discussed in Section 2.3.4. Because we are dealing with a small number of levels of concatenation and a finite computation, we are less interested in the threshold itself than a specific calculation of the success probability for a chosen arrangement. A detailed estimate would differ slightly because we have three separate error sources in memory, local gates, and teleportation, along the lines of Steane’s simulations [308]; here we restrict ourselves to a simple analysis. Table 7.3 shows rough teleportation counts for the complete modular exponentiation for Shor’s factoring algorithm, based on Table 6.2 (page 145) and the teledata entries of Table 7.6 (page 185). The number of multiplier blocks has no significant impact on the number of teleportations we must execute. The choice of node size and adder are important; the carry-lookahead adder requires ten to fifteen times as many teleportations (for 16 to 1,024 bits), but may be faster under some circumstances, as we will show in Section 7.5; this accounts for the range of values in Table 7.3.

7.4.1 Distributed Logical Zeroes

In Equation 2.48 (p. 51) and Figure 2.7 (p. 52), we showed the logical zero state ($|0_L\rangle$) for the Steane $[[7,1,3]]$ quantum error correcting code and a circuit to create the state. This state is used in the fault-tolerant construction of quantum error correction. In the multicomputer, we may need to perform QEC on states that span two (or more) nodes, when moving data between nodes in a quantum multicomputer, or simply trying to maintain the integrity of a static state that spans multiple nodes. Thus, we must find a way to either

1. create a distributed $|0_L\rangle$ state;
2. do four-qubit parity (error syndrome) measurement using only weak nonlinearity on four qubits; or

3. find some other way to do syndrome measurement without the full, distributed $|0_L\rangle$ state.

Of these three options, we have chosen the first. We have also invested some effort in looking for a way to calculate the parity of n qubits using the weak nonlinearity, but all of the schemes we have found so far for more than three qubits scale poorly in terms of noise; Yamaguchi et al. have designed a method that works for three qubits but not more [353]. Bacon has developed a new method for creating self-correcting memories, using the original Shor $[[9,1,3]]$ code, that may not require the creation of logical zeroes; its implications for actual implementation are exciting but still poorly understood [28, 324]. Thus, $|0_L\rangle$ states must be created, and this chapter discusses the performance and error characteristics of the creation process.

The logical $|0_L\rangle$ can be created using the same two methods as any other distributed quantum computation: we can directly create the state in a distributed fashion, using teleported gates (telegate), or we can create the state within a single node and teleport several of the qubits to the remote node before using the state in our QEC (teledata). First, consider the use of teleported gates to create the $|0_L\rangle$ state. Figure 7.2 shows that splitting the $|0_L\rangle$ state across two nodes, as at the line labeled “c”, forces the execution of four teleported CNOTs, consuming four EPR pairs; breaking at “d” would require only three. In the figure, the subscripts again represent the bit number in the QEC block; the qubits have been reordered compared to Figure 2.7 for efficiency. Our second alternative is to teleport portions of a locally-created $|0_L\rangle$ state. If enough qubits and computational resources are available at both nodes, we are free to create the state in either location and teleport some of the qubits; thus, the maximum number of qubits that must be teleported is $\lfloor n/2 \rfloor$, or 3 for the 7-bit Steane code. Table 7.4 shows the number of gate or data teleportations necessary, depending on the breakdown of qubits to nodes, showing that teledata requires the same or fewer EPR pairs, and so is preferred.

7.4.2 Distributed Data

Static Distributed States

If a logical data qubit $|\psi_L\rangle$ is split between nodes A and B in the same fashion as Figure 7.2, we will use the $|0_L\rangle$ states to calculate the syndromes for the error correction. Each syndrome calculation consumes one $|0_L\rangle$ state, first executing some gates to entangle it with the logical data qubit, then measuring the zero state. The $[[7,1,3]]$ code

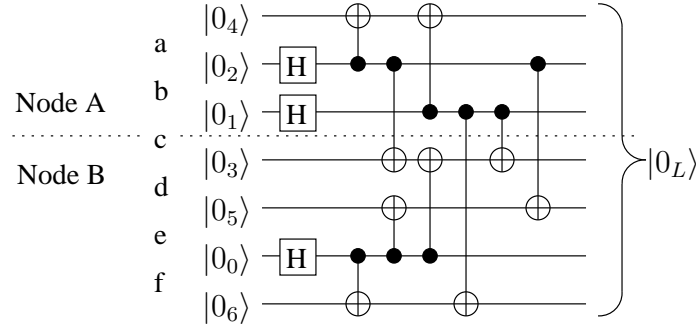


Figure 7.2: Distributed circuit to create the $|0_L\rangle$ state for the Steane $[[7,1,3]]$ code.

breakpoint	telegate	teledata
a	2	1 ($B \rightarrow A$)
b	3	2 ($B \rightarrow A$)
c	4	3 ($B \rightarrow A$)
d	3	3 ($A \rightarrow B$)
e	3	2 ($A \rightarrow B$)
f	2	1 ($A \rightarrow B$)

Table 7.4: Breakpoints (corresponding to Figure 7.2) and the cost of telegate v. teledata to create a logical zero state for the Steane $[[7,1,3]]$ code, in EPR pairs consumed. Also shown is the direction qubits must be teleported.

requires six syndrome measurements (three value and three phase), and Steane recommends measuring each syndrome at least twice, so each QEC cycle consumes at least a dozen logical zero states. With $|\psi_L\rangle$ divided at the “d” point, each $|0_L\rangle$ requires three teleportations, for a total of $3 \times 12 = 36$ EPR pairs destroyed to execute a single, full cycle of QEC.

The split described here allows a single logical qubit plus its QEC ancillae, a total of fourteen physical qubits, to be split between two nodes. The same principles apply to states split among a larger number of nodes, potentially allowing significantly smaller nodes to be useful, or allowing larger logical encoding blocks to be used, spread out among small, fixed-size nodes. More importantly for our immediate purposes, this analysis serves as a basis for considering the movement of logical states from node to node.

States in Motion

When considering the teleportation of logical qubits and their error correction needs, two general approaches are possible:

1. Transfer the entire QEC block, then perform QEC locally at the destination; or

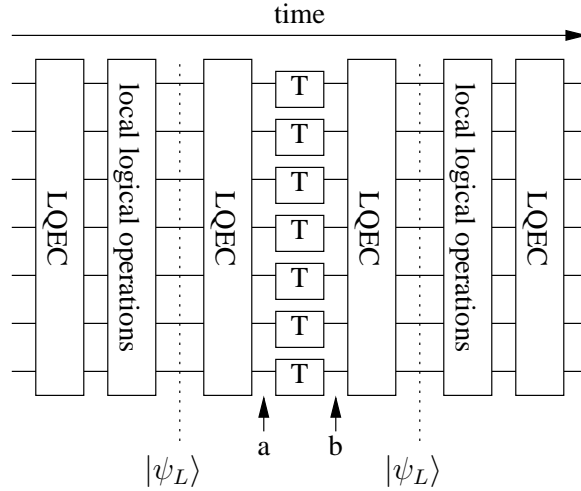


Figure 7.3: Teleporting logical state using local QEC only, no intermediate QEC. The box holding a “T” is the teleportation circuit. Each line represents a qubit variable, independent of its location, so that the teleportation operation does not explicitly show the movement of the qubit from one node to another.

2. use one of the methods described above for distributed QEC *between* the teleportations of the component qubits.

The first approach is conceptually simpler; does the second offer any advantages in either performance or failure probability?

We will examine one-level QEC and two-level concatenated QEC. Steane prefers the $[[23,1,7]]$ code as the lowest layer of a multi-layer code [308]. This code can defend against three errors, so we are interested in the probability of four errors. All of the one- and two-layer combinations of $[[7,1,3]]$ and $[[23,1,7]]$ are examined.

The first approach, illustrated in Figure 7.3, obviously consumes seven EPR pairs to transfer the seven-qubit code word from one node to the other. Assume, for the moment, that local gates and quantum memory are perfect, so that our only source of errors is teleportation. As we saw in Chapter 2.3, for an $[[n,k,d]]$ -qubit error correction code, we use n physical qubits to hold k logical qubits, and can correct up to $(d-1)/2$ errors. If p_t is the probability of an error occurring during the teleportation of a single qubit, then the probability of m errors occurring is

$$p_e(n, m) = \binom{n}{m} (1 - p_t)^{n-m} p_t^m \approx \binom{n}{m} p_t^m \quad (7.2)$$

for small p_t . For $p_t \ll 1$, most failures will occur in the lowest failure mode, $((d-1)/2) + 1 = (d+1)/2$ errors. We will approximate our total failure probability as the

probability of $(d + 1)/2$ errors occurring.

If p_a is the failure probability of our total algorithm and t is the *total* number of *logical* qubit teleportations we use in the computation, then

$$p_a = 1 - (1 - p_e)^t \approx \binom{t}{1} p_e \approx t p_e. \quad (7.3)$$

For the $[[7,1,3]]$ code,

$$p_e(7, 2) = \binom{7}{2} (1 - p_t)^5 p_t^2 \approx 21 p_t^2 \quad (7.4)$$

is the probability of two errors occurring in our block of seven qubits. Two qubit errors, of course, is more than the $[[7,1,3]]$ code can correct. Our probability of algorithm failure becomes

$$p_a \approx t p_e = 21 t p_t^2. \quad (7.5)$$

Thus, we can say that, to have a reasonable probability of success, we should have $p_t \ll 1/\sqrt{21t}$. This is a significant improvement over the case with no error correction seen at the beginning of this chapter.

Using a two-level concatenated code, the picture is less grim. For two levels of the $[[7,1,3]]$ code, our total encoding will consist of seven blocks of seven qubits each, and the computation will fail only if *two* or more of those blocks fail.

Of course, the two codes need not be the same. Adapting Steane's terminology and notation, will refer to the physical-level code as the “inner” code, and the code built on top of that as the “outer” code [308]. $[[n^i, k^i, d^i]]$ or $[[n, k, d]]^i$ is the inner code, and $[[n^o, k^o, d^o]]$ or $[[n, k, d]]^o$ is the outer code. Approximating the error probability according to Equations 7.2 and 7.3, we have

$$p_a \approx t \binom{n^o}{m^o} \left(\binom{n^i}{m^i} p_t^{m^i} \right)^{m^o} \quad (7.6)$$

where $m^i = (d^i + 1)/2$ and likewise for m^o .

Table 7.5 shows the estimates for the teleportation failure probability p_t that will give us a total algorithm failure probability of $p_a < 0.1$. Although $[[23,1,7]]^i + [[7,1,3]]^o$ and $[[7,1,3]]^i + [[23,1,7]]^o$ are different, by coincidence, their failure probabilities are almost identical, so they are listed together. Note that $[[23,1,7]]$ offers essentially the same error protection as $[[7,1,3]] + [[7,1,3]]$, despite using half the number of qubits and being conceptually simpler.

error-correcting code	scale-up	teleportations	p_t for $p_a < 0.1$
(none)	1	10^5 10^8 10^{11}	$0.1/t = 10^{-6}$ $0.1/t = 10^{-9}$ $0.1/t = 10^{-12}$
[[7,1,3]]	7	10^5 10^8 10^{11}	$1/\sqrt{21t} = 7 \times 10^{-4}$ $1/\sqrt{21t} = 2 \times 10^{-5}$ $1/\sqrt{21t} = 7 \times 10^{-7}$
[[23,1,7]]	23	10^5 10^8 10^{11}	$1/(17t^{1/4}) \approx 3 \times 10^{-3}$ $1/(17t^{1/4}) \approx 6 \times 10^{-4}$ $1/(17t^{1/4}) \approx 1 \times 10^{-4}$
$[[7,1,3]]^i + [[7,1,3]]^o$	49	10^5 10^8 10^{11}	$1/(17t^{1/4}) \approx 3 \times 10^{-3}$ $1/(17t^{1/4}) \approx 6 \times 10^{-4}$ $1/(17t^{1/4}) \approx 1 \times 10^{-4}$
$[[23,1,7]]^i + [[7,1,3]]^o$ and $[[7,1,3]]^i + [[23,1,7]]^o$	161	10^5 10^8 10^{11}	$1/(19t^{1/8}) \approx 0.012$ $1/(19t^{1/8}) \approx 5 \times 10^{-3}$ $1/(19t^{1/8}) \approx 2 \times 10^{-3}$
$[[23,1,7]]^i + [[23,1,7]]^o$	529	10^5 10^8 10^{11}	$1/(20t^{1/16}) \approx 0.025$ $1/(20t^{1/16}) \approx 0.016$ $1/(20t^{1/16}) \approx 0.010$

Table 7.5: An estimate of the necessary error rate of teleportation (p_t) to achieve a specific number of logical teleportations with 90% probability of success, for different error-correction schemes.

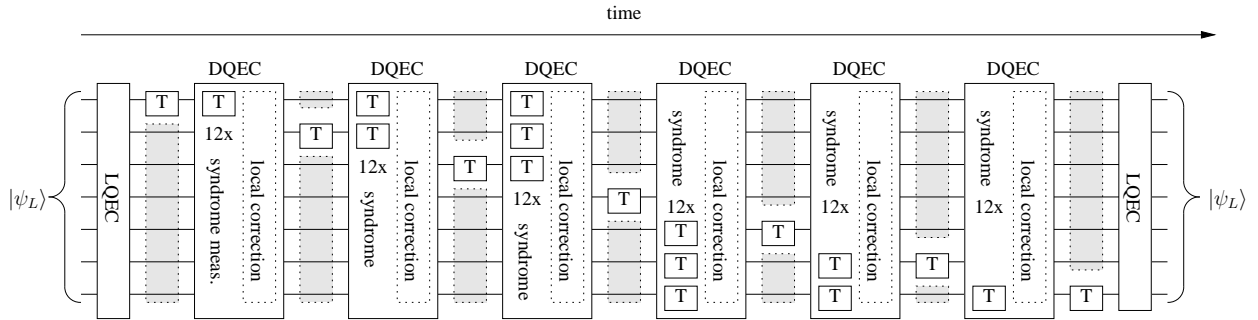


Figure 7.4: Teleporting logical state using intermediate, teledata distributed QEC.

The second approach described above, doing error correction after serially sending each qubit, is shown in Figure 7.4. Using this approach, we attempt to reduce the overall error probability by incrementally correcting the logical state as it is teleported; to teleport the seven-bit state we perform local QEC before beginning, then do distributed QEC after each of the first six teleportations, then local QEC again after the seventh teleportation. Each distributed QEC (DQEC) block performs twelve distributed syndrome measurements. We can again choose telegate or teledata for the $|0_L\rangle$ state creation; the figure illustrates teledata. Using telegate, we would need the sum of the telegate column in Table 7.4, or $2 + 3 + 4 + 3 + 3 + 2 = 17$, inter-node gates, for each syndrome that must be measured. To perform twelve measurements we consume a total of $12 \times 17 = 204$ EPR pairs. Using teledata, we would need only $1 + 2 + 3 + 3 + 2 + 1 = 12$ per syndrome, or 144 EPR pairs for the full twelve syndromes in a cycle. The worst-case DQEC block is $3 \times 12 = 36$ teleportations. Obviously, the probability of error is higher for 36 teleportations than for seven. Therefore, unless someone develops a means of measuring syndromes without using the $|0_L\rangle$ states, this second approach does not achieve its goal of reducing the total error probability. Performance-wise, the penalty for doing step-wise QEC is also stiff; we conclude that this approach is not useful.

7.4.3 Implications for Link Design

Figure 7.3 shows a $[[7,1,3]]$ state being transferred in parallel and Figure 7.5 shows the serial equivalent. In these diagrams, each line represents a qubit that is a member of a code block, essentially following the variable rather than the storage locations; at a T block, representing teleportation, of course the qubit moves from one node to the other. If the transfer is done serially, the wait to *start* the QEC sequence is seven times

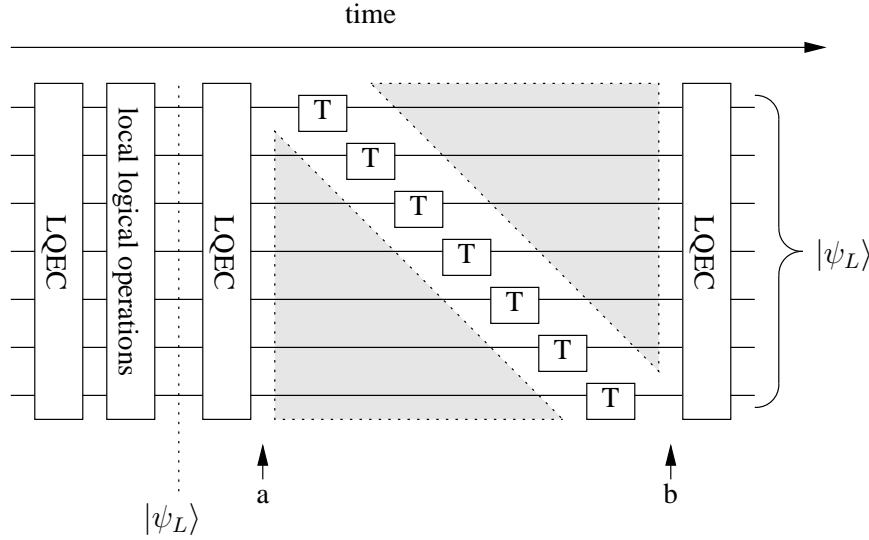


Figure 7.5: Local QEC only, no intermediate QEC, serial interface.

as long, but the *total* time for transfer plus QEC (that is, time from the start of one QEC cycle to the next, from the first $|\psi_L\rangle$ to the point marked “b” in the figures) won’t grow by nearly as large a factor if local QEC requires significant time compared to a teleportation. Thus, we need to determine if the increase in wait time caused by the lengthening of the interval the point marked “a” to the point marked “b” in Figures 7.3 and 7.5 has an unacceptably large impact on our overall failure rate.

The gray areas in the serial figure indicate increased wait time for the qubits. Each qubit spends one cycle teleporting, and six waiting for the other teleportations. If p_m is the probability of error for a single qubit during the time to execute a single teleportation, then the probability of no error on one bit during that time is $(1 - p_m)^6$ for a $[[7,1,3]]$ code. For an $[[n,k,d]]$ code, the failure probability of that qubit during the serial transfer waiting time is $p'_m = 1 - (1 - p_m)^{n-1}$. The probability of m memory errors is

$$p_M(n, m) = \binom{n}{m} p'_m{}^m (1 - p'_m)^{n-m} \approx \binom{n}{m} p'_m{}^m \approx \binom{n}{m} (n-1) p_m^m. \quad (7.7)$$

Combining Equations 7.7 and 7.2, we need the two error sources together to generate less than $m = (d+1)/2$ errors. We will constrain the final combined memory and teleportation error rate p_f for the serial link to be similar to the teleportation errors for

the parallel link,

$$p_f(n, m) = \sum_{i=0}^m p_M(n, i) p_e(n, m - i) \sim p_e(n, m). \quad (7.8)$$

For the error codes we are considering, $[[7,1,3]]$ and $[[23,1,7]]$, numeric evaluation for $p_m = p_t/10(n - 1)$ gives 25% and 50% increase in failure probability compared to the $p_m = 0$ (perfect memory) case. Thus, we can say, very roughly, that a memory failure probability two orders of magnitude less than the failure probability of the teleportation operation will mean that the choice of serial or parallel buses has minimal impact on the overall system error rate.

Although this section has focused on reliability rather than performance, the choice of serial or parallel links also affects performance. It is easy to see that choosing a serial link does not result in a factor of n degradation in system performance when QEC is taken into account. Let t_t be our teleportation time, and t_{LQEC} be the time to perform local error correction. t_t is related to the qubus detector time and t_{LQEC} is related to the local qubit measurement time.

If $nt_t \ll t_{LQEC}$, then in accordance with Amdahl's Law the choice also has minimal impact on our overall performance [18]. Of course, if the resources available at each node are large enough, teleportation and error correction can be pipelined, but the growth in resources is significant if t_{LQEC} is large and the performance gains are small if t_{LQEC} is small. In addition, as we will see in the next section, arithmetic algorithms rarely have enough data waiting for teleportation that pipelining will be effective, so pipelining here would be a second-order effect on overall system performance. Therefore, we recommend using serial links without pipelining, if the qubus detector time is reasonable.

7.4.4 Summary

I originally believed that the issues of serial v. parallel and intermediate QEC v. block transfer were tied together. However, it is now clear that the two are separate issues, and that, unless a better method for creating logical zeroes is found or Bacon's method of calculating syndromes without using logical zeroes proves to be practical, intermediate QEC offers no benefit. I therefore recommend block-wise error correction, shipping the entire QEC block from source to destination before performing QEC.

The results in Table 7.5 show that a teleportation error rate (really, EPR pair infidelity) of $\sim 1\%$ will allow computations as large as the factoring of a 1,024-bit number to proceed with a high probability of success. This estimate is for a data encoding of $[[23,1,7]]^i + [[23,1,7]]^o$ on the link and a memory error rate in the time it takes to perform a teleportation at least two orders of magnitude better than the teleportation failure rate. Our analysis, though somewhat simpler than Steane's, supports his recommendation of the $[[23,1,7]]$ code. Replacing one level with the $[[7,1,3]]$ code still allows an error rate of one part in a thousand or better, with a noticeable savings in storage requirements. Of course, we do not have to compute or store data using the same encoded states that we use during data transport [324]. In this dissertation, for simplicity, we have assumed that the system uses only a single choice of encoding.

This section has argued that the difference in both performance and reliability between serial and parallel network links will be small for a reasonable set of assumptions. Serial links will dramatically simplify our hardware design by reducing the number of required transceiver qubits in each node, and eliminating concerns such as jitter and skew between pairs of conductors or wave guides. Moreover, if we do choose to have multiple transceiver qubits in each node, system performance on some workloads may be boosted more by creating a richer node-to-node interconnect topology than by creating parallel channels between pairs of nodes in a simpler topology, as we will see in the next section.

7.5 Distributed Form of Shor's Algorithm

This section evaluates the performance of quantum arithmetic algorithms run on a quantum multicomputer. We vary the node capacity and I/O capabilities, and the network topology. The tradeoff of choosing between telegate and teledata is examined. We show that the teledata approach performs better, and that carry-ripple adders perform well when the teleportation block is decomposed so that the key quantum operations can be parallelized. A node size of only a few logical qubits performs adequately, provided that the nodes have two transceiver qubits. A linear network topology performs acceptably for a broad range of system sizes and performance parameters. We therefore recommend pursuing small, high-I/O bandwidth nodes and a simple network, as described at the end of Section 7.1.

The first question in considering a multicomputer is whether the system performance will be acceptable *if* the implementation problems can be solved. Chapter 6 provided the tools and algorithms for this analysis; here they are applied. Our evaluation criterion is the latency to complete one addition. The goal is to achieve “reasonable” performance for Shor’s factoring algorithm for numbers up to a thousand bits. This analysis is done attempting to minimize the required number of qubits in a node while retaining reasonable performance; we investigate node sizes of one to five logical qubits per node.

This section shows that:

- teleportation of data is better than teleportation of gates;
- decomposition of teleportation into a series of smaller operations brings big benefits in performance, making a carry-ripple adder effective even for large problems;
- a linear topology is an adequate network for the foreseeable future; and
- small nodes (only a few logical qubits) perform acceptably, but I/O bandwidth is critical.

A multicomputer built around these principles and based on solid-state qubit technology will perform well on Shor’s algorithm. These results collectively represent a large step in the design and performance analysis of distributed quantum computation.

Next, we discuss the mapping of arithmetic algorithms to our system. The bulk of this section progressively refines performance estimates, including decomposing the teleportation operation to make the performance of carry-ripple adders competitive with the carry-lookahead adder, with a simpler network and smaller nodes.

7.5.1 Algorithm

We evaluate three different addition algorithms: the Vedral-Barenco-Ekert (VBE) style of carry-ripple adder (Sec. 3.4.2) [342], the faster, smaller Cuccaro-Draper-Kutin-Moulton (CDKM) carry-ripple adder (Sec. 3.4.2) [88], and the carry-lookahead adder (Sec. 3.4.3) [103]. In this section, we discuss the adders without regard to the network topology; the following section presents numeric values for different topologies and gate timings.

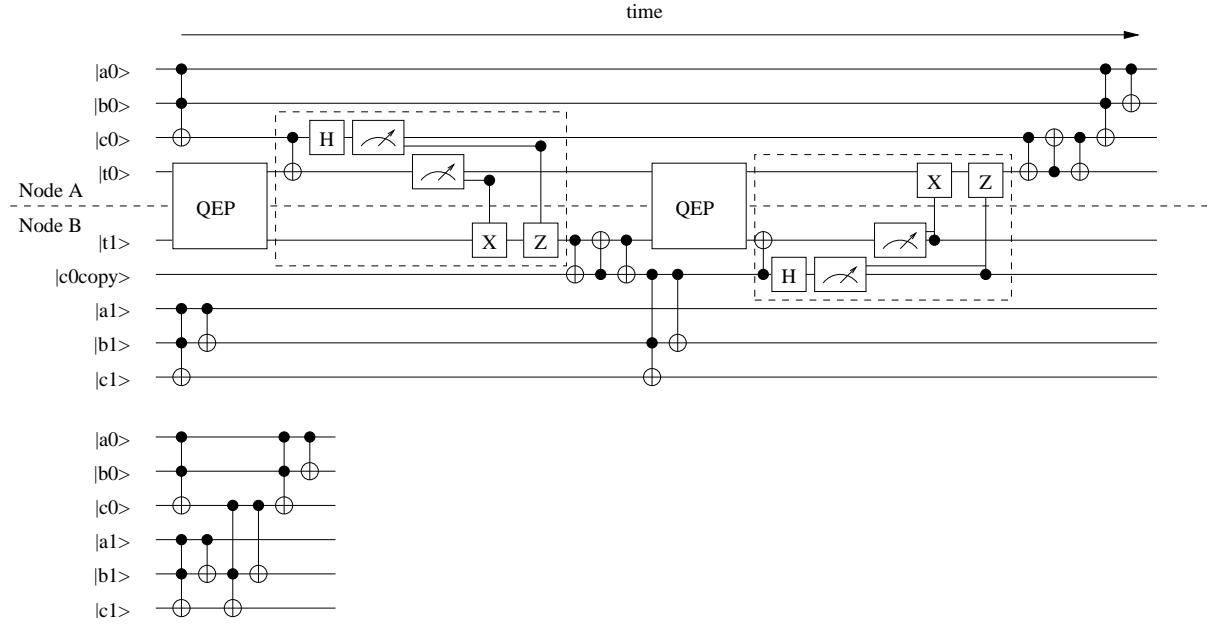


Figure 7.6: Details of a distributed 2-qubit VBE adder. The top circuit is the distributed form using the teledata method; the bottom circuit is the monolithic equivalent. The solid box (QEP) is the qubus EPR pair generator; the circuits in dashed boxes are standard quantum teleportation circuits. Graphical notation as in Fig. 2.3 on page 36.

Carry-Ripple Adders

Figure 7.6 shows a two-qubit VBE carry-ripple adder in its monolithic (bottom) and distributed (top) forms. The QEP block creates an EPR pair using the qubus entanglement protocol described in Sec. 5.1. The dashed boxes delineate the teleportation circuit (which is assumed to be perfect) that moves the qubit $c0$ from node A to node B. $c0$ is used in computation at node B, then moved back to node A via a similar teleportation to complete the computation. The two qubits $t0$ and $t1$ are used as transceiver qubits, and are reinitialized as part of the QEP sub-circuit.

Figure 7.7 shows a larger VBE adder circuit and illustrates a visual method for comparing telegate and teledata. For telegate, we can draw a line across the circuit, with the number of gates (vertical line segments) crossed showing our cost. For teledata, the line must *not* cross gates, instead crossing the qubit lines. The number of such crossings is the number of teleportations required. This approach works well for analyzing the VBE and CDKM adders, but care must be taken with the carry-lookahead adder, because it uses long-distance gates that may be between e.g. nodes 1 and 3.

The VBE adder latency to add two n -qubit numbers on an m -node machine using the teledata method is $2m - 2$ teleportations plus the circuit cost. For the telegate

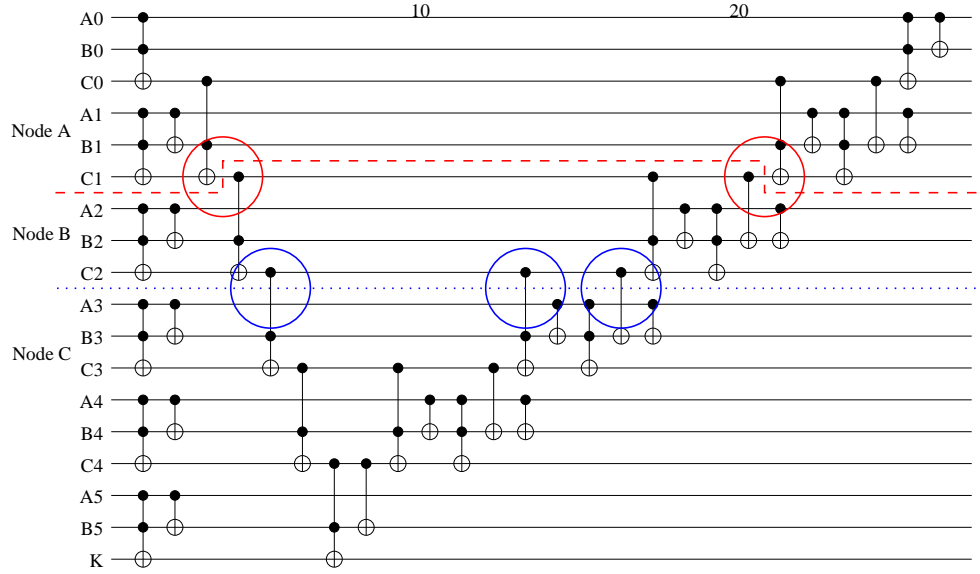


Figure 7.7: Visual approach to determining relative cost of teleporting data versus teleporting gates for a VBE adder. The upper, dashed (red) line shows the division between two nodes (A and B) using data teleportation. The circles show where the algorithm will need to teleport data. The lower, dotted line (blue) shows the division using gate teleportation (nodes B and C). The circles show where teleported gates must occur. Note that two of these three are CCNOT gates, which may entail multiple two-qubit gates in actual implementation. The numbers at the top are clock cycles.

approach, using the five-gate breakdown for CCNOT built from \sqrt{X} gates and CNOTs, as in Figure 6.1 on page 123, would require three teleported two-qubit gates to form a CCNOT. Therefore, implementing telegate, the latency is $7m - 7$ gate teleportations, or 3.5x the cost.

For the CDKM carry-ripple adder, which more aggressively reuses data space, tele-data requires a minimum of six movements, whereas telegate requires two CCNOTs and three CNOTs, or a total of nine two-qubit gates, as shown in figure 7.8. The CDKM adder pipelines extremely well, so the actual latency penalty for more than two nodes is only $2m + 2$ data teleportations, or $6m$ gate teleportations, when there is no contention for the inter-node links, as in our line and fully-connected topologies. The bus topology performance is limited by contention for access to the interconnect.

Carry Lookahead

Analyzing the carry-lookahead adder is more complex, as its structure is not regular, but grows more intertwined toward the middle bits. Gate scheduling is also variable, and the required concurrency level is high. The latency is $O(\log n)$, making it one of

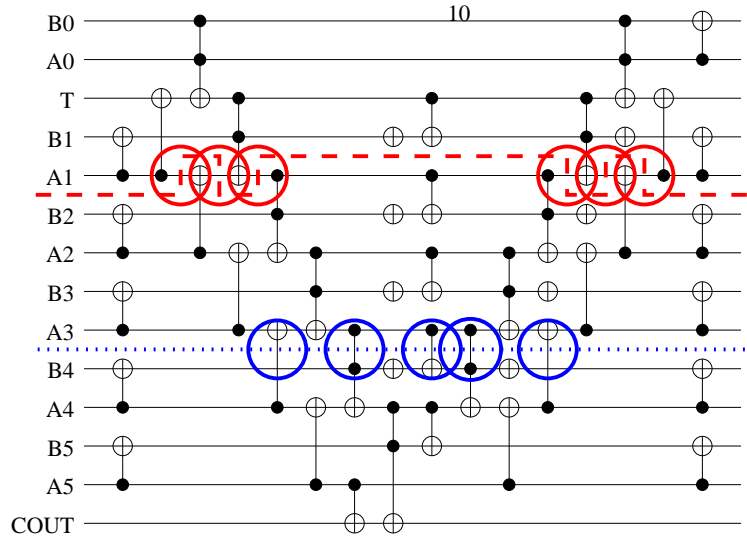


Figure 7.8: Visual approach to determining relative cost of teleporting data versus teleporting gates for a CDKM adder. The upper, dashed (red) line shows the division between two nodes using data teleportation. The circles show where the algorithm will need to teleport data. The lower, dotted line (blue) shows the division using gate teleportation. The circles show where teleported gates must occur. Note that two of these five are CCNOT gates, which may entail multiple two-qubit gates in actual implementation.

the fastest forms of adder for large numbers [103, 334, 109].

Let us look at the performance in a monolithic quantum computer, for n a power of two. Based on table 1 from Draper et al. [103], for $n = 2^k$, the circuit depth of $4k + 3$ Toffoli gates is 19, 31, and 43 Toffoli gates, for 16, 128, and 1,024 bits, respectively. We assume a straightforward mapping of the circuit to the distributed architecture. Most nodes are assigned four logical qubits (A_i , B_i , C_i , and one temporary qubit used as part of the carry propagation). In the next subsection, we see that the transceiver qubits are the bottleneck; we cannot actually achieve this $4k + 3$ latency.

7.5.2 Performance

The modular exponentiation to run Shor’s factoring algorithm on a 1,024-bit number requires approximately 2.1 million calls to the integer adder [334]. With a 100 μsec adder, one run of the algorithm will require less than five minutes; with a 1 msec adder, it will take just over half an hour, allowing about twelve hundred “runs” per month. Even a system two to three orders of magnitude slower than this will have attractive performance, provided that error correction can sustain the system state for that long, and

that the system can be built and operated economically. This section presents numerical estimates of performance which show that this criterion is easily met by a quantum multicomputer under a variety of assumptions about logical operation times, providing plenty of headroom for quantum error correction.

Initial Estimate

Our initial results are shown in table 7.6. Units are in number of complete teleportations, treating teleportation and EPR pair generation as a single block, and assuming zero cost for local gates. In the following subsections these assumptions are revisited. We show three approaches (baseline, telegate, and teledata) and three adder algorithms (VBE, CDKM, carry-lookahead) for five networks (bus, 2bus, line, fully, 2fully) and three problem sizes (16, 128, and 1024 bits). In the baseline case, each node contains only a single logical qubit; gates are therefore executed using the telegate approach. For the telegate and teledata columns, we chose node sizes to suit the algorithms: two, three, and four qubits per node for the CDKM, VBE, and carry-lookahead adders, respectively, when using telegate, and three, four and five qubits when using teledata.

The VBE adder, although larger than CDKM and slower on a monolithic computer, is faster in a distributed environment. The VBE adder exhibits a large (3.5x) performance gain by using the teledata method instead of telegate. For teledata, the performance is independent of the network topology, because only a single operation is required at a time, moving a qubit to a neighboring node. The CDKM adder also communicates only with nearest neighbors, but performs more transfers. The single bus configuration is almost 3x slower than the line topology. On a line, in most time slots, three concurrent transfers are conducted (e.g., between nodes $1 \rightarrow 2$, $3 \rightarrow 2$, and $3 \rightarrow 4$).

An unanticipated but intuitive result is that the performance of the carry-lookahead adder is better in the baseline case than the telegate case, for the fully-connected network. This is due to the limitation of having a single transceiver qubit per node. Putting more qubits in a node increases contention for the transceiver qubit, and reduces performance even though the absolute number of gates that must be executed via teleportation has been reduced. Our numbers also show that the carry-lookahead adder is not a good match for a bus architecture, despite the favorable long-distance transport, again because of excessive contention for the bus.

The carry-lookahead adder is easily seen to be inappropriate for the line architecture, since the carry-lookahead requires long-distance gates to propagate carry information quickly. Using the linear network naturally degenerates to linear cost to share data over a long distance. Using nested purification techniques, as with quantum repeaters [71, 57], it might be possible to reduce the linear time to $O(\log n)$ time, but even the factor of ten introduced for a 1,024-bit number will make the carry-lookahead adder slower than the carry-ripple adders. If the required resources on the line are spatially overlapping, the penalty might actually exceed ten times, exacerbating the problem. Therefore, we have ruled out using the carry-lookahead adder on a linear network, and do not analyze it further.

For telegate, performing some adjustments to eliminate intra-node gates, we find $8n - 9k - 8$ total Toffoli gates that need arguments that are originally stored on three separate nodes, plus $n - 2$ two-node CNOTs. For the bus case, which allows no concurrency, this is our final cost. For the fully-connected network, we find a depth of $8k - 10$ three-node CCNOTs, 8 two-node CCNOTs, and 1 CNOT. These numbers must be multiplied by the appropriate CCNOT breakdown. For the teledata fully-connected case, each three-node Toffoli gate requires four teleportations (in and out for each of two variables). For the 2fully network, the latency of the three-node Toffolis is halved, but the two-node Toffolis do not benefit, giving us a final cost of slightly over half the fully network cost.

algo.	size	Baseline			Telegate					Teledata				
		bus	line	fully	bus	2bus	line	fully	2fully	bus	2bus	line	fully	2fully
VBE	16	360	305	182	105	105	105	105	105	30	30	30	30	30
	128	3048	2545	1526	889	889	889	889	889	254	254	254	254	254
	1024	24552	20465	12278	7161	7161	7161	7161	7161	2046	2046	2046	2046	2046
CDKM	16	232	160	160	138	96	96	97	96	90	60	34	90	34
	128	1912	1280	1280	1146	768	768	768	768	762	508	258	762	258
	1024	15352	10240	10240	9210	6144	6144	6145	6144	6138	4092	2050	6138	2050
Carry-look-ahead	16	644	N/A	99	444	222	N/A	136	135	260	178	N/A	96	56
	128	6557	N/A	159	4901	2451	N/A	256	255	3176	2028	N/A	192	104
	1024	54806	N/A	219	41502	20751	N/A	376	375	27260	17206	N/A	288	152

Table 7.6: Estimate of latency necessary to execute various adder circuits on different topologies of quantum multicomputer, assuming monolithic teleportation blocks (Sec. 7.5.2). Units are in number of teleportation blocks, including EPR pair creation (bus transaction), local gates and classical communication. Size, length of the numbers to be added, in bits. Lower numbers are faster (better).

Improved Performance

The analysis in Section 7.5.2 assumed that a teleportation operation is a monolithic unit. However, Figure 7.6 makes it clear that a teleportation actually consists of several phases. The first portion is the creation of the entangled EPR pair via the qubus. The second portion is local computation and measurement at the sending node, followed by classical communication between nodes, then local operations at the receiving node. The EPR pair creation is not data-dependent; it can be done in advance, as resources (bus time slots, qubits) become available, for both telegate and teledata. With these assumptions, we are free to reduce the entire performance problem to making all needed EPR pairs as quickly as possible.

Our initial execution time model treats local gates and classical communication as zero cost, assuming that EPR pair creation is the most expensive portion of the computation. For example, for the teledata VBE adder on a linear topology, all of the EPR pairs needed can be created in two time steps at the beginning of the computation. The execution time would therefore be 2, constant for all n and m . Table 7.7 shows the performance under this assumption. The performance of the carry-lookahead adder does not change compared to the initial estimate, as the bottleneck link is busy full-time creating EPR pairs.

This model gives a misleading picture of performance once EPR pair creation is decoupled from the teleportation sequence. When the cost of the teleportation itself or of local gates exceeds $\sim 1/n$ of the cost of the EPR pair generation, the simplistic model breaks down; in the next subsection, we examine the performance with a more realistic model.

algo.	size	Baseline			Telegate					Teledata				
		bus	line	fully	bus	2bus	line	fully	2fully	bus	2bus	line	fully	2fully
VBE	16	360	16	16	105	53	7	14	7	30	15	2	4	2
	128	3048	16	16	889	445	7	14	7	254	127	2	4	2
	1024	24552	16	16	7161	3581	7	14	7	2046	1023	2	4	2
CDKM	16	232	21	19	135	68	11	18	9	90	60	6	12	6
	128	1912	21	19	1146	573	11	18	9	762	508	6	12	6
	1024	15352	21	19	9210	4605	11	18	9	6138	4092	6	12	6
Carry-look-ahead	16	644	N/A	99	444	222	N/A	89	45	260	178	N/A	96	56
	128	6557	N/A	159	4901	2451	N/A	149	75	3176	2028	N/A	192	104
	1024	54806	N/A	219	41502	20751	N/A	209	105	27260	17206	N/A	288	152

Table 7.7: Estimated latency to execute various adders on different topologies, for decomposed teleportation blocks (sec. 7.5.2), assuming classical communication and local gates have zero cost. Units are in EPR pair creation times. Size, length of the numbers to be added, in bits. Lower numbers are faster (better).

Detailed Estimate

To create Figures 7.9-7.11, we make assumptions about the execution time of various operations. Classical communication between nodes is 10nsec. A CCNOT (Toffoli) gate on encoded qubits takes 50nsec, CNOT 10nsec, and NOT 1nsec. These numbers can be considered realistic but optimistic for a technology with physical gate times in the low nanoseconds. For quantum error correction-encoded solid-state systems, the bottleneck is likely to be the time for qubit initialization or reliable single-shot measurement, which is still being designed, so actual performance may be one to two orders of magnitude slower.

We vary the EPR pair creation time from 10nsec to 1280nsec. This creation process is influenced by the choice of parallel or serial bus and the cycle time of an optical homodyne detector, as discussed in the last section. Photodetectors may be inherently fast, but their performance is limited by surrounding electronics [21, 315]. Final performance may be faster or slower than our model, but the range of values we have analyzed is broad enough to demonstrate clearly the important trends.

Figures 7.9 and 7.10 show, top to bottom, the fully, 2fully, and line networks for the telegate and teledata methods. The graphs plot adder time against EPR pair creation time and the length of the numbers to be added. The left hand plot shows the shape of the surfaces, with the z axis being latency to complete the addition. The right hand plot, with the same x and y axes, shows the region in which each type of adder is the fastest.

These figures show that the teledata method is faster than telegate. They also show that the carry-lookahead adder is very dependent on EPR pair creation time, while neither type of carry-ripple adder is. In Figure 7.11 we show this in more detail. For fast (10nsec) EPR pair creation, the carry-lookahead adder is faster for all problem sizes. For slow (1280nsec) EPR pair creation time, carry-lookahead is not faster until we reach 512 bits.

Although I have not includes graphs, we have also varied the time for classical communication and the other types of gates. The performance of an adder is fairly insensitive to these changes; it is dominated by the relationship between CCNOT and EPR pair creation times.

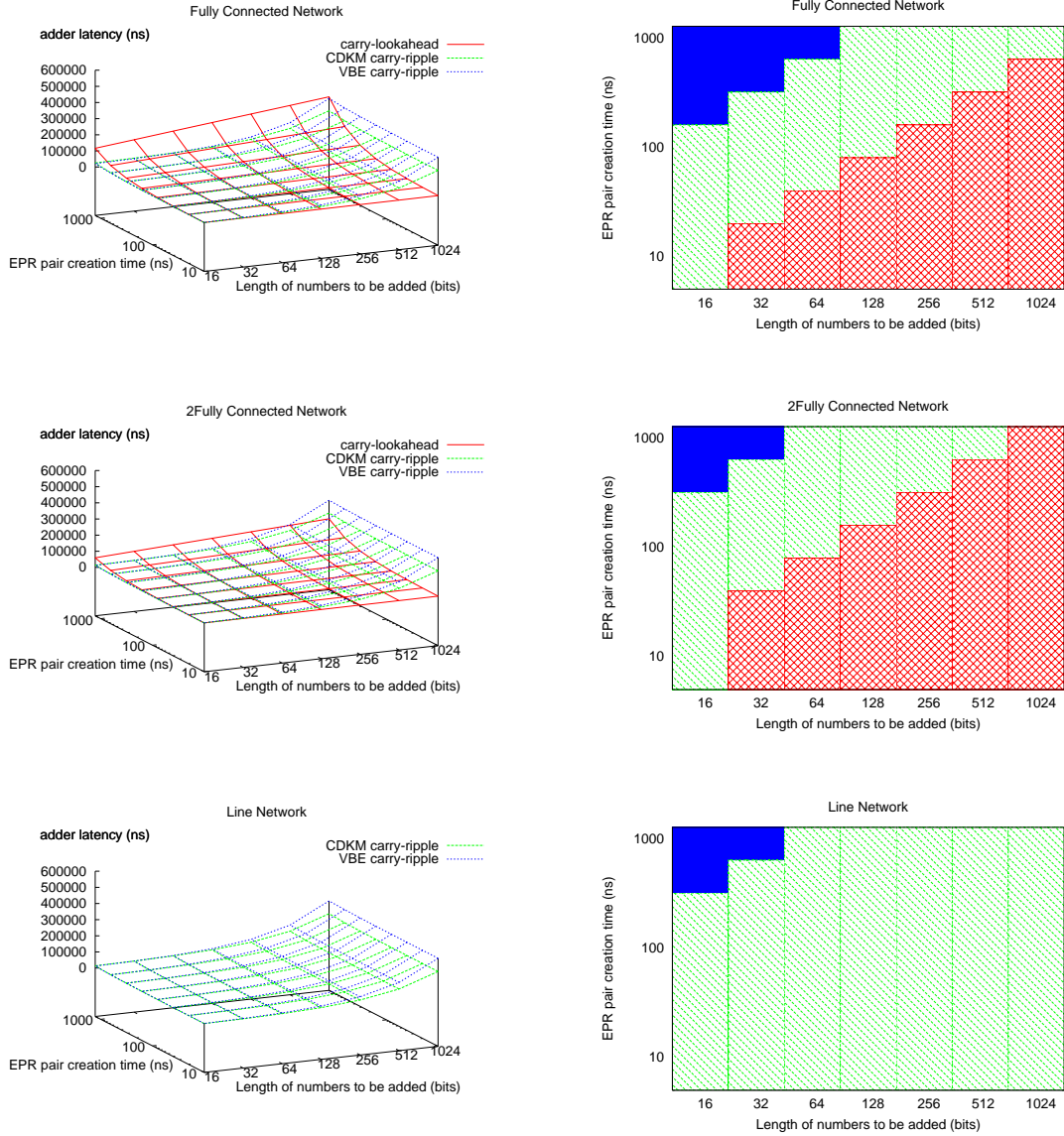


Figure 7.9: (Telegate) Performance of different adders on three different networks, one fully-connected with a single link and one with two links per node (2fully), and one line configuration. In this graph, we vary the latency to create a high-quality EPR pair and the length of the numbers we are adding. Classical communication time is assumed to be 10nsec, Toffoli gate time 50nsec, CNOT gate time 10nsec. The left hand graph of each pair plots adder execution time (vertical axis) against EPR pair creation time and number length. In the right hand graph of each pair, the hatched red area indicates areas where carry-lookahead is the fastest, the diagonally lined green area indicates CDKM carry-ripple, and solid blue indicates VBE carry-ripple. The performance of the carry-lookahead adder is very sensitive to the EPR pair creation time. If EPR pair creation time is low, the carry-lookahead adder is very fast; if creation time is high, the adder is very slow.

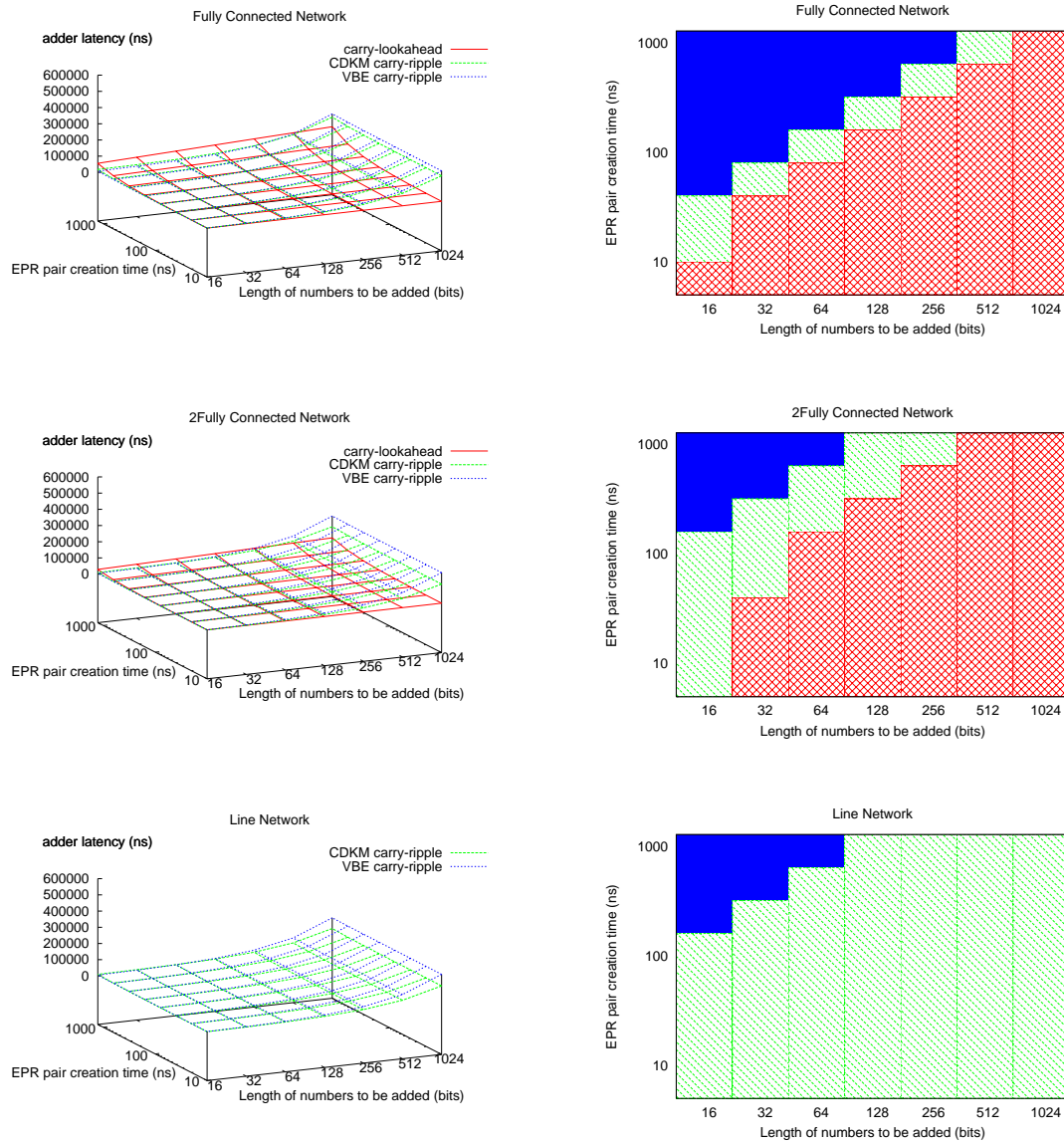


Figure 7.10: (Teledata) Performance of different adders on three different networks, one fully-connected with a single link and one with two links per node (2fully), and one line configuration. In this graph, we vary the latency to create a high-quality EPR pair and the length of the numbers we are adding. Classical communication time is assumed to be 10nsec, Toffoli gate time 50nsec, CNOT gate time 10nsec. In the right hand graph of each pair, the hatched red area indicates areas where carry-lookahead is the fastest, the diagonally lined green indicates CDKM carry-ripple, and solid blue indicates VBE carry-ripple. The performance of the carry-lookahead adder is very sensitive to the EPR pair creation time. If EPR pair creation time is low, the carry-lookahead adder is very fast; if creation time is high, the adder is very slow.

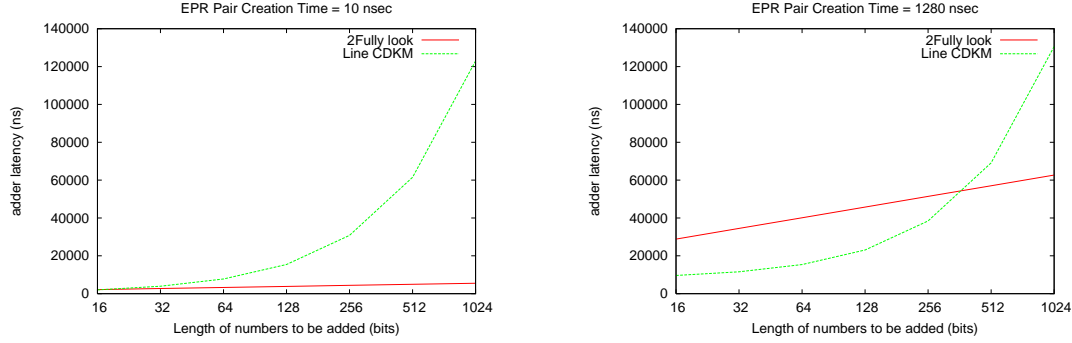


Figure 7.11: (Teledata) Comparison of CDKM on a line network with carry-lookahead on a 2fully network. These are the “front” and “back” cross-sections of figure 7.10.

7.6 Summary

This chapter has covered the overall quantum multicomputer architecture, including justifying the need for distributed quantum computation, investigating distributed quantum error correction and network link design, and ended by evaluating the performance of arithmetic circuits on a quantum multicomputer for different problem sizes, interconnect topologies, and gate timings. Although we have assumed that the interconnect is based on the qubus entanglement protocol creation of EPR pairs, our analysis, especially Table 7.6, applies equally well to any two-level structure with low-latency local operations and high-latency long-distance operations. The details of the cost depend on the interconnect topology, number of transceiver qubits, and the chosen breakdown for CCNOT. Gate time ratios are more important than actual gate times for this analysis. The time values presented here are reasonable for solid-state qubits under optimistic assumptions about advances in the underlying technology. Applying our results to slower technologies (or the same technology using more layers of quantum error correction) is a simple matter of scaling by the appropriate clock speed and storage requirements.

We found that the teledata method is faster than the telegate method, that separating the actual data teleportation from the necessary EPR pair creation allows a carry-ripple adder to be efficient for large problems, and that a linear network topology is adequate for up to a hundred nodes or more, depending on the cost ratio of EPR pair creation to local gates. For very large systems, switching interconnects, which are well understood in the optical domain [172, 218, 319], may become necessary, though we recommend deferring adding switching due to the complexity and the inherent signal loss; switching time in such systems also must be considered.

These results show that node size, interconnect topology, distributed gate approach (teledata v. telegate), and choice of adder affect overall performance in sometimes unexpected ways. Increasing the number of logical qubits per node, for example, reduces the total number of interconnect transfers but concentrates them in fewer places, causing contention for access. Therefore, increasing node size is not favorable *unless node I/O bandwidth increases proportionally*; we recommend keeping the node size small and fixed for the foreseeable future.

This data presents a clear path forward. I recommend pursuing a node architecture consisting of only a few logical qubits and initially two transceiver (quantum I/O) qubits. This will allow construction of a linear network, which will perform adequately with a carry-ripple adder up to moderately large systems. Engineering emphasis should be placed on supporting more transceiver qubits in each node, which can be used to parallelize transfers, decrease the network diameter, and provide fault tolerance. Significant effort is warranted on minimizing the key parameter of EPR pair creation time. Only once these avenues have been exhausted should the node size be increased and a switched optical network introduced. This approach should lead to the design of a viable quantum multicomputer.

Chapter 8

Conclusion

Now this is not the end. It is not even the beginning of the end.
But it is, perhaps, the end of the beginning.

Winston Churchill, November 1942

This dissertation has described the architecture of a quantum multicomputer and the structure of the algorithms to run on it. Shor's factoring algorithm has served as a convenient, concrete benchmark, but the overall architecture, building blocks and analysis methods are general. Although small-scale quantum computers exist, prospects for large-scale ones remain uncertain. The physicists have many problems to solve, of course, including decoherence time and gate quality, both of which are affected by many physical sources. The engineers, as well, have many problems to solve. At the highest levels, the process of balancing performance, reliability, physical feasibility and system cost has just begun. Utilization of heterogeneous structures, continued progress in error management, and further optimization of application algorithms for particular architectures continue to be promising areas of research. At lower levels, integration of system components, thermal engineering, and packaging remain issues. Once these problems are solved, a quantum multicomputer built on many nodes based on solid-state qubits is a viable, highly scalable, high-performance architecture.

The creation of the quantum multicomputer began with the optimization of quantum modular exponentiation for Shor's factoring algorithm, first in an architecture-independent fashion, then considering two specific architectural models, AC and NTC. The primary difference is that AC allows two qubits anywhere in the system to interact without penalty, while NTC allows only nearest neighbors in a line topology to interact. Both models are somewhat simplistic, but serve as useful upper and lower bounds.

Classical computation can be traded for quantum; increasing the classical computation by a factor of 2^w allows a factor of w decrease in quantum, a good trade for small values of w . Two new adder algorithms, the carry-select and conditional-sum adders, were developed. The carry-select adder runs in $O(\sqrt{n})$ time to add two n -bit numbers, and the conditional-sum adder, which is similar but uses a more complex demultiplexer, runs in $O(\log n)$ time. These techniques, as well as the fast, efficient CDKM carry-ripple adder, the $O(\log n)$ -depth carry-lookahead adder, Cleve-Watrous parallel multiplication, and some original optimizations, are used to create complete modular exponentiation algorithms. The algorithms presented here will reduce wall-clock time by a factor of one million for a six-thousand bit number on the AC architecture, or a factor of 13,000 on NTC. These circuits are $O(n \log^2 n)$ and $O(n^2 \log n)$ in circuit depth, respectively, and demonstrate the paramount importance of architecture when planning for performance. The primary architectural features of interest are the ability to execute multiple gates concurrently, the number of application-level qubits available, and the interconnection network of qubits.

The quantum multicomputer transcends the physical limitations of an individual quantum computer by combining the power of multiple quantum computers, in direct analogy to classical, distributed-memory multicomputers. It is obvious that a multicomputer can store more data than any individual quantum computer; what was less certain before this research was done was the performance of such a system. Extracting performance improvements, as in classical distributed systems, depends on finding parallelism in the algorithms and on minimizing the costs of communication. This research has shown that application-level parallelism is plentiful, and that the communication costs are reasonable. A linear network of nodes, each containing just a few logical qubits and two transceiver qubits for the quantum links, performs well up to several hundred nodes. Subdividing quantum teleportation of the data into the EPR pair creation and the later teleportation act allows high levels of parallelism in the EPR pair creation to be used, and a simple carry-ripple adder performs well. As the problem size approaches a thousand bits, the linear costs of the carry-ripple adder begin to dominate, and the logarithmic depth carry-lookahead adder becomes attractive. Efficient implementation of distributed carry-lookahead requires a more complex network. Increasing the size of individual nodes risks turning I/O into the system bottleneck, making it necessary to increase the number of transceiver qubits as node size grows.

With this summary, the detailed technical work of this thesis draws to a close. The remainder of this final chapter of the dissertation is more speculative: first, some rough

length	adder calls	tot. teleportations (t)
16	481	14000–125000
128	32544	8×10^6 – 10^8
1024	2.1×10^6	4×10^9 – 6×10^{10}

Table 8.1: Number of teleportations and adder calls necessary to execute the full modular exponentiation for different problem sizes.

estimates of the wall clock time that will actually be required to execute modular exponentiation on the quantum multicomputer are presented, then future work and some thoughts on the prospects for quantum computation, and the dissertation ends with some final, personal comments.

8.1 Complete Performance Estimates

Table 8.1 shows the number of adder calls for the complete modular exponentiation. These values assume that $w = 4$ and that p is large enough for the modulo arithmetic to have no impact, giving a required $2n^2$ calls to the adder routine. These numbers are combined with the data presented in the previous chapter to create total teleportation counts; the range of numbers is due to the difference between carry-ripple and carry-lookahead adders, with the carry-lookahead adder being more expensive. These total numbers were used in Section 7.4 to derive the necessary reliability of teleportation operations.

Because of the manner in which EPR pair creation and the actual gates are composed, it is now no longer possible to talk about performance strictly in units of “gate times”; we must now talk in terms of clock time for certain operations. Table 8.2 shows performance estimates derived from the figures and extrapolated for the complete algorithm.

These EPR pair creation times are for enough high-quality EPR pairs to transfer an entire logical qubit. Using the $[[23,1,7]]^i + [[7,1,3]]^o$ error correction code, we must transfer 161 physical qubits for a single logical qubit. Using a serial link, performing 161 transfers in 1280nsec (the upper end of the graphs shown) requires a physical EPR pair creation time of about 8nsec. Although this time is faster than what has been achieved experimentally, much of the time in adaptive homodyne measurements is spent on (classical digital) calculations, usually carried out on FPGAs [315, 21]. The qubus measurement time therefore seems amenable to significant improvement as technology advances.

length	CDKM, linear			Lookahead, 2fully		
	10nsec	160nsec	1280nsec	10nsec	160nsec	1280nsec
16	960 μ sec	1.4msec	4.6msec	1.0msec	2.5msec	14msec
128	500msec	530msec	750msec	125msec	290msec	1.5sec
1024	260sec	260sec	270sec	12sec	26sec	130sec

Table 8.2: Estimated time to complete a single run of distributed modular exponentiation. The data are for the CDKM adder on a linear network and a carry-lookahead adder on a 2fully network, each for three different *logical* EPR pair creation times, 10, 160, and 1280nsec. Other gate times as described in text.

Likewise, the gate times we have chosen, such as 50nsec for a Toffoli gate, must be seen in the light of fault tolerance and error correcting techniques; the $[[23,1,7]]$ code requires about three dozen time steps to measure and correct, while using significant concurrent gate execution [308]. The exact performance when combined with the upper-layer $[[7,1,3]]$ code is unclear, and the implementation of both codes is very different for AC and NTC, but the total performance penalty is likely around two orders of magnitude. A 50nsec logical Toffoli gate would therefore require physical gates well under a nanosecond, significantly faster than current physical implementations.

Thus, it is likely that the absolute performance numbers for the adder circuits presented in Section 7.5 are one to two orders of magnitude too optimistic. However, the basic analysis depends primarily on the ratio of gate times to teleportation and communication times, so the qualitative results are valid and the numbers need only scaling by the appropriate factors, which remain unclear.

Moreover, the numbers presented here are for a *single* run of the algorithm. For a perfect quantum computer, it is known that the probability of success with Shor's algorithm is $\geq 40\%$, independent of n , meaning that a very small number of runs will produce a good answer [298, 178]. However, for an imperfect quantum computer, decoherence and the precision required in the gates for the QFT ($O(2^{-k})$ for bit k) present problems. The approximate QFT (AQFT) is a reduced-precision form of the QFT [82], which has been investigated by various researchers who have produced differing estimates of the success probability, based on differing sets of assumptions [31, 121]. Resolving this discrepancy for real-world conditions is a very high priority issue.

One final factor throws a large uncertainty into the wall-clock time estimates: the number of concurrent multiplications (s) we implement. We saw in Section 6.4.2 that $s = n$ units will allow us to complete the full modular exponentiation in $\log_2 n$ times the latency for one multiplication. With the full $s = 1024$ multiplier units, the modular

exponentiation for a 1,024-bit number would run one hundred times as fast as for $s = 1$. For this approach to be economically and physically viable, integration must increase one hundred fold over that proposed in Chapter 7.1, to about 50,000 physical qubits per pod, whether in one node or multiple nodes, or the cost and floor space per dilution refrigerator must decline by a similar amount.

8.2 Future Work

The pursuit of performance in computing systems is never-ending. In classical computing systems, we have half a century of experience; in quantum computing, the race has just begun. It could be said that, at the moment, answering many questions about quantum computer architecture requires a great deal of insight and only moderate amounts of sweat. In the classical world, deep insight is also required, beginning with an understanding of where the bottlenecks in existing systems lie; however, in a mature field such as classical architecture, acting on that insight, first demonstrating that your insight is useful in limited circumstances, then achieving wide-spread adoption, often requires an *enormous* amount of effort¹. Over the next decade or so, as quantum computer architecture matures, this will no doubt become true in this field as well.

The future work presented here blends smoothly from specific, low-level continuations of the research in this dissertation to a research agenda for the larger quantum computer architecture community. Further refinement of the quantum multicomputer design requires the selection of a node technology and improvement in the detail of hardware design. Specifically, we must determine with some precision the number of qubits that can fit on a single chip, investigate on-chip demultiplexers for external control signals, and move as much control as possible into the device. Heterogeneous node types and heterogeneous qubit types within a node need to be investigated, as well as multi-level interconnect architectures. QEC optimized for ion trap is progressing rapidly; similar optimizations for solid state are desirable. And, of course, supporting experimental implementation of qubus and multi-qubit nodes will advance the architecture also.

Improving the accuracy of estimates for the number of runs of Shor's algorithm on QEC-encoded states on machines with limited physical accuracy, and the detailed cost

¹For example, the TRIPS microprocessor team is over twenty-five faculty, staff and students, and in turn is only a small fraction of the size of a microprocessor team in a major semiconductor manufacturer [61].

of high-precision operations on the encoded states, tops the list of follow-on work on algorithms. Continued algorithmic improvements in arithmetic, such as the completion of the smaller, faster conditional-sum adder mentioned in Section 6.3.1, is necessary. Optimizations for NTC and more complex topologies and more work to balance quantum and classical computation will also contribute to reduced run times for quantum algorithms, with consequent improvements in reliability and economic benefits.

Can technologies with disparate characteristics be combined into a hybrid, heterogeneous quantum computer, much as CPU, cache, RAM, and magnetic disks are combined into a classical computer? This will depend on development of the ability to transfer qubits from one technology to another and back, e.g. nuclear spin \leftrightarrow electron spin \leftrightarrow photon [227, 159, 71]. It will also require development of algorithms capable of taking advantage of such an architectural feature, presumably based on the classical techniques of caching, virtual memory, and out-of-core algorithms [171, 186].

For all quantum computing technologies, we are entering the era where automatic and semi-automatic design tools are needed [327, 316, 87]. A primary theme of architecture research going forward will no doubt be creating and utilizing heterogeneity in structures. Optimizing the choice of hardware structures, their layout and interconnections, and the algorithms to be run on them is a complex problem that will require powerful tools. Even for algorithms as simple and regular as arithmetic, many mappings of qubits to nodes (and gates to bus time slots) are possible; I do not claim the arrangements presented here are optimal. We are investigating further layouts using evolutionary algorithms, and expect to report those results at a future date. Other researchers have been doing excellent work on tools for automatic generation of QEC algorithms and structures, especially for ion traps; continued improvement in these tools holds the key to fast, accurate research into quantum computer architectures.

In the early 1980s, although chip layout was done *on* a computer, it was mostly done *by* a human being — including much of the verification (at Caltech, it was common to post a plot of a chip layout on the wall for visual inspection and correction by passers-by). A decade later, engineers often mused that it had become impossible to design a computer without using one; the layout and especially validation of the design, including design rule checking and simulation at both logical and electrical levels, could only be done by computer, and designs were far too complex to get right without the validation. Obviously, detailed simulation of a large quantum computer requires a quantum computer; the first large-scale quantum computers must be built without data from the most desirable simulations. When will a quantum computer first be used to

design its successor, and when will it become indispensable to do so?

8.3 Prospects

Few of the researchers working on implementations of quantum computing will commit to a timetable for delivering a machine large enough, reliable enough, and fast enough to solve classically intractable problems. Off the record, some are optimistic that “step functions” in total capabilities are on the horizon; others are pessimistic enough to say, “I’m not sure we will have a useful quantum computer in my lifetime.”

Personally, I am optimistic. I believe we are on the verge of stepping onto a Moore’s Law-like growth curve, with the number of qubits entangled in a single state growing exponentially over a sustained period. Ion trap systems are generating enormous excitement, and the technical problems surrounding them seem to be well on their way to being solved; a Moore’s Law-like curve seems very plausible for this technology. System architects have already begun making serious contributions in this area. Solid-state technologies such as quantum dot and Josephson junction still have hurdles to clear for individual qubits, including coherence time, gate quality and fast, reliable single-shot measurement. Once those problems are solved, it seems possible that the number of qubits on a chip can grow quite rapidly; when this step function happens, the need for system-level architects will be immediate. All technologies, as integration levels grow, will need improved control systems. The existing rack-mount equipment will quickly become prohibitive in both space and money.

Once any of these technologies becomes “turn-key” ready, so that system design, fabrication and experimentation are available to lay systems folk rather than the initiates of physics, interest in quantum computation will explode and systems will develop rapidly. When the physical technology reaches the point that individual researchers can create quantum computer designs and fabricate them without dedicated facilities, as the MOSIS project did more than two decades ago for VLSI, the base of capable researchers will broaden dramatically [325, 267]. Putting these systems in the hands of hackers may also result in useful algorithms. We are, in effect, in the time of Babbage asking what Knuth, Lampson and Torvalds will do with the machines we build.

The most prominent proposed use of quantum computers today is Shor’s algorithm for factoring large numbers, which has the potential to make the widely used RSA public-key cryptosystem and Diffie-Hellman key exchange protocol insecure. The encrypting operations and the execution of Shor’s algorithm are, not coincidentally, both

$O(n^3)$ for n -bit keys. The number of qubits we can build in a quantum system is much smaller than the number of classical bits we build in a system, and both manufacturing and operating costs for qubits and quantum gates will remain many orders of magnitude more expensive than classical bits and gates for the foreseeable future. Classical systems can therefore afford to go to larger key lengths far more easily than a quantum system, staying ahead in the cryptographic arms race (although this cost must be borne by all users, not those breaking the codes). However, the known existence (or even imminent delivery) of even a single large quantum computer may prompt a shift away from cryptosystems perceived to be vulnerable². Thus, Shor's algorithm alone is unlikely to be adequate economic incentive for the development and purchase of more than a handful of large quantum computers.

Whether or not a specific quantum computing technology is useful depends on the availability of important algorithms (e.g., Shor's algorithm) and supporting algorithms or subroutines (e.g., the modular exponentiation necessary to run Shor's algorithm) that map efficiently to a system built on the technology. Future developments in algorithms, therefore, can make an architecture useful which had earlier been dismissed due to lack of interesting, practical applications.

The need for hardware/software co-design is very much in evidence here. Because quantum computation in general, and architecture in particular, is immature as a field, we start adrift on Lampson's Sea. This thesis charts a course toward a particular goal, and maps out some of the major shoals. Course corrections, some major, are inevitable, but our sails are full and we have a guide star to follow. To be a complete system, many subsystems must be developed. Indeed, not just the subsystems themselves, but the development *tools* must be built. Chip layout tools must integrate smoothly with one or more of the commercial successors to early VLSI tools such as the Magic toolkit [257]. We need to develop the quantum equivalent of classical design rules [225], and may ultimately wish to use direct silicon compilation to physical circuits from programs [26]. Compilers that optimize a circuit are already being developed; new back ends to create both hardware and software will allow better optimization, at the expense of tool complexity.

²We wish to point out here that quantum key distribution does not solve the problems that Shor's algorithm creates [261].

8.4 Final Words

When I began working on quantum computing three years ago, I was naive about a great many of the technical aspects. I wanted to focus on software for quantum computers, and I was especially curious about how our classical mechanisms for resource management (such as semaphores) and naming — two of the key functions of an operating system — would translate into the quantum world. I quickly discovered that the structure of the machines themselves was not yet advanced enough to work seriously on such topics. Surveying the state of hardware proposals, it became clear that there was much room for jacks-of-all-system-trades like me to contribute. Each time I opened one door, I found another. Sometimes I found that someone had unlocked the door before me, and I was happy to walk through on their work. Sometimes, I found the door locked, and faced the task of picking the lock myself. I am pleased with what I have accomplished, but not satisfied; I imagine many, many productive years yet pushing beyond what we currently know, though it is not always obvious exactly what it *is* that we don't know.

I wish to close with two of my favorite quotes. “Life is either a daring adventure or nothing,” Heller Keller said. Even when things don't work out according to the original plan, you accomplish something along the way, if you are flexible and work hard. You must let the path teach you, as much as you choose the path.

Butter tea and wind pictures, the crystal mountain, and blue sheep dancing on the snow — it's quite enough! Did you see the snow leopard? No! Isn't that wonderful?

Peter Matthiessen, *The Snow Leopard*

Appendix A

Glossary

In such an interdisciplinary thesis, a glossary would seem to be essential. The mathematical terms are defined here *extremely* informally, for the benefit of newcomers to the field.

ancilla (plural ancillae) Bits holding temporary variables used during a reversible computation that must be returned to their initial state at the end of the computation.

bisection In a network, the number of links that must be cut to divide the network in half.

bra Dirac notation for a complex-conjugate row vector: $\langle\psi|$. See also *ket*.

cluster state computing

Also called *one-way computing* or *measurement-based computing* [277, 250].

Has nothing to do with classical computing clusters; the cluster state is a very large entangled state which serves as a computing substrate.

decoherence

The degradation of the state of a quantum system as it interacts with its environment in ways that are impossible to adequately characterize; causes errors in qubits.

decoherence free subspace (DFS)

A form of error management in which logical states are encoded in the *relative* state of multiple qubits [206, 140, 205].

degree The number of links, or connections to the network, at each node.

density matrix

Describes the statistical state of a quantum system. For an n -qubit system, a $2^n \times 2^n$ matrix. Also called the *density operator*, and usually written ρ . A valid density matrix has trace $\text{Tr}(\rho) = 1$, and the diagonal elements are the probability of finding the system in the corresponding state when measured.

diameter The largest number of hops through the network to get from any node to any other.

entanglement

The property of two or more qubits in which operations on one affect the state of the other. For pure states, corresponds roughly to the qubits having dependent probabilities for their states. *Karami-tsuki* in Japanese.

full-duplex

A type of link in which data can be transferred in both directions at the same time. Telephones are generally full-duplex.

half-duplex

A type of link in which data can be transferred in either direction, but only in one direction at a time. Many computer buses are half-duplex; push-to-talk walkie-talkies are half-duplex.

ket Dirac notation for a column vector: $|\psi\rangle$. For an n -qubit system, consists of 2^n entries. See also *bra*.

link A physical connection in a network between two nodes, or a node and a piece of dedicated networking equipment such as a router. May be serial or parallel.

mixed state

A state which has partially decohered due to interaction with its environment; must be represented by a density matrix ρ which does not have $\text{Tr}(\rho^2) = 1$

mux Multiplexer.

network In this dissertation, a collection of links that connect quantum computer nodes together. Often used in the quantum computing literature to mean circuit or program.

node A computational element attached to a network.

probe beam

For the qubus, the high-intensity beam that interacts with the qubits.

pure state

A quantum state about which we have maximal knowledge; it is not entangled with the environment. A pure state has $\rho = \rho^2$ and $\text{Tr}(\rho^2) = 1$. A pure state can be written in state-vector form as $|\psi\rangle$.

qubit

A two-level quantum system that obeys DiVincenzo's criteria; the basic unit of quantum information. A qubit may be in a superposition of its two states. Qubits may be physical or logical.

qubus

A system that uses a strong probe beam and weak nonlinearities to entangle two or more qubits over a distance.

qubyte

Eight qubits.

separable

Two quantum systems that are not entangled are separable.

simplex

A unidirectional link.

superposition

Two or more solutions to Schrödinger's equation added together to form a single state, with their weights adjusted so that the total weight is still one. *Kasane-awase* in Japanese.

trace

The sum of the diagonal of a matrix.

transceiver qubit

A physical qubit that connects to a qubus.

unitary transform

The most common mathematical representation of a quantum gate; for an n -qubit gate, a $2^n \times 2^n$ unitary matrix that effects a rotation in the appropriate space. A unitary transform U satisfies the condition that $U^\dagger U = U U^\dagger = I$.

Appendix B

List of Papers and Presentations

Peer-Reviewed Journals

1. R. Van Meter and M. Oskin. Architectural implications of quantum computing technologies. *ACM J. Emerging Tech. in Comp. Sys.*, 2(1), Jan. 2006.
2. R. Van Meter and K. M. Itoh. Fast quantum modular exponentiation. *Physical Review A*, 71(5):052320, May 2005.

International Conferences

1. R. Van Meter, W. J. Munro, K. Nemoto, and K. M. Itoh. Distributed arithmetic on a quantum multicomputer. In *Proc. Int. Symp. on Computer Architecture (ISCA33)*, Jun. 2006.
2. R. Van Meter, K. M. Itoh, and T. D. Ladd. Architecture-dependent execution time of Shor's algorithm, In *Proc. Int. Symp. on Mesoscopic Superconductivity and Spintronics (MS+S2006)*, Feb. 2006.
3. R. Van Meter. Trading classical for quantum computation using indirection. In *Realizing Controllable Quantum States: Proc. Int. Symp. on Mesoscopic Superconductivity and Spintronics (MS+S2004)*, Mar. 2004.

National Conferences and Workshops

1. R. Van Meter. Communications topology and distribution of the quantum Fourier transform. In *Proc. Tenth Symposium on Quantum Information Technology (QIT10)*, pages 19–24, May 2004.

Teaching

1. Jun. 2005: WIDE Project School of Internet, “Introduction to Quantum Computing”, a 3-day intensive short course on quantum computing offered via satellite and Internet. Attended by approximately fifty students from Nepal, Indonesia, Laos, Thailand, Japan, Malaysia, and Bangladesh.
2. Sept. 2004: U. Aizu, “Introduction to Quantum Computing”, a 3-day intensive short course on quantum computing offered to U. Aizu students for credit.

Other Presentations

1. “Fast Quantum Modular Exponentiation,” Caltech Workshop on Classical and Quantum Information Security (CQIS), Dec. 2005.
2. “The Design of a Quantum Multicomputer,” USC/ISI, Dec. 2005.
3. “Fast Quantum Modular Exponentiation,” BBN, Aug. 2005.
4. “Quantum Computing *Systems*: State of the Art, Summer 2005,” Carnegie Mellon University, Aug. 2005.
5. “Fast Quantum Modular Exponentiation,” HP Labs, Bristol, Jan. 2005.
6. “Fast Quantum Modular Exponentiation,” Oxford University, Jan. 2005.
7. “Fast Quantum Modular Exponentiation,” MIT, Nov. 2004.
8. “Accelerating Shor’s Algorithm Using Fast Quantum Modular Exponentiation,” 2004 Workshop on Information Security Research (invited), Fukuoka, Japan, Oct. 2, 2004.
9. “Introduction to Quantum Computing,” Keio Shonan Fujisawa Campus, June 3, 2004 (in Japanese).
10. “Trading Classical for Quantum Computation Using Indirection,” ERATO Kyoto, April 15, 2004 (in Japanese).
11. “A Computer Systems Research Agenda for Quantum Computing,” Nara Institute of Science and Technology, April 16, 2004 (in Japanese).

12. “Communications Topology and Distribution of the Quantum Fourier Transform,” National Institute of Informatics, April 22, 2004.
13. “A Computer Systems Research Agenda for Quantum Computing,” NTT Basic Research Laboratory, October 7, 2003.

Bibliography

- [1] *Proc. ERATO Conference on Quantum Information Science (EQIS2003)*, Sept. 2003.
- [2] S. Aaronson. Complexity zoo. http://qwiki.caltech.edu/wiki/Complexity_Zoo.
- [3] S. J. Aaronson. *Limits on Efficient Computation in the Physical World*. PhD thesis, U.C. Berkeley, 2004.
- [4] E. Abe. *Pulsed Electron Sping Resonance in Phosphorus Doped Isotopically Controlled Silicon*. PhD thesis, Keio University, 2006.
- [5] E. Abe, K. M. Itoh, J. Isoya, and S. Yamasaki. Electron-spin phase relaxation of phosphorus donors in nuclear-spin-enriched silicon. *Physical Review B*, 70:033204, 2004.
- [6] H. Abelson, D. Allen, D. Coore, C. Hanson, E. Rauch, G. Homsy, T. F. K. Jr., R. Nagpal, G. J. Sussman, and R. Weiss. Amorphous computing. *Commun. ACM*, 43(5):74–82, May 2000.
- [7] D. S. Abrams and S. Lloyd. Simulation of many-body Fermi systems on a universal quantum computer. *Physical Review Letters*, 79:2586–2589, 1997.
- [8] ACM. *Computer Architecture News, Proc. 33rd Annual International Symposium on Computer Architecture*, June 2006.
- [9] M. Acton, K.-A. Brickman, P. Haljan, P. Lee, L. Deslauriers, and C. Monroe. Near-perfect simultaneous measurement of a qubit register. <http://arXiv.org/quant-ph/0511257>, Nov.
- [10] L. M. Adleman. Molecular computation of solutions to combinatorial problems. *Science*, 266:1021–1024, 1994.

- [11] D. Aharonov and M. Ben-Or. Fault-tolerant quantum computation with constant error rate. <http://arXiv.org/quant-ph/9906129>, June 1999. extended version of STOC 1997 paper.
- [12] D. Aharonov, W. van Dam, J. Kempe, Z. Landau, S. Lloyd, and O. Regev. Adiabatic quantum computation is equivalent to standard quantum computation. In *Proc. 45th Annual Symposium on Foundations of Computer Science*. ACM, 2004.
- [13] Y. Aharonov, L. Davidovich, and N. Zagury. Quantum random walks. *Physical Review A*, 48(2):1687–1690, 1993.
- [14] A. V. Aho and K. M. Svore. Compiling quantum circuits using the palindrome transform. <http://arXiv.org/quant-ph/0311008>, Nov. 2003.
- [15] G. Ahokas, R. Cleve, and L. Hales. The complexity of quantum fourier transforms and integer multiplication. In *Proc. ERATO Conference on Quantum Information Science (EQIS2003)* [1].
- [16] V. A. Aksyuk et al. 238x238 micromechanical optical cross connect. *IEEE Photonics Technology Letters*, 15(4):587–589, 2003.
- [17] O. Alter and Y. Yamamoto. *Quantum Measurement of a Single System*. Wiley, 2001.
- [18] G. Amdahl. Validity of the single processor approach to achieving large-scale computing capabilities. In *AFIPS Conference Proceedings*, pages 483–485, 1967.
- [19] D. P. Anderson and G. Fedak. The computational and storage potential of volunteer computing. available at <http://boinc.berkeley.edu/papers.php>, Dec. 2005.
- [20] ARDA. *A quantum information science and technology roadmap*, v2.0 edition, Apr. 2004.
- [21] M. A. Armen, J. K. Au, J. K. Stockton, A. C. Doherty, and H. Mabuchi. Adaptive homodyne measurement of optical phase. *Physical Review Letters*, 89:133602, 2002.
- [22] I. Asimov. *I, Robot*. Gnome Press, 1950.

- [23] A. Aspuru-Guzik, A. D. Dutoi, P. J. Love, and M. Head-Gordon. Simulated quantum computation of molecular energies. *Science*, 309:1704–1707, 2005.
- [24] W. C. Athas and C. L. Seitz. Multicomputers: message-passing concurrent computers. *IEEE Computer*, 21:9–24, Aug. 1988.
- [25] W. C. Athas and L. J. Svensson. Reversible logic issues in adiabatic CMOS. In *Proc. IEEE 1994 Workshop on Physics and Computing*. IEEE, 1994.
- [26] R. F. Ayres. *Silicon Compilation and the Art of Automatic Microchip Design*. Prentice-Hall, Englewood Cliffs, NJ, 1983.
- [27] D. Bacon. Quantum computational complexity in the presence of closed timelike curves. *Physical Review A*, 70:032309, 2004.
- [28] D. Bacon. Operator quantum error correcting subsystems for self-correcting quantum memories. <http://arxiv.org/quant-ph/0506023>, June 2005.
- [29] S. Balensiefer, L. Kregor-Stickles, and M. Oskin. An evaluation framework and instruction set architecture for ion-trap based quantum micro-architectures. In *Proc. 32nd Annual International Symposium on Computer Architecture*, June 2005.
- [30] A. Barenco, C. H. Bennett, R. Cleve, D. P. DiVincenzo, N. Margolus, P. Shor, T. Sleator, J. Smolin, and H. Weinfurter. Elementary gates for quantum computation. *Phys. Rev. A*, 52:3457, 1995.
- [31] A. Barenco, A. Ekert, K.-A. Suominen, and P. Törmä. Approximate quantum fourier transform and decoherence. *Physical Review A*, 54:139–146, 1996.
- [32] T. Bauch, T. Lindström, F. Tafuri, G. Rotoli, P. Delsing, T. Claeson, and F. Lombardi. Quantum dynamics of a d-wave josephson junction. *Science*, 311:57–60, 2006.
- [33] J. Baugh, O. Moussa, C. A. Ryan, A. Nayak, and R. Laflamme. Experimental implementation of heat-bath algorithmic cooling using solid-state nuclear magnetic resonance. *Nature*, 438:470–473, 2005.
- [34] S. Beauregard. Circuit for Shor’s algorithm using $2n + 3$ qubits. *Quantum Information and Computation*, 3(2):175–185, 2003. <http://arXiv.org/quant-ph/0205095>.

- [35] D. Beckman, A. N. Chari, S. Devabhaktuni, and J. Preskill. Efficient networks for quantum factoring. *Phys. Rev. A*, 54:1034–1063, 1996. <http://arXiv.org/quant-ph/9602016>.
- [36] R. Beckman, E. Johnston-Halperin, Y. Luo, J. E. Green, and J. R. Heath. Bridging dimensions: Demultiplexing ultrahigh-density nanowire circuits. *Science*, 310:465–468, 2005.
- [37] M. Beeler, R. W. Gosper, and R. Schroepel. HAKMEM. Technical Report AIM-239, MIT, 1972.
- [38] C. G. Bell, A. Kotok, T. N. Hastings, and R. Hill. The evolution of the DECsystem-10. In C. G. Bell, J. C. Mudge, and J. E. McNamara, editors, *Computer Engineering: A DEC View of Hardware Systems Design*. Digital, 1978.
- [39] P. Benioff. Quantum mechanical models of Turing Machines that dissipate no energy. *Physical Review Letters*, 48:1581–1585, 1982.
- [40] C. H. Bennett. Logical reversibility of computation. *IBM J. Res. Develop.*, 17:525–532, 1973.
- [41] C. H. Bennett. Notes on the history of reversible computation. *IBM J. of Research and Development*, 32(1), 1988. reprinted in *IBM J. R.&D.* Vol. 44 No. 1/2, Jan./Mar. 2000, pp. 270–277.
- [42] C. H. Bennett, E. Bernstein, G. Brassard, and U. Vazirani. Strengths and weaknesses of quantum computing. *SIAM J. Comput.*, 26(5):1510–1523, 1997. <http://arXiv.org/quant-ph/9701001>.
- [43] C. H. Bennett, H. J. Bernstein, S. Popescu, and B. Schumacher. Concentrating partial entanglement by local operations. *Physical Review A*, 53:2046, 1996.
- [44] C. H. Bennett and G. Brassard. Quantum cryptography: Public key distribution and coin tossing. In *Proc. IEEE International Conference on Computers, Systems, and Signal Processing*, pages 175–179. IEEE, Dec. 1984.
- [45] C. H. Bennett, G. Brassard, C. Crépeau, R. Josza, A. Peres, and W. Wootters. Teleporting an unknown quantum state via dual classical and EPR channels. *Physical Review Letters*, 70:1895–1899, 1993.

- [46] C. H. Bennett, D. P. DiVincenzo, J. A. Smolin, and W. K. Wootters. Mixed-state entanglement and quantum error correction. *Physical Review A*, 54:3824–3851, 1996.
- [47] C. H. Bennett and S. J. Wiesner. Communication via one- and two-particle operators on Einstein-Podolsky-Rosen states. *Physical Review Letters*, 69:2881–2884, 1992.
- [48] E. Bernstein and U. Vazirani. Quantum complexity theory. *SIAM J. Computing*, 26(5):1411–1473, 1997.
- [49] P. Bertet, C. J. P. M. Harmans, and J. E. Mooij. Parametric coupling for superconducting qubits. *Physical Review B*, 73:064512, 2006.
- [50] B. M. Boghosian and W. Taylor IV. Simulating quantum mechanics on a quantum computer. *Physica D*, 120:30–42, Sept. 1998.
- [51] M. Bohr. Silicon trends and limits for advanced microprocessors. *Commun. ACM*, 41(3):80–87, Mar. 1998.
- [52] N. Boulant, K. Edmonds, J. Yang, M. A. Pravia, and D. G. Cory. Experimental demonstration of an entanglement swapping operation and improved control in NMR quantum-information processing. *Physical Review A*, 68:032305, 2003.
- [53] G. Bourianoff. The future of nanocomputing. *IEEE Computer*, pages 44–53, Aug. 2003.
- [54] D. Bouwmeester, J.-W. Pan, K. Mattle, M. Eibl, H. Weinfurter, and A. Zeilinger. Experimental quantum teleportation. *Nature*, 390:575–579, Dec. 1997.
- [55] G. Brassard, P. Høyer, and A. Tapp. Quantum counting. In *Proc. 25th Int. Colloquium on Automata, Languages and Programming (ICALP’98)*, pages 820–831. Springer, July 1998.
- [56] G. K. Brennen, C. M. Caves, P. S. Jessen, and I. H. Deutsch. Quantum logic gates in optical lattices. *Physical Review Letters*, 82(5):1060–1063, Feb. 1999.
- [57] H.-J. Briegel, W. Dür, J. Cirac, and P. Zoller. Quantum repeaters: the role of imperfect local operations in quantum communication. *Physical Review Letters*, 81:5932–5935, 1998.

- [58] K. R. Brown, R. J. Clark, and I. L. Chuang. Limitations of quantum simulation examined by simulating a pairing Hamiltonian using nuclear magnetic resonance. *quant-ph/0601021*, Jan. 2006.
- [59] D. E. Browne and T. Rudolph. Resource-efficient linear optical quantum computation. *Physical Review Letters*, 95:010501, 2005.
- [60] J. W. Bruce, M. A. Thornton, L. Shivakumaraiah, P. S. Kokate, and X. Li. Efficient adder circuits based on a conservative reversible logic gate. In *Proc. IEEE Computer Society Annual Symposium on VLSI*. IEEE Computer Society, Apr. 2002.
- [61] D. Burger, S. W. Keckler, K. S. McKinley, M. Dahlin, L. K. John, C. Lin, C. R. Moore, J. Burrill, R. G. McDonald, and W. Yode. Scaling to the end of silicon with EDGE architectures. *IEEE Computer*, 37(7):44–55, 2004.
- [62] G. Burkard, D. Loss, D. P. DiVincenzo, and J. A. Smolin. Physical optimization of quantum error correction circuits. *Physical Review B*, 60(16):11404–11416, 1999.
- [63] T. Byrnes and Y. Yamamoto. Simulating lattice gauge theories on a quantum computer. *Physical Review A*, 73:022328, 2006.
- [64] A. R. Calderbank and P. W. Shor. Good quantum error-correcting codes exist. *Physical Review A*, 54:1098–1105, 1996.
- [65] K. Čapek. *R.U.R.: Rossum’s Universal Robots*. 1920.
- [66] A. Carlini, A. Hosoya, T. Koike, and Y. Okudaira. Time-optimal quantum evolution. *Physical Review Letters*, 96:060503, 2006.
- [67] S. Cavallar, B. Dodson, A. K. Lenstra, W. Lioen, P. L. Montgomery, B. Murphy, H. te Riele, K. Aardal, J. Gilchrist, G. Guillerm, P. Leyland, J. Marchand, F. Morain, A. Muffett, C. Putnam, C. Putnam, and P. Zimmermann. Factorization of a 512-bit RSA modulus. In *Advances in Cryptology - EUROCRYPT 2000: International Conference on the Theory and Application of Cryptographic Techniques*, volume 1807 of *Lecture Notes in Computer Science*, page 1, Jan. 2000.
- [68] T. Chanelière, D. N. Matsukevich, S. D. Jenkins, S.-Y. Lan, T. A. B. Kennedy, and A. Kuzmich. Storage and retrieval of single photons transmitted between remote quantum memories. *Nature*, 438:833–836, 2005.

- [69] J. Chiaverini, J. Britton, D. Leibfried, E. Knill, M. D. Barrett, R. B. Blakestad, W. M. Itano, J. D. Jost, C. Langer, R. Ozeri, T. Schaetz, and D. J. Wineland. Implementation of the semiclassical quantum fourier transform in a scalable system. *Science*, 308:997–1000, 2005.
- [70] J. Chiaverini, D. Leibfried, T. Schaetz, M. D. Barrett, R. B. Blakestad, J. Britton, W. M. Itano, J. D. Jost, E. Knill, C. Langer, R. Ozeri, and D. J. Wineland. Realization of quantum error correction. *Nature*, 432:602–605, 2004.
- [71] L. Childress, J. M. Taylor, A. S. Sørensen, and M. Lukin. Fault-tolerant quantum repeaters with minimal physical resources, and implementations based on single-photon emitters. <http://arXiv.org/quant-ph/0502112>, Feb. 2005.
- [72] I. Chiorescu, P. Bertet, K. Semba, Y. Nakamura, C. J. P. M. Harmans, and J. E. Mooij. Coherent dynamics of a flux qubit coupled to a harmonic oscillator. *Nature*, 431:159–162, Sept. 2004.
- [73] C. W. Chou, H. de Riedmatten, D. Felinto, S. V. Polyakov, S. J. van Enk, and H. J. Kimble. Measurement-induced entanglement for excitation stored in remote atomic ensembles. *Nature*, 438:828–832, 2005.
- [74] I. L. Chuang, N. Gershenfeld, and M. Kubinec. Experimental implementation of fast quantum searching. *Physical Review Letters*, 80:2408–3411, 1998.
- [75] I. L. Chuang, R. Laflamme, P. Shor, and W. H. Zurek. Quantum computers, factoring and decoherence. *Science*, 270(5242):1633–1635, 1995.
- [76] I. L. Chuang, L. M. K. Vandersypen, X. Zhou, D. W. Leung, and S. Lloyd. Experimental realization of a quantum algorithm. *Nature*, 393:143–146, 1998.
- [77] J. Cirac, A. Ekert, S. Huelga, and C. Macchiavello. Distributed quantum computation over noisy channels. *Physical Review A*, 59:4249, 1999.
- [78] J. I. Cirac and P. Zoller. Quantum computations with cold trapped ions. *Phys. Rev. Lett.*, 74:4091–4094, 1995.
- [79] R. G. Clark et al. Progress in silicon-based quantum computing. *Phil. Trans. R. Soc. London A*, 361:1451–1471, 2003.

- [80] R. Cleve and J. Watrous. Fast parallel circuits for the quantum Fourier transform. In *Proc. 41st Annual Symposium on Foundations of Computer Science*, pages 526–536. ACM, 2000.
- [81] E. Collin, G. Ithier, A. Aassime, P. Joyez, D. Vion, and D. Esteve. NMR-like control of a quantum bit superconducting circuit. *Physical Review Letters*, 93:157005, Oct. 2004.
- [82] D. Coppersmith. An approximate Fourier transform using quantum factoring. Technical Report 19642, IBM Research, 1994. <http://arXiv.org/quant-ph/0201067>.
- [83] D. Copsey, M. Oskin, F. T. Chong, I. Chuang, and K. Abdel-Gaffar. Memory hierarchies for quantum data. In *1st Workshop on Non-Silicon Computing*, 2002.
- [84] D. Copsey, M. Oskin, T. Metodiev, F. T. Chong, I. Chuang, and J. Kubiatawicz. The effect of communication costs in solid-state quantum computing architectures. In *Proceedings of the fifteenth annual ACM Symposium on Parallel Algorithms and Architectures*, pages 65–74, 2003.
- [85] C. Cosmelli, M. G. Castellano, F. Chiarello, R. Leoni, D. Simeone, G. Torrioli, and P. Carelli. Controllable flux coupling for the integration of flux qubits. *cond-mat/0403690*, Mar. 2004.
- [86] N. Craig and T. Lester. The hitchhiker’s guide to the dilution refrigerator. http://marcuslab.harvard.edu/how_to/Fridge.pdf, Aug. 2004.
- [87] A. W. Cross. Synthesis and evaluation of fault-tolerant quantum computer architectures. Master’s thesis, MIT, 2005.
- [88] S. A. Cuccaro, T. G. Draper, S. A. Kutin, and D. P. Moulton. A new quantum ripple-carry addition circuit. <http://arXiv.org/quant-ph/0410184>, Oct. 2004.
- [89] W. J. Dally and B. Towles. *Principles and Practices of Interconnection Networks*. Elsevier, 2004.
- [90] C. M. Dawson, H. L. Haselgrove, and M. A. Nielsen. Noise thresholds for optical quantum computers, 2005. <http://arXiv.org/quant-ph/0509060>.
- [91] E. P. DeBenedictis. Reversible logic for supercomputing. In *Proc. 2nd conference on Computing Frontiers*, pages 391–402. ACM, 2005.

- [92] E. Dennis, A. Kitaev, A. Landahl, and J. Preskill. Topological quantum memory. *J. Math. Phys.*, 43:4452–4505, 2002.
- [93] D. Deutsch. Quantum theory, the Church-Turing principle, and the universal quantum computer. *Proc. Royal Soc. London A*, 400:97–117, 1985.
- [94] D. Deutsch and R. Jozsa. Rapid solution of problems by quantum computation. *Proc. R. Soc. London, Ser. A*, 439:553, 1992.
- [95] S. J. Devitt, A. G. Fowler, and L. C. Hollenberg. Simulations of Shor’s algorithm with implications to scaling and quantum error correction. <http://arXiv.org/quant-ph/0408081>, Aug. 2004.
- [96] E. D’Hondt. *Distributed quantum computation: A measurement-based approach*. PhD thesis, Vrije Universiteit Brussel, July 2005.
- [97] D. P. DiVincenzo. Quantum Computation. *Science*, 270(5234):255–261, 1995.
- [98] D. P. DiVincenzo. Two-bit gates are universal for quantum computation. *Physical Review A*, 51:1015–1022, 1995.
- [99] D. P. DiVincenzo. Quantum gates and circuits. *Proc. Royal Soc. London A*, 1998.
- [100] D. P. DiVincenzo, D. Bacon, J. Kempe, G. Burkard, and K. B. Whaley. Universal quantum computation with the exchange interaction. *Nature*, 408:339–342, 2000.
- [101] J. J. Dongarra, S. W. Otto, M. Snir, and D. Walker. An introduction to the MPI standard. *Commun. ACM*, Jan. 1995.
- [102] T. G. Draper. Addition on a quantum computer. <http://arXiv.org/quant-ph/0008033>, Aug. 2000. first draft dated Sept. 1998.
- [103] T. G. Draper, S. A. Kutin, E. M. Rains, and K. M. Svore. A logarithmic-depth quantum carry-lookahead adder. <http://arXiv.org/quant-ph/0406142>, June 2004.
- [104] M. I. Dyakonov. Quantum computing: a view from the enemy camp. In S. Luryi, J. Xu, and A. Zaslavsky, editors, *Future Trends in Microelectronics: The Nano Millenium*, pages 307–318. Wiley, 2002.

- [105] M. D. Eisaman, A. Andr, F. Massou, M. Fleischhauer, A. S. Zibrov, and M. D. Lukin. Electromagnetically induced transparency with tunable single-photon pulses. *Nature*, 438:837–841, 2005.
- [106] J. Eisert, M. Wilkens, and M. Lewenstein. Quantum games and quantum strategies. *Physical Review Letters*, 83(15):3077–3080, Oct. 1999.
- [107] A. Ekert and R. Jozsa. Quantum computation and Shor’s factoring algorithm. *Review of Modern Physics*, 68(3):733–753, 1996.
- [108] C. Elliott, D. Pearson, and G. Troxel. Quantum cryptography in practice. In *Proc. SIGCOMM 2003*. ACM, ACM, Aug. 2003. <http://arXiv.org/quant-ph/0307049>.
- [109] M. D. Ercegovac and T. Lang. *Digital Arithmetic*. Morgan Kaufmann, San Francisco, CA, 2004.
- [110] ESIA, JEITIA, KSIA, TSIA, and SIA. International technology roadmap for semiconductors. Technical report, ESIA and JEITIA and KSIA and TSIA and SIA, 2005. <http://public.itrs.net/>.
- [111] E. Farhi, J. Goldstone, S. Gutmann, J. Lapan, A. Lundgren, and D. Preda. A quantum adiabatic evolution algorithm applied to random instances of an NP-complete problem. *Science*, 292:472–476, 2001.
- [112] R. P. Feynman. *Feynman Lectures on Computation*. Addison Wesley, 1996.
- [113] R. P. Feynman. Computing machines in the future. In Hey [148].
- [114] R. P. Feynman. Simulating physics with computers. In Hey [148].
- [115] R. P. Feynman, R. B. Leighton, and M. Sands. *The Feynman Lectures on Physics*. Addison-Wesley, Reading, Massachusetts, 1963.
- [116] M. Fleischhauer and M. D. Lukin. Dark-state polaritons in electromagnetically induced transparency. *Physical Review Letters*, 84:5094–5097, May 2000.
- [117] R. Folman, P. Krüger, D. Cassettari, B. Hessmo, T. Maier, and J. Schmiedmayer. Controlling cold atoms using nanofabricated surfaces: Atom chips. *Physical Review Letters*, 84:4749–4752, 2000.
- [118] A. G. Fowler. Constructing arbitrary single-qubit fault-tolerant gates. [quant-ph/0411206](http://arXiv.org/quant-ph/0411206), Dec. 2005.

- [119] A. G. Fowler, S. J. Devitt, and L. C. Hollenberg. Implementation of Shor's algorithm on a linear nearest neighbor qubit array. *Quantum Information and Computation*, 4(4):237, 2004. <http://arXiv.org/quant-ph/0402196>.
- [120] A. G. Fowler, C. D. Hill, and L. C. L. Hollenberg. Quantum error correction on linear nearest neighbor qubit arrays. *Physical Review A*, 69:042314, 2004.
- [121] A. G. Fowler and L. C. L. Hollenberg. Scalability of Shor's algorithm with a limited set of rotation gates. *Physical Review A*, 70:032329, 2004.
- [122] M. P. Frank. *Reversibility for Efficient Computing*. PhD thesis, MIT, 1999.
- [123] E. Fredkin and T. Toffoli. Conservative logic. *Int. J. Theoretical Physics*, 21:219–253, 1982.
- [124] T. Fujisawa, T. H. Oosterkamp, W. G. van der Wiel, B. W. Broer, R. Aguado, S. Tarucha, and L. P. Kouwenhoven. Spontaneous emission spectrum in double quantum dot devices. *Science*, 282:932–935, 1998.
- [125] A. Furusawa, J. L. Sørensen, S. L. Braunstein, C. A. Fuchs, H. J. Kimble, and E. S. Polzik. Unconditional Quantum Teleportation. *Science*, 282(5389):706–709, 1998.
- [126] A. Galindo and M. A. Martin-Delgado. Information and computation: classical and quantum aspects. *Review of Modern Physics*, 74:347–423, Apr. 2002.
- [127] S. Gasparoni, J. Pan, P. Walther, T. Rudolph, and A. Zeilinger. Realization of a photonic controlled-NOT gate sufficient for quantum computation. *Physical Review Letters*, 93:020504, 2004.
- [128] S. Gay. Quantum programming languages: Survey and bibliography. *Bulletin of the European Association for Theoretical Computer Science*, June 2005.
- [129] C. Gilbert. *The Design and Use of Electronic Analogue Computers*. Chapman and Hall, Ltd., 1964.
- [130] P. Gossett. Quantum carry-save arithmetic. <http://arXiv.org/quant-ph/9808061>, Aug. 1998.
- [131] D. Gottesman. *Stabilizer Codes and Quantum Error Correction*. PhD thesis, California Institute of Technology, May 1997.

- [132] D. Gottesman. Fault tolerant quantum computation with local gates. <http://arXiv.org/quant-ph/9903099>, Mar. 1999.
- [133] D. Gottesman and I. L. Chuang. Demonstrating the viability of universal quantum computation using teleportation and single-qubit operations. *Nature*, 402:390–393, 1999.
- [134] M. Greiner, I. Bloch, O. Mandel, T. W. Hänsch, and T. Esslinger. Exploring phase coherence in a 2D lattice of bose-einstein condensates. *Physical Review Letters*, 87:160405, 2001.
- [135] L. Grover. A fast quantum-mechanical algorithm for database search. In *Proc. 28th Annual ACM Symposium on the Theory of Computation*, pages 212–219, 1996. <http://arXiv.org/quant-ph/9605043>.
- [136] L. K. Grover. Quantum telecomputation. <http://arXiv.org/quant-ph/9704012>, Apr. 1997.
- [137] L. K. Grover. Fixed-point quantum search. *Physical Review Letters*, 95:150501, 2005.
- [138] S. Gulde, M. Riebe, G. P. T. Lancaster, C. Becher, J. Eschner, H. Haffner, F. Schmidt-Kaler, I. L. Chuang, and R. Blatt. Implementation of the Deutsch-Jozsa algorithm on an ion-trap quantum computer. *Nature*, 421:48–50, 2003.
- [139] H. Häffner, W. Hänsel, C. F. Roos, J. Benhelm, D. C. al kar, M. Chwalla, T. Körber, U. D. Rapol, M. Riebe, P. O. Schmidt, C. Becher, O. Gühne, W. Dür, and R. Blatt. Scalable multiparticle entanglement of trapped ions. *Nature*, 438:643–646, 2005.
- [140] H. Häffner, F. Schmidt-Kaler, W. Haensel, C. F. Roos, T. Koerber, M. Chwalla, M. Riebe, J. Benhelm, U. D. Rapol, C. Becher, and R. Blatt. Robust entanglement. *Appl. Phys. B*, 81:151, 2005.
- [141] L. Hales and S. Hallgren. An improved quantum Fourier transform algorithm and applications. In *Proc. 41st Annual Symposium on Foundations of Computer Science*. ACM, ACM, Nov. 2000.
- [142] J. Hall. A reversible instruction set architecture and algorithms. *Physics and Computation*, pages 128–134, 1994.

- [143] S. Hallgren. Polynomial-time quantum algorithms for Pell's equation and the principal ideal problem. In *Proc. Symposium on Theory of Computing*. ACM, 2002.
- [144] S. E. Harris. Electromagnetically induced transparency. *Physics Today*, 50(7):36–42, July 1997.
- [145] A. W. Harrow, B. Recht, and I. L. Chuang. Efficient discrete approximations of quantum gates. *Journal of Mathematical Physics*, 43(9):4445–4451, 2002.
- [146] J. L. Hennessy and D. A. Patterson. *Computer Architecture: A Quantitative Approach*. Morgan Kaufman, 3rd edition, 2003.
- [147] W. K. Hensinger, S. Olmschenk, D. Stick, D. Hucul, M. Yeo, M. Acton, L. Deslauriers, and C. Monroe. T-junction ion trap array for two-dimensional ion shuttling, storage, and manipulation. *Applied Physics Letters*, 88:034101, 2006.
- [148] A. J. G. Hey, editor. *Feynman and Computation*. Westview Press, 2002.
- [149] M. Hillery, V. Bužek, and M. Ziman. Probabilistic implementation of universal quantum processors. *Physical Review A*, 65:022301, 2002.
- [150] J. Hughes. private communication, Jan. 2006.
- [151] K. Hwang and F. A. Briggs. *Computer Architecture and Parallel Processing*. McGraw Hill, 1984.
- [152] M. Jeong, B. Doris, J. Kedzierski, K. Rim, and M. Yang. Silicon device scaling to the sub-10-nm regime. *Science*, 306:2057–2060, Dec. 2004.
- [153] A. Imre, G. Csaba, L. Ji, A. Orlov, G. H. Bernstein, and W. Porod. Majority logic gate for magnetic quantum-dot cellular automata. *Science*, 311:205–208, 2006.
- [154] N. Isailovic, Y. Patel, M. Whitney, and J. Kubiawicz. Interconnection networks for scalable quantum computers. In *Computer Architecture News, Proc. 33rd Annual International Symposium on Computer Architecture* [8].

- [155] N. Isailovic, M. Whitney, Y. Patel, J. Kubiawicz, D. Copsey, F. T. Chong, I. L. Chuang, and M. Oskin. Datapath and control for quantum wires. *ACM Transactions on Architecture and Code Optimization*, 1(1), Mar. 2004.
- [156] K. M. Itoh. An all-silicon linear chain NMR quantum computer. *Solid State Communications*, 133:747–752, 2005.
- [157] D. Jaksch, H.-J. Briegel, J. Cirac, C. W. Gardiner, and P. Zoller. Entanglement of atoms via cold controlled collisions. *Physical Review Letters*, 82(9):1975–1978, 1999.
- [158] D. F. V. James and P. G. Kwiat. Atomic-vapor-based high efficiency optical detectors with photon number resolution. *Physical Review Letters*, 89:183601, 2002.
- [159] F. Jelezko, T. Gaebel, I. Popa, M. Domhan, A. Gruber, and J. Wrachtrup. Observation of coherence oscillation of a single nuclear spin and realization of a two-qubit conditional quantum gate. *Physical Review Letters*, 93:130501, Sept. 2004.
- [160] J. Johansson et al. Vacuum Rabi oscillations in a macroscopic superconducting qubit LC oscillator system. <http://arXiv.org/cond-mat/0510457>, 2005.
- [161] J. A. Jones, M. Mosca, and R. H. Hansen. Implementation of a quantum search algorithm on a quantum computer. *Nature*, 393:344–346, 1998.
- [162] R. Jozsa and N. Linden. On the role of entanglement in quantum computational speedup. *Proc. Royal Soc. London A*, 459:2011–2032, 2003. <http://arXiv.org/quant-ph/0201143>.
- [163] B. E. Kane. A silicon-based nuclear spin quantum computer. *Nature*, 393:133–137, May 1998.
- [164] N. Katz, M. Ansmann, R. C. Bialczak, E. Lucero, R. McDermott, M. Neeley, M. Steffen, E. M. Weig, A. N. Cleland, J. M. Martinis, and A. N. Korotkov. Coherent state evolution in a superconducting qubit from partial-collapse measurement. *Science*, 312:1498–1500, June 2006.
- [165] Y. Kawano, S. Yamashita, and M. Kitagawa. Explicit implementation of quantum circuits on a unidirectional periodic structure. *Physical Review A*, 72:012301, 2005.

- [166] J. Kempe. Quantum random walks: an introductory overview. *Contemporary Physics*, 44(4):307–327, 2003.
- [167] V. M. Kendon and W. J. Munro. Entanglement and its role in Shor’s algorithm. <http://arXiv.org/quant-ph/0412140>, Dec. 2004.
- [168] P. Kerntopf. Synthesis of multipurpose reversible logic gates. In *Proc. Euromicro Symposium on Digital System Design*. IEEE, IEEE, 2002.
- [169] R. Keyes. Is quantum computing with solid state devices possible? *Applied Physics A: Materials Science & Processing*, 76(5):737–741, Mar. 2003.
- [170] D. Kielpinski, C. Monroe, and D. J. Wineland. Architecture for a large-scale ion-trap quantum computer. *Nature*, 417:709–711, 2002.
- [171] T. Kilburn, D. Edwards, M. Lanigan, and F. Sumner. One-level storage system. *IRE Transactions*, EC-11(2):223–235, 1962.
- [172] J. Kim et al. 1100x1100 port MEMS-based optical crossconnect with 4-dB maximum loss. *IEEE Photonics Technology Letters*, 15(11):1537–1539, 2003.
- [173] J. Kim et al. System design for large-scale ion trap quantum information processor. *Quantum Information and Computation*, 5(7):515–537, 2005.
- [174] J. Kim, J.-S. Lee, , S. Lee, and C. Cheong. Implementation of the refined Deutsch-Jozsa algorithm on a three-bit NMR quantum computer. *Physical Review A*, 62:022312, 2000.
- [175] T. Kishimoto, H. Hachisu, J. Fujiki, K. Nagato, M. Yasuda, and H. Katori. Electrodynamical trapping of spinless neutral atoms with an atom chip. <http://arxiv.org/physics/0603157>, Mar. 2006.
- [176] A. Y. Kitaev. Quantum computations: algorithms and error correction. *Russian Math. Surveys*, 52(6):1191–1249, 1997.
- [177] A. Y. Kitaev, A. H. Shen, and M. N. Vyalyi. *Classical and Quantum Computation*. American Mathematical Society, 2002.
- [178] E. Knill. On Shor’s factor finding algorithm: Increasing the probability of success and tradeoffs involving the Fourier transform modulus. Available online but apparently unpublished., Aug. 1995.

- [179] E. Knill. Bounds on the probability of success of postselected nonlinear sign shifts implemented with linear optics. *Physical Review A*, 68:064303, 2003.
- [180] E. Knill. Quantum computing with very noisy devices. <http://arXiv.org/quant-ph/0410199>, Nov. 2004.
- [181] E. Knill, R. Laflamme, R. Martinez, and C. Negrevergne. Benchmarking quantum computers: the five-qubit error correcting code. *Physical Review Letters*, 86(25):5811–5814, June 2001.
- [182] E. Knill, R. Laflamme, R. Martinez, and C.-H. Tseng. An algorithmic benchmark for quantum information processing. *Nature*, 404:368–370, 2000.
- [183] E. Knill, R. Laflamme, and G. J. Milburn. Thresholds for linear optics quantum computation, 2000. <http://arXiv.org/quant-ph/0006120>.
- [184] E. Knill, R. Laflamme, and G. J. Milburn. A scheme for efficient quantum computation with linear optics. *Nature*, 409:46–52, 2001.
- [185] E. Knill, R. Laflamme, and W. H. Zurek. Resilient quantum computation. *Science*, 279:342–345, Jan. 1998.
- [186] D. E. Knuth. *The Art of Computer Programming, volume 3 / Sorting and Searching*. Addison-Wesley, Reading, MA, 1973.
- [187] D. E. Knuth. *The Art of Computer Programming, volume 2 / Seminumerical Algorithms*. Addison-Wesley, Reading, MA, 3rd edition, 1998.
- [188] J. G. Koller and W. C. Athas. Adiabatic switching, low energy computing, and the physics of storing and erasing information. In *Proc. IEEE 1992 Workshop on Physics and Computing*. IEEE, 1992.
- [189] G. A. Korn and T. M. Korn. *Electronic Analog Computers*. McGraw-Hill, 2nd edition, 1956.
- [190] C. E. Kozyrakis, S. Perissakis, D. A. Patterson, T. E. Anderson, K. Asanovic, N. Cardwell, R. Fromm, J. Golbus, B. Gribstad, K. Keeton, R. Thomas, N. Treuhaft, and K. A. Yelick. Scalable processors in the billion-transistor era: Iram. *IEEE Computer*, 30(9):75–78, 1997.

- [191] N. Kunihiro. Practical running time of factoring by quantum circuits. In *Proc. ERATO Conference on Quantum Information Science (EQIS2003)* [1].
- [192] N. Kunihiro. A new requirement for implementation of quantum computers. private communication, Jan. 2004.
- [193] N. Kunihiro. Exact analyses of computational time for factoring in quantum computers. *IEICE Trans. Fundamentals*, E88-A(1):105–111, 2005.
- [194] T. Kutsuzawa et al. Coherent control of a flux qubit by phase-shifted resonant microwave pulses. <http://arXiv.org/cond-mat/0501592>, 2005.
- [195] T. D. Ladd. *Quantum Computing With Nuclear Spins in Semiconductors*. PhD thesis, Stanford University, 2005.
- [196] T. D. Ladd, J. R. Goldman, F. Yamaguchi, Y. Yamamoto, E. Abe, and K. M. Itoh. All-silicon quantum computer. *Physical Review Letters*, 89(1):17901, July 2002.
- [197] T. D. Ladd, D. Maryenko, Y. Yamamoto, E. Abe, and K. M. Itoh. Coherence time of a solid-state nuclear qubit, 2005. <http://arXiv.org/quant-ph/0309164>.
- [198] R. Laflamme, C. Miquel, J. P. Paz, and W. H. Zurek. Perfect quantum error correcting code. *Physical Review Letters*, 77:198–201, 1996.
- [199] B. W. Lampson. Hints for computer system design. In *Proc. 9th ACM Symposium on Operating Systems Principles*, pages 33–48, 1983.
- [200] R. Landauer. Irreversibility and heat generation in the computing process. *IBM J. of Research and Development*, 5(3):183–191, 1961. reprinted in *IBM J. R.&D.* Vol. 44 No. 1/2, Jan./Mar. 2000, pp. 261–269.
- [201] J. Lantz, M. Wallquist, V. S. Shumeiko, and G. Wendin. Josephson junction qubit network with current-controlled interaction. *Physical Review B*, 70:140507, 2004.
- [202] D. Leibfried, E. Knill, S. Seidelin, J. Britton, R. B. Blakestad, J. Chiaverini, D. B. Hume, W. M. Itano, J. D. Jost, C. Langer, R. Ozeri, R. Reichle, and D. J. Wineland. Creation of a six-atom ‘schrodinger cat’ state. *Nature*, 438:639–642, 2005.

- [203] A. Lenstra, E. Tromer, A. Shamir, W. Kortsmit, B. Dodson, J. Hughes, and P. Leyland. Factoring estimates for a 1024-bit RSA modulus. In *AsiaCrypt 2003*, Lecture Notes in Computer Science, New York, 2003. Springer-Verlag.
- [204] D. W. Leung, I. L. Chuang, F. Yamaguchi, and Y. Yamamoto. Efficient implementation of selective recoupling in heteronuclear spin systems using Hadamard matrices. *Phys. Rev. A*, 61, 2000. <http://arXiv.org/quant-ph/9904100>.
- [205] D. A. Lidar, I. L. Chuang, and K. B. Whaley. Decoherence-free subspaces for quantum computation. *Physical Review Letters*, 81(12):2594–2597, Sept. 1998.
- [206] D. A. Lidar and K. B. Whaley. *Irreversible Quantum Dynamics*, volume 622 of *Lecture Notes in Physics*, chapter Decoherence-Free Subspaces and Subsystems. Springer, 2003.
- [207] Y. L. Lim, S. D. Barrett, A. Beige, P. Kok, and L. C. Kwek. Repeat-Until-Success quantum computing using stationary and flying qubits. <http://arXiv.org/quant-ph/0508218>, Aug. 2005.
- [208] Y. Liu, L. F. Wei, J. S. Tsai, and F. Nori. Controllable coupling between flux qubits. *cond-mat/0507496*, July 2005.
- [209] Y. Liu, J. Q. You, L. F. Wei, C. P. Sun, and F. Nori. Optical selection rules and phase-dependent adiabatic state control in a superconducting quantum circuit. *Physical Review Letters*, 95:087001, 2005.
- [210] S. Lloyd. A potentially realizable quantum computer. *Science*, 261:1569–1571, 1993.
- [211] S. Lloyd. Universal quantum simulators. *Science*, 273:1073–1078, 1996.
- [212] S. Lloyd. Ultimate limits to computation. *Nature*, 406:1047–1054, 2000.
- [213] S. Lloyd. Computational capacity of the universe. *Physical Review Letters*, 88:237901, 2002.
- [214] D. Loss and D. P. DiVincenzo. Quantum computation with quantum dots. *Phys. Rev. A*, 57:120, 1998.
- [215] P. J. Love and B. M. Boghosian. Type-II quantum algorithms. *Physica A*, 2005, to appear.

- [216] A. Maassen van den Brink, A. Berkley, and M. Yalowsky. Mediated tunable coupling of flux qubits. *New Journal of Physics*, 7:230, 2005.
- [217] F. Magniez, D. Mayers, M. Mosca, and H. Ollivier. Self-testing of quantum circuits. <http://arXiv.org/quant-ph/0512111>, Dec. 2005.
- [218] P. J. Marchand, A. V. Krishnamoorthy, G. I. Yayla, S. C. Esener, and U. Efron. Optically augmented 3-d computer: System technology and architecture. *J. Parallel and Distributed Computing*, 41(1):20–35, Feb. 1997.
- [219] D. J. H. Markham. *Local Distinguishability, Entanglement and Mixedness of Quantum States*. PhD thesis, Imperial College, University of London, 2004.
- [220] R. Martel, T. Schmidt, H. R. Shea, T. Hertel, and P. Avouris. Single- and multi-wall carbon nanotube field-effect transistors. *Applied Physics Letters*, 73(17):2447–2449, 1998.
- [221] J. M. Martinis, S. Nam, J. Aumentado, and C. Urbina. Rabi oscillations in a large Josephson-junction qubit. *Physical Review Letters*, 89:117901, 2002.
- [222] D. N. Matsukevich and A. Kuzmich. Quantum State Transfer Between Matter and Light. *Science*, 306(5696):663–666, 2004.
- [223] K. Mattle, H. Weinfurter, P. G. Kwiat, and A. Zeilinger. Dense coding in experimental quantum communication. *Physical Review Letters*, 76:4656–4659, 1996.
- [224] C. Mead. *Analog VLSI and Neural Systems*. Addison Wesley, 1989.
- [225] C. Mead and L. Conway. *Introduction to VLSI Systems*. Addison-Wesley Longman Publishing Co., Boston, MA, 1979.
- [226] C. A. Mead. Scaling of MOS technology to submicrometer feature sizes. In Hey [148].
- [227] M. Mehring, J. Mende, and W. Scherer. Entanglement between an electron and a nuclear spin 1/2. *Physical Review Letters*, 90:153001, Apr. 2003.
- [228] J. D. Meindl, Q. Chen, and J. A. Davis. Limits on silicon nanoelectronics for terascale integration. *Science*, 293:2044–2049, 2001.

- [229] T. S. Metodi, D. D. Thaker, A. W. Cross, F. T. Chong, and I. L. Chuang. A quantum logic array microarchitecture: Scalable quantum data movement and computation. In *Proceedings of the 2005 International Symposium on Microarchitecture (MICRO-38)*, 2005.
- [230] T. Metodiev, A. Cross, D. Thaker, K. Brown, D. Copsey, F. T. Chong, and I. L. Chuang. Preliminary results on simulating a scalable fault tolerant ion-trap system for quantum computation. In *Proceedings of the 3rd Workshop on Non-Silicon Computation [NSC-3]*, 2003.
- [231] D. A. Meyer. Quantum games and quantum algorithms. <http://arXiv.org/quant-ph/0004092>, 2000.
- [232] A. J. Miller, S. W. Nam, J. M. Martinis, and A. V. Sergienko. Demonstration of a low-noise near-infrared photon counter with multiphoton discrimination. *Applied Physics Letters*, 83:791–793, 2003.
- [233] C. Miquel, J. P. Paz, and W. H. Zurek. Quantum computation with phase drift errors. *Physical Review Letters*, 78:3971–3974, 1997.
- [234] J. E. Mooij, T. P. Orlando, L. Levitov, L. Tian, C. H. van der Wal, and S. Lloyd. Josephson persistent-current qubit. *Science*, 285:1036–1039, Aug. 1999.
- [235] C. Moore and M. Nilsson. Parallel quantum computation and quantum codes. *SIAM J. Computing*, 31(3):799–815, 2001. <http://arxiv.org/abs/quant-ph/9808027>.
- [236] G. E. Moore. Cramming more components onto integrated circuits. *Electronics*, 38(8), Apr. 1965.
- [237] W. Munro, K. Nemoto, and T. Spiller. Weak nonlinearities: a new route to optical quantum computation. *New Journal of Physics*, 7:137, May 2005.
- [238] W. Munro, K. Nemoto, and A. White. The Bell inequality: a measure of entanglement? *J. Modern Optics*, 48(7):1239–1246, June 2001.
- [239] K. V. R. M. Murali, N. Sinha, T. S. Mahesh, M. H. Levitt, K. V. Ramanathan, and A. Kumar. Quantum information processing by nuclear magnetic resonance: Experimental implementation of half-adder and subtractor operations using an oriented spin-7/2 system. *Physical Review A*, 66(022313), 2002.

- [240] E. S. Myrgren and K. B. Whaley. Implementing a quantum algorithm with exchange-coupled quantum dots: a feasibility study. *Quantum Information Processing*, 2003. to appear; <http://arXiv.org/quant-ph/0309051>.
- [241] Y. Nakajima, Y. Kawano, and H. Sekigawa. A new algorithm for producing quantum circuits using KAK decompositions, 2005. <http://arXiv.org/quant-ph/0509196>.
- [242] Y. Nakamura, Y. A. Pashkin, and J. S. Tsai. Coherent control of macroscopic quantum states in a single-Cooper-pair box. *Nature*, 398:786–788, Apr. 1999.
- [243] C. Negrevergne, T. Mahesh, C. Ryan, M. Ditty, F. Cyr-Racine, W. Power, N. Boulant, T. Havel, D. Cory, and R. Laflamme. Benchmarking quantum control methods on a 12-qubit system. *Physical Review Letters*, 96:170501, 2006.
- [244] K. Nemoto and W. J. Munro. Nearly deterministic linear optical controlled-NOT gate. *Physical Review Letters*, 93:250502, 2004.
- [245] M. A. Nielsen. Simple rules for a complex quantum world. In *The Edge of Physics*. Scientific American, 2003.
- [246] M. A. Nielsen. Cluster-state quantum computation. <http://arxiv.org/abs/quant-ph/0504097>, Apr. 2005.
- [247] M. A. Nielsen and I. L. Chuang. Programmable quantum gate arrays. *Physical Review Letters*, 79:321–324, 1997.
- [248] M. A. Nielsen and I. L. Chuang. *Quantum Computation and Quantum Information*. Cambridge University Press, 2000.
- [249] M. A. Nielsen and I. L. Chuang. *Quantum Computation and Quantum Information*, pages 266–268. Cambridge University Press, 2000.
- [250] M. A. Nielsen and C. M. Dawson. Fault-tolerant quantum computation with cluster states, 2004. <http://arXiv.org/quant-ph/0405134>.
- [251] M. A. Nielsen, M. R. Dowling, M. Gu, and A. C. Doherty. Quantum computation as geometry. *Science*, 311:1133–1135, 2006.
- [252] A. O. Niskanen, Y. Nakamura, and J.-S. Tsai. Tunable coupling scheme for flux qubits at the optimal point. *cond-mat/0512238*, Dec. 2005.

- [253] J. L. O'Brien, G. J. Pryde, A. G. White, T. C. Ralph, and D. Branning. Demonstration of an all-optical quantum controlled-NOT gate. *Nature*, 426:264–267, Nov. 2003.
- [254] B. Ömer. Classical concepts in quantum programming. In *Proc. Quantum Structures*, 2002.
- [255] M. Oskin, F. T. Chong, and I. Chuang. A practical architecture for reliable quantum computers. *IEEE Computer*, Jan. 2002.
- [256] M. Oskin, F. T. Chong, I. L. Chuang, and J. Kubiawicz. Building quantum wires: The long and short of it. In *Computer Architecture News, Proc. 30th Annual International Symposium on Computer Architecture*. ACM, June 2003.
- [257] J. K. Ousterhout, G. T. Hamachi, R. N. Mayo, W. S. Scott, and G. S. Taylor. Magic: A VLSI layout system. In *Proc. 21st Design Automation Conference*, pages 152–159. IEEE, 1984.
- [258] E. Ozbay. Plasmonics: merging photonics and electronics at nanoscale dimensions. *Science*, 311:189–193, 2006.
- [259] J.-W. Pan, S. Gasparoni, R. Ursin, G. Weihs, and A. Zeilinger. Experimental entanglement purification of arbitrary unknown states. *Nature*, 423:417–422, May 2003.
- [260] Y. A. Pashkin, T. Yamamoto, O. Astafiev, Y. Nakamura, D. V. Averin, and J. S. Tsai. Quantum oscillations in two coupled charge qubits. *Nature*, 421:823–826, Feb. 2003.
- [261] K. G. Paterson, F. Piper, and R. Schack. Why quantum cryptography? <http://arxiv.org/quant-ph/0406147>, June 2004.
- [262] Y. N. Patt, S. J. Patel, M. Evers, D. H. Friendly, and J. Stark. One billion transistors, one uniprocessor, one chip. *IEEE Computer*, 30(9):51–57, 1997.
- [263] D. A. Patterson, G. Gibson, and R. H. Katz. A case for redundant arrays of inexpensive disks (RAID). In *Proc. ACM SIGMOD Conference*, pages 109–116, June 1988.
- [264] J. P. Paz and A. Roncaglia. Quantum gate arrays can be programmed to evaluate the expectation value of any operator. *Physical Review A*, 68:052316, 2003.

- [265] T. Pellizzari, S. A. Gardiner, J. I. Cirac, and P. Zoller. Decoherence, continuous observation, and quantum computing: A cavity QED model. *Physical Review Letters*, 75:3788–3791, 1995.
- [266] J. R. Petta, A. C. Johnson, J. M. Taylor, E. A. Laird, A. Yacoby, M. D. Lukin, C. M. Marcus, M. P. Hanson, and A. C. Gossard. Coherent manipulation of coupled electron spins in semiconductor quantum dots. *Science*, 309:2180–2184, 2005.
- [267] C. A. Piña. MOSIS: IC prototyping and low volume production service. In *Proc. 2001 International Conference on Microelectronic Systems Education (MSE'01)*. IEEE, 2001.
- [268] T. Pittman, B. Jacobs, and J. Franson. Demonstration of quantum error correction using linear optics. *Physical Review A*, page 052332, May 2005.
- [269] T. B. Pittman, M. J. Fitch, B. C. Jacobs, and J. D. Franson. Experimental controlled-NOT logic gate for single photons in the coincidence basis. *Physical Review A*, 68:032316, 2003.
- [270] T. B. Pittman, B. C. Jacobs, and J. D. Franson. Demonstration of nondeterministic quantum logic operations using linear optical elements. *Physical Review Letters*, 88:257902, 2002.
- [271] B. L. T. Plourde, T. L. Robertson, P. A. Reichardt, T. Hime, S. Linzen, C.-E. Wu, and J. Clarke. Flux qubits and readout device with two independent flux lines. *Physical Review B*, 72:060506(R), 2005.
- [272] B. L. T. Plourde, J. Zhang, K. B. Whaley, F. K. Wilhelm, T. L. Robertson, T. Hime, S. Linzen, P. A. Reichardt, C.-E. Wu, and J. Clarke. Entangling flux qubits with a bipolar dynamic inductance. *Physical Review B*, 70:140501(R), 2004.
- [273] J. Preskill. Lectures notes on quantum computation. <http://www.theory.caltech.edu/~preskill/ph219/index.html>, Oct. 1998.
- [274] J. Preskill. Reliable quantum computers. *Proc. Roy. Soc. Lond. A*, 454:385–410, 1998.

- [275] T. C. Ralph. Time displaced entanglement and non-linear quantum evolution. <http://arXiv.org/quant-ph/0510038>, Oct. 2005.
- [276] T. C. Ralph, A. J. F. Hayes, and A. Gilchrist. Loss-tolerant optical qubits. *Physical Review Letters*, 95:100501, Sept. 2005.
- [277] R. Raussendorf, D. E. Browne, and H. J. Briegel. Measurement-based quantum computation on cluster states. *Physical Review A*, 68(022312), 2003.
- [278] H. Rheingold. *Smart Mobs: The Next Social Revolution*. Perseus Books Group, 2002.
- [279] C. Rigetti, A. Blais, and M. Devoret. Protocol for universal gates in optimally biased superconducting qubits. *Physical Review Letters*, 94:240502, 2005.
- [280] R. Rivest, A. Shamir, and L. Adleman. A method for obtaining digital signatures and public-key cryptosystems. *Commun. ACM*, 21(2):120–126, 1978.
- [281] C. F. Roos, M. Riebe, H. Häffner, W. Hänsel, J. Benhelm, G. P. Lancaster, C. Becher, F. Schmidt-Kaler, and R. Blatt. Control and measurement of three-qubit entangled states. *Science*, 304:1478–1480, June 2004.
- [282] M. Roško, V. Bužek, P. R. Chouha, and M. Hillery. Generalized measurements via a programmable quantum processor. *Physical Review A*, 68:062302, 2003.
- [283] RSA Security Inc. web page, May 2004. <http://www.rsasecurity.com/rsalabs/node.asp?id=2096>.
- [284] T. Rueckes, K. Kim, E. Joselevich, G. Y. Tseng, C.-L. Cheung, and C. M. Lieber. Carbon nanotube-based nonvolatile random access memory for molecular computing. *Science*, 289:94–97, 2000.
- [285] K. Sanaka, T. Jennewein, J. Pan, K. Resch, and A. Zeilinger. Experimental nonlinear sign shift for linear optics quantum computation. *Physical Review Letters*, 92:017902, 2004.
- [286] C. Santori, D. Fattal, J. Vuckovic, G. S. Solomon, and Y. Yamamoto. Indistinguishable photons from a single-photon device. *Nature*, 419:594–597, 2002.
- [287] S. Scheel, K. Nemoto, W. J. Munro, and P. L. Knight. Measurement-induced nonlinearity in linear optics. *Physical Review A*, 68:032310, 2003.

- [288] F. Schmidt-Kaler, H. Haffner, M. Riebe, S. Gulde, G. P. T. Lancaster, T. Deuschle, C. Becher, C. F. Roos, J. Eschner, and R. Blatt. Realization of the Cirac-Zoller controlled-NOT quantum gate. *Nature*, 422:408, 2003.
- [289] B. Schneier. *Applied Cryptography*. J. Wiley, 2nd edition, 1996.
- [290] N. Schuch and J. Siewert. Programmable networks for quantum algorithms. *Physical Review Letters*, 91:027902, 2003.
- [291] L. J. Schulman and U. V. Vazirani. Molecular scale heat engines and scalable quantum computers. In *Proc. 31st ACM Symposium on the Theory of Computing*, page p. 322, 1999.
- [292] T. Sekiguchi, S. Yoshida, and K. M. Itoh. Self-assembly of parallel atomic wires and periodic clusters of silicon on a vicinal Si(111) surface. *Physical Review Letters*, 95:106101, 2005.
- [293] K. Semba. private communication, Nov. 2005.
- [294] M. S. Shahriar, P. R. Hemmer, S. Lloyd, P. S. Bhatia, and A. E. Craig. Solid-state quantum computing using spectral holes. *Physical Review A*, 66:032301, 2002.
- [295] A. Shnirman, G. Schön, and Z. Hermon. Quantum manipulations of small josephson junctions. *Physical Review Letters*, 79:2371–2374, 1997.
- [296] P. W. Shor. Algorithms for quantum computation: Discrete logarithms and factoring. In *Proc. 35th Symposium on Foundations of Computer Science*, pages 124–134, Los Alamitos, CA, 1994. IEEE Computer Society Press.
- [297] P. W. Shor. Fault-tolerant quantum computation. In *Proc. 37th Symposium on Foundations of Computer Science*, pages 56–65, Los Alamitos, CA, 1996. IEEE Computer Society Press.
- [298] P. W. Shor. Polynomial time algorithms for prime factorization and discrete logarithms on a quantum computer. *SIAM J. Comp.*, 26(5):1484–1509, 1997. <http://arXiv.org/quant-ph/9508027>.
- [299] D. R. Simon. On the power of quantum computation. In *Proc. 35th Annual Symposium on Foundations of Computer Science*, pages 116–124. ACM, 1994.

- [300] A. J. Skinner, M. E. Davenport, and B. E. Kane. Hydrogenic spin quantum computing in silicon: A digital approach. *Physical Review Letters*, 90:087901, 2003. <http://arXiv.org/quant-ph/0206159>.
- [301] A. Sørensen and K. Mølmer. Entanglement and quantum computation with ions in thermal motion. *Phys. Rev. A*, 62, 2000.
- [302] T. P. Spiller, W. J. Munro, S. D. Barrett, and P. Kok. An introduction to quantum information processing: applications and realisations. Technical Report HPL-2005-192, Oct. 2005.
- [303] T. P. Spiller, K. Nemoto, S. L. Braunstein, W. J. Munro, P. van Loock, and G. J. Milburn. Quantum computation by communication. *New Journal of Physics*, 8:30, Feb. 2006.
- [304] A. Steane. Error correcting codes in quantum theory. *Physical Review Letters*, 77:793–797, 1996.
- [305] A. Steane. The ion trap quantum information processor. *Appl. Phys. B*, 64:623–642, 1997.
- [306] A. Steane et al. Speed of ion trap quantum information processors. *Phys. Rev. A*, 62, 2000. <http://arXiv.org/quant-ph/0003087>.
- [307] A. M. Steane. Quantum computer architecture for fast entropy extraction. *Quantum Information and Computation*, 2(4):297–306, 2002. <http://arxiv.org/quant-ph/0203047>.
- [308] A. M. Steane. Overhead and noise threshold of fault-tolerant quantum error correction. *Physical Review A*, 68:042322, 2003.
- [309] A. M. Steane. How to build a 300 bit, 1 Gop quantum computer. <http://arxiv.org/abs/quant-ph/0412165>, Dec. 2004.
- [310] A. M. Steane and B. Ibinson. Fault-tolerant logical gate networks for CSS codes. <http://arXiv.org/quant-ph/0311014>, Nov. 2003.
- [311] A. M. Steane and D. M. Lucas. Quantum computing with trapped ions, atoms, and light. *Fortschritte der Physik*, Apr. 2000. <http://arXiv.org/quant-ph/0004053>.

- [312] G. L. Steele Jr. and W. D. Hillis. Connection Machine Lisp: Fine-grained parallel symbolic processing. In *Proceedings of the 1986 ACM conference on LISP and functional programming*, pages 279–297. ACM, 1986.
- [313] M. Steffen, W. van Dam, T. Hogg, G. Breyta, and I. Chuang. Experimental implementation of an adiabatic quantum optimization algorithm. *Physical Review Letters*, 90:067903, 2003.
- [314] T. L. Sterling, D. Savarese, D. J. Becker, J. E. Dorband, U. A. Ranawake, and C. V. Packer. BEOWULF: A parallel workstation for scientific computation. In *Proc. Int. Conf. on Parallel Processing, Volume I: Architecture*, pages 11–14, 1995.
- [315] J. Stockton, M. Armen, and H. Mabuchi. Programmable logic devices in experimental quantum optics. *J. Opt. Soc. Am. B*, 19:3019, 2002.
- [316] K. M. Svore, A. V. Aho, A. W. Cross, I. Chuang, and I. L. Markov. A layered software architecture for quantum computing design tools. *IEEE Computer*, pages 74–83, Jan. 2006.
- [317] K. M. Svore, B. M. Terhal, and D. P. DiVincenzo. Local fault-tolerant quantum computation. *Physical Review A*, 72:022317, 2005.
- [318] T. Szkopek, P. Boykin, H. Fan, V. Roychowdhury, E. Yablonovitch, G. Simms, M. Gyure, and B. Fong. Threshold error penalty for fault tolerant computation with nearest neighbour communication. <http://arxiv.org/abs/quant-ph/0411111>, 2004.
- [319] T. Szymanski and H. Hinton. Design of a terabit free-space photonic backplane for parallel computing. In *Proc. Second Workshop on Massively Parallel Processing Using Optical Interconnections*. IEEE, 1995.
- [320] Y. Takahashi, Y. Kawano, and M. Kitagawa. Constant-depth quantum circuits with gates for addition. In *Proc. ERATO Conference on Quantum Information Science (EQIS2003)* [1].
- [321] S. Tani, H. Kobayashi, and K. Matsumoto. Exact quantum algorithms for the leader election problem. In *Proc. STACS 2005: 22nd Annual Symposium on Theoretical Aspects of Computer Science*, volume 3404 of *Lecture Notes in Computer Science*, pages 581–592. Springer-Verlag, 2005.

- [322] S. J. Tans, A. R. M. Verschueren, and C. Dekker. Room-temperature transistor based on a single carbon nanotube. *Nature*, 393:49–52, 1998.
- [323] J. Taylor, H.-A. Engel, W. Dür, A. Yacoby, C. Marcus, P. Zoller, and M. Lukin. Fault-tolerant architecture for quantum computation using electrically controlled semiconductor spins. *Nature Physics*, 1:177–183, Dec. 2005.
- [324] D. D. Thaker, T. Metodi, A. Cross, I. Chuang, and F. T. Chong. CQLA: Matching density to exploitable parallelism in quantum computing. In *Computer Architecture News, Proc. 33rd Annual International Symposium on Computer Architecture* [8].
- [325] C. Tomovich. MOSIS – a gateway to silicon. *IEEE Circuits and Devices Magazine*, 4(2):22–23, 1988.
- [326] P. Treutlein, T. Steinmetz, Y. Colombe, P. Hommelhoff, J. Reichel, M. Greiner, O. Mandel, A. Widera, T. Rom, I. Bloch, and T. W. Hänsch. Quantum information processing in optical lattices and magnetic microtraps. <http://arXiv.org/quant-ph/060513>, May 2006.
- [327] M. Udrescu, L. Prodan, and M. Vlădăţiu. Using HDLs for describing quantum circuits: A framework for efficient quantum algorithm simulation. In *Proc. Conference on Computing Frontiers*, pages 96–110. ACM, 2004.
- [328] W. Unruh. Maintaining coherence in quantum computers. *Physical Review A*, 51:992–997, 1995.
- [329] I. Žutić, J. Fabian, and S. D. Darma. Spintronics: Fundamentals and applications. *Review of Modern Physics*, 76:323, 2004.
- [330] J. Vala, Z. Amitay, B. Zhang, S. R. Leone, and R. Kosloff. Experimental implementation of the Deutsch-Jozsa algorithm for three-qubit functions using pure coherent molecular superpositions. *Physical Review A*, 66:062316, 2002.
- [331] R. Van Meter. <http://www.tera.ics.keio.ac.jp/person/rdv/quantum/arithmetic.html>.
- [332] R. Van Meter. Communications topology and distribution of the quantum Fourier transform. In *Proc. Tenth Symposium on Quantum Information Technology (QIT10)*, pages 19–24, May 2004.

- [333] R. Van Meter. Trading classical for quantum computation using indirection. In *Realizing Controllable Quantum States: Proc. Int. Symp. on Mesoscopic Superconductivity and Spintronics (MS+S2004)*, Mar. 2004.
- [334] R. Van Meter and K. M. Itoh. Fast quantum modular exponentiation. *Physical Review A*, 71(5):052320, May 2005.
- [335] R. Van Meter, K. M. Itoh, and T. D. Ladd. Architecture-dependent execution time of Shor's algorithm. In *Proc. Int. Symp. on Mesoscopic Superconductivity and Spintronics (MS+S2006)*, Feb. 2006.
- [336] R. Van Meter, W. J. Munro, K. Nemoto, and K. M. Itoh. Distributed arithmetic on a quantum multicomputer. In *Computer Architecture News, Proc. 33rd Annual International Symposium on Computer Architecture* [8], pages 354–365.
- [337] R. Van Meter and M. Oskin. Architectural implications of quantum computing technologies. *Journal of Emerging Technologies in Computing Systems*, 2(1), Jan. 2006.
- [338] L. M. Vandersypen and I. Chuang. NMR techniques for quantum computation and control. *Rev. Modern Phys.*, 76:1037, 2004.
- [339] L. M. K. Vandersypen. *Experimental Quantum Computation with Nuclear Spins in Liquid Solution*. PhD thesis, Stanford University, 2001. <http://arXiv.org/quant-ph/0205193>.
- [340] L. M. K. Vandersypen, M. Steffen, G. Breyta, C. S. Yannoni, M. H. Sherwood, and I. L. Chuang. Experimental realization of Shor's quantum factoring algorithm using nuclear magnetic resonance. *Nature*, 414:883–887, Dec. 2001.
- [341] J. J. Vartiainen, A. O. Niskanen, M. Nakahara, and M. M. Salomaa. Implementing Shor's algorithm on Josephson charge qubits. *Physical Review A*, 70:012319, 2004.
- [342] V. Vedral, A. Barenco, and A. Ekert. Quantum networks for elementary arithmetic operations. *Phys. Rev. A*, 54:147–153, 1996. <http://arXiv.org/quant-ph/9511018>.
- [343] C. Vieri, M. J. Ammer, M. Frank, N. Margolus, and T. Knight. A fully reversible asymptotically zero energy microprocessor.

- [344] C. J. Vieri. *Reversible Computer Engineering and Architecture*. PhD thesis, MIT, 1999.
- [345] E. Waks, K. Inoue, W. Oliver, E. Diamanti, and Y. Yamamoto. High-efficiency photon-number detection for quantum information processing. *IEEE Journal of Selected Topics in Quantum Electronics*, 9:1502–1511, 2003.
- [346] A. Wallraff, D. I. Schuster, A. Blais, L. Frunzio, R.-S. Huang, J. Majer, S. Kumar, S. M. Girvin, and R. J. Schoelkopf. Strong coupling of a single photon to a superconducting qubit using circuit quantum electrodynamics. *Nature*, 431:162–167, Sept. 2004.
- [347] P. Walther, K. J. Resch, T. Rudolph, E. Schenck, H. Weinfurter, V. Vedral, M. Aspelmeyer, and A. Zeilinger. Experimental one-way quantum computing. *Nature*, 434:169–176, 2005.
- [348] D. F. Wang, A. Takahashi, Y. Matsumoto, K. M. Itoh, Y. Yamamoto, T. Ono, and M. Esashi. Magnetic mesa structures fabricated by reactive ion etching with CO/NH₃/Xe plasma chemistry for an all-silicon quantum computer. *Nanotechnology*, pages 990–994, 2005.
- [349] C. P. Williams and S. H. Clearwater. *Ultimate Zero and One: Computing at the Quantum Frontier*. Copernicus Books, 1999.
- [350] D. J. Wineland et al. Quantum control, quantum information processing, and quantum-limited metrology with trapped ions. In *Proceedings of the International Conference on Laser Spectroscopy (ICOLS)*, Aug. 2005. <http://arxiv.org/quant-ph/0508025>.
- [351] S. A. Wolf, D. D. Awschalom, R. A. Buhrman, J. M. Daughton, S. von Molnár, M. L. Roukes, A. Y. Chtchelkanova, and D. M. Treger. Spintronics: A spin-based electronics vision for the future. *Science*, 294:1488–1495, 2005.
- [352] W. K. Wootters and W. H. Zurek. A single quantum cannot be cloned. *Nature*, 299:802, Oct. 1982.
- [353] F. Yamaguchi, K. Nemoto, and W. J. Munro. Quantum error correction via robust probe modes. *Physical Review A*, 73:060302, June 2006.

- [354] A. Yao. Quantum circuit complexity. In *Proceedings of the 34th Annual Symposium on Foundations of Computer Science*, pages 352–361, Los Alamitos, CA, 1993. Institute of Electrical and Electronic Engineers Computer Society Press.
- [355] J. Yepez. Type-II quantum computers. *International Journal of Modern Physics C*, 12(9):1273–1284, 2001.
- [356] A. Yimsiriwattana and S. J. Lomonaco Jr. Distributed quantum computing: A distributed Shor algorithm. <http://arxiv.org/quant-ph/0403146>, Mar. 2004.
- [357] N. Yoran and B. Reznik. Deterministic linear optics quantum computation with single photon qubits. *Physical Review Letters*, 91:037903, 2003.
- [358] S. Yoshida, T. Sekiguchi, and K. M. Itoh. Atomically straight steps on vicinal Si(111) surfaces prepared by step-parallel current in the kink-up direction. *Applied Physics Letters*, 87:031903, 2005.
- [359] J. Q. You, J. S. Tsai, and F. Nori. Scalable quantum computing with Josephson charge qubits. *Phys. Rev. Lett.*, 89, Nov. 2002. <http://arXiv.org/cond-mat/0306209>.
- [360] J. Q. You, J. S. Tsai, and F. Nori. Quantum computing with many superconducting qubits, June 2003. <http://arXiv.org/cond-mat/0306208>.
- [361] Y. Yu, S. Han, X. Chu, S.-I. Chu, and Z. Wang. Coherent temporal oscillations of macroscopic quantum states in a Josephson junction. *Science*, 296(5569):889–892, 2002.
- [362] C. Zalka. Fast versions of Shor’s quantum factoring algorithm. <http://arXiv.org/quant-ph/9806084>, June 1998. <http://arXiv.org/quant-ph/9806084>.
- [363] Z. Zhong, D. Wang, Y. Cui, M. W. Bocrath, and C. M. Lieber. Nanowire crossbar arrays as address decoders for integrated nanosystems. *Science*, 302:1377–1379, 2003.